Surfactant Mediated and Green Approach to Fabricate Nano ZnO and Doped System for Industrial Applications

Thesis submitted in partial fulfillment of the requirements for the award of the degree of

DOCTOR OF PHILOSOPHY

In

CHEMISTRY

by

Nitesh
(Roll No: 719118)

Supervisor:
Prof. Srilakshmi V. Patri

Co-supervisor:
Dr. Sergey M. Melnikov

DEPARTMENT OF CHEMISTRY
NATIONAL INSTITUTE OF TECHNOLOGY
WARANGAL-506 004, (T. S.), INDIA

September-2023

Dedicated to

Waheguru ji

My parents: Smt. Ranjana and Sh. Om Parkash

Wife: Mrs. Rashmi N. Bhalla

Children: Gunmay and Yatharth

Brothers: Dr. Sandeep and Mr. Jitesh

Special Thanks to

IFFCO Group

IFFCO BEAUTY

Mr. Isa Allana

Mr. Sunil Singh

Mrs. Shubhalaxmi Sharma

Prof. D. Haranath

Mr. Kultar Singh

Mr. Vivek Sirohi

"Great leaders don't have all the answers, but they know where and how to find them"

-Anonymous

Dr. P. V. Srilakshmi
Professor
Department of Chemistry
National Institute of Technology
Warangal - 506 004
Telangana, India

Mobile: +91-9441965575
Email: patrisrilakshmi@nitw.ac.in

CERTIFICATE

This is to certify that the research work presented in this thesis entitled **"Surfactant Mediated and Green Approach to Fabricate Nano ZnO and Doped System for Industrial Applications"** submitted by **Mr. Nitesh** for the Degree of Doctor of Philosophy in Chemistry, National Institute of Technology, Warangal (Telangana), under my supervision and co-supervision of Dr. Sergey M. Melnikov of IFFCO group. This research work has not been submitted elsewhere for any degree.

Date: 08-05-2023
Place: NIT Warangal

Dr. P. V. Srilakshmi
Thesis Supervisor

DEPARTMENT OF CHEMISTRY
NATIONAL INSTITUTE OF TECHNOLOGY
WARANGAL – 506 004

Thesis Approval for Ph.D.

The thesis entitled ***"Surfactant Mediated and Green Approach to Fabricate Nano ZnO and Doped System for Industrial Applications"*** by **Mr. NITESH** (Roll No. 719118) is approved for the degree of Doctor of Philosophy.

Examiner (Online):

C. Shivakumara

Prof. C. Shivakumara
Principle Research Scientist
Solid State Structural Chemistry
Indian Institute of Science (IISc)
Bangalore, Karnataka

P.V. Srilakshmi 5th Sept. 2023

(Prof. Srilakshmi Patri)
Supervisor

प्राध्यापक / Professor
रसायन विभाग / Department of Chemistry
राष्ट्रीय प्रौद्योगिकी संस्थान, वरंगल - ५०६ ००४ आं.प्र
National Institute of Technology,
Warangal - 506 004

Sergey Melnikov

(Dr. Sergey M. Melnikov)
Co-Supervisor

05/9/2023

(Prof. D. Kashinath)
Chairman

विभागाध्यक्ष / Professor & Head
रसायन विभाग / Department of Chemistry
राष्ट्रीय प्रौद्योगिकी संस्थान, वरंगल - ५०६ ००४
National Institute of Technology,
Warangal - 506 004

Date: 05th September, 2023
Place: NIT Warangal

DECLARATION

I hereby declare that the matter embodied in this thesis entitled **"Surfactant Mediated and Green Approach to Fabricate Nano ZnO and Doped System for Industrial Applications"** is based entirely on the results of the investigations and research work carried out by me under the supervision of **Prof. Srilakshmi V. Patri**, Department of Chemistry, National Institute of Technology, Warangal and under the co-supervision of **Dr. Sergey M. Melnikov** of IFFCO group. I declare that this work is original and has not been submitted in part or full, for any degree or diploma to this or any other University.

Date: 08-05-2023

Place: NIT Warangal

(NITESH)

Roll No. 719118

CONTENTS

Acknowledgments

It is my privilege to express a deep gratitude to my research supervisor, ***Professor Srilakshmi V. Patri*** *for her exceptional support throughout my PhD journey. Her constant encouragement, constructive criticisms and full support from the introductory to the concluding level of my Doctoral thesis work. Also, heartfelt thanks to my co-guide* ***Dr. Sergey M. Melnikov****, Director R&D-IFFCO for his valuable inputs and guidance.*

I owe a sincere debt of gratitude to the ***IFFCO group especially Mr. Isa Allana (Board) for being a partner in pursuing my dream, encourgament and*** *for providing the financial support and extending the necessary laboratory facilities respectively, to carry out my research work and* ***Director, NIT Warangal*** *for all the support in PhD program. Sincere thanks to* ***Mr. Serhad C. Kelemci (CEO)*** *and* ***Mr. Sunil Singh (Technical Director)*** *of IFFCO group for their kind support.*

I would like to express my sincere thanks to my DSC members: ***Prof. K. V. Gobi, Dr. Raghu Chitta,*** *and* ***Prof. D. Haranath*** *for their progressive directions and fruitful suggestions. I am also indebted to other* ***Faculty Members*** *of the Department of Chemistry for their timely support and co-operation during my research work.*

I would like to express my deep sense of respect and gratitude to Asst. Prof. ***Dr. Ajeet Kaushik,*** *Department of Natural Sciences, Florida, Polytechnic University for his valuable technical inputs during my research work.*

It is a pleasure to thank my colleagues ***Nitin N. Ingle, Athira Jayaprakash and Hiral Patel for*** *their continuous support and enjoyable company during my research work.*

The continuous support and co-operation rendered by ***Non-Teaching*** *staff members and other* ***Ph.D. scholars*** *of the Department of Chemistry is gratefully acknowledged.*

Date: May 08, 2023 ***Nitesh Om Parkash Bhalla***

Abstract

Nanotechnology is a multidisciplinary and promising technology that entails the advancement of organic and inorganic materials, as well as the conversion and manipulation of these materials on an atomic and molecular scale, to produce materials with tailored biological, chemical, and physical properties. ZnO is an important member of the wurtzite family having a hexagonal crystal lattice and wide bandgap II-VI group semiconductor. Nanoscale ZnO has several significant benefits such as tunable morphological characteristics, chemical stability, efficient blockers of sun rays and ultraviolet radiations, non-irritant, compatible with various skin types, protects the skin from inflammation and have thus used as a crucial material for applications in diverse fields in personal care industry. Personal care products are self-care items that are commonly used for personal hygiene, cleaning, and grooming. Shampoos, soaps, handwash, and shower gels are examples of hygienic products that should be rinsed immediately after use. However, antibacterial agents that have been present in personal hygiene products for years are now becoming incredibly inefficient and toxic as a result of the worldwide rise in genetic variations and antibacterial resistance, which makes pathogens difficult to manage. Moreover, synthesis methods are either expensive, time and energy consuming or solvents/generated by-products are either not permitted or affects stability of health and hygiene products. Therefore, existing methodologies and antibacterial actives are not compatible or not preferred, there is still a lot to unleash in ZnO fabrication methodologies as well as selection of appropriate precursors suitable for health and hygiene products.

Motivated by the above facts, current thesis is dedicated towards fabrication and characterization of surfactant mediated and green based nano ZnO and doped system for industrial applications. The fabricated nanomaterials and infused products were systematically characterized using various advanced and appropriate techniques.

This research demonstrates, a facile approach to fabricate the nano ZnO and silver doped ZnO system in an unique combination of surfactant-polyol-assembly (SPA) acting as a caging agent restricting the ZnO crystallite size in nano-regime. This SPA is suitable for health and hygiene products and such optimized technique is among the very few researches exploring the impact of embedding low concentrations of nano ZnO system into the matrix of sodium salt of long chain fatty acids (soap bar) and liquid cleansing personal care products.

Results: XRD evaluation of nano ZnO-SPA and silver doped system exhibit an average crystallite size as 20.18 nm and 15.14 nm. The SEM suggests monodisperse spherical particles. UV-Vis spectra indicate Burstein-Moss-effect and bandgap energy from 3.55 to 3.64 eV with higher silver doping. Nano ZnO (3.66 eV) embedded in soap bar acted as a UV-blocker that prevents oxidation and increase photostability. The antibacterial efficacy of nanomaterials and infused products are investigated against *Staphylococcus aureus* and *Escherichia coli* by zone of inhibition and European standard EN:1276. Nano ZnO-SPA infused products exhibited high antibacterial efficacy up to 4.43 log reduction equivalent to >99.99% germ kill while ZnOS infused exhibit ZOI up to 11.75 mm with a log reduction of 5.41 i.e. >99.999% germ kill.

This thesis further explores phytochemical analysis on the aqueous and methanolic moringa leaves extracts using GCMS and their free radical scavenging potency studied using DPPH. Moringa based green synthesis is carried out as a strategic and sustainable route to fabricate potent zinc oxide nanoparticles. Moringa oleifera comprises various phytochemicals that act as non-toxic stabilizing and reducing agents.

Results: GCMS analysis revealed an extraction of phytochemicals in 25 aqueous and 54 bio components methanolic extracts. The half-maximal inhibitory concentration (IC_{50}) of moringa aqueous extract observed is 4.65 µL/mL and for methanolic extract 1. 83 µL/mL. XRD of GsZnO-Nps, the average crystallite size is 13.82 nm. SEM suggests the formation of spherical nanoparticles having a diameter of 50 nm. UV-Vis spectrum shows high bandgap energy of 3.36 eV. IC_{50} value of GsZnO-Nps was 21.72 µg/mL and AR-Grade ZnO was 345.57 µg/mL. Antibacterial efficacy of GsZnO-Nps was established which is comparatively higher than or equal to standard antibiotics/drugs; high ZOI of 26 mm and 30 mm against *Staphylococcus aureus* and *Escherichia coli* respectively. *Cutibacterium acne* organism have average ZOI of 33 mm.

Surfactant mediated and green approach is an excellent method to developing eco-friendly, safe and multi-functional versatile products having strong antioxidants, anti-acne and advanced antibacterial efficacy for industrial applications such as food, cosmetics, medicine etc.

The Doctoral thesis comprises of nine chapters and the highlights are given here under:

Chapter 1

- The current chapter deals a brief introduction about nanomaterials and nanostructures and their applications in personal care industry.

- Comprehensive overview of zinc oxide nanoparticles has been described along with significant industrial and product applications have been explored.

- A detailed review of literature on different synthesis methods of zinc oxide have been presented.

- The current chapter gives an outline about personal care products and industry. Various types personal care products and the market size is presented.

- Extensive review of soap and liquid cleansing products have been conducted to understand their history, chemistry and manufacturing. Efforts have also been placed to understand the antibacterial products market and drawbacks.

- Finally, current drawbacks in the industry and motivation for the current research work were detailed.

Chapter 2

- The current chapter describes the experimental procedures used for fabrication of zinc oxide and silver doped zinc oxide nano systems

- Surfactant mediated fabrication and green synthesis methods have been discussed in detail.

- This chapter also explores the principles of characterization instruments and methods that have been employed in the understanding properties of fabricated nanomaterial

Chapter 3

- This research demonstrates, a facile approach to fabricate the nano ZnO system in a unique combination of surfactant-polyol-assembly (SPA) acting as a caging agent restricting the ZnO crystallite size in nano-regime.

- The fabricated nano ZnO in SPA were systematically characterized using various advanced and appropriate techniques. This SPA is suitable for health and hygiene products.

- The antibacterial efficacy of nano ZnO-SPA were investigated against Staphylococcus aureus (*S. aureus*) and Escherichia coli (*E. coli*) by Zone of Inhibition (ZOI) and European standard EN:1276.

- This research demonstrates, optimized technique that is among the very few researches exploring the impact of embedding low concentrations of nano ZnO system into the matrix of sodium salt of long chain fatty acids (soap bar) and liquid cleansing personal care products.
- The infused products were systematically characterized using various advanced and appropriate techniques. Soap bar without ZnO experienced photodegradation and reduction in whiteness which clearly reflects the increased photostability of soap bar.

- The antibacterial efficacy of infused products is investigated against Staphylococcus aureus (*S. aureus*) and Escherichia coli (*E. coli*) by Zone of Inhibition (ZOI) and European standard EN:1276. Infused products exhibited high antibacterial efficacy up to >99.99% germ kill.

Chapter 4

- This chapter explores a strategic approach to fabricate nano scale silver (100-2000 ppm) doped zinc oxide (ZnOS) in a unique Surfactant-Polyol-Assembly (SPA) that acts as a caging agent, restricting the growth of particles.

- This highly suitable approach for health and hygiene products is among the few works of literature exploring the fabrication and infusion of nano ZnOS to elevate the germicidal efficacy of liquid cleansing products significantly.

- Infused products with 0.2% of ZnOS exhibit ZOI up to 13.25 mm with a log reduction of 2.13 while nano ZnOS 2000 ppm shows ZOI up to 11.75 mm with a log reduction of 5.41 which corresponds to >99.999% germ kill.

Chapter 5

- In this present study phytochemical analysis have been done on the aqueous and methanolic Moringa leaves extracts using Gas Chromatography-Mass spectrometry (GCMS) and their free radical scavenging potency (FRSP) studied using 2, 2-diphenyl-1-picrylhydrazyl (DPPH) free radical for further applications.

- GCMS analysis revealed an extraction of range of phytochemicals in aqueous and methanolic extracts.

- These extracts can act as very powerful antioxidants, anti-inflammatory ingredient for various applications in diverse field of food, cosmetics, medicine etc.

- Moringa oleifera comprises various phytochemicals that act as non-toxic stabilizing and reducing agents. Green synthesized ZnO nanoparticles (GsZnO-Nps) were investigated for their morphological and physicochemical properties using various advanced characterizing techniques.

- Anti-oxidant activity is recommended to improve general health by helping to neutralize free radicals in our systems. Strong anti-acne efficacy established against C. acne bacteria which is mostly responsible for causing acne on skin, the average inhibition zone was 33.00 mm.

- Antibacterial efficacy of GsZnO-Nps was established at different concentrations (10, 50, 100, and 200 µg/mL) against Gram-positive and Gram-negative pathogens by zone-of-inhibition (ZOI) method with respect to standard drugs.

Chapter 6

- The current chapter summarizes the thesis's significance and noteworthy successes.

- Details overall findings and remarks developed in the present study.

- The scope of future work has also been discussed.

List of Figures

List of Tables

Abbreviations

CB	Conduction Band
EDS/X	Energy Dispersive Spectroscopy
EN 1276	European Standard
FTIR	Fourier Transform Infrared Spectroscopy
FRSP	Free Radical Scavenging Potency
GsZnO-Nps	Green Synthesized Zinc Oxide Nanoparticles
GC-MS	Gas Chromatography–Mass Spectrometry
SEM	Scanning Electron Microscopy
TEM	Transmission Electron Microscopy
ICDD	International Centre For Diffraction Data
MIC	Minimal Inhibitory Concentration
SEM	Scanning Electron Microscopy
SLES	Sodium Lauryl Ether Sulfate/Sodium Laureth Sulfate
SPA	Surfactant Polyol Assembly
UV	Ultra Violet
VB	Valence Band
XRD	X-Ray Diffraction
ZnO	Zinc Oxide
ZnOS	Silver Doped Zinc Oxide
ZOI	Zone Of Inhibition
GC-FID	Gas Chromatography-Flame Ionization Detector

Chapter 1

Introduction to Nanomaterials and Personal Care Industry

Highlights of the Chapter:

- *The current chapter deals a brief introduction about nanomaterials and nanostructures and their applications in personal care industry.*
- *Comprehensive overview of zinc oxide nanoparticles has been described along with significant industrial and product applications have been explored.*
- *A detailed review of literature on different synthesis methods of zinc oxide have been presented.*
- *An outline about personal care products and industry. Various types personal care products and the market size is presented.*
- *Extensive review of soap and liquid cleansing products have been conducted to understand their history, chemistry and manufacturing. Efforts have also been placed to understand the antibacterial products market and drawbacks.*
- *Finally, current drawbacks in the industry, motivation and objectives of the current research work were detailed.*

1.1. Nanoscience and Nanotechnology

Nanomaterials are classified as structured components that have at least one of its dimensions lesser than 100 nm. Specifically, the four classifications are (i) zero dimensional materials which have all dimensions within the 100 nm (ii) one dimensional materials that have one dimension out of the nano range such as nano rods, nano wires etc. (iii) two dimensional materials having two dimensions more than 100 nm and usually it looks in form of layers acting like surface coatings or thin films (iv) three dimensional materials which have all three dimensions outside the nano meter range for example, nano flowers, bulk powders or bundles of nanorods and nanolayers. Materials with two dimensions in nanoscale (and extended in one dimension) are referred to as quantum wire. A quantum dot has all three dimensions in the nano range.

Nanotechnology, in spite of decades of research, is an evolving interdisciplinary field of science that has been flourishing in several zones. Nanostructures have gained tremendous research attention because of its extraordinary properties along with different industrial approaches and applications [1]–[6]. In order to build materials with oriented arrays and novel properties nanotechnology endeavours are focusing on manipulating molecules, atoms, and nano-size particles using accurate and skilful methods. Interested size range starts from 100 nm until atomic level (approximately 0.2 nm).

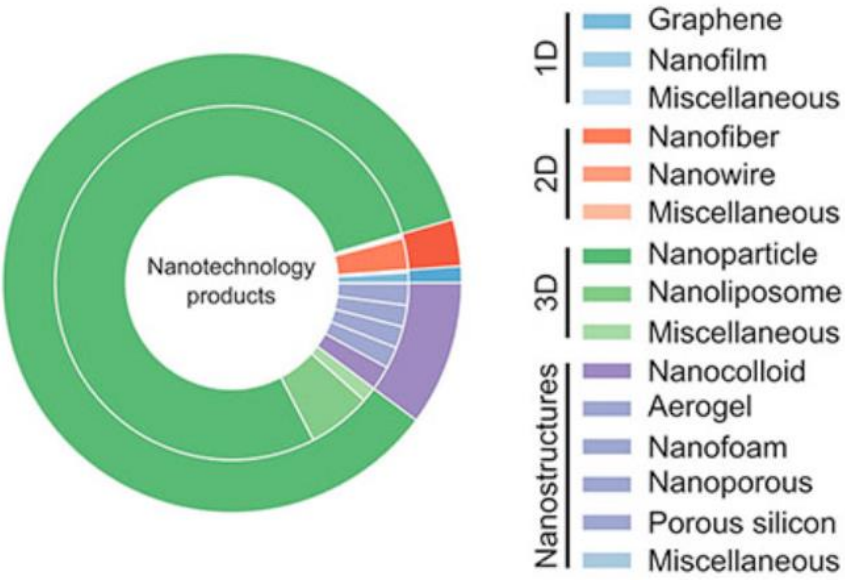

Figure 1.1. *Distribution and classifications of nanomaterial in commercialized products* [7].

The Figure 1.1. depicts the classification distribution of marketed nanomaterials. According to statistics, three dimensional nanomaterials are the most common with over 85%, with nanoparticles accounting for 78% of all nano based products.

There are two primary factors, which affects nanomaterials properties that contrast tremendously in comparison with its bulk counterparts: (i) quantum effect and (ii) higher relative surface area to volume ratio. These factors improve properties like strength, reactivity, electrical characteristics etc. With particle size reduction, rise in surface-area to volume ratio is observed; hence, more amounts of atoms are being created over the surface in comparison with bulk region. (Table 1.1)

Table 1.1. Relation between particle size and surface atom percentages

S. No.	Particle size	Number of surface atoms in %
1	1 mm	3×10^{-4}
2	30 nm	5
3	10 nm	20
4	3 nm	50

Therefore, nanoparticles in comparison to larger particles have higher surface area per unit mass. While catalytic chemical reactions along with growth happens near surfaces, it emphasizes that more reactivity will be seen in specific material mass in form of nano particulate as compared to same material mass in larger bulk form.

As reduction in size to nanoscale occurs, effect of quantum starts to lead matter properties mainly due to surface area effects. As a result, electrical, optical and magnetic material behaviour is affected predominantly since particle size or structure approaches towards smallest end of nanoscale. Materials exhibiting this effect include quantum well lasers and quantum dots for optoelectronics. Amongst semiconducting nanocrystals, ZnO, metal chalcogenides and their doped system were paid much attention because of its enormous applications in different areas and have shown fascinating phenomena such as visible light emission and size induced absorption [7]–[9], radiative life time shortening[10], photo blinking effec[11], electroluminescence [12].

Nanotechnology has historically made headway into key industries, such as materials and manufacturing, electronics and information technology, healthcare and life sciences, and energy and the environment depicted in Figure 1.2 [13][14]. Despite development in field of nanotechnology has been especially noticeable since the start of the century, the overall purpose is to translate research into commercially viable goods and gadgets that improve society. Nanotechnology provide opportunities for social progress, and their existence in our everyday routines is becoming frequent.

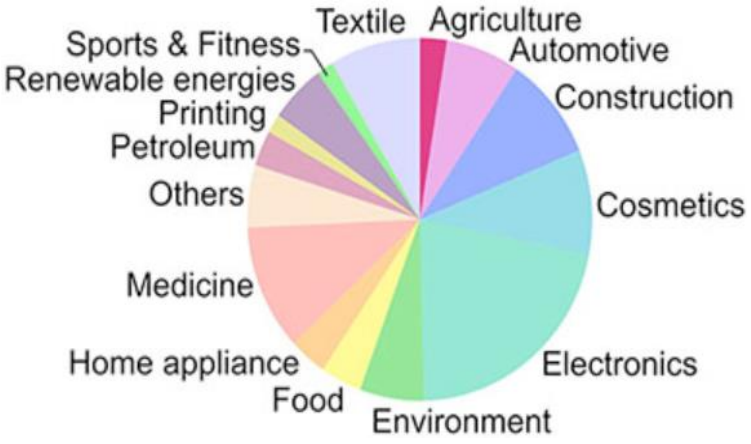

Figure 1.2. *Global nanotechnology market by industry branches*[7]

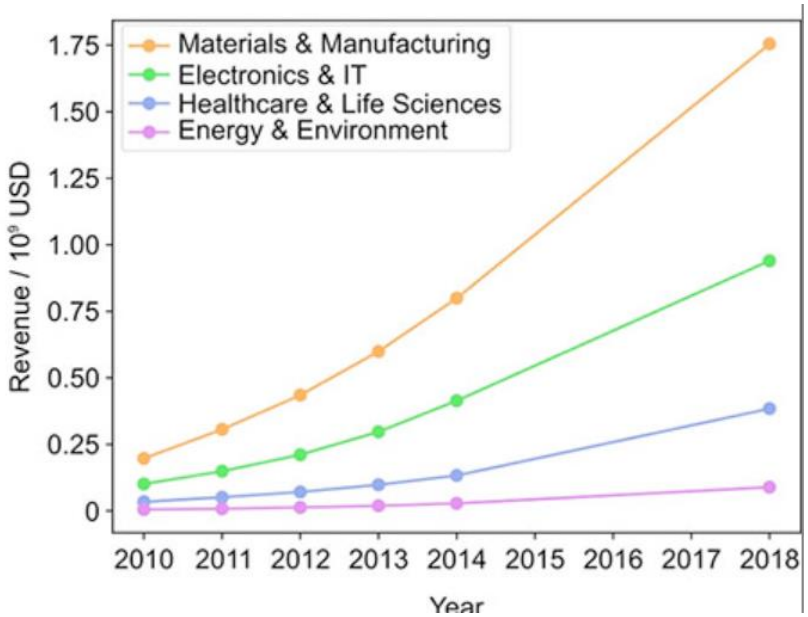

Figure 1.3. *Gross income earned by nanotechnology solutions, broken out by industry sector and year* [7].

When nanostructures revenues (Figure 1.3) is studied by industry, it is clear that materials and manufacturing caused more to overall nanotechnology income. This is to be expected given that the initial developmental stage for all technology requires fundamental multidisciplinary research, and this in the context of nanotechnology equates to the exploration of material characteristics and the fabrication of nanostructured materials. Nevertheless, if nanodevices are combined with current innovations, we should expect this tendency to move further towards product industries in the future years.

Nano products are quickly penetrating the commercial market across a wide variety of uses, and the prospects for the future are high. This demands for worldwide action to broaden guidelines, licenses, and restrictions for the next phase of nano products to assure their successful and safe usage. In the foreseeable future, substantial GDP growth and employment generation are predicted to grow and expand. Such an endeavour, in particular, will enable the later introduction of nano products with superior productivity and imminent public benefit. Moderna's COVID-19 mRNA nano based vaccines and Pfizer/COVID-19 BioNTech's mRNA nano based vaccines are indeed two prime case studies of how nanomaterials aided solutions can dramatically affect society everyday, especially in challenging topics like public health [15-[16]. These will undoubtedly raise public knowledge and confidence in nanoscience, accelerating progress in the sector. Nanoparticles and nano products are no more prospective possibilities in the significant multinational commercial market, but rather well-established value enhancers.

1.2. Metal and Metal Oxide Nanomaterials

Semiconductor metals and metal oxides have received a lot of interest due to their benefits. Due to their distinctive features, tailored metal oxide nanoparticles are one of the most widely utilized and produced nanomaterials. The numerous optoelectronic features, better flexibility at raised temperatures over poorly graded ceramics, cool welding capabilities, super - paramagnetic behaviour, remarkable catalytic, sensitivity, and selective activity of nanomaterials make them vital instruments in current nanotechnology. The melting point of a nanoparticle, for instance, is significantly smaller compared to a macroscopic substance of the same composition. The high density and small size of external surfaces of these nanoparticles contribute to their distinctive chemical and physical capabilities. Metal oxide nanostructures' possible technical uses are crucial, drawing scientists from the domains of material science, healthcare, agribusiness, informatics,

pharmaceutical, optoelectronic, telecommunications, electrochemistry, environment, fuel, and sensing. Modifications in cell characteristics have been found in nanoparticles of CuO, ZnO, SnO_2, Al_2O_3, MgO, ZrO_2, AgO, TiO_2, CeO_2, and others owing to size-related structural alterations.

Magnetic metal oxide nanoparticles have piqued the curiosity of researchers because their characteristics can be modified depending on their dimensions and structure. The magnetic, electrical, and chemical characteristics of nanomaterials can be affected by the nanoparticle size [17]. Iron oxides, including magnetite, are of keen importance to researchers and scientists due to a variety of possible uses ranging from magnetic storage devices (MSD) to magnetic resonance imaging (MRI) contrast agents [18]. Size dependence in -Fe_2O_3 nanoparticles was discovered, with 55 nm particles exhibiting ferromagnetic behaviour and 12 nm nanoparticles exhibiting super paramagnetic behaviour without hysteresis [19]. The reduction in particle size reduces overall magnetic anisotropy while causing the transition to super paramagnetic [20]. Novel and simple techniques of producing the desired sized metal oxide nanoparticles are necessary to achieve any of the preferred magnetic, electrical, and chemical characteristics. Since oxygen vacancies enhance surface conductivity while absorbed ions reduce it, metal oxide conductance is highly reliant on surface covalent bonding. Binding of compounds such as oxygen gas or nitrogen dioxide at vacant sites of the oxides causes electrons to move away from the conduction band and reduces conductivity, while carbon monoxide or hydrogen under oxygen rich environment reacts with adsorbed O_2, liberating electrons and boosting conductivity [21].

Metal oxide nanoparticles with high surface areas, such as nano ZnO, have chemical and thermal stability, as well as antibacterial capabilities. Therefore, nanoscale ZnO are utilized as effective nano adsorbents. Dehaghi *et al.* created ZnO enhanced chitosan particles that were utilized to remove permethrin (a neurotoxic insecticide) from water samples [22]. Permethrin was effectively reduced with 96% success utilizing a tiny quantity of ZnO enhanced chitosan material, according to the findings (500 mg).

Metal nanoparticles, including silver and gold, are sometimes found in personal care and beauty products. Silver is well recognized for the antimicrobial qualities, and its utilization in the shape of nanostructures finds numerous uses as an antiacne, antidandruff, and antiscaring ingredient in various personal care products such as skincare products, hair products, and soaps. Amorphous silica (SiO_2), zinc oxide (ZnO), and titanium dioxide (TiO_2) are the most common

metal oxide nanomaterials found in personal care products. Since they have a hydrophilic surface, their active surface is utilized to control, support, and deliver certain cosmeceutical components to the epidermis, as well as to promote skin penetration of encapsulated compounds.

The intrinsic qualities of nanoparticles, including their great capability to absorb epidermis, antibacterial effects, ultraviolet rays shielding, and lastly their unique optical characteristics, make them appropriate and valuable personal care product ingredients [23]. Sunscreens, moisturizers, balms, cosmetics, and loose powders, lip glosses, highlighters, eye makeup, nail polish, antiaging creams, soaps, body wash, hygiene products, shampoos, hair conditioners, antiperspirants, fragrances, and other cosmetic goods include metal and metal oxide nanoparticles [24]–[26].

1.3. Zinc Oxide (ZnO) Overview

1.3.1. Brief history

In history, zinc was observed as an exceptional and unique material. In 1st century A.D., Romans used zinc for making metals. It was in 14th century; in Zewar Rajasthan, India, zinc in the form of metal was considered. Through smelting technique, production of ZnO was achieved as a byproduct. This byproduct was in the form of white powder, was used to cure sore eyes. In 16th century, China initiated zinc-refining framework where high zinc material was used to make brass [27]. Europeans used to import zinc from China and in 1789, Antoine Lavoisier recorded Zinc as an element of periodic table. Possibly, in 1920's ZnO was first used in electronic applications for building radio sets [28]. In twentieth century, material science really blossomed and ZnO was considered as one of the important materials requested in detailed. During 1935, electron diffraction data on ZnO was first generated [29]. Three years down the line, for the first time, an image was obtained with the help of scanning transmission electron microscope and crystal structure of ZnO was studied [30]. Temperature-dependent Hall estimation of ZnO was first stated in 1954 asserting the naturally n-sort nature of this material [31]. During 1930's in Germany, preliminary work on the light discharge from ZnO was taking consideration. Previous ZnO research and finding has increase the eagerness to study the nano look of ZnO particles.

1.3.2. Zinc Oxide Crystal Structure

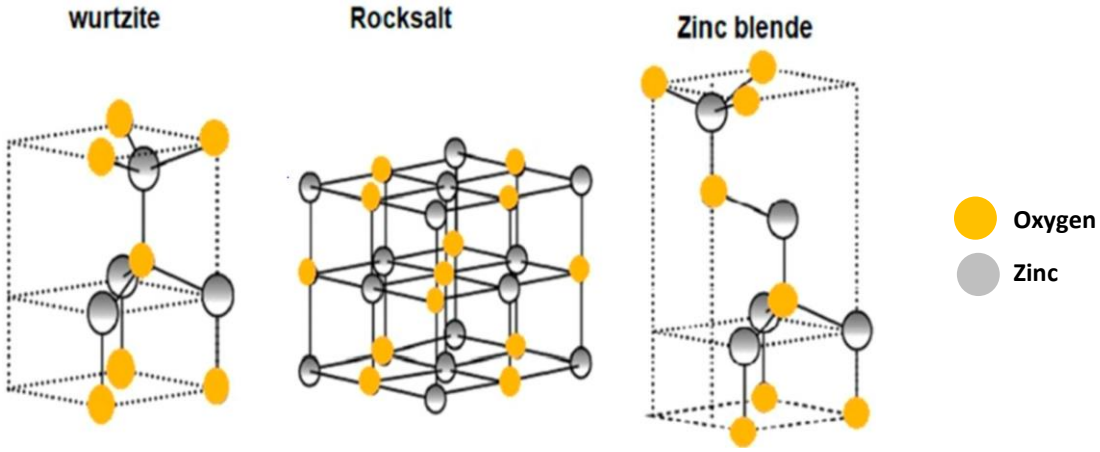

Figure 1.4. *ZnO crystal structures (a) wurtzite, (b) zinc blende and (c) cubic rock salt* [32]

ZnO is a II-VI semiconductor compound with a large, direct band gap of 3.4 eV. Its high exciton binding energy of 60 meV qualifies it as a desirable candidate for application in photodetectors such as LEDs and fiber lasers generating in the blues and UV spectral ranges. Figure 1.4(a)–(c) shows the crystal structures of zinc blende, wurtzite, and cubic rock salt. Figure 1.4(a) to (c) shows crystallization of zinc oxide in wurtzite (B4 type) structure. ZnO looks like hexagonal crystal lattice, which is considered by two interconnecting sublattices i.e. Zn^{2+} and O^{2-}, the interconnection is in such a way that Zn ion is surrounded by O ion in a tetrahedral manner, and vice-versa. Tetrahedral harmonization provides polar symmetry at the hexagonal axis and inherently accountable for the ZnO properties. Each Zn atom is bonded with four O atoms.

The wurtzite structure looks like hexagonal unit cell which has two cross-section parameters i.e. "a" and "c" within extent of c/a = 1.633 which goes to space group of of C^4_{6v} and $P6_3mc$ are within the Schoenflies and Hermann–Mauguin notations respectively [33]. At surrounding temperature, wurtzite structure is steadiest. Adjusting of zinc blende shape may be possible by forming zinc oxide onto substrates along with cross section cubic structures. In both the above cases, oxide and zinc centers considered as tetrahedral.

Semicodnuctors lattice parameters influenced by various factors like: (i) Foreign atom concentration, their defects and difference in their radii in comparison to replaced ions of matrix. (ii) Conduction band having free-electron with varying concentration influence the parmeters due to deformation potential, (iii) External strains like induced by substrate, and (iv) temperature. High resolution X-ray technique is very suitable to do the accurate mesurement of lattice parameters of

any crystalline material by utilizing bond method for a symmetrical reflections and asymmetrical reflections set. Lattice constants for wurtzite ZnO, extend from 3.2475 to 3.2501 Å (a–parameter) and range of 5.2042 to 5.2075 Å (c-parameter). Slightly wider variation reported for the c/a proportion and u parameter, from 1.593-1.6035 and from 0.383-0.3856 respectively. Lattice stability and ionicity could be most probable reasons for the deviation from an ideal wurtzite crystal structure [33].

At room temperature (RT), ZnO wurtzite bandgap has gap energy ~3.37 eV. Zinc oxide is one highly important material of wurtzite family. Polar surfaces and non-central symmetry are two critical features for wurtzite structure. Large band gap of ZnO make it a versatile material for various distinctive applications. Additionally, due to large exciton binding energy (approx 60 meV), and high thermal stability of these exciton in ZnO at RT make it significantly preferred material in certain optoelectronic applications like Ultraviolet lasing etc. Reports have been published demonstrating the Optically Pump Stimulated Emission (OPSE) within ZnO films along with Zinc oxide nano-wires [34], [35].

1.3.3. Industrial Applications of ZnO

Historically ZnO is being used as pigments and protective coatings on metals. ZnO is also used as a standard material for various appliactions in semiconductor electrochemistry, conventional catalysis and photochemistry and so on [36], [37]. Due to its wide applications in multiple fields, ZnO nanoparticles have gain lot more attention. For instance, in environmental fields it can be used to photo catalytically degrade inorganic or organic pollutants in water or air.

In early 1950s, studies on ZnO as an antimicrobial agent initiated. However, in last few decades, real work towards the usage of zinc oxide as an antimicrobial agent started. Also, nanosize ZnO is been investigated for their potential antimicrobial actions and properties, that have an immense advantage owing to its biocompatibility, less-toxic to human, the ability to withstand insensitive condition, and are more durable, in comparison with the usual organic materials, which make a potential candidate for antibacterial applications, medical and other industrial applications. Currently, U.S. Food and Drug Administration (FDA) has recognized ZnO as safe material (21CFR182.8991) (FDA, 2011) and made it among one of the five listed zinc compounds in "Generally Recognized as Safe" (GRAS).

The industry is dominated by large-scale global corporations with a solid and robust global marketing system Table 1.2. Competitors are increasing their investments in R&D to manufacture

elevated goods. The United States Zinc industries are the global leaders in the production of ZnO. It serves a variety of finished goods sectors, including rubber, chemicals, ceramics, and others. Among the key companies in the global zinc oxide market are [38]:
U.S. Zinc , Zinc Oxide LLC, EverZinc, Rubamin, Grupo Promax, Weifang Longda Zinc Industry Co., Ltd., Yongchang zinc industry Co., Ltd.

Table 1.2. Zinc oxide market scope analysis[38]

Report Attribute	Details
Market size value in 2022	USD 4.67 billion
Revenue forecast in 2030	USD 8.1 billion
Growth rate	CAGR of 6.9% from 2022 to 2030
Base year for estimation	2021
Historical data	2018 - 2020
Forecast period	2022 - 2030
Quantitative units	Volume in kilotons, revenue in USD million/billion, and CAGR from 2022 to 2030
Report coverage	Volume and revenue forecast, company ranking, competitive landscape, growth factors, and trends
Segments covered	Process, application, region
Regional scope	North America; Europe; Asia Pacific; South America; MEA
Country scope	U.S.; Canada; Mexico; Germany; Italy; Spain; Russia; Belgium;The Netherlands; China; India; Australia; South Korea; Peru; Bolivia; Brazil; Iran; South Africa
Key companies profiled	U.S. Zinc; Zinc Oxide LLC; EverZinc; Rubamin; Grupo Promax; Weifang Longda Zinc Industry Co., Ltd.; Yongchang Zinc IndustryCo. Ltd.

The worldwide zinc oxide business was estimated at $ 4.43 billion in 2021, with a compound annual growth rate (CAGR) of 6.9% anticipated from 2022 to 2030. The material is utilized in several sectors. Rubber, ceramics, medicines, and cosmetics are just a few examples. The increased requirement for zinc oxide nanoparticles is likely to present the market with several potential

possibilities throughout the projected timeframe. Rubber, ceramics, chemicals, cosmetics & personal care, paints & coatings, pharmaceuticals, agriculture, and other applications comprise the global market.

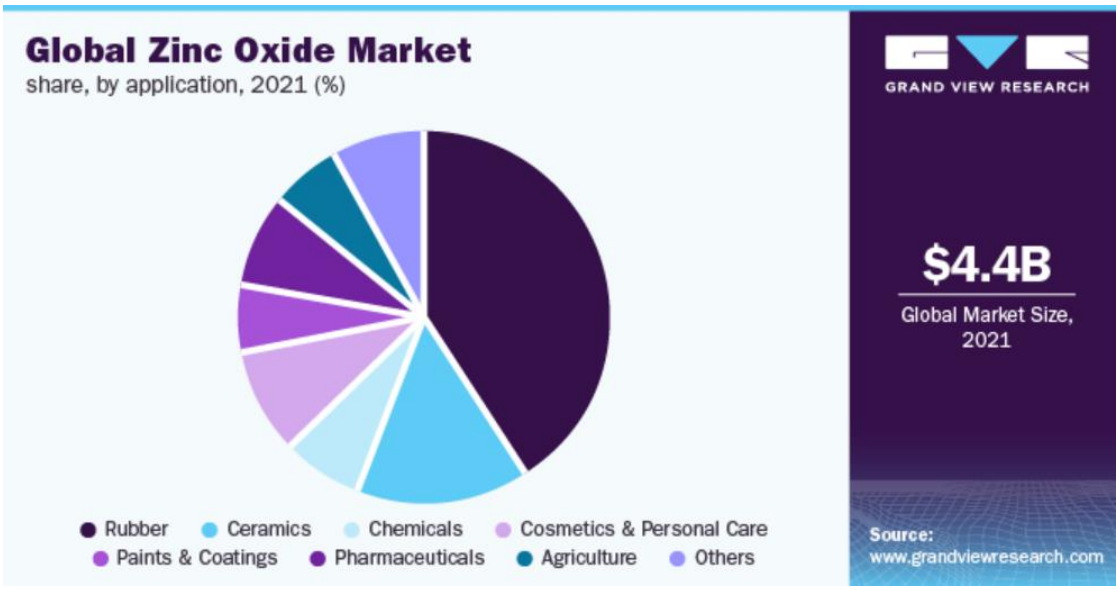

Figure 1.5. *Global zinc oxide market share by application, 2021%* [38]

In 2021 as seen in Figure 1.5, the rubber category had the highest marketshare of higher than 41%. This is due to the increased usage of zinc oxide in the rubber sector as a result of increased tire manufacture. ZnO is utilized as a vulcanizing activator, which is a material that is used in tiny amounts to boost the efficiency of the vulcanization accelerator. It's employed to cure or cross-link halogen-containing elastomers like neoprene and polysulfides. Ceramics are expected to have the next highest market share by 2030. ZnO has favorable characteristics in the manufacturing of ceramics, including relatively high heat capacity, large stability, thermal conductivity, and a low expansion coefficient.

Furthermore, ZnO nano-particles is well known for the medicinal properties as an astringent and anti-irritant in the pharmaceuticals industry. It is also used as sunscreen due to its UV blocking properties [39]. The nanosize zinc oxide particles act as a sunblock by dispersing in suitable matrix of formulations and transmitting visible light. One of the key marketing advantage of nanoparticles ZnO is its capability to provide broad spectrum UV protection in sunscreen products that are non-irritating. Certain organic active agents like avobenzene also known as Parsol-1789 gives full UVA

protection can sometime cause irritation to skin. In result, Zinc oxide is gaining attention for various applications like for sensitive skin and products for baby and many renowned brand organizations like Clinique, Johnson & Johnson etc. sunscreen brands like Cellex-C International are using ZnO significantly, and also for daily skin foundation and lotions like oil of Olay, Revlon which provides UV protection.

However, fine particle size may be able to maintain the skin protection against UV radiation but the inherent photoactivity of such materials may lead to increase in the generation rate of hydroxyl radicals. Therefore, with personal care products, increase in photocatalytic activity may show negative impact on skin cells. Moreover, there is few data published which correlates nanoparticles photoactivity with biological effects. In vitro study showed damaged to supercoiled DNA in presence of nanoparticulate metal oxides, and the rate of unwinding itself could be utilized as a measurement of metal oxide photoactivity [40], [41]. In personal care products, material‘s photoactivity needs to be quenched for preventing potential damage to skin cells. There are different methods through which we can achieve quenching effect like capping the sites where generation of surface hydroxyl radicals occur, alteration of band gap and particles encapsulation through insulating layer. Consideration towards band gap are gaining interest, where reduction of energy gap was achieved through introducing dopant species into system. Majority of the data published is mainly towards utilization of dopants to change photoactivity in titania [42], [43]. In current article, the nano ZnO and its doped system has been microvisioned because of its enormous potential applications in various fields.

1.4. Various synthesis methods

Nowadays, various innovative methods are developed and explored to synthesize nanomaterial and engineered thei properties. Investigating all those approaches and methodlogies extesnively in this article is beyond the scope. However, few of the novel nanosize material synthesis routes for ZnO and their doped systems, which are well established, and underdevelopment are included:

1.4.1. Attrition methods

The strategies endeavor to reduce micron-size coarse particles to fine particles by utilizing the energy, through process called as milling. Few other analysts are finding different method to conduct milling with cautiously organized warm, chemical situations and shear. Whereas for few applications, such strategies communicated to abandon contaminated item either due to the vessel utilized to break particles or media.

Salah et al [44] utilized energy intensive ball milling method which differs from the traditional milling methodology. In this method, on magnetic milling balls to apply strong magnetic pulling force, a magnet is positioned closer to the cell, and hence higher impact energy is observed as compared to conventional ball milling energy to break the particles. Moreover, with adjustment of cell rotation and magnet position different milling intensities can be achieved to break coarse particles. ZnO powder available commercially with purity of 99.9% and having size of ≈ 0.6–1 μm was subjected for milling within steel cells by utilizing hard steel balls having diameter of 15mm and weight of about 32 gm at ambient conditions with different time point that starting from 2 hours and reaching to 50 hours. The mechanical milling method was conducted in a horizontal oscillatory mill (Retsch-PM 400) operating at frequency of 25 Hz. Steel balls and Zinc oxide powders mixture ratio was maintained around 15:1 weight by percent. In this process, direct usage of milled materials without any added milling media was done. Each cell comprised of 10 g of powdered sample along with five balls. In this experiment, two parallel cells were utilized (total weight of sample powder was 20 g). Resultant nanomaterials were characterized using X-ray diffraction (XRD), whereas field emission scanning electron microscopy (FESEM) and transmission electron microscopy (TEM) was used to analyze powder morphologies and nano details. At room temperature (RT), Photoluminescence (PL) emission spectra was recorded using fluorescence spectro fluorophotometer. For measuring photoluminescence, equal amounts of nanomaterials were dispersed in ethanol i.e. around 5 mg in about 5 mL and subjected for recording spectra.

From SEM images, the average particle size was estimated and plotted as function of milling time, Figure 1.6. At around 365nm, new band observed in PL spectrum result, whose intensity increases with decrease in particle size. Such type of optical and structural modifications induced in zinc oxide nanoparticles can be useful for different applications.

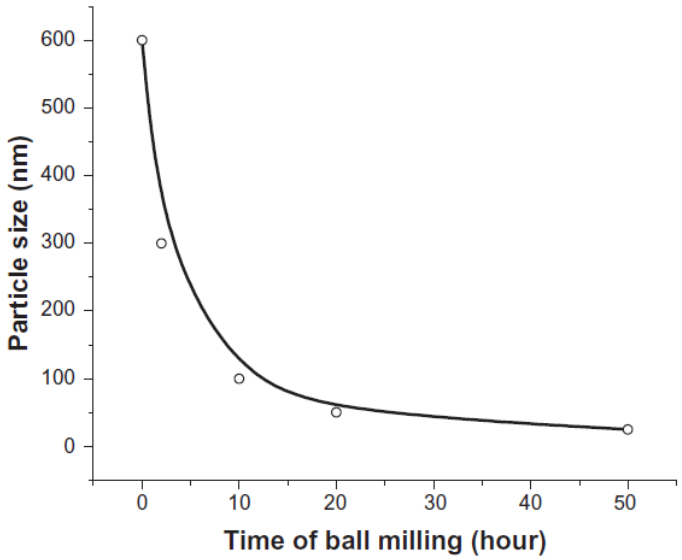

Figure 1.6. *Milling time and resultant particle sizes* [44]

Zahra et al [45] synthesized ZnO nanoparticles by a mechanochemical method using Na_2CO_3 and $ZnCl_2$ as precursors along with Sodium chloride as a diluent. The initial materials were then mixed in a 300 ml stainless steel vessel enclosed with three stainless steel balls with 20 mm diameters, nine balls with 15 mm diameters, and 17 balls with 10 mm diameters. The milling rate was set to 300 rpm. Milling was conducted in a high-energy planetary ball mill with a range of milling times between eight and 14 hours and with ball to powder mass ratios of 15:1 and 20:1. After completion of milling, three groups of samples were obtained. Factors such as ball to powder mass ratio and milling time influenced the effects of milling energy and impact of synthesis processes on the structure, morphology and optical properties of the synthesized nanoparticles were characterized by XRD, SEM, TEM, UV-visible and photoluminescence spectroscopies. It was reflected from the results that longer milling times and ball to powder mass ratios ccontribute to the increased crystallite sizes of the nanoparticles due to cold welding. Nanoparticles of ZnO with crystallite sizes in the range between 16 nm and 19 nm was produced through optimization of the order of processes and milling energy.

Variety of morphologies were obtained in different samples because of changing the synthetic steps order, Table 1.3. The optical band gap values for different ZnO nanoparticles were observed to be much smaller than the known bulk ZnO. This result was consistent with PL studies and correlated to the presence of intrinsic defects in the generated nanoparticles.

Table 1.3. The mechanochemical processes, conditions, and the resultant properties of various samples

Samples Code	A	B	C	D	E
Process	Milled, Washed, Heated	Milled, Washed, Heated	Milled, Washed	Milled, Washed	Milled, Heated, Washed
Milling Time (hour)	8	10	12	14	8
Ball:Powder Mass ratio	15:1	20:1	15:1	20:1	15:1
Morphology	spherical	spherical	spherical	spherical	flakes
Crystallite Size (nm)	16.6	17.5	16.1	18.9	16.5
Band gap (eV)	3.2	3.17	3.25	3.18	3.27

1.4.2. Solution method

This method also well considered as chemical synthesis, wet method, precipitation technique, sol-gel etc. This method involves the usage of reactants in solution form and attempt to precipitate nanoparticles. The sol-gel approach is well established and used to create nanoparticles known as quantum dots in which quantum mechanical properties plays key role for the particles valuable behavior. The striking feature of solution process is their low processing temperature low capital expenditure. Additionally, for controlling the final shape of the particles, they are much better and convenient than vapor condensation techniques.

Sue *et al.* [46] in methanol solution synthesized the colloidal ZnO nanoparticles by hydrolyzing methanolic $Zn(CH_3COO)_2$ solution. In general, KOH base solution was introduced to methanolic $Zn(CH_3COO)_2$ solution and the formation $Zn(OH)_2$ turbid solution occurs before the ZnO colloids formation. In their method, powder $Zn(CH_3COO)_2$ was added to methanolic solution of KOH and subjected to heating at 60^oC and ZnO nanoparticles synthesized without forming the suspension of $Zn(OH)_2$. The solvent was removed using rotary evaporator and ZnO were taken out for further studies. The PL spectrum shows prominent near-band edge excitonic emission of ZnO nanoparticle as shown in Figure 1.7. The peak observed at wavelength of 378 nm (3.28 eV) is showing blue shift to a certain extent in comparison to bulk ZnO emission. Strong emission band at wavelength 381 nm (3.25 eV) was shown by 300 μm thick ZnO bulk substrate.

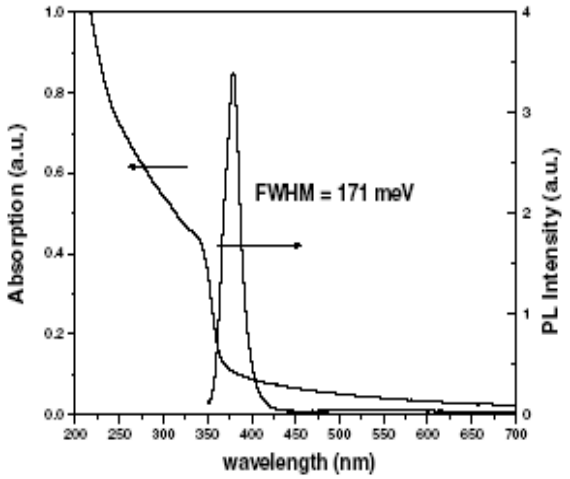

Figure 1.7 *UV-Vis and PL spectra of ZnO nanoparticles post evaporation of the solvent* [46]

Through UV–vis absorption peak the estimated size was 3.6 nm of the ZnO dry powders. Further, investigation on particle size was done by using TEM and results shows that particles are narrowly distributed and are of 4 nm average diameter. In the range of 200–3100 cm^{-1} Micro-Raman spectra recorded in from 200 cm^{-1} to 3100 cm^{-1}.

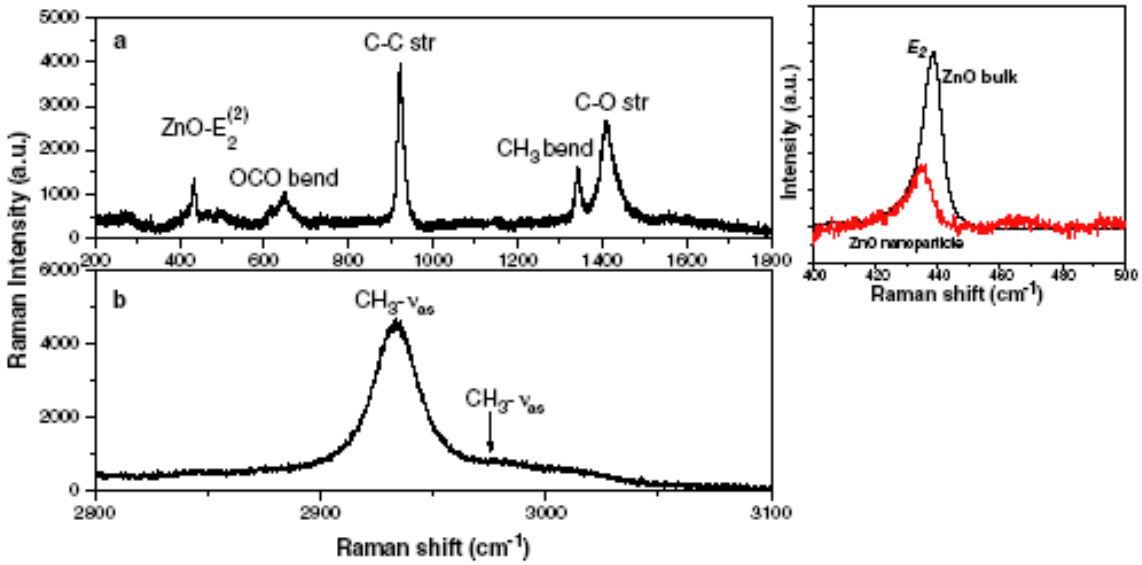

Figure 1.8 *Micro-Raman Spectra (a) and (b) of dried nano ZnO powder. Shifting of E_2 phonon in bulk ZnO versus nano ZnO is shown in the inset [46].*

Figure 1.8 shows the vibration modes because of acetate and ZnO. The $E_2^{(2)}$ phonon mode of ZnO at 436.5 cm^{-1} is markedly resolved in the z(x_) $\bar{z}$ geometry. The $E_2^{(2)}$ phonon frequency of bulk ZnO observed to be red-shifted by 2.0 cm^{-1} and appearing strongly at 438.5 cm^{-1}. Other Raman vibrational mode frequencies due to acetate group are assigned in Figure 1.8 and

summarized in Table 1.4. The ZnO surfaces can have bounded acetate ligand available in free form as potassium acetate and/or zinc acetate ligand.

Table 1.4 The assignment of wavenumbers of various different modes of metal with acetate group

Modes of Acetate with Metal	$_{C=O}$ (cm^{-1})	$_{C-O}$ (cm^{-1})
Unidentate	1579	1425
Bidentate	1547	1456
Bridging	1600	1441

Basis the characterization employed, it was concluded that adsorption of acetate group on nano ZnO surfaces and passivation of oxygen vacancies leading to UV emission and show green luminescence. The redshifted CO stretching mode indicates the formation of bonds between oxygen of carboxylic groups and Zn atoms available on surface of particles.

Yang et al [47] synthesized ZnO nanostructure by hydrothermal process at 120°C using cetyltrimethylammonium bromide (CTAB), $Zn(AC)_2$ and NaOH as starting materials. Resultant nanomaterial had interesting flowerlike nanostructures, which comprise of sword like nanorods of ZnO. Synthesis process involves the mixing of aqueous Zinc acetate solution with CTAB and with continuous stirring and subsequently added aqueous NaOH of 2 M concentration for the hydrolysis. The resultant white aqueous mixture was transferred to stainless steel autoclave having Teflon lining, sealed and was subjected to 120°C temperature for 20 h.

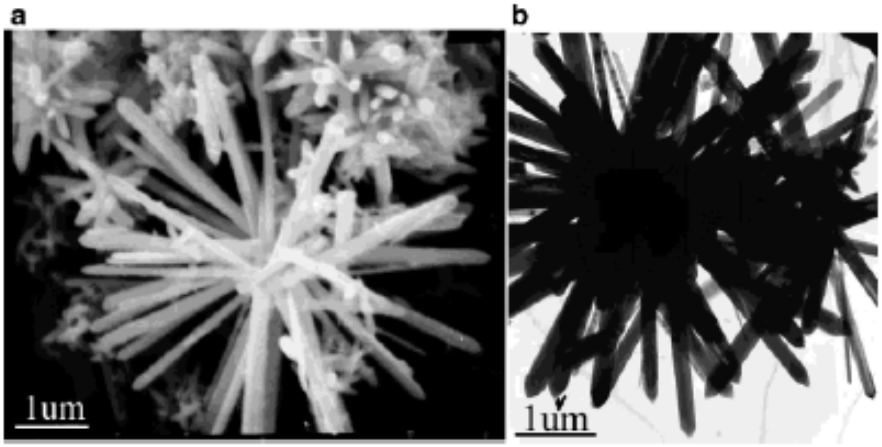

Figure 1.9. *Electron Microscopic images of Flowerlike ZnO nanostructures obtained from hydrothermal synthesis route (a) SEM image and (b) TEM image* [47]

Similarly tow more experiments were carried out for the comparison study one without CTAB and second by heating to 160°C temperature. White precipitates were then centrifuged, washed with distilled water followed by ethanol to remove the unreacted substances and ionic species and then were air dried at 60°C.

XRD investigations revealed that flower like ZnO nanostructures were hexagonal crystals. SEM and TEM images of flower like ZnO nanostructures are presented in Figure 1.9 (a, b) having sword like ZnO nanorods with 60-200 nm in width and length in several micrometers.

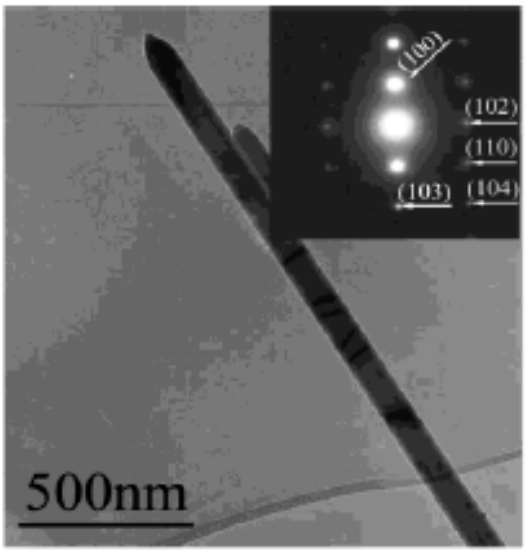

Figure 1.10. *TEM image of an individual sword like ZnO nanorod synthesized at 120℃ by hydrothermal process, it comprises of flowerlike ZnO nanostructures. SAED pattern of the sword like nanorod of ZnO is shown as an inset on upper right of the image* [47].

TEM image of an individual sword like ZnO nanostructure with pointed end is shown in Figure 1.10, and the inset having selected area electron diffraction (SAED) patterns reveals that nanorod is actually a single crystal and possess hexagonal phase and these results correlates with XRD findings.

It was concluded that CTAB plays an important role in generating actives sites on surface of ZnO nuclei which eventually led to the growth of nanorods. This mainly occurs by the CTAB interaction with growth ZnO units and results in building the flower like ZnO nanostructures. At low temperature (120^{o}C), sword like ZnO nanorods did not grow as there was not enough driving force without CTAB.

Deepak et al [48] reported the synthesis of nano ZnO doped with variety of transition metal ions Mn^{2+}, Ni^{2+} and Co^{2+} by making acetate solid solutions and subjecting them to water for the

decomposition. Nanoparticles of ZnO doped with Mn^{2+} was synthesized using $Zn(CH_3COO)_2.2H_2O$ and $Mn(CH_3COO)_2.4H_2O$ as solid precursors and were mixed at different molar ratios of Mn ranging from 1 to 7%. A clear solution was obtained by dissolving the solid mixture into 20 ml of water and the resultant solution was subjected to dry at 100^oC for around 10 h. The resultant powder was further heated for 3h at 600^oC in air and polycrystalline ZnO:Mn^{2+} was obtained. Similar process was performed for the doping of Co^{2+} and Ni^{2+} in ZnO with slight change in heating temperature. Optical absorption spectra of Mn^{2+} doped ZnO indicates the bandgap reduction for low dopant concentrations, and linear increase in bandgap with increased concentration. Progressive reduction in the bandgap with concentration of dopant was observed in ZnO doped with Co^{2+} and $Ni^{2+.}$

1.4.3. Surfactant aided microemulsion and nanoemulsion methods

These techniques are gaining attention from the ease of process and various applications perspective. Microemulsions are transparent and thermodynamically stable system having two immiscible liquids usually stabilized by the presence of high concentration of surfactants and co-surfactants. Whereas nanoemulsions are kinetically stable system. The surfactant molecules are amphiphilic having hydrophobic tail and hydrophilic head group and play an important role in these techniques by reducing interfacial tensions and by creating confined domains for the synthesis of nanoparticles. For the synthesis of nanoparticles, water in oil microemulsion has been effectively utilized. Promising results are reported in certain studies however there is still dearth of extensive reports on synthesis of ZnO and doped system and demonstration of their industrial applications using these techniques but gaining attention recently.

Lopez et al [49] using bicontinuous microemulsions reported the synthesis of nano ZnO with high purity, high yield and having size range 6 to 22 nm. Figure 1.11 shows the phase diagram which was generated for the mixture of Sodium bis-2-ethylhexyl sulfosuccinate (AOT)/Sodium dodecyl sulfate (SDS) at the ratio of 2:1 by weight in toluene and their titration with varying concentration of surfactant 5% to 70% by weight and 0.9M of $Zn(NO_3)_2$ aqueous solution to identify the bicontinuous microemsulsion region at reaction temperature 70°C.

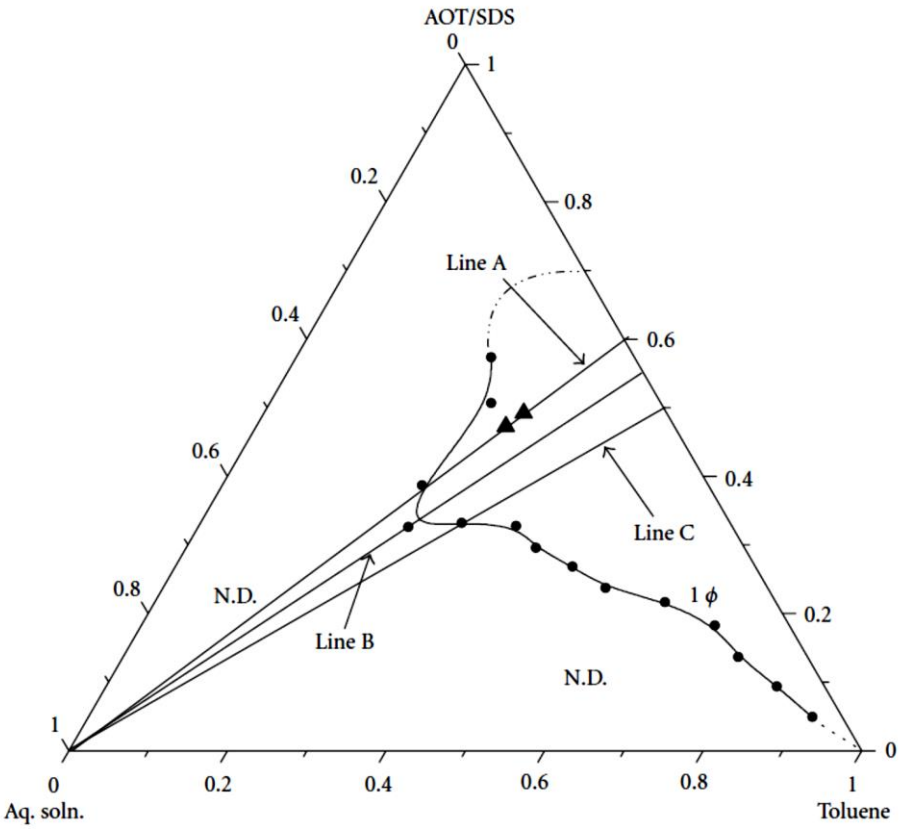

Figure 1.11. *Partial phase diagram achieved at temperature 70℃ for the blends of toluene, AOT/SDS (2/1w/w), and aqueous solution of 0.9M Zn(NO$_3$)$_2$. The one-phase microemulsion area (1φ) is found between the surfactant's mixture/toluene axis and the solid line; here, lines A, B, and C demonstrates where conductivity estimations were performed to look at the structure of the microemulsions. Strong triangles show the compositions where the precipitation responses were made* [49]

Bicontinuous microemulsion having Zn(NO$_3$)$_2$ was subjected for the hydrolysis at 70°C by using 1.4 times of stoichiometric amount of NaOH at varying rate to achieve different addition times 100 min, 125 min and 150 min. The resultant precipitates were filtered and suspended in acetone/aqueous mixture while doing sonication (15 min) for the removal of adsorbed surfactant and residual reactants/ impurities. This process was executed several times and eventually obtained wet powder was subjected to dry at 60°C and further exposed to calcination at 400°C. Nanoparticles characterization was done by using various techniques like TEM, atomic absorption spectroscopy (AAS), and XRD which confirmed their nano dimensions.

Li et al [50] synthesized nano ZnO using microemulsion and hydrothermal method in the presence of PEG400 as a passivant and reported the variety of morphologies and sizes of nanostructures. Separate microemulsions (ME1 and ME2) in the presence of surfactant polyoxyethylene tert-octylphenyl ether were prepared having precursors $Zn(NO_3)_2$, PEG400 and NaOH. These microemsulison were mixed and then transferred to autoclave for the hydrothermal process at 140°C. Characterization of the resultant powder material was done by using FTIR, UV-Vis, XRD, TEM and TG-DTA analysis. XRD investigations confirmed the formation of hexagonal wurtzite structure of ZnO nanocrystals. Variation in PEG400 concentration influences the morphologies needle-like, columnar, and spherical ZnO samples were obtained. TGA analysis and TEM images indicates that the passivant PEG400 and microemulsion interface synergistically influences the morphologies of ZnO nanomaterial. Bandgaps of various nanomaterial samples were estimated by using UV-Vis absorption technique. Proposed mechanism of the synthesis of nano ZnO with variety of morphologies in the presence of PEG400 is shown in Figure 1.12.

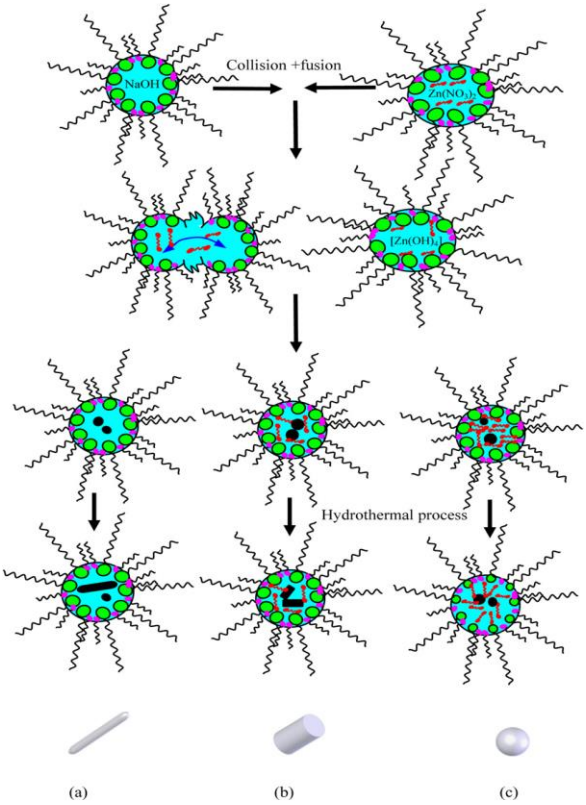

Figure 1.12. *A schematic diagram for synthesis of crystalline ZnO particles in microemulsions and their morphologies at varying PEG400 concentrations: (a) 0.0%, (b) 12.5% or 25.0%, (c) 50.0%. Surfactant molecule:* 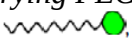 *co-surfactant molecule:* 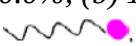 *PEG400 molecule:*  [50]

1.4.4. Green plant-based routes

Various techniques are established and reported to synthesize nanoparticles such as vaporization technique, ball milling, co-precipitation, sol-gel, sputtering etc. In last decade, immense interest has been demonstrated by researchers to synthesize nanoparticles of metals and their oxides using green routes along with evolving eco-friendly biological methodologies. These evolutionary green techniques nowadays have become a vital branch of nanoscience and technology while establishing the benefits and applications [51], [52]. These green methodologies involve the natural extracts of plant, fruits, byproducts, fungi, vegetables, microbes etc. as an important starting materials to synthesize metal and metal oxide nanoparticles in eco-friendly ways. These methodologies have various advantages as clean technology involving easy process, low energy, cost effectiveness etc.

Sivaraj et al [53] using aloe leaf broth synthesized the nanoparticles of ZnO. Synthesis process involve the zinc nitrate as precursor and its complete dissolution into the aloe extract and subjecting the mixture to vigorous stirring at 150°C for about 6h. Resultant mixture was cooled to RT while allowing for the settling of precipitates, decanted supernatant liquid, and centrifuged twice at more than 3000 rpm for about 15 min to obtain the pale yellow precipitates which were washed thoroughly with water and subjected to dry for around 8h at 80°C to ensure the conversion of intermediate hydroxides if any to ZnO. The particles of 40 nm Size of ZnO were obtained by this green synthesis method. The uniform colloidal suspension of nanoparticles was prepared in distilled water by sonication. These green synthesized nanoparticles of ZnO were studied for their antimicrobial efficacy against fungal and bacterial pathogens. The results reflect their promising biocidal efficacy against variety of pathogens in comparison to ZnO nanoparticle of chemical route.

Buazar et al [54] using microalgae Chlorella extract synthesized nanoparticle of ZnO (ZnO NPs) with high purity. Zinc nitrate as source of zinc and Microallgae chlorella extracts as reducing agent were used as starting materials to synthesize the desired nanoparticles of ZnO at ambient temperature.

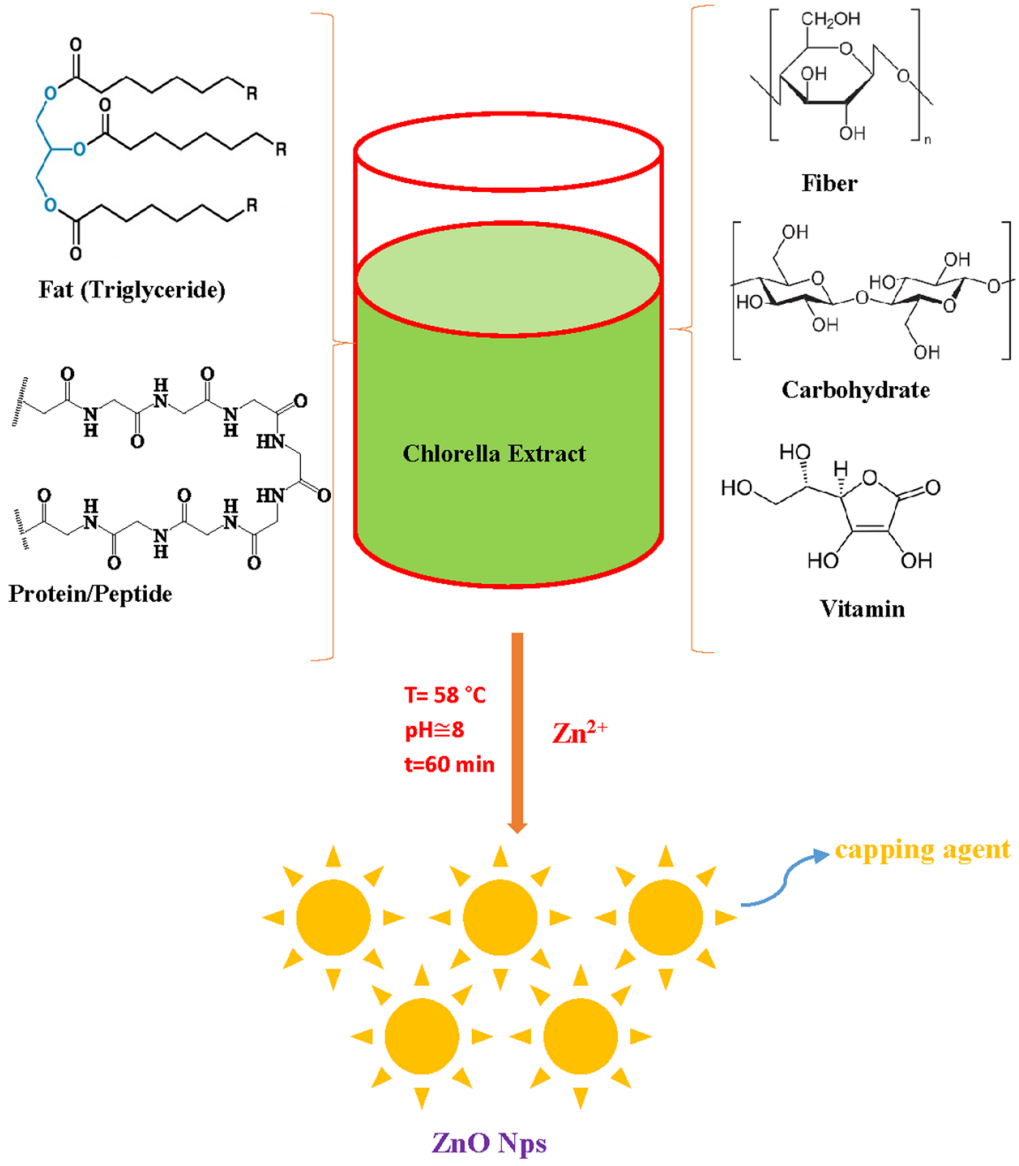

Figure 1.13. *A schematic presentation of biosynthesis of zinc oxide nanoparticles while utilizing chlorella (algae) extract as reducing and capping agent* [54]

Figure 1.13 is the proposed mechanism of ZnO NPs indicating the Chlorella extract also playing the role of stabilizing layer in addition to reducing agent action.

SEM, UV-Vis spectra clearly reflect the formation of nanosize ZnO particles and XRD confirms their hexagonal structure. These nanoparticles were studied for their photocatalytic activity and established the degradation of hazardous pollutant Dibenzothiophene (DBT) using Gas chromatography and UV-Vis techniques. Also, demonstrated that these nanoparticles have reusability up to five cycle in degrading the DBT.

1.5. Other techniques and methodologies reported in literature

Table 1.5. Summary of various methods and studies of synthesizing Nano ZnO and doped system.

Method	Starting material	Solvent	Other Reagents	Temperature	Morphology	Properties studied	Characterization Techniques	Ref.	Year
Thermal evaporation	Zn Powder	Nil	Nil	850-950^{o}C	ZnO Nanowires	Photoluminescence (PL)	XRD,SEM,TEM, HR-TEM,PL	[55]	2003
Sol-gel	$Zn(OAC)_2.2H_2O$	Ethanol (C_2H_5OH)	$Al(NO_3)_2.9H_2O$,Lactic acid,aetyl acetone, Diethanolamine (DEA)	75^{o}C	Film of spherical particles on glass substrate	Nil	XRD, EDX, AFM,FT-IR	[56]	2002
Solvothermal	Zn powder	Toluene	Trimethylamine N-oxide (Me_3NO), Ethylendiamine (EDA) tetarmethylenediamine (TEDA)	180^{o}C	Rod-like, particle like	Nil	XRD, TEM	[57]	2003
Complex formation/decomposition	$Zn(OAC)_2.2H_2O$	H_2O	Beta-cyclodextrin	RT/500^{o}C	Spherical particle	Nil	TGA-DTA, XRD, TEM, AFM	[58]	2003
Precipitation/Calcination	$ZnSO_4.7H_2O$	H_2O	NaOH, NH_4HCO_3	RT/80^{o}C/320-550^{o}C	Particle	Photocatalysis (degradation of phenol)	XRD,TEM, Surface area, surface voltage spectroscopy, XPS, EPR	[59]	2001
Solid-vapor deposition	ZnO powder	Nil	Nil	860^{o}C	Nanobelts	PL	SEM, TEM, HR-TEM	[60]	2004

Hydrolysis	$Zn(OAC)_2.2H_2O$	Isopropyl Alcohol (IPA)	NaOH, Polyvinyl pyrolidone (PVP)	0^oC/RT	Nanoparticle, Nanofibre	PL	TEM, HR-TEM, XRD, EXFAS, UV-Vis, FT-IR	[61]	2000
Sol-gel	$Zn(OAC)_2.2H_2O$	H_2O	H_2SO_4:H_2O, Na_2S, $Mn(OAC)_2.4H_2O$, NaOH,	RT	ZnO:Mn spherical nanoparticle on Si-wafer	PL	Ellipsometry, AFM, XPS, UV-Vis	[62]	2000
Electrophoresis deposition (EPD)	ZnO powder, $Mg(NO_3).6H_2O$	$O(CH2CH_2OH)_2$	Nil	RT/450^oC	ZnO:Mg spherical particle	PL	SEM, XRD	[63]	2001
Sol-gel	$Zn(OAC)_2.2H_2O$	Diethylene glycol (DEG),	Ethylenediamine tetraethyl acetate (EDTA)	RT	Spherical particle	PL	TEM, XRD, UV-Vis	[64]	2005
Solid-state reaction	$Zn(OAC)_2.2H_2O$	Nil	Triethanolamine (TEA), NaOH	RT	Nanorod	Nil	XRD, TEM	[65]	2003
Sol-gel	$Zn(OAC)_2.2H_2O$, $Zn_4O(OAC)_6$	Ethanol	$LiOH.H_2O$, Succinic acid, acetic acid	80^oC	Nanoparticle	Nil	XRD, EXAFS, TGA-DTA	[36]	2003
Microemulsion/annealing	$Zn(NO_3)$	Iso-Octane	Oxalic acid, sodium di-2-ethylhexylsulfosuccinate (AOT)	RT/Annealing	Nanoparticle	Electrical property	TEM-XRD	[66]	1997
Seeding/Annealing	$Zn(OAC)_2.2H_2O$	IPA	TEA	85^oC /RT/150^oC	ZnO nanorods and dumb-bell on cotton fabric	UV-protection	SEM, EDX, XRD, UV-protection factor (UPF)	[67]	2004
Hydrolysis	$Zn(OAC)_2.2H_2O$	IPA	NaOH	RT	Nanoparticles	Nil	UV-Vis	[68]	2005
Thermal evaporation	ZnO powder	Nil	Nil	1350^oC	ZnO nanobelts	PL	HR-TEM, TEM, EDS, PL	[69]	2004
Microemulsion/annealing	$Zn(NO_3).6H_2O$	H_2O, Cyclohexane	Polyethylene glycol mono-4-nonylphenylether	600-800^oC	Spherical particles	PL	SEM, XRD, PL	[70]	2005

			and hexamethylene diisocyanate, NaOH						
Hydrolysis	$Zn(OAC)_2.2H_2O$	Ethanol	$LiOH.H_2O$, Hexane	$70^oC/0^oC$	Spherical particles	PL	SEM, XRD, UV-Vis, PL	[71]	2005
Microemulsion/annealing	$ZnCL_2$, $MnCl_2$, $EuCl_3$	H_2O, Octane	Cetyltrimethylammoniumbromide (CTAB), NH_4OH, Butanol	RT/220-350^{o}C	ZnO:Mn, ZnO:Eu particles	PL	PL	[72]	2002,
Microemulsion/annealing	$Zn(OAC)_2.2H_2O$	Ethanol, Xylene	Dodecyl benzene sulfonic acid sodium salt (DBS), Hydrazine monohydrate	$140^oC/70^oC$	ZnO nanorods	PL	SEM, XRD, PL	[73]	2002
Hydrothermal	$Zn(NO_3).6H_2O$	H_2O	KOH	400 ^{o}C	ZnO spherical nanoparticles and nanorods	Nil	XRD, TEM	[74]	2004
Complex formation/decomposition	$Zn(OAC)_2.2H_2O$	H_2O, Heptane, Ethanol	NaOH, NH_4OH	180 ^{o}C	Flower like, snow flake, prism like, prickly sphere like, rod like morphologies	PL	XRD, SEM, PL	[75]	2002
Thermal evaporation	Zn Powder	Nil	$Ar:O_2$ (10:1)	500 ^{o}C	ZnO nanoshells	PL	SEM, TEM, HR-TEM, Selected area electron diffraction (SAED), PL, XRD	[76]	2005
Hydrolysis	$Zn(OAC)_2.2H_2O$, $Co(OAC)_2.4H_2O$, $Ni(ClO_4).6H_2O$	Dimethyl sulfoxide (DMSO)	TMAH, TOPO	180 ^{o}C	ZnO:Co, ZnO:Ni	Magnetism	UV-Vis, XRD, TEM, HR-TEM, SEM	[77]	2003

					spherical nanoparticles				
Mechnochemical process	$ZnCl_2$	Nil	Oxalic acid	450°C	ZnO nanoparticles	Nil	XRD, Raman Spectra, SEM	[78]	2011
Precipitation process	$ZnNO_3$	Demineralized water, Ethanol	NaOH, Starch	100°C	ZnO nanoparticles	Dielectric constant, conductivity	XRD, TEM, FT-IR	[79]	2013
Precipitation process	$ZnSO_4$	Ethanol	NH_4CO_3	300-500°C	ZnO nanoparticles	Surface area	XRD, TEM, BET	[80]	2010
Sol-gel	$Zn(OAC)_2.2H_2O$	Dichloro methane	Oxalic acid.$2H_2O$	Reaction at room temp. followed by heating at 500°C	Nanocrystalline ZnO	Nil	XRD, SEM, FT-IR, TG, BET	[81]	2009
Sol-gel	$Zn(OAC)_2.2H_2O$	Ethanol	Oxalic acid.$2H_2O$	Reaction at 50°C followed by calcination at 650°C	Crystalline Nano ZnO	Photocatalytic activity	SEM, XRD	[82]	2013
Solvothermal-Microwave technique	Zinc acetylacetonate monohydrate	methoxy ethanol, ethoxyethanol, and n-butoxyethanol		Teflon vessel, heating in microwave (800W, 4 min)	Nano sized ZnO	Nil	SEM, XRD, TEM, TG, IR,	[83]	2010
Emulsion	$Zn(OAC)_2.2H_2O$	Cyclohexane	Non-ionic surfactant, NaOH and KOH	Reaction at ambient temperature followed by drying 24h at 120°C	Hexagonal wurtzite structure solid, ellipsoid, rods, flakes	Photocatalysis	XRD, SEM, FT-IR, Thermal analysis	[84]	2012

Green Synthesis	$ZnNO_3.6H_2O$	Deionized water	Moringa oleifera leaves	Reaction at ambient temperature followed by heating at 500°C for 1h	Nano ZnO	Electrochemical properties	TGA/DSC, XRD, HRTEM, SEAD, FT-IR, UV-vis	[85]	2017
co-precipitation method	$ZnNO_3.6H_2O$	double distilled water	NaOH	Reaction at ambient temperature for 4h	ZnO nanoparticles	Supercapacitor electrode application	XRD, SEM, FTIR, Impedance spectroscopy, Bode plots, Cyclic voltammetry	[86]	2018
Green Synthesis	$ZnNO_3$	Analytical grade water	leaves from the *Solanum torvum L*	Reaction at 60°C for 24h	Nanoparticles	Subchronic toxicity	XRD, UV-vis, DLS, Zeta potential, SEM	[87]	2019
Ecofriendly Routes	$Zn(NO_3)_2 \cdot 6H_2O$	Distilled water	Aloe vera gel broth extracts and Cassava starch	Reaction at RT followed by calcination at 750°C	Nanoparticles	Adsorbent for Copper Removal From Waste water	XRD, SEM, Raman spectroscopy, Zeta potential, XPS, UV Vis	[88]	2020
Hydrothermally Synthesized	$ZnCl_2$, $CoCl_2 \cdot 6H_2O$	Distilled water	KOH	Reaction at RT followed by heating at 120°C for 23 h	Co-Doped ZnO Cylindrical Microcrystals	Enhanced Optical and Antibacterial Activity	FE-SEM, XRD, XPS, Raman spectroscopy, UV-vis, PL spectra,	[89]	2021

1.6. Personal Care Products and Industry an overview:

Cosmetic and personal care product formulation is an old art. Historically, these items comprised of crushed minerals found in oil or fat mixtures. Originally, men wore colored cosmetics to enhance their appearance during combat, to perform tribal rites, and to distinguish native groups or tribes. Women first used cosmetics in Egyptian civilization. Color items were utilized to draw attention to face characteristics, animal and vegetable extracts were used to perfume the clothes and hair, and greases and oils were applied to soothe the skin [90]. Skin care has remained mostly unchanged throughout the years, with the use of essential oils or glycerin and plant extract concoctions.

The personal care sector has grown tremendously in past decades. Increased understanding of physical care and personal hygiene goods, the development of new technologies to fuel the industry, and a rise in per capita disposable income are among the primary factors contributing to the industry's expansion. Soaps bar, shampoos, toothpastes, and shower gels are examples of personal care items that should be rinsed off soon after use. However, some personal care products, such as sanitizers, sunscreen lotion, and so on, are leave-on items. Cosmetics are typically leave-on items that remain on the skin for several hours, such as body and face creams, insect repellant, cosmetics, fragrances, and antiperspirants (Table 1.6).

Table 1.6. List of different personal care and cosmetic product categories

Personal Care Products	Hair Care Products	Shampoo
		Conditioners
		Hair Oil
		Hair Coloring Products
	Skin Care Products	Facial Care Products
		Body Care Products
		Lip Care Products
		Hand Care Products
	Bath And Shower	Shower Gels
		Bar Soaps
		Toothpaste
		Mouthwashes and Rinses
		Deodorants and Antiperspirants
Colour Cosmetics Products	Facial Cosmetics	
	Eye Cosmetics Products	
	Lip and Nail Makeup Products	

As per Technavio's recent market data analyses, the personal care industry is expected to increase by USD 148.89 billion between 2020 and 2025, at a rate of 5.68% (Figure 1.14) [91]. Technavio's studies give a deep examination through the compilation and summarization of data from different sources, with an emphasis on identifying prominent industry players. This study provides an up-to-date overview of the current market landscape, the most recent trends and drivers, as well as the general industry environment.

Figure 1.14. *Global personal care market 2021- 2025* [91]

Some prominent players in the global beauty and personal care products market include: Unilever, The Estée Lauder Companies Inc., Shiseido Co., Ltd., Revlon, Procter & Gamble L'Oréal S.A

Green personal care ranges are getting increasingly popular among consumers and manufacturers. This is seen in their use of a wide range of natural personal care raw materials and products as seen in Figure 1.15 which is reinforced by the negative impact of various surfactants on customers with damaged, sensitive, or delicate skin. Harsh surfactants and chemicals have an especially potent cleansing efficiency, however they can potentially harm the delicate skin's natural protective layer, triggering tightening, dryness, barrier damage, discomfort, and even stinging [92]. The advantages of "green" personal care products go further than aesthetics; expanding research demonstrates the toxicity of traditional skincare products [93]. This makes skin more susceptible to external contaminants and sometimes causes dry and scaly patches. Furthermore, as consumer

interest in sustainability grows, many personal care producers are looking for natural and ecologically viable surfactants and active additives for their formulations. A product can be called "green" if it incorporates active compounds obtained from plants, such as herbs and flowers, rather than comparable active chemicals artificially synthesized in the factory. It is preferable if it is developed in an environmentally friendly manner using production techniques that recognize the value of the environment.

Figure 1.15. *Some of the leading green personal care products in the market*

Table 1.7. Plant-based Skincare Products Market Outlook [94]

Base Year Value (2020A)	US$ 640 Million
Projected Year Value (2031F)	US$ 1.4 Billion
Value CAGR (2021-2031)	7.5%
Collective Value Share (U.S., U.K., Germany): Top 3 Countries	54.7%

Growth of plant-based skincare products is anticipated to reach $683.4 million in 2021 (Table 1.7) [94]. As per Fact.MR, the global market size of plant-based personal care products is predicted to more than double by 2031, expanding at a compound annual growth rate (CAGR) of 7.5% throughout the same time. As a result, many researchers are currently concentrating on investigating the various qualities of natural extracts that may be beneficial for personal care products.

1.6.1. Soap products

The Hittites of Asia Minor invented soap and body washing around four thousand years ago, when they cleansed their palms with ash from the soap nut (Saponaria officinalis) floating in water [95]. The Phoenicians created the initial modern soap formulation in 600 B.C. by saponifying goat fat, water, and potassium carbonate-rich ash into a hard, waxy substance [96]. Utilizing soap to wash the skin was not usually thought to be healthy. In the Middle Ages, Churches prohibited the use of soap because it considered that revealing the skin, even to take showers, was sinful. When the concept of microbes infected illness became popular, the consumption of soap skyrocketed. Soap is now a medically recognized element of the everyday hygiene practice.

The molecular association is significant not just for explaining the phase behavior of soaps and surfactants, but also for determining the product qualities. The diverse packing orientations in solid soaps have resulted in the production of distinct solid phases, whereas in liquid phases, it is vital to understand these relationships in order to manufacture products in the form of isotropic micelle solutions (liquid soap, shampoo, shower gel etc). At greater concentrations, the creation of hexagonal and lamellar liquid crystalline phases allows for the development of high viscosity products such as gels or flowable viscous liquids [97].

1.6.2. Basic soap chemistry

The basic principles of soap composition apply to all varieties of bar soap. The "saponification" technique entails combining triglyceride oils found in nature such as tallow (animal fat), coconut oil, palm oil etc. with sodium hydroxide and heating it. Soaps are salts of saturated and unsaturated fatty acids having C10- C18 carbon chains [98], [99].

The saponification value is the amount of potassium hydroxide milligrams necessary to saponify one gram of neutral oil [100]. The acid value is the amount of milligrams of potassium hydroxide required to neutralize one gram of fatty acid [101]. These two characteristics are critical in determining the amount of sodium hydroxide necessary for saponification or neutralization of oils and fatty acids.

To prepare soap from oil, the oil blend is reacted with strong sodium hydroxide to give soap, glycerin and high heat.

$$\text{Fats/Oils} + \text{Strong Base} \rightarrow \text{Soaps} + \text{Glycerin} + \text{Heat}$$

$$\begin{array}{lcl} R_1COOCH_2 & & R_1COONa \quad\quad CH_2OH \\ \quad | & & \quad\quad\quad\quad\quad\quad | \\ R_2COOCH & + \; 3\,NaOH \rightarrow & R_2COONa \quad + \quad CHOH \quad + \quad Heat \\ \quad | & & \quad\quad\quad\quad\quad\quad | \\ R_3COOCH_2 & & R_3COONa \quad\quad CH_2OH \end{array}$$

Splitting method involves first splitting of triglyceride oil into fatty acid and glycerin using high temperature and high pressure. The fatty acid and glycerin can be easily separated in this method. The separated fatty acid is further distilled and reacted with strong base such as sodium hydroxide to prepare soap.

Fats/Oils + Water → Fatty Acids + Glycerin

$$\begin{array}{lcl} R_1COOCH_2 & & R_1COOH \quad\quad CH_2OH \\ \quad | & & \quad\quad\quad\quad\quad\quad | \\ R_2COOCH & + \; 3\,H_2O \rightarrow & R_2COOH \quad + \quad CH_2OH \\ \quad | & & \quad\quad\quad\quad\quad\quad | \\ R_3COOCH_2 & & R_3COOH \quad\quad CH_2OH \end{array}$$

Distillation of fatty acids

Fatty Acids + Strong Base → Soaps + Water

$$\begin{array}{lcl} R_1COOH & & R_1COONa \\ R_2COOH & + \; 3\,NaOH \rightarrow & R_2COONa \quad + \quad Water \\ R_3COOH & & R_3COONa \end{array}$$

The alkyl chains R on the fat/oil triglyceride molecules possess both saturated and unsaturated fatty acid types of carbon atoms chain.

$$\begin{array}{l} CH_2 - (CH_2)_{14} - COOH \\ \quad | \\ CH_3 - (CH_2)_7 - CH = CH - (CH_2)_7 - COOH \\ \quad | \\ CH_2 - (CH_2)_4 - CH = CH - CH_2 - CH = CH - (CH_2)_7 - COOH \end{array}$$

The above triglyceride has saturated fatty acid chains palmitic acid with C16 chain and two unsaturated fatty acid chain with oleic acid C18:1 and linoleic acid C18:2. The combinations of the saturated and unsaturated fatty acid as well as their chain lengths give different chains of glycerin and highly influences the intrinsic properties such as melting point. Since glycerin is

costlier than soap, the majority of it is extracted to be used in relatively luxury cosmetic items. Additional glycerin is left in the soap to make it soften and creamy. For soap preparation the ratio of saturated and unsaturated fatty acids and their chain lengths are significant. Moreover, the presence of largely unstable double bonds makes *unsaturated fatty acids less stable than saturated fatty* acids. As a result, they are more prone to rancidity [102], [103]. The oxidation of lipids or fatty acid chains due to *water, atmospheric oxygen, sunlight, metal ions, or microorganisms* is referred to as rancidity. Rancidity is frequently characterized by an unpleasant odor hence it is crucial to add antioxidants [103].

For example, oxidation of different carbon atoms in methyl oleate a long chain fatty acids used in soap gives rise to different colour product.

$$CH_3 - (CH_2)_6 - CH_2 - CH = CH - CH_2 - (CH_2)_6 - COOR$$

If oxygen attacks the C8 carbon atom gives the following hydro peroxide,

$$CH_3 - (CH_2)_6 - CH_2 - CH = CH - \overset{8}{C}H - (CH_2)_6 - COOR$$
$$\Big|$$
$$O - OH$$

This then decomposes to form the following products,

(i) The unsaturated aldehyde 2-undecenal that is quite odorous

$$CH_3 - (CH_2)_6 - CH_2 - CH = CH - CH$$
$$\Big\|$$
$$O$$

(ii) Hydroxide and C7 hydrocarbon radicals

$$OH^{\bullet} \quad + \quad {}^{\bullet}(CH_2)_6 - COOR$$

If oxygen attacks the C9 carbon atom gives the following hydro peroxide,

$$CH_3 - (CH_2)_6 - CH_2 = CH - \overset{9}{C}H - CH - (CH_2)_6 - COOR$$
$$\Big|$$
$$O - OH$$

This then decomposes to form the following products,

(i) The unsaturated aldehyde 2-decenal that is highly odorous well known to attract insects

$$CH_3 - (CH_2)_6 - CH = CH - CH$$
$$\Big\|$$
$$O$$

(ii) Hydroxide and C8 hydrocarbon radicals

$$OH^{\bullet} \quad + \quad {}^{\bullet}CH_2 - (CH_2)_6 - COOR$$

Oxidation of C10 carbon atom gives –Nonanal with fatty/green odor and that of C11 gives –octanol with fatty green soapy odor.

Most soap bar are made using a mixture of different oils to achieve required characteristics. These oils can be divided into two types, nut oil and non-nut oils. Nut oils are oils derived from coconut and palm kernels while non-nut oils are obtained from animal fat/tallows or palm trees [104]. Non-nut oils are long chain saturated fatty acids such as palmitic and stearic acids are insoluble in normal water temperatures which add to hardness that increases lather stability and makes soap solid. Nut oil are short chain fatty acids such as lauric acid that gives soap solubility and high lather. An optimized mixture of both is required to prepare the perfect soap bar [104].

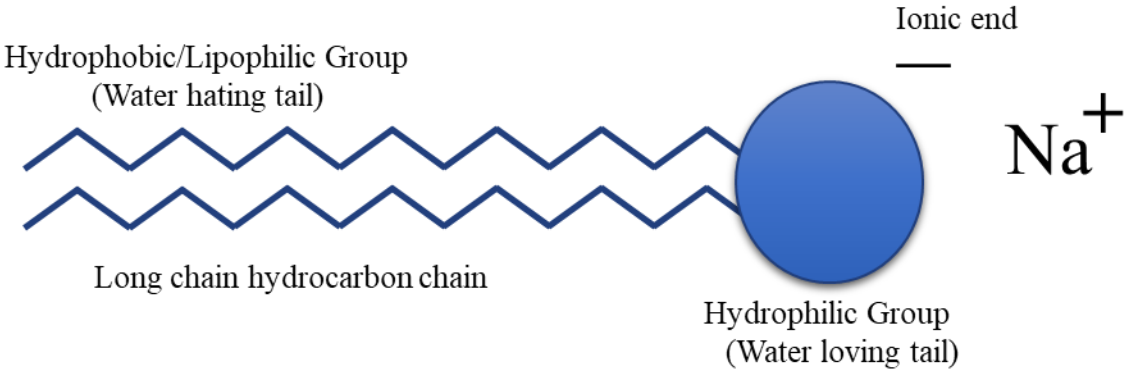

Figure 1.16. *Molecular structure of soap*

The molecular structure of soap described in Figure 1.16 contains surfactants molecules with a carboxylate group that is the hydrophilic head and aliphatic chain that is the hydrophobic chain. This dual nature gives soap the power to dissolve in both aqueous and organic phase as well as form structures in air-liquid interface such as foam. The soap structure consists of packed bilayers of soap molecules, arranged head to head and tail to tail. In presence of water, this forms a hydrated crystal structure consisting of water hydration in between the packed carboxylate heads in the bilayer structure. Depending on the oil/fat used the aliphatic chain lengths can vary from C8 to C22 as well as unsaturation including oleic (C18:1) and linoleic (C18:2) chains [97], [104]. The completing step of the commercial soap production process comprises the addition of compounds such as colors, preservatives, and scent to the soap, which is subsequently formed into bars for selling.

1.6.3. Manufacturing of soap

For the creation of regular bar soap finishing comprises of the following processing processes.

1. Mixing the main dry soap noodles with additional ingredients using double-arm sigma mixers.

2. Refining and extruding the finished product into compact slug/billets. The process of combining of soap and other additives through the simultaneous presence of pressure and shear is known as refining. For refining, plodders or plodders in conjunction with a roll mill are employed.

3. Cutting the extruded slugs into individual lengths. Soap is produced as a single slug (billet) from the duplex vacuum plodder in a form defined by an extrusion die set.

4. Stamping into a bar and packaging the finished stamped bars. To stamp all unique shaped items, soap stamping machines only utilize dies and related counter-dies

The soap manufacturing process is represented in Figure 1.17 below:

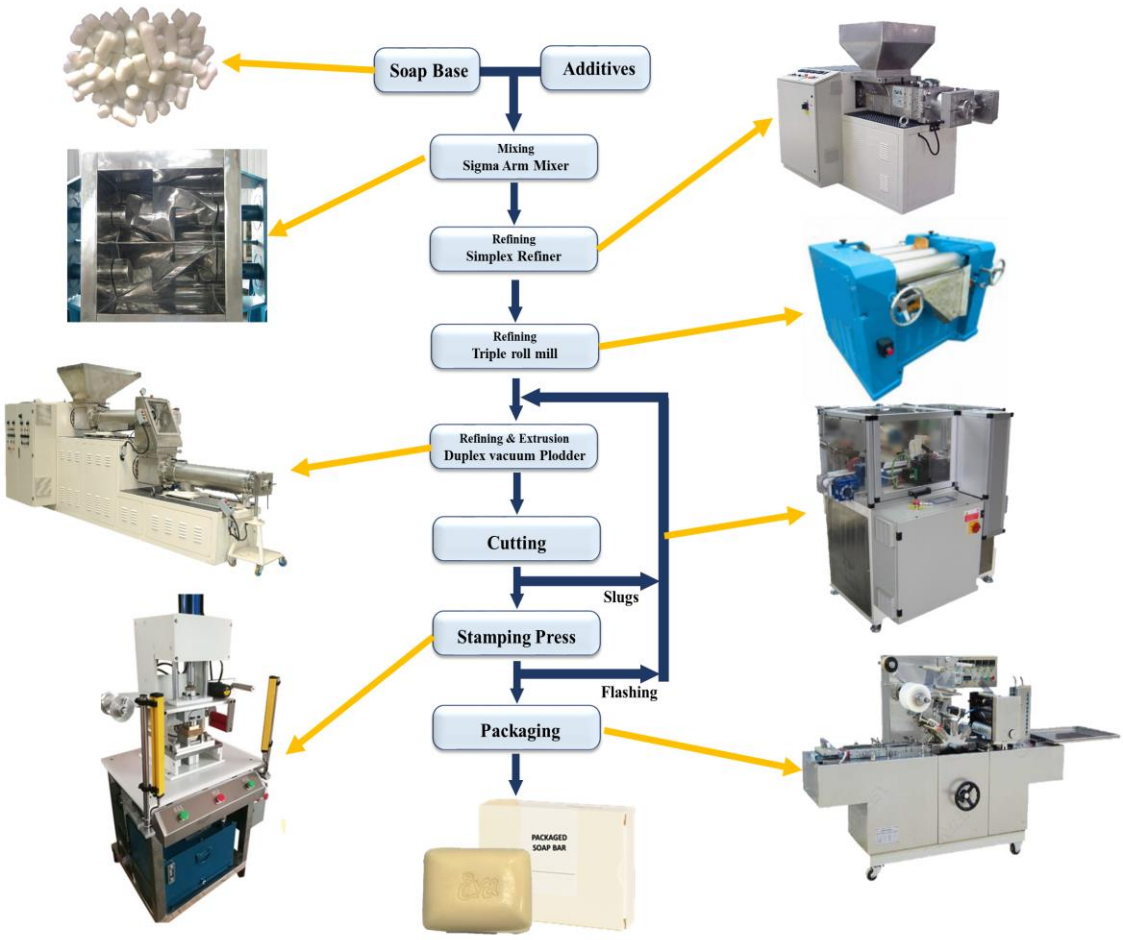

Figure 1.17. *Bar soap finishing process flow chart*

1.6.4. Liquid personal care products

Personal care products are intended to provide a practical advantage while also improving consumers' mental health through increased physical appeal. Most cosmetic and personal care products are intended to clean hair, skin, and so forth while also imparting a nice fragrance, making the skin feel silky, providing moisturizing properties, protecting against sun exposure etc. Usually personal care products are complicated systems comprising emulsions, moisturizers, lotions, etc. All of these intricate processes are comprised of various ingredients such as oil, water, surfactants, coloring additives, perfumes, stabilizers, nutrients, and etc. [105].

Personal care products are intended to provide a practical advantage while also improving consumers' mental health through increased physical appeal. Most cosmetic and personal care products are intended to clean hair, skin, and so forth while also imparting a nice fragrance, making the skin feel silky, providing moisturizing properties, protecting against sun exposure etc. Usually personal care products are complicated systems comprising emulsions, moisturizers, lotions, etc. All of these intricate processes are comprised of various ingredients such as oil, water, surfactants, coloring additives, perfumes, stabilizers, nutrients, and etc [105].

Liquid cleansers are typically made up of a significant amount of water and surfactants, moisturizing agents such as glycerin or polyols, and additives such as antibacterial and anti-dandruff actives, extracts, whitening agents, vitamins, preservatives, stabilizing agents, color, and perfumes (Figure 1.18).

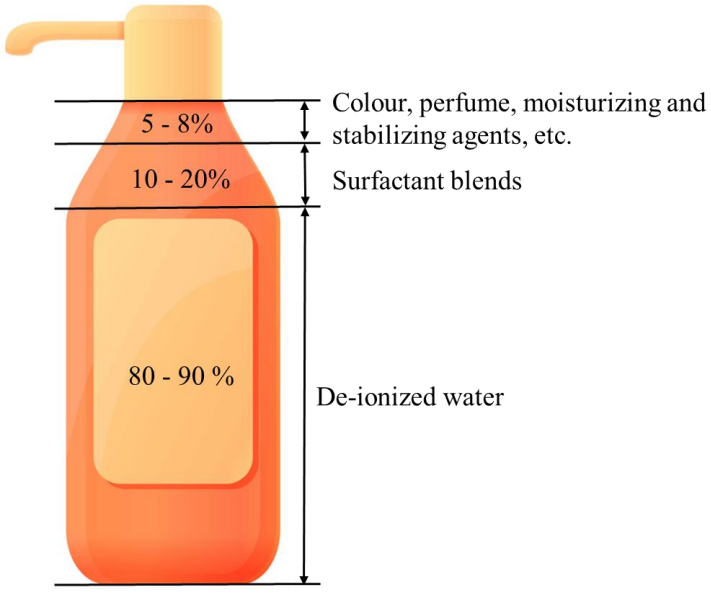

Figure 1.18. *Basic composition of a liquid cleanser*

Surfactants play a critical part in the development of these intricate formulations, ensuring long term storage stability and the desired feel on usage. In cosmetics and personal care applications different types of surfactants used are anionic, cationic, amphoteric, and nonionic surfactants. Surfactants are surface active agents that form highly ordered molecular aggregates termed micelles in a mixture (water or oil phase) and adhere to the interface of two immiscible fluids, therefore reducing interfacial tension [106]. A surfactant possesses molecular structure with two specialized functional groups (hydrophilic and lipophilic) with differing affinities within a single molecule to exhibit these two specific characteristics. Surfactant molecules often have a hydrocarbon chain with 8-22 carbon atoms known as a hydrophobic group, which has little affinity for water, or lipophilic groups (lipid loving) in lipid systems. Surfactant molecules also include a chemical group known as the hydrophilic group, which has an attraction to water. These groups can change the interaction between different stages. Their interface effects are caused by their capacity to position themselves in line with the polarities of the two different phases. As a result, the polar hydrophilic half of the functional group can face the more polar phase of the interface, whereas the non-polar lipophilic/hydrophobic half can face the non-polar phase. A structure with two conflicting functions is referred to as an amphiphilic structure [106], [107].

Surfactants are classified into following four categories:

(i) Anionic surfactants

Surfactants with a negatively charged on the hydrophilic group, dissociates into anions in aqueous phase. Alkylbenzene sulfonates (cleaning agents), soaps (fatty acids), lauryl sulfate (foaming agent), and others are among them. Anionic surfactants account for almost half of global output. Table 1.8 lists the structures of the most prevalent anionic surfactants.

Sodium lauryl ether sulfate/sodium laureth sulfate (SLES) is the principal anionic surfactant in the large percentage of cleansing products in the industry. The key markets for this commodity are India, Egypt, Malaysia, and China, which generate global supply to companies around the globe [108], [109]. SLES 70% (Sodium Lauryl Ether Sulphate) has good detergency, emulsifying, and foaming properties (Figure 1.19). SLES is less expensive than other sulphate or sulphate-free surfactants [110]. It is also beneficial in terms of hard water resistance and disinfection, stability, dispersion, flowability, solubilizing efficiency, and foaming. Good solubility, viscosity building, broad compatibility and high biodegradability with minimal skin and eye discomfort.

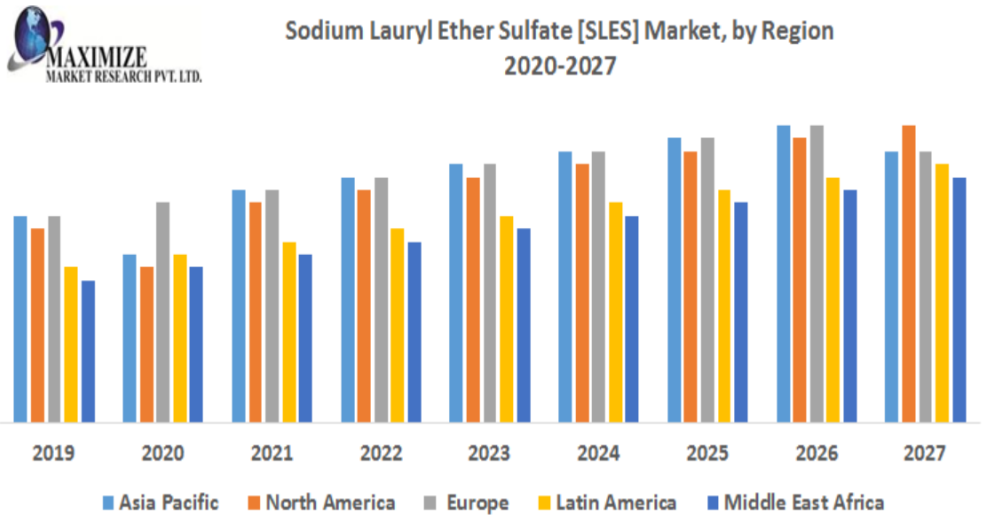

Figure 1.19. *SLES market by region 2020- 2027* [109]

Table 1.8. Common anionic surfactants are sulphonic acid and carboxylic acids derivatives

S.No	Common anionic surfactants	Structure
1.	Sodium Dodecyl Sulfate	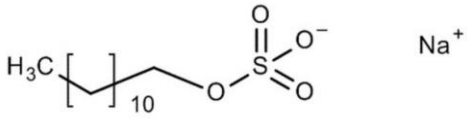
2.	Sodium Laureth Sulfate	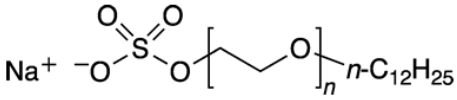
3.	Sodium lauryl sulfate	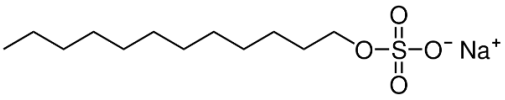
4.	Alpha-Olefin Sulfonates	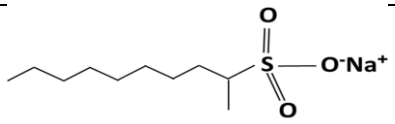

(ii) Cationic Surfactants

Cationic surfactants carry a positive charge and as a result can be used to neutralize the negative charges on hair that cause frizz to give a smoothing effect. This charge may be either permanent or only present in certain pH value ranges. Commonly used aliphatic quaternary ammonium compounds are cetrimonium bromide (CTAB) ($C_{16}H_{33}N(CH_3)_3$ Br), Cetyltrimethylammonium chloride (CTAC) ($C_{19}H_{42}ClN$), cetylpyridinium chloride (CPC) ($C_{21}H_{38}ClN$), benzethonium chloride (BZT) ($C_{27}H_{42}ClNO_2$), etc [111].

(iii) Zwitterionic surfactants

The charges on the hydrophilic head of such surfactants can alter as a result of pH. They have a positive charge at low pH and a negative charge at high pH, and they can neutralize to produce a neutralized ionic species [111]. These features are depicted below with an example of lauraminopropionic acid:

Low pH, the surfactant molecule is a cation

$$[R - NH_2 - CH_2 - CH_2 - COOH]^+ \quad X^-$$

Intermediate pH, the surfactant molecule is a zwitterion

$$[R - NH_2 - CH_2 - CH_2 - COOH]^{+\,-}$$

High pH, the surfactant molecule is a anion

$$[R - NH_2 - CH_2 - CH_2 - COOH]^- \quad C^+$$

R represents alkyl groups, X^- and C^+ are required counter ions.

(iv) Nonionic surfactants

Surfactants that do not dissociate into ions in aqueous solutions, and they are further divided depending on the type of their hydrophilic group [111]. Common hydrophilic groups of ionic surfactants are carboxylate (–COO^-), sulfate (–OSO_3^-), sulfonate (SO_3^-), carboxybetaine (–$NR_2CH_2COO^-$), sulfobetaine (–$N(CH_3)_2C_3H_6SO_3^-$), and quaternary ammonium (–R_4N^+).

Once those surfactants are introduced to a medium (water or oil), they self-assemble to produce micelles, which are highly ordered molecular groups. Micelle production or micellization is an essential characteristic because the presence of micelles in solution is required for a variety of vital interfacial phenomenon such as detergency and solubility [112]. The critical micelle concentration is the concentration of surfactant at which micellization occurs (CMC). The micellar structure is determined by the material's tail length (l), head group area (a), and molecular volume (v). According to Israelachvili *et al.*16, the surfactant aggregates can take on varied morphologies based on the value of the packing parameter p (= v/al) (Figure 1.20) [113].

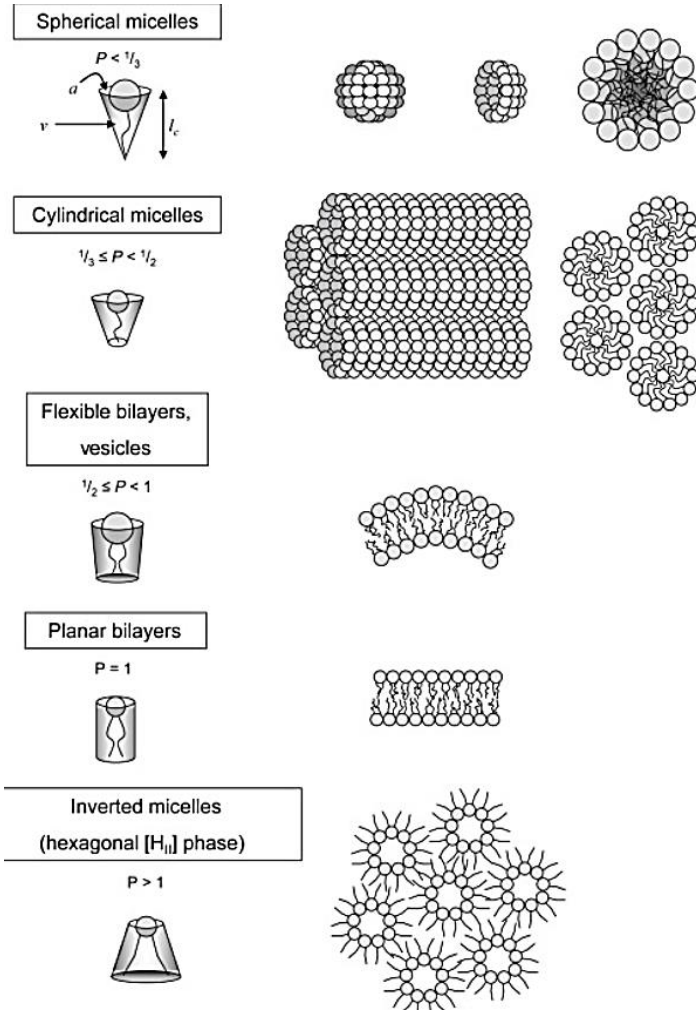

Figure 1.20*. Packing parameters of surfactant molecule and the different structure the form in solution* [112]

Micelles are spherical for 1/3 p 1/2 and ellipsoidal and cylidrical for 1/3 p 1/2. Surfactant aggregates tend to be bilayers when p > 1/2, resulting in the creation of vesicles in appropriate instances. It should be noted that altering the temperature of the mixture or adding salt to the micellar system can modify the functional head group area a, causing modifications in micellar shape. The introduction of inert salts to a solution of surfactant often reduces the CMC of ionic surfactants and hence increases micelle formation. This impact is more prominent in surfactants like SLES and less evident in nonionic surfactants. Salts tend to shield intra- and inter-micelle repulsive interactions, essentially making the surfactant more hydrophobic. As the hydrophobic interactions between the surfactants strengthen, they form bigger aggregates at lower concentrations, causing spherical [112]–[114].

1.6.5. Manufacturing of liquid products

Manufacturing of liquid cleansing products are done in few stages, as seen in Figure 1.21.

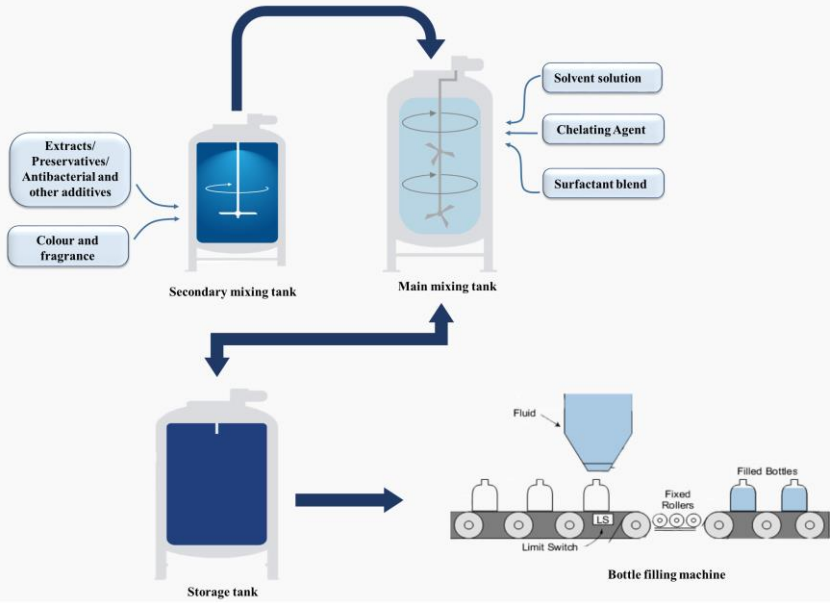

Figure 1.21. *Manufacturing of liquid cleansing products*

Mixing tanks are the primary piece of machinery used in the production of liquid cleansing solutions. It is primarily used for homogeneous mixing of various liquid items such as surfactants, extracts, medical medications, dairy, sugar, and other materials depending on the application. Bottle filling machines are devices used to fill fluids into bottles folowwed by capping and labelling.

1.6.6. Anti-bacterial personal care products

Figure 1.22. *Some of the leading antibacterial personal care products in the market*

Since the beginning the development of personal care products was rooted in the need to kill microbes that cause harmful diseases.The range of popular antibac prodcts shown in (Figure 1.22). The worldwide antibacterial products market was worth USD 27.04 billion in 2020, and it is predicted to increase at a CAGR of 2.3% between 2021 and 2028 [115]. Growing demands for antibacterial products as a consequence of growing consumer hygiene concerns are driving market expansion. Furthermore, the rising frequency of bacterial and viral infections such as COVID-19, ringworm, dermatitis, and measles has increased customer demands for such goods throughout the world. The COVID-19 outbreak has had an important part in growing market for these goods, since customer's preferences have switched toward antibacterial skin and personal care products, as seen by the rise of antibacterial products on the market (Figure 1.23). These incidents are predicted to increase the use of antibacterial products in the future years.

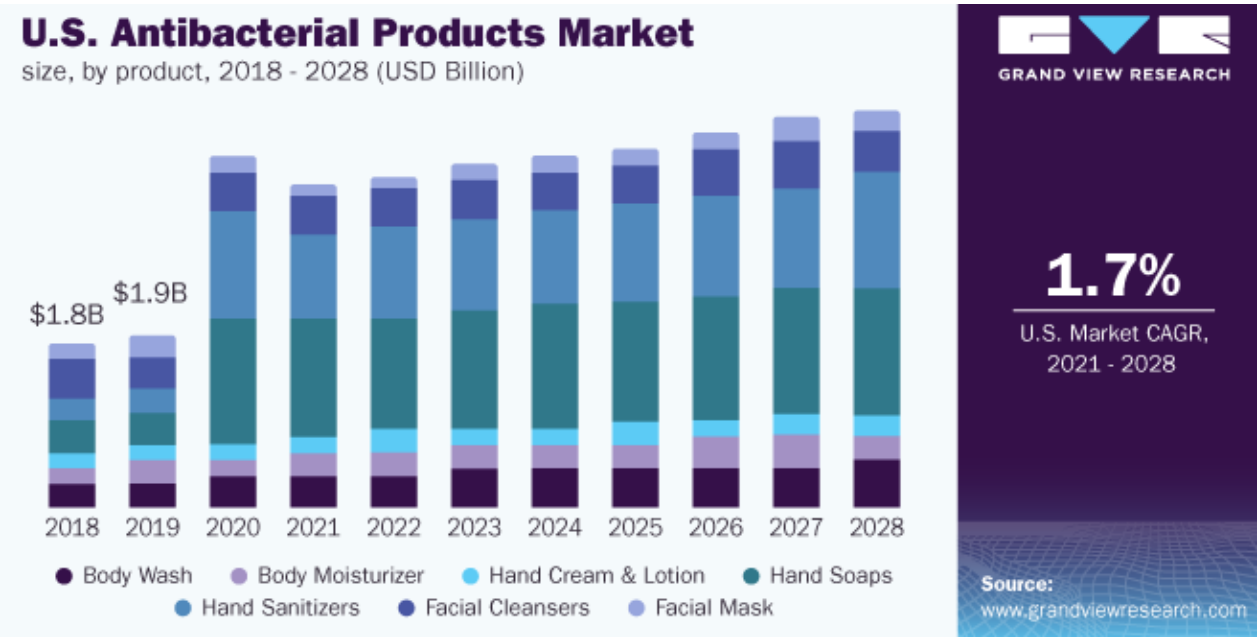

Figure 1.23. *United States antibacterial product market 2018-2028* [115]

Hand washes had the biggest market share of 35.0% in 2020 and is predicted to retain its lead throughout the forecast period [40]. The introduction of hand hygiene recommendations in the aftermath of the COVID-19 epidemic has resulted in an increase in demand for hand soap bars and liquids in 2020. This has led to large purchases of antibacterial items, providing the industry with tremendous development prospects.

The most common infections for children and adults worldwide are *Escherichia coli (E. Coli), Staphylococcus aureus (S. aureus), Pseudomonas aeruginosa (P. aeruginosa),* and *Enterococcus hirae (E. hirae). E. coli* is the most prevalent bacterium responsible for simple cystitis, as well as causes pneumonia, bacteremia, and gastrointestinal illnesses such as bacterial peritonitis [116] *S.aureus* is a prominent cause of bacteremia, blood infections such as bacterial endocarditis, osteoarticular infections, soft tissue infections, bronchitis and bronchiolitis, etc [117]. *P. aeruginosa* is a prominent source of hospital - acquired infections, including pneumonia, infection in immunosuppressed patients, and illness in people with structural lung disease such as cystic fibrosis [118], [119]. *E. hirae* infection is more likely to be found in animals however cases have been found to be causing endocarditis, liver failure, and renal dysfunction condition [120]. Despite the fact that *E. hirae* has been discovered to cause serious infections in people, limited instances have been recorded to date due to the difficulty in detecting the bacteria, as well as a lack of detailed studies on clinical features and therapies [121]. Most antibacterial agents are tested against *E. coli* and *S.aureus* using different standard methods such as Zone of inhibition (ZOI), Minimum inhibitory concentration (MIC), minimum bacterial concentration (MBC) or contact kill method EN 1276.

Triclosan, Triclocarban, trichlorocarbanilide and P-chloro-in-xylenol (PCMX/Chloroxylenol) are the commonly used anti-bacterial in medicated soaps such as Lifebuoy, protex, Dettol, safeguard, head & shoulder, activex etc, however many of these chemicals have been banned by authorities in recent years. Thus new technologies such as silver oxides and silver nanoparticles are being explored. Table 1.9 describes some renowned antibacterial soaps and handwash with active ingredients as per label disclosure in last decade:

Table 1.9. Antibacterial personal care products of different brands and their actives as per label

Ingredients	Structure	Application	Toxicity
Triclosan	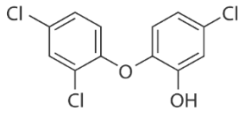	Antimicrobial/soaps, fragrances	Endocrine disruptor effects, reproduction, carcinogenic, resistant bacteria, bioaccumulation, aquatic toxicity [122]–[124]
Triclocarban	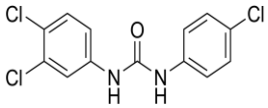	Antimicrobial, soaps, body washes, lotions, detergents, and wipes for its sanitizing properties.	Carcinogenic, endocrine disruptor, teratogenicity, bioaccumulation, weight loss, abortion [122]
Zinc Pyrithione	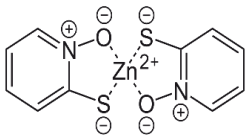	Antidandruff/ Antimicrobial, soap, shampoos	Fertility and reproduction toxicity, weight loss, abortion, Developmental Toxicity [125]

The industry is now shifting to alternate antibacterial agents such as silver oxide, thymol, terpinol, chloroxylenol (PCMX) or green natural based ingredients such as tea tree oil, flax seed oil etc Table 1.10.

Table 1.10. Alternate antibacterial agents in personal care products as per label

Ingredients	Structure	Properties
Thymol	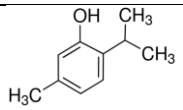	antiseptic, antibacterial , antioxidant, anti-inflammatory, local anaesthetic, antinociceptive, cicatrizing, , and antifungal
Terpinol	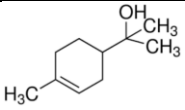	anti-microbial, antioxidant, anticancer, anticonvulsant, antiulcer, antihypertensive, anti-nociceptive compound
Chloroxylenol	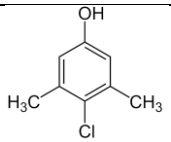	antiseptic disinfectant, to control bacteria, algae and fungi

1.7. Demerits in current system and motivation of work

Challenges in antibacterial agents and antibacterial resistance:

- Antibacterial agents that have been in market for many decades used in personal care products are becoming extremely inefficient and toxic. This is due to the increase of mutations and antibacterial resistance throughout the world, making illnesses and death more challenging to manage.

- Most frequently used antibacterial agents such as Triclosan, Triclocarban, phenolic compounds and their carcinogenic byproducts are known to cause cancer, reproductive toxicity, highly destructive to the environment [K. Z. Sanidad et al 2022, X. Wang et al 2015, L. M. Weatherly et al 2017]. The chemicals are banned by the FDA since 2016.

- Zinc pyrithione (ZPT) an antifungal agent with extensive use in anti-dandruff shampoos that has been banned in many countries as of 2022 despite years of commercial use [*www.cirs-group.com*]. Therefore, once common antibacterial agents are getting phased out from the personal care products in many countries. Therefore, industry viable efficacious and sustainable solutions are highly required.

- European authorities have recently (February 2022) withdrawn authorization of commonly used ingredient TiO_2 from application as additives and has given a grace period to phase out the ingredient and reformulate the products with other alternatives [https://www.fas.usda.gov/data/european-union-titanium-dioxide-banned-food-additive-eu].

- Few natural green based antibacterial agents and alternatives are being slowly introduced in the market however there is a dearth in green approach moringa based zinc oxide nanoparticles in personal care products and establishing efficacy

- New antibacterial agents are hence desperately required for personal care products, keeping researchers on their toes as they explore new and effective actives to fight disease-causing microbes like *Staphylococcus aureus (S. aureus), Escherichia coli (E. coli)* as well as recent world-wide pandemic Covid-19 causing respiratory syndrome. At the same time, selection of material which are allowed to be used as per regulations.

Key demerits associated with existing synthesis methodologies of zinc oxide nanomaterials are:

- Vapour, solid state, combustion, methods are either highly energy extensive or expensive

- hydrothermal method requiring increased pressure and sonoelectrodeposition methods requiring mechanical waves of ultrasound etc.

- used solvents are expensive, toxic if exposed to human skin and flammable which can be discarded into marine and wildlife posing irreparable damage to our ecosystems

- solvents or generated by-products during synthesis are either not permitted or affects stability of health and hygiene products for example in liquid products these unwanted by-products often affect the foaming, rheological parameters of the products, colours etc.

- Therefore, majority of these methods are not compatible and not preferred for personal care products, there is still a lot to unleash in ZnO fabrication methodologies as well as selection of appropriate precursors suitable for health and hygiene products.

- Another major challenge is oxidation of unsaturated long chain fatty acids of soap bars. Oxidation of soap bars cause photo-degradation under sunlight resulting into rancid and unpleasant yellow–brown colored product.

Inspired by the above-mentioned facts, the research work in thesis has been focused on fabricating nanomaterial suitable for health and hygiene products using appropriate synthesis methods.

1.8. Research Objectives of the Thesis

Fabrication of nano ZnO and doped system (Surfactant mediated and Green Approach):

- Basis extensive literature survey and in-depth understanding of personal care formulations. Select suitable, compatible matrix and dopant to fabricate nano ZnO and doped system for health and wellness applications.

- Establish the industry viable methodologies (Surfactant polyol mediated and Green approach) for the fabrication of nano ZnO and doped system while optimizing their physico-chemical parameters. Silver doped ZnO fabrication in surfactant polyol matrix to advance germicidal efficacy and suitable for health and hygiene applications

- Green synthesis of nano scale zinc oxide nanoparticles (GsZnO-Nps) using Moringa leaves extracts while investigating phytochemical of Moringa oleifera and establishing their antioxidant property. Establish the efficacy of GsZnO-Nps and the added benefits of moringa phytochemicals for anti-acne, anti-oxidant and anti-microbial efficacies

- Study and characterization of the as prepared samples for their structural and morphological analysis using techniques like Scanning Electron Microscopy (SEM), X-Ray Diffraction (XRD), UV-Visible spectroscopy and Fourier transform infrared Spectroscopy (FTIR).

Product applications:

- **Industrial application in products** by infusing nanoparticles in soap bars and liquid cleansing products for enhanced anti-oxidant and anti-microbial properties. Incorporation of zinc oxide nanomaterial can enhance different characteristic properties of soap bars and liquid cleansing products hence efforts were made to understand the influence of nanomaterials in these systems

- **Study of antibacterial efficacy** of prepared product samples using methods such as *zone of inhibition (ZOI), minimal inhibitory concentration (MIC),* and contact kill test (EN 1276). Antibacterial efficacy depends on particle size hence efforts were made to explore the effect of particle size by comparing synthesized nano zinc oxide with commercial AR grade zinc oxide samples.

References

[1] R. H. Baughman, A. A. Zakhidov, and W. A. de Heer, "Carbon Nanotubes--the Route Toward Applications," *Science (80-.).*, vol. 297, no. 5582, pp. 787–792, Aug. 2002, doi: 10.1126/science.1060928.

[2] D. L. Klein, R. Roth, A. K. L. Lim, A. P. Alivisatos, and P. L. McEuen, "A single-electron transistor made from a cadmium selenide nanocrystal," *Nature*, vol. 389, no. 6652, pp. 699–701, Oct. 1997, doi: 10.1038/39535.

[3] Z. W. Pan, Z. R. Dai, and Z. L. Wang, "Nanobelts of Semiconducting Oxides," *Science (80-.).*, vol. 291, no. 5510, pp. 1947–1949, Mar. 2001, doi: 10.1126/science.1058120.

[4] H. Yan, R. He, J. Johnson, M. Law, R. J. Saykally, and P. Yang, "Dendritic Nanowire Ultraviolet Laser Array," *J. Am. Chem. Soc.*, vol. 125, no. 16, pp. 4728–4729, Apr. 2003, doi: 10.1021/ja034327m.

[5] J. C. Johnson, H. Yan, P. Yang, and R. J. Saykally, "Optical Cavity Effects in ZnO Nanowire Lasers and Waveguides," *J. Phys. Chem. B*, vol. 107, no. 34, pp. 8816–8828, Aug. 2003, doi: 10.1021/jp034482n.

[6] D. Haranath, H. Chander, N. Bhalla, P. Sharma, and K. N. Sood, "Surface distribution studies and improved photoluminescence characteristics of silica coated ZnS:Mn nanophosphor layers," *Appl. Phys. Lett.*, vol. 86, no. 20, p. 201904, May 2005, doi: 10.1063/1.1929076.

[7] S. Talebian, T. Rodrigues, J. das Neves, B. Sarmento, R. Langer, and J. Conde, "Facts and Figures on Materials Science and Nanotechnology Progress and Investment," *ACS Nano*, vol. 15, no. 10, pp. 15940–15952, Oct. 2021, doi: 10.1021/acsnano.1c03992.

[8] C. B. Murray, D. J. Norris, and M. G. Bawendi, "Synthesis and characterization of nearly monodisperse CdE (E = sulfur, selenium, tellurium) semiconductor nanocrystallites," *J. Am. Chem. Soc.*, vol. 115, no. 19, pp. 8706–8715, Sep. 1993, doi: 10.1021/ja00072a025.

[9] D. Haranath, N. Bhalla, H. Chander, Rashmi, M. Kar, and R. Kishore, "Controlled growth of ZnS:Mn nanophosphor in porous silica matrix," *J. Appl. Phys.*, vol. 96, no. 11, pp. 6700–6705, Dec. 2004, doi: 10.1063/1.1806552.

[10] Z. Lin-Li, G. Chang-Xin, Z. Jun-Jing, and H. Jun-Tao, "Photoluminescence of Eu(III)-Doped ZnO Nanopowder and Energy Transfer from ZnO to Eu(III) Ions," *Chinese Phys. Lett.*, vol. 22, no. 5, pp. 1225–1227, May 2005, doi: 10.1088/0256-307X/22/5/056.

[11] R. N. Bhargava, D. Gallagher, X. Hong, and A. Nurmikko, "Optical properties of manganese-doped nanocrystals of ZnS," *Phys. Rev. Lett.*, vol. 72, no. 3, pp. 416–419, Jan. 1994, doi: 10.1103/PhysRevLett.72.416.

[12] M. Nirmal *et al.*, "Fluorescence intermittency in single cadmium selenide nanocrystals," *Nature*, vol. 383, no. 6603, pp. 802–804, Oct. 1996, doi: 10.1038/383802a0.

[13] D. Schaming and H. Remita, "Nanotechnology: from the ancient time to nowadays," *Found. Chem.*, vol. 17, no. 3, pp. 187–205, Oct. 2015, doi: 10.1007/s10698-015-9235-y.

[14] Z. I. Mahmoud Nasrollahzadeh, Mohammad Sajadi, Monireh Atarod, Mohadeseh Sajjadi, *An Introduction to Green Nanotechnology*. Elsevier, 2019.

[15] A. Khurana *et al.*, "Role of nanotechnology behind the success of mRNA vaccines for COVID-19," *Nano Today*, vol. 38, p. 101142, Jun. 2021, doi: 10.1016/j.nantod.2021.101142.

[16] S. M. Kapnick, "The Nanoparticle-Enabled Success of COVID-19 mRNA Vaccines and the Promise of Microneedle Platforms for Pandemic Vaccine Response," *DNA Cell Biol.*, vol. 41, no. 1, pp. 25–29, Jan. 2022, doi: 10.1089/dna.2021.0538.

[17] F. J. O. Charles P. Poole Jr., *Introduction to Nanotechnology*. 2003.

[18] C. Lang, D. Schüler, and D. Faivre, "Synthesis of Magnetite Nanoparticles for Bio- and Nanotechnology: Genetic Engineering and Biomimetics of Bacterial Magnetosomes," *Macromol. Biosci.*, vol. 7, no. 2, pp. 144–151, Feb. 2007, doi: 10.1002/mabi.200600235.

[19] Y. Jun, J. Seo, and J. Cheon, "Nanoscaling Laws of Magnetic Nanoparticles and Their Applicabilities in Biomedical Sciences," *Acc. Chem. Res.*, vol. 41, no. 2, pp. 179–189, Feb. 2008, doi: 10.1021/ar700121f.

[20] M. T. Klem, D. A. Resnick, K. Gilmore, M. Young, Y. U. Idzerda, and T. Douglas, "Synthetic Control over Magnetic Moment and Exchange Bias in All-Oxide Materials Encapsulated within a Spherical Protein Cage," *J. Am. Chem. Soc.*, vol. 129, no. 1, pp. 197–201, Jan. 2007, doi: 10.1021/ja0667561.

[21] M. S. Chavali and M. P. Nikolova, "Metal oxide nanoparticles and their applications in nanotechnology," *SN Appl. Sci.*, vol. 1, no. 6, p. 607, Jun. 2019, doi: 10.1007/s42452-019-0592-3.

[22] S. Moradi Dehaghi, B. Rahmanifar, A. M. Moradi, and P. A. Azar, "Removal of permethrin pesticide from water by chitosan–zinc oxide nanoparticles composite as an adsorbent," *J. Saudi Chem. Soc.*, vol. 18, no. 4, pp. 348–355, Sep. 2014, doi: 10.1016/j.jscs.2014.01.004.

[23] S. Raj, S. Jose, U. Sumod, and M. Sabitha, "Nanotechnology in cosmetics: Opportunities and challenges," *J. Pharm. Bioallied Sci.*, vol. 4, no. 3, p. 186, 2012, doi: 10.4103/0975-7406.99016.

[24] S. Kaul, N. Gulati, D. Verma, S. Mukherjee, and U. Nagaich, "Role of Nanotechnology in Cosmeceuticals: A Review of Recent Advances," *J. Pharm.*, vol. 2018, pp. 1–19, Mar. 2018, doi: 10.1155/2018/3420204.

[25] D.-H. Kim, J. Bae, J. H. Heo, C. H. Park, E. B. Kim, and J. H. Lee, "Nanoparticles as Next-Generation Tooth-Whitening Agents: Progress and Perspectives," *ACS Nano*, vol. 16, no. 7, pp. 10042–10065, Jul. 2022, doi: 10.1021/acsnano.2c01412.

[26] A. Weir, P. Westerhoff, L. Fabricius, K. Hristovski, and N. von Goetz, "Titanium Dioxide Nanoparticles in Food and Personal Care Products," *Environ. Sci. Technol.*, vol. 46, no. 4, pp. 2242–2250, Feb. 2012, doi: 10.1021/es204168d.

[27] V. Deshpande, "A Note on Ancient Zinc-Smelting in India and China," *Indian jounal Hist. Sci.*, vol. 31, no. 3, pp. 275–279, 1996.

[28] C. Jagadish and S. Pearton, Eds., *Zinc Oxide Bulk, Thin Films and Nanostructures Processing, Properties and Applications*. 2006.

[29] H. J. Yearian, "OCTOBER 1 , 1935 PHYSICAL REVIEW."

[30] M. von Ardenne, "Das Elektronen-Rastermikroskop. Praktische Ausfuhrung in Zeitschrift fur Technische," *Physik*, pp. 407–416, 1938.

[31] N. B. Er and S. E. Harrison, "PH YSI CAL REVI EWV Conductivity and Hall Effect of Zno at Low Temperatures*t," 1954.

[32] S. Sagadevan, K. P. Raj, F. A. Aziz, Z. Z. Chowdhury, M. R. Bin Johan, and J. Podder, "Structure, properties, photocatalytic and antibacterial activity and applications of zinc oxide nanoparticles-An overview," *Journal of Bionanoscience*, vol. 12, no. 4. American Scientific Publishers, pp. 457–468, Aug. 01, 2018, doi: 10.1166/jbns.2018.1557.

[33] G. F. Neumark, I. L. Kuskovksy, and H. X. Jiang, *Wide bandgap light emitting materials and devices*. .

[34] D. M. Bagnall *et al.*, "Optically pumped lasing of ZnO at room temperature," *Appl. Phys. Lett.*, vol. 70, no. 17, pp. 2230–2232, Apr. 1997, doi: 10.1063/1.118824.

[35] M. H. Huang *et al.*, "Room-Temperature Ultraviolet Nanowire Nanolasers." [Online]. Available: http://science.sciencemag.org/.

[36] M. S. Tokumoto, S. H. Pulcinelli, C. V. Santilli, and V. Briois, "Catalysis and temperature dependence on the formation of ZnO nanoparticles and of zinc acetate derivatives prepared by the sol-gel route," *J. Phys. Chem. B*, vol. 107, no. 2, pp. 568–574, Jan. 2003, doi: 10.1021/jp0217381.

[37] D. Li and H. Haneda, "Morphologies of zinc oxide particles and their effects on photocatalysis." [Online]. Available: www.elsevier.com/locate/chemosphere.

[38] "https://www.grandviewresearch.com/industry-analysis/zinc-oxide-market-report." .

[39] F. P. Gasparro, M. Mitchnick, and J. F. Nash3, "Invited Review A Review of Sunscreen

Safety and Efficacy," 1998.

[40] J. Musarrat, Q. Saquib, A. Azam, and S. A. H. Naqvi, "Zinc oxide nanoparticles-induced DNA damage in human lymphocytes," *Int. J. Nanoparticles*, vol. 2, no. 1–6, pp. 402–415, 2009, doi: 10.1504/ijnp.2009.028775.

[41] H. Hidaka"', S. Horikoshi, N. Serpone ~"'~, and J. Knowland, "In vitro photochemical damage to DNA. RNA and their bases by an inorganic sunscreen agent on exposure to UVA and UVB radiation," 1097.

[42] M. Hirano, C. Nakahara, K. Ota, O. Tanaike, and M. Inagaki, "Photoactivity and phase stability of ZrO 2-doped anatase-type TiO 2 directly formed as nanometer-sized particles by hydrolysis under hydrothermal conditions," 2003.

[43] G. Sivalingam, K. Nagaveni, M. S. Hegde, and G. Madras, "Photocatalytic degradation of various dyes by combustion synthesized nano anatase TiO2," *Appl. Catal. B Environ.*, vol. 45, no. 1, pp. 23–38, Sep. 2003, doi: 10.1016/S0926-3373(03)00124-3.

[44] N. Salah *et al.*, "High-energy ball milling technique for ZnO nanoparticles as antibacterial material.," *Int. J. Nanomedicine*, vol. 6, pp. 863–869, 2011, doi: 10.2147/ijn.s18267.

[45] Z. M. Kakhaki, A. Youzbashi, and N. Naderi, "Effect of Milling Energy and Process Ordering on the Morphologies and Optical Properties of ZnO Nanoparticles Obtained Through a Mechanochemical Technique," 2015.

[46] R. D. Yang, S. Tripathy, Y. Li, and H. J. Sue, "Photoluminescence and micro-Raman scattering in ZnO nanoparticles: The influence of acetate adsorption," *Chem. Phys. Lett.*, vol. 411, no. 1–3, pp. 150–154, Aug. 2005, doi: 10.1016/j.cplett.2005.05.125.

[47] H. Zhang, D. Yang, Y. Ji, X. Ma, J. Xu, and D. Que, "Low Temperature Synthesis of Flowerlike ZnO Nanostructures by Cetyltrimethylammonium Bromide-Assisted Hydrothermal Process," *J. Phys. Chem. B*, vol. 108, no. 13, pp. 3955–3958, Apr. 2004, doi: 10.1021/jp036826f.

[48] S. V. Bhat and F. L. Deepak, "Tuning the bandgap of ZnO by substitution with Mn2+, Co 2+ and Ni2+," *Solid State Commun.*, vol. 135, no. 6, pp. 345–347, Aug. 2005, doi: 10.1016/j.ssc.2005.05.051.

[49] S. López-Cuenca *et al.*, "High-yield synthesis of zinc oxide nanoparticles from bicontinuous microemulsions," *J. Nanomater.*, vol. 2011, 2011, doi: 10.1155/2011/431382.

[50] X. Li, G. He, G. Xiao, H. Liu, and M. Wang, "Synthesis and morphology control of ZnO nanostructures in microemulsions," *J. Colloid Interface Sci.*, vol. 333, no. 2, pp. 465–473, May 2009, doi: 10.1016/j.jcis.2009.02.029.

[51] S. Ahmed, Annu, S. A. Chaudhry, and S. Ikram, "A review on biogenic synthesis of ZnO nanoparticles using plant extracts and microbes: A prospect towards green chemistry,"

Journal of Photochemistry and Photobiology B: Biology, vol. 166. Elsevier B.V., pp. 272–284, Jan. 01, 2017, doi: 10.1016/j.jphotobiol.2016.12.011.

[52] H. Agarwal, S. Venkat Kumar, and S. Rajeshkumar, "A review on green synthesis of zinc oxide nanoparticles – An eco-friendly approach," *Resour. Technol.*, vol. 3, no. 4, pp. 406–413, Dec. 2017, doi: 10.1016/j.reffit.2017.03.002.

[53] S. Gunalan, R. Sivaraj, and V. Rajendran, "Green synthesized ZnO nanoparticles against bacterial and fungal pathogens," *Prog. Nat. Sci. Mater. Int.*, vol. 22, no. 6, pp. 693–700, 2012, doi: 10.1016/j.pnsc.2012.11.015.

[54] T. Khalafi, F. Buazar, and K. Ghanemi, "Phycosynthesis and Enhanced Photocatalytic Activity of Zinc Oxide Nanoparticles Toward Organosulfur Pollutants," *Sci. Rep.*, vol. 9, no. 1, Dec. 2019, doi: 10.1038/s41598-019-43368-3.

[55] Y. Dai, Y. Zhang, Y. Q. Bai, and Z. L. Wang, "Bicrystalline zinc oxide nanowires," *Chem. Phys. Lett.*, vol. 375, no. 1–2, pp. 96–101, Jun. 2003, doi: 10.1016/S0009-2614(03)00823-6.

[56] R. F. Silva and M. E. D. Zaniquelli, "Morphology of nanometric size particulate aluminium-doped zinc oxide films." [Online]. Available: www.elsevier.com/locate/colsurfa.

[57] S. J. Chen, L. H. Li, X. T. Chen, Z. Xue, J. M. Hong, and X. Z. You, "Preparation and characterization of nanocrystalline zinc oxide by a novel solvothermal oxidation route," *J. Cryst. Growth*, vol. 252, no. 1–3, pp. 184–189, May 2003, doi: 10.1016/S0022-0248(02)02495-8.

[58] Y. Yang, X. Li, J. Chen, H. Chen, and X. Bao, "ZnO nanoparticles prepared by thermal decomposition of β-cyclodextrin coated zinc acetate," *Chem. Phys. Lett.*, vol. 373, no. 1–2, pp. 22–27, May 2003, doi: 10.1016/S0009-2614(03)00562-1.

[59] L. Jing, Z. Xu, X. Sun, J. Shang, and W. Cai, "The surface properties and photocatalytic activities of ZnO ultra®ne particles."

[60] X. Wang, Y. Ding, C. J. Summers, and Z. L. Wang, "Large-scale synthesis of six-nanometer-wide ZnO nanobelts," *J. Phys. Chem. B*, vol. 108, no. 26, pp. 8773–8777, Jul. 2004, doi: 10.1021/jp048482e.

[61] L. Guo *et al.*, "Synthesis and characterization of poly(vinylpyrrolidone)-modified zinc oxide nanoparticles," *Chem. Mater.*, vol. 12, no. 8, pp. 2268–2274, 2000, doi: 10.1021/cm9907817.

[62] N. I. Kovtyukhova, E. V. Buzaneva, C. C. Waraksa, B. R. Martin, and T. E. Mallouk, "Surface sol-gel synthesis of ultrathin semiconductor films," *Chem. Mater.*, vol. 12, no. 2, pp. 383–389, Feb. 2000, doi: 10.1021/cm990395p.

[63] Y. Jin *et al.*, "Room temperature UV emission of Mg x Zn 12x O ®lms q." [Online]. Available: www.elsevier.com/locate/ssc.

[64] K. F. Lin, H. M. Cheng, H. C. Hsu, L. J. Lin, and W. F. Hsieh, "Band gap variation of size-controlled ZnO quantum dots synthesized by sol-gel method," *Chem. Phys. Lett.*, vol. 409, no. 4–6, pp. 208–211, Jun. 2005, doi: 10.1016/j.cplett.2005.05.027.

[65] C.-F. Jin, X. Yuan, W.-W. Ge, J.-M. Hong, and X.-Q. Xin, "Synthesis of ZnO nanorods by solid state reaction at room temperature," 2003. [Online]. Available: http://iopscience.iop.org/0957-4484/14/6/319.

[66] M. Singbal, V. Cbbabra, P. Kang, and D. O. Shah, "Pergamon PI1 SOO2s-5408(96)00175-4 SYNTHESIS OF ZnO NANOPARTICLES FOR VARISTOR APPLICATION USING Zn-SUBSTITUTED AEROSOL OT MICROEMULSION," 1997.

[67] R. Wang, J. H. Xin, X. M. Tao, and W. A. Daoud, "ZnO nanorods grown on cotton fabrics at low temperature," *Chem. Phys. Lett.*, vol. 398, no. 1–3, pp. 250–255, Nov. 2004, doi: 10.1016/j.cplett.2004.09.077.

[68] Z. Hu, J. F. Herrera Santos, G. Oskam, and P. C. Searson, "Influence of the reactant concentrations on the synthesis of ZnO nanoparticles," *J. Colloid Interface Sci.*, vol. 288, no. 1, pp. 313–316, Aug. 2005, doi: 10.1016/j.jcis.2005.02.058.

[69] C. Ronning, P. X. Gao, Y. Ding, Z. L. Wang, and D. Schwen, "Manganese-doped ZnO nanobelts for spintronics," *Appl. Phys. Lett.*, vol. 84, no. 5, pp. 783–785, Feb. 2004, doi: 10.1063/1.1645319.

[70] T. Hirai and Y. Asada, "Preparation of ZnO nanoparticles in a reverse micellar system and their photoluminescence properties," *J. Colloid Interface Sci.*, vol. 284, no. 1, pp. 184–189, Apr. 2005, doi: 10.1016/j.jcis.2004.09.069.

[71] L. Dong *et al.*, "Preparation of ZnO colloids by aggregation of the nanocrystal subunits," *J. Colloid Interface Sci.*, vol. 283, no. 2, pp. 380–384, Mar. 2005, doi: 10.1016/j.jcis.2004.09.044.

[72] R. N. Bhargava, V. Chhabra, T. Som, A. Ekimov, and N. Taskar, "Quantum Confined Atoms of Doped ZnO Nanocrystals."

[73] L. Guo, Y. L. Ji, H. Xu, P. Simon, and Z. Wu, "Regularly shaped, single-crystalline ZnO nanorods with wurtzite structure," *J. Am. Chem. Soc.*, vol. 124, no. 50, pp. 14864–14865, Dec. 2002, doi: 10.1021/ja027947g.

[74] K. Sue, K. Kimura, M. Yamamoto, and K. Arai, "Rapid hydrothermal synthesis of ZnO

nanorods without organics," *Mater. Lett.*, vol. 58, no. 26, pp. 3350–3352, 2004, doi: 10.1016/j.matlet.2004.06.036.

[75] J. Zhang, Sun, Yin, Su, Liao, and Yan, "Control of ZnO Morphology via a Simple Solution Route," *Chem. Mater.*, vol. 14, no. 10, pp. 4172–4177, Oct. 2002, doi: 10.1021/cm020077h.

[76] Y. H. Leung *et al.*, "Zno nanoshells: Synthesis, structure, and optical properties," *J. Cryst. Growth*, vol. 283, no. 1–2, pp. 134–140, Sep. 2005, doi: 10.1016/j.jcrysgro.2005.05.061.

[77] D. A. Schwartz, N. S. Norberg, Q. P. Nguyen, J. M. Parker, and D. R. Gamelin, "Magnetic Quantum Dots: Synthesis, Spectroscopy, and Magnetism of Co 2+ - and Ni 2+ -Doped ZnO Nanocrystals," *J. Am. Chem. Soc.*, vol. 125, no. 43, pp. 13205–13218, Oct. 2003, doi: 10.1021/ja036811v.

[78] A. Stanković, L. Veselinović, S. D. Škapin, S. Marković, and D. Uskoković, "Controlled mechanochemically assisted synthesis of ZnO nanopowders in the presence of oxalic acid," *J. Mater. Sci.*, vol. 46, no. 11, pp. 3716–3724, Jun. 2011, doi: 10.1007/s10853-011-5273-6.

[79] A. S. Lanje, S. J. Sharma, R. S. Ningthoujam, J.-S. Ahn, and R. B. Pode, "Low temperature dielectric studies of zinc oxide (ZnO) nanoparticles prepared by precipitation method," *Adv. Powder Technol.*, vol. 24, no. 1, pp. 331–335, Jan. 2013, doi: 10.1016/j.apt.2012.08.005.

[80] Y. Wang, C. Zhang, S. Bi, and G. Luo, "Preparation of ZnO nanoparticles using the direct precipitation method in a membrane dispersion micro-structured reactor," *Powder Technol.*, vol. 202, no. 1–3, pp. 130–136, Aug. 2010, doi: 10.1016/j.powtec.2010.04.027.

[81] T. H. Mahato, G. K. Prasad, B. Singh, J. Acharya, A. R. Srivastava, and R. Vijayaraghavan, "Nanocrystalline zinc oxide for the decontamination of sarin," *J. Hazard. Mater.*, vol. 165, no. 1–3, pp. 928–932, Jun. 2009, doi: 10.1016/j.jhazmat.2008.10.126.

[82] H. Benhebal *et al.*, "Photocatalytic degradation of phenol and benzoic acid using zinc oxide powders prepared by the sol–gel process," *Alexandria Eng. J.*, vol. 52, no. 3, pp. 517–523, Sep. 2013, doi: 10.1016/j.aej.2013.04.005.

[83] J. J. Schneider *et al.*, "Synthesis, Characterization, Defect Chemistry, and FET Properties of Microwave-Derived Nanoscaled Zinc Oxide," *Chem. Mater.*, vol. 22, no. 7, pp. 2203–2212, Apr. 2010, doi: 10.1021/cm902300q.

[84] A. Kołodziejczak-Radzimska, E. Markiewicz, and T. Jesionowski, "Structural Characterisation of ZnO Particles Obtained by the Emulsion Precipitation Method," *J. Nanomater.*, vol. 2012, pp. 1–9, 2012, doi: 10.1155/2012/656353.

[85] N. Matinise, X. G. Fuku, K. Kaviyarasu, N. Mayedwa, and M. Maaza, "ZnO nanoparticles via Moringa oleifera green synthesis: Physical properties & mechanism of formation," *Appl. Surf. Sci.*, vol. 406, pp. 339–347, Jun. 2017, doi: 10.1016/j.apsusc.2017.01.219.

[86] M. S. Yadav, N. Singh, and A. Kumar, "Synthesis and characterization of zinc oxide nanoparticles and activated charcoal based nanocomposite for supercapacitor electrode application," *J. Mater. Sci. Mater. Electron.*, vol. 29, no. 8, pp. 6853–6869, Apr. 2018, doi: 10.1007/s10854-018-8672-5.

[87] K. M. Ezealisiji, X. Siwe-Noundou, B. Maduelosi, N. Nwachukwu, and R. W. M. Krause, "Green synthesis of zinc oxide nanoparticles using Solanum torvum (L) leaf extract and evaluation of the toxicological profile of the ZnO nanoparticles–hydrogel composite in Wistar albino rats," *Int. Nano Lett.*, vol. 9, no. 2, pp. 99–107, Jun. 2019, doi: 10.1007/s40089-018-0263-1.

[88] J. de O. Primo *et al.*, "Synthesis of Zinc Oxide Nanoparticles by Ecofriendly Routes: Adsorbent for Copper Removal From Wastewater," *Front. Chem.*, vol. 8, Nov. 2020, doi: 10.3389/fchem.2020.571790.

[89] A. Khalid *et al.*, "Enhanced Optical and Antibacterial Activity of Hydrothermally Synthesized Cobalt-Doped Zinc Oxide Cylindrical Microcrystals," *Materials (Basel).*, vol. 14, no. 12, p. 3223, Jun. 2021, doi: 10.3390/ma14123223.

[90] J. M. Wilmott, D. Aust, B. E. Brockway, and V. Kulkarni, "The Delivery Systems' Delivery System," in *Delivery System Handbook for Personal Care and Cosmetic Products*, Elsevier, 2005, pp. 437–472.

[91] "https://www.prnewswire.com/news-releases/personal-care-market-to-grow-by-usd-148-89-billion--17-000-technavio-research-reports-301411858.html."

[92] K. P. Ananthapadmanabhan, D. J. Moore, K. Subramanyan, M. Misra, and F. Meyer, "Cleansing without compromise: the impact of cleansers on the skin barrier and the technology of mild cleansing," *Dermatol. Ther.*, vol. 17, no. s1, pp. 16–25, Jan. 2004, doi: 10.1111/j.1396-0296.2004.04S1002.x.

[93] E. Lémery *et al.*, "Skin toxicity of surfactants: Structure/toxicity relationships," *Colloids Surfaces A Physicochem. Eng. Asp.*, vol. 469, pp. 166–179, Mar. 2015, doi: 10.1016/j.colsurfa.2015.01.019.

[94] "https://www.factmr.com/report/plant-based-skincare-products-market." .

[95] K. Ertel, "MODERN SKIN CLEANSERS," *Dermatol. Clin.*, vol. 18, no. 4, pp. 561–575, Oct. 2000, doi: 10.1016/S0733-8635(05)70207-2.

[96] "https://www.ancientmesopotamiagifts.com/blogs/a-little-history." .

[97] M. Hill and T. Moaddel, "Soap Structure and Phase Behavior," in *Soap Manufacturing*

Technology, Elsevier, 2016, pp. 35–54.

[98] E. G. Myers, "Soap and Detergents," in *Inedible Meat by-Products*, Dordrecht: Springer Netherlands, 1992, pp. 149–176.

[99] H. I. M. Frank Dreher, Elsa Jungman, Kazutami Sakamoto, Ed., *Handbook of Cosmetic Science and Technology*. 2022.

[100] R. Barret, "Importance and Evaluation of Lipophilicity," in *Therapeutical Chemistry*, Elsevier, 2018, pp. 53–78.

[101] H. B. W. Patterson, "Quality and Control," in *Hydrogenation of Fats and Oils*, Elsevier, 2011, pp. 329–350.

[102] J. B. Marcus, "Lipids Basics: Fats and Oils in Foods and Health," in *Culinary Nutrition*, Elsevier, 2013, pp. 231–277.

[103] M. N. Riaz and G. J. Rokey, "Impact of particle size and other ingredients on extruded foods and feeds," in *Extrusion Problems Solved*, Elsevier, 2012, pp. 55–63.

[104] N. Hall, "Implications of Soap Structure for Formulation and User Properties," in *Soap Manufacturing Technology*, Elsevier, 2016, pp. 1–33.

[105] T. F. Tadros, *Pharmaceutical, Cosmetic and Personal Care Formulations*. De Gruyter, 2018.

[106] J. Eastoe and R. F. Tabor, "Surfactants and nanoscience," in *Colloidal Foundations of Nanoscience*, Elsevier, 2022, pp. 153–182.

[107] R. J. Farn, Ed., *Chemistry and Technology of Surfactants*. Wiley, 2006.

[108] "Sodium Lauryl Ether Sulphate (SLES) - What is it and how is it used in global industries?," [Online]. Available: https://www.ipsingredis.com/markets/sodium-lauryl-ether-sulphate-sles-what-is-it-and-how-is-it-used-in-global-industries/.

[109] "[30] 'Sodium Lauryl Ether Sulfate [SLES] Market: Industry Analysis and Forecast (2019 to 2027): By Application, Type, Form, and Region,' MAXIMIZE MARKET RESEARCH," [Online]. Available: https://www.maximizemarketresearch.com/market-report/sodium-lauryl-ether-sulfate-market/40608/.

[110] "Sulfate vs. Sulfate-free: Information to Make a Choice," *Cosmetics & Toiletries*, 2013.

[111] B. E. Rapp, "Surface Tension," in *Microfluidics: Modelling, Mechanics and Mathematics*, Elsevier, 2017, pp. 421–444.

[112] V. A. P. Goyal, "Micellar structure and inter-micelle interactions in micellar solutions:

Results of small angle neutron scattering studies," 2001.

[113] J. N. Israelachvili, D. J. Mitchell, and B. W. Ninham, "Theory of self-assembly of hydrocarbon amphiphiles into micelles and bilayers," *J. Chem. Soc. Faraday Trans. 2*, vol. 72, p. 1525, 1976, doi: 10.1039/f29767201525.

[114] A. S. Rafique, S. Khodaparast, A. S. Poulos, W. N. Sharratt, E. S. J. Robles, and J. T. Cabral, "Micellar structure and transformations in sodium alkylbenzenesulfonate (NaLAS) aqueous solutions: effects of concentration, temperature, and salt," *Soft Matter*, vol. 16, no. 33, pp. 7835–7844, 2020, doi: 10.1039/D0SM00982B.

[115] "Antibacterial Products Market Size & Share Report," 2022. [Online]. Available: https://www.grandviewresearch.com/industry-analysis/antibacterial-products-market-report.

[116] M. Mueller and C. R. Tainter, "Escherichia Coli," 2020, [Online]. Available: https://www.ncbi.nlm.nih.gov/books/NBK564298/.

[117] S. Y. C. Tong, J. S. Davis, E. Eichenberger, T. L. Holland, and V. G. Fowler, "Staphylococcus aureus Infections: Epidemiology, Pathophysiology, Clinical Manifestations, and Management," *Clin. Microbiol. Rev.*, vol. 28, no. 3, pp. 603–661, Jul. 2015, doi: 10.1128/CMR.00134-14.

[118] M. Wu and X. Li, "Klebsiella pneumoniae and Pseudomonas aeruginosa," in *Molecular Medical Microbiology*, Elsevier, 2015, pp. 1547–1564.

[119] A. M. Spagnolo, M. Sartini, and M. L. Cristina, "Pseudomonas aeruginosa in the healthcare facility setting," *Rev. Med. Microbiol.*, vol. 32, no. 3, pp. 169–175, Jul. 2021, doi: 10.1097/MRM.0000000000000271.

[120] N. Bourafa, L. Loucif, N. Boutefnouchet, and J.-M. Rolain, "Enterococcus hirae, an unusual pathogen in humans causing urinary tract infection in a patient with benign prostatic hyperplasia: first case report in Algeria," *New Microbes New Infect.*, vol. 8, pp. 7–9, Nov. 2015, doi: 10.1016/j.nmni.2015.08.003.

[121] D. Piccinini, E. Bernasconi, C. Di Benedetto, G. Martinetti Lucchini, and M. Bongiovanni, "Enterococcus hirae infections in the clinical practice," *Infect. Dis. (Auckl).*, vol. 55, no. 1, pp. 71–73, Jan. 2023, doi: 10.1080/23744235.2022.2125066.

[122] K. Z. Sanidad, G. Wang, A. Panigrahy, and G. Zhang, "Triclosan and triclocarban as potential risk factors of colitis and colon cancer: Roles of gut microbiota involved," *Sci. Total Environ.*, vol. 842, p. 156776, Oct. 2022, doi: 10.1016/j.scitotenv.2022.156776.

[123] X. Wang *et al.*, "Triclosan causes spontaneous abortion accompanied by decline of estrogen sulfotransferase activity in humans and mice," *Sci. Rep.*, vol. 5, no. 1, p. 18252, Dec. 2015, doi: 10.1038/srep18252.

[124] L. M. Weatherly and J. A. Gosse, "Triclosan exposure, transformation, and human health effects," *J. Toxicol. Environ. Heal. Part B*, vol. 20, no. 8, pp. 447–469, Nov. 2017, doi: 10.1080/10937404.2017.1399306.

[125] "BREAKING NEWS: The Ban on the Cosmetic Anti-dandruff Agent Zinc Pyrithione (ZPT) in the EU will come into force on March 1, 2022 - Regulatory News - Personal and Home Care Products," 2022. https://www.cirs-group.com/en/cosmetics/breaking-news-the-ban-on-the-cosmetic-anti-dandruff-agent-zinc-pyrithione-zpt-in-the-eu-has-come-into-force-on-march-1-2022.

Chapter 2

Experimental Methodologies, Characterization and Evaluation Techniques

Highlights of the Chapter:

- *The current chapter describes the experimental procedures used for fabrication of zinc oxide and silver doped zinc oxide nano systems*
- *Surfactant mediated fabrication and green synthesis methods have been discussed in detail.*
- *This chapter also explores the principles of characterization instruments such as XRD, SEM, UV-vis etc. and evaluation techniques ZOI, EN-1276, FRSP, Rheology, etc. that have been employed in the understanding properties of fabricated nanomaterial and products infused with fabricated materials*

2.1. Fabrication Approaches

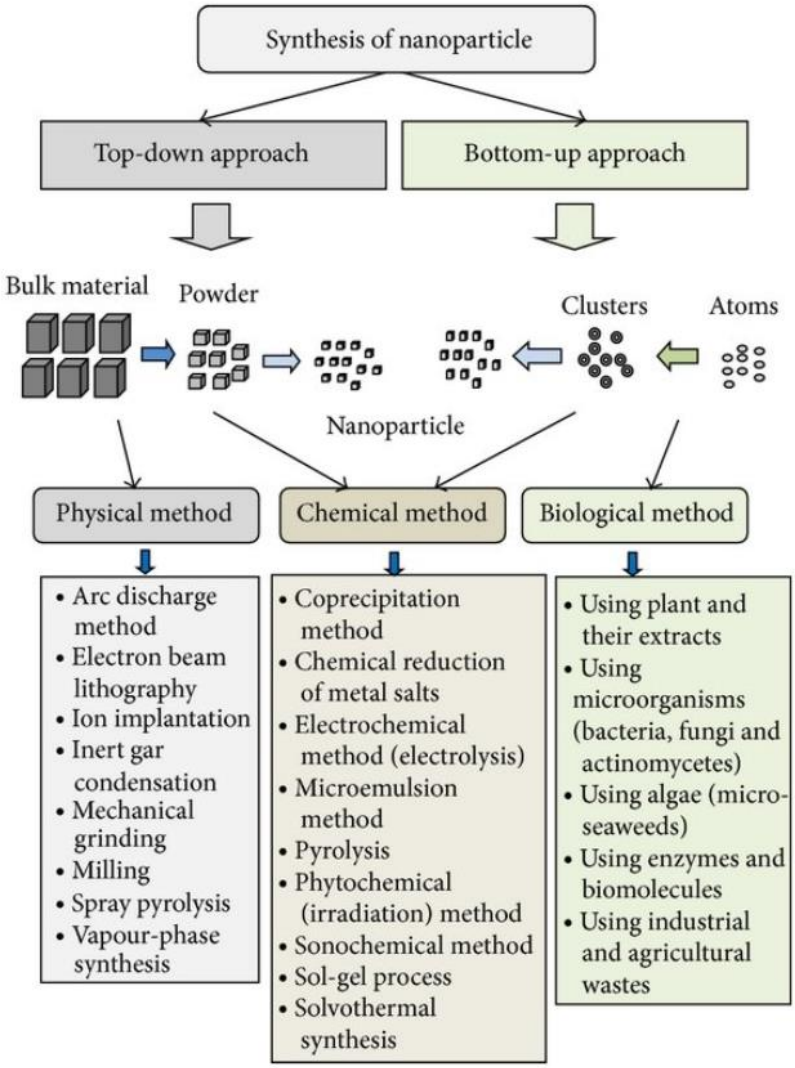

Figure 2.1. *Various physical, chemical and biological fabrication approaches of nano-scale materials* [1]

Nanoparticles are generally synthesized using either a top-down or bottom-up strategy (Figure 2.1). Bottom-up approaches rely on nucleating atoms or molecules of elements into nanostructures. While the specific technique of synthesis varies on the substance being produced, some typical processes include co precipitation, solvothermal, chemical reduction, the sol-gel process, and, more recently, microbial and plant-based synthesis. Top-down processes include ball milling, laser ablation, and spark ablation, in which a bulk substance is mechanically broken up to generate tiny particles.

Bottom-up methods are sometimes referred to as "wet" approaches because they employ significant quantities of solvents and other reagents. Furthermore, the nanoparticles must frequently be stabilized or encapsulated in solution to guarantee that they stay in the nanometer level [2], [3].

In order to fabricate potent nanomaterials and confine nanoparticle growth, the current approach utilizes the unique capabilities of surfactant and polyol combinations such as micellar assembly and their caging structure. Green strategy to fabricate ZnO and its various enhanced properties are also established using the added power of *Moringa oleifera* leaves phytochemicals. Arrangements and caging agents are used in this approach to create fabricated materials suited for industrial purposes such as health and hygiene, personal care, and cosmetics.

2.1.1. Surfactant mediated

Nanotechnology involves the fabrication of desired nanomaterial dimensions and structure for their suitable uses. Surfactants are commonly employed to lower surface and interfacial tension between two or more phases due to their structural distinctiveness. Surfactants have shown to have ideal morphological directing agents in the formation of nanomaterials, with the surface adsorption of surface active compounds on distinct crystallographic planes of nucleating centers influencing their overall form. Surfactants, a distinct family of surface active chemicals, have a remarkable capacity to influence crystal development in a shape and size controlled way. Controlling the surfactant framework in addition to its self-assembled activity allows for careful tailoring of the targeted morphologies. Surfactants of various types have been utilized in the shape control formation of nanoparticles, with ionic surfactants exhibiting significant shape regulating actions [4], [5].

This work may be the first or among the very few reports where authors have explored this unique surfactant and polyol combination, perfectly suitable precursors for personal care industry that aid in keeping the crystallite size of nanomaterial in nanoregime (Figure 2.2). SLES is an anionic surfactant that is cost effective material that is commonly used in health and hygiene industry especially cleansing products. Glycerin is also a well-known co-surfactant for engineering nanoscale materials when additionally acts as humectant preventing the trans epidermal water loss to keep the skin moisturized [6]. Therefore, presented SPA based nanomaterial synthesis strategy has several advantages such as high compatibility with health

and hygiene, personal care products especially liquid cleansing products, non-toxic, low cost solvents, low energy consuming, non-intensive process and is a one-step fast synthesis without any additional process like calcinations and milling.

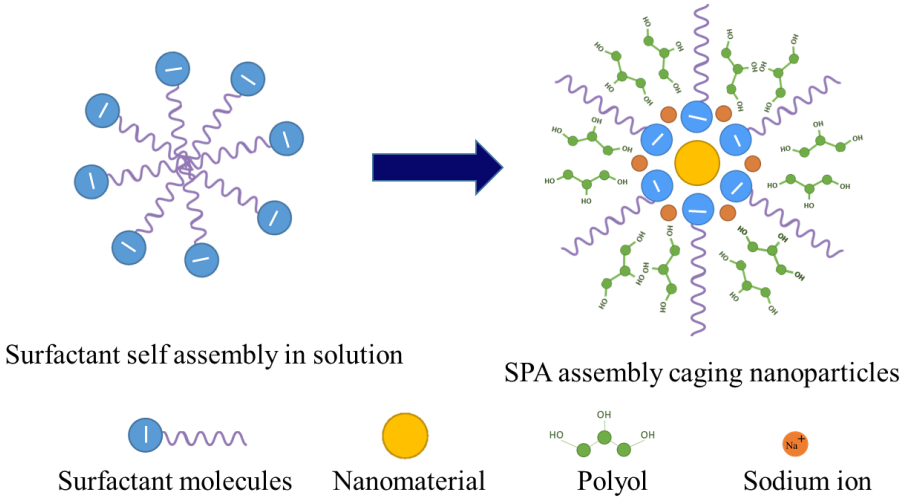

Figure 2.2. *Illustrative fabrication of nanomaterial in SPA*

The current method takes advantage of unique properties of surfactant and polyol combination such as micellar formation and their cage-like matrix to synthesize materials in nanoscale and restricting the particle growth. This method thus uses assemblies and caging agents specifically to make synthesized ZnO suitable for industrial applications like health and hygiene, personal care and cosmetic products.

Basic steps involved in the ZnO-SPA fabrication include:

- homogenously mixing Sodium Lauryl Ether Sulphate and Glycerine
- addition of zinc precursors such as zinc chloride or zinc nitrate and silver precursors such as silver nitrate
- stoichiometric steady addition of sodium hydroxide solution and with continuous stirring until uniform homogeneous mix obtained indicating successful synthesis

2.1.2. Green synthesis using Moringa Oleifera

Due to various innovative methodologies and alternatives to physical and chemical processes, phytochemical-mediated green sustainable synthesis is gaining popularity. The reducing agents engaged in nanoparticle production in this bottom-up strategy, where the phytochemicals stabilized and encapsulated nanomaterial, include alkaloids, polyphenols, terpenoids, etc (Figure 2.3). Green synthesis is a one-step process that is nontoxic, sustainable;

hence, botanical research has increased fast. Every component of the plant, including the leaves, stem, stalks, flower, and root, may be utilized to synthesize nanoparticles [7], [8].

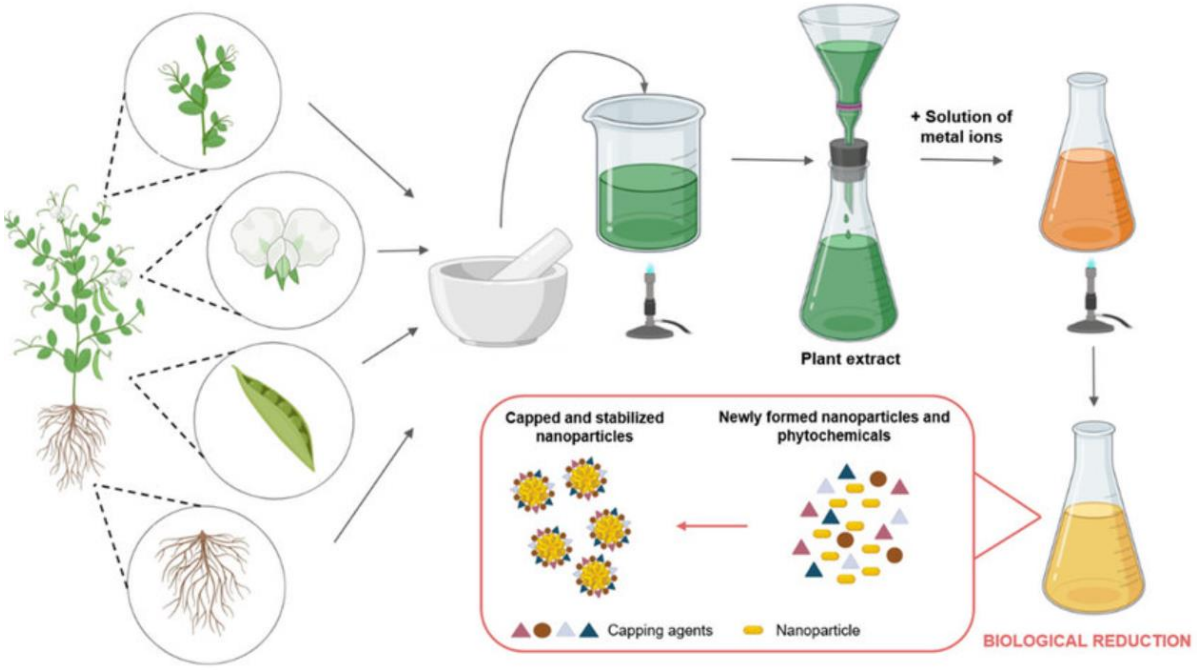

Figure 2.3. *General steps of green synthesis of inorganic nanoparticles using plant extracts*[8]

Green synthesis is employed not just to minimize environmental impact, but also to create large amounts of harsh chemical free nanomaterials with unique dimensions and shapes. The properties of the nanostructures were affected by the elements of the plant extract since they contain varying quantities and compositions of biological phytochemicals and reducing agents. A green extract mediated reduction consists of the plant extract with an aqueous solution of the related metal salt precursor at ambient temperature and thus is conducted in a couple of hours.

Basic steps involved:

- decoction of *Moringa oleifera* leaves powder were done using 1:20 ratio with distilled water under continuous stirring

- To the filtrate metal precursor is added with continuously stirring until precipitation observed. The phytochemicals such as phenolic compounds and flavonoids (Ar-(OH)n) present in *Moringa oleifera* leaves extract are responsible for reduction process.

- Set aside solution for in order to facilitate reaction completion and formation of nano ZnO.

2.2. Characterization techniques for nanomaterials

2.2.1. Scanning Electron Microscope (SEM)

SEM is a versatile sophisticated device that is mostly used to examine material surface characteristics (Figure 2.4). SEM may offer qualitative data about a sample such as its topography, morphology, composition information. In other regards, it describes the surface morphology and texture, as well as the structure, size, and organization of the particles on the sample's surface [9].

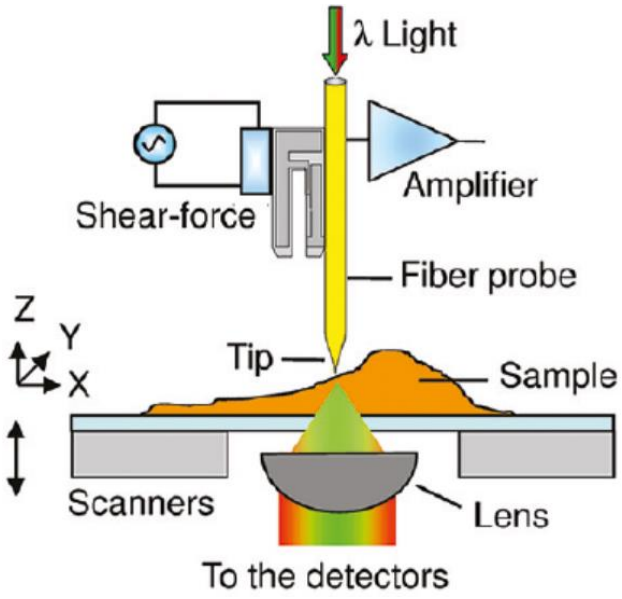

Figure 2.4. *Illustration of SEM instrumentation*

The surface morphology of powdered nanomaterials in the current study was investigated by using SEM Model-JSM-6010 PLUS ILA in the range magnification of 2000x to 6000x, parameter was 20 kV, WD 12 mm, SS50. The SEM measurement (Figure 2.5) is built on the concept that the primary electrons generated from the source offer energy to the atomic electrons of the test sample, causing them to emit as secondary electrons (SEs), and the compiling these released secondary electrons from test sample, the prerequisite for SEM to function effectively is to be done under a vacuum to prevent interactions of electrons with gas particles to generate maximum resolution. Furthermore, the initial electrons created and released by the electron cannon are accelerated by thermal treatment or providing high energy [10]. These released

electrons are concentrated and restricted to a monochromatic beam (width of approximately 100 nm) within a vacuumed section using magnetic field lenses and metallic apertures. When the main beam of electrons strikes the surface of the sample, it interacts with the sample's surface area in a range of methods up to a particular depth. The impinging electrons driven towards the samples contain significant amounts of kinetic energy, which they dissipate by creating multiple signals from electron interactions with the sample molecules and these signals can be used to obtain pictures [11].

Figure 2.5. *Photograph of Scanning Electron Microscope (SEM)*

The illuminating light is emitted by the probe and passes through the aperture at the tip before interacting with the sample surface. The absorbance or fluorescence generated by the tagged molecules on the sample surface may be collected when light travels through the sample. Topographic and optical pictures with great spatial resolution can be created together [11].

2.2.2. X-ray diffraction (XRD)

X-ray diffraction (XRD) is used to characterize material characteristics such as crystal structure, crystallite size, and strain. XRD operates on the basis of Bragg's equation [12],

$$2d_{hkl}\sin\theta = n\lambda$$

θ is the Bragg angle, d_{hkl} is the lattice spacing for (h k l) planes under consideration and n is the order of reflection (n=1,2,3…). The Braggs equation can be explained in perspective of the incidence of a collimated X-ray radiation on a crystallographic planes of the sample to be examined (Figure 2.6). The mechanism of X-ray diffraction is caused by a scattering process

wherein X-rays are scattered by electrons of atoms found in the object without affecting the wavelength.

(a)

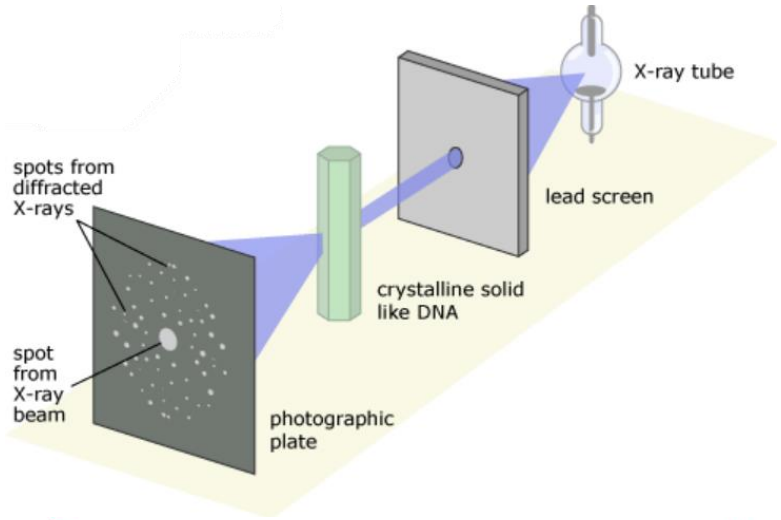

(b)

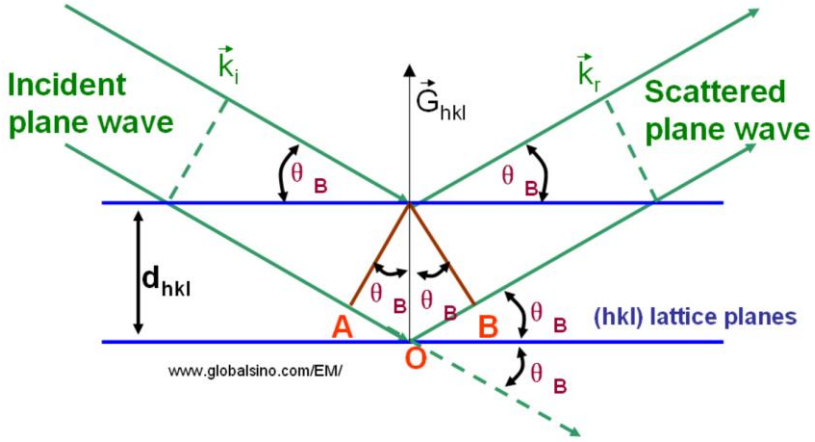

Figure 2.6. *(a) Schematic representation of XRD instrument (b) Braggs law diagram* [12]

When X-rays have wavelengths equivalent to the interatomic spacing of a crystalline material which is in the nanometer range, the incoming X-ray beam diffracts in certain directions predicted by Bragg's equation [13]. The resultant diffraction pattern is a characteristic fundamental feature of the object, giving not just identification but also thorough understanding of its structure [14]. The crystalline structure, size and phase analysis of nanomaterials was determined by using X-ray diffractometer (XRD Shimadzu-6100) having parameters CuK1 radiation (k = 1.54056 A°), voltage 40 kV and, Current 30 mA.

2.2.3. Energy-dispersive X-ray (EDX) Spectroscopy

Energy dispersive X-ray spectroscopy (EDX) is an analytical technique used to characterize materials analytically or chemically. EDX systems are typically used in conjunction with an electron microscopy equipment such as transmission electron microscopy (TEM) or scanning electron microscopy (SEM). The generation of a test sample's distinctive X-rays is the basic principle for EDX. A pulse of high-energy charged ions i.e. electrons or protons is aimed at the test sample under investigation. When an electron from a higher binding energy electron level drops into the lower energy level, it emits an X-ray with the energy equal to the gap between the electron level binding energies which is depicted as speaks in the spectra. The elemental constitution of the studied sample is associated with the peaks in the EDX spectrum [15], [16]. A schematic describing the EDX spectroscopy method is shown in Figure 2.7. The qualitative and quantitative analyses of nanomaterial system were done by EDX-8100-Shimadzu, Japan. Nano material was placed in sample holder and measurement was done using 10 mm collimator (Figure 2.8). However, The key limitations of EDX are (a) data generation is mainly on surface and or only from few microns depth (b) accuracy of detection reduces as atomic number approaches below eleven.

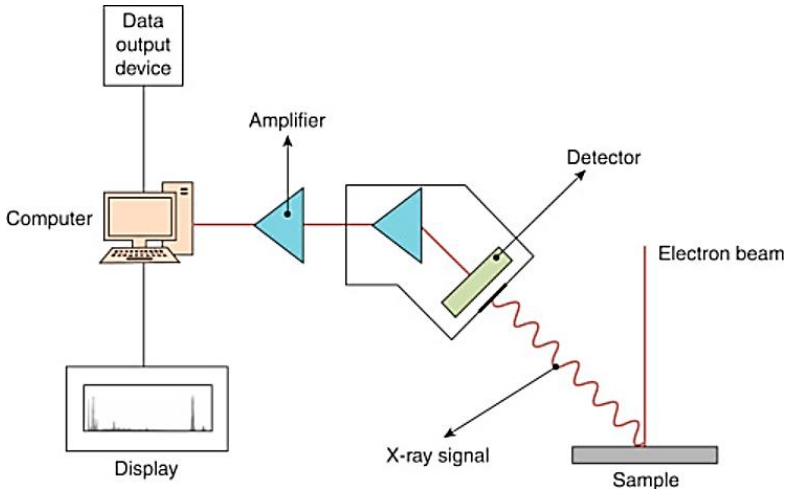

Figure 2.7. *Schematic representation of EDX instrument* [15]

Figure 2.8. *Photograph of energy-dispersive X-ray*

2.2.4. Fourier-Transform Infrared (FTIR) spectroscopy

Fourier Transform Infrared (FTIR) spectroscopy is a tool for obtaining the infrared spectrum of solid, liquid, and gas absorbance, transmittance, and photoconductivity. It is utilized to identify distinct functional groups in a variety of compounds.

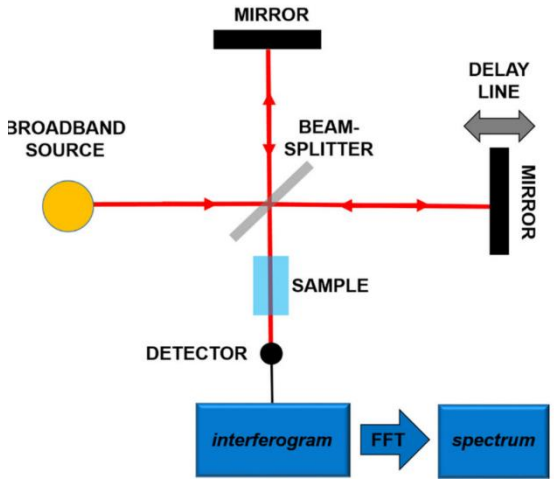

Figure 2.9. *Schematic representation of EDX instrument* [15]

FTIR analysis is used to identify organic and inorganic compounds by scanning the samples with IR radiation. FTIR may be used to identify and characterize unknown components, discover impurities in a substance, locate additives, and detect decomposition. Infrared radiation of approximately 10,000-100 cm^{-1} is transmitted through the sample, with most absorbed and some passed through (Figure 2.9). The sample converts received radiation into vibrational or rotational energy. The detector output signal is a spectra ranging from 4000 to 400 cm^{-1}, representing the samples' chemical fingerprint [17] and because each molecule has a distinct imprint we can identify unknown molecules present.

Figure 2.10. *Photograph of Fourier Transform Infrared (FTIR) spectrometer*

FTIR spectrums were recorded by using Model-IRAffinity-1S make by Shimadzu, Japan (Figure 2.10) attenuated total reflection (ATR) from SPECAC, U.K. measurement mode was transmittance vs wavenumber, Scanning-45, spectrum recorded through ATR.

2.2.5. Ultraviolet visible (UV Vis) spectroscopy

UV-Vis absorption spectroscopy is an apparatus for measuring the attenuation of light as it travels through a material or after light is reflection from the material. UV-Vis spectroscopy is a useful method for identifying, characterizing, and investigating these materials, as well as assessing the stability of nanoparticle solutions.

The electronic transitions of organic molecules absorbing light which excite electrons from a lesser energy orbit (highest occupied molecular orbital HOMO) to a greater energy free orbit (lowest unoccupied molecular orbital LUMO) are the basis of UV-visible spectroscopy (Figure 2.11). Light absorption causes atomic excitation, that explains the transition of atoms from a low energy ground state to an excited state. The energy required for atoms to undergo these transitions is distinct. Employing a UV-Vis spectrophotometer, this theory may be used to determine the molecules in a sample depending on their absorption characteristics [18].

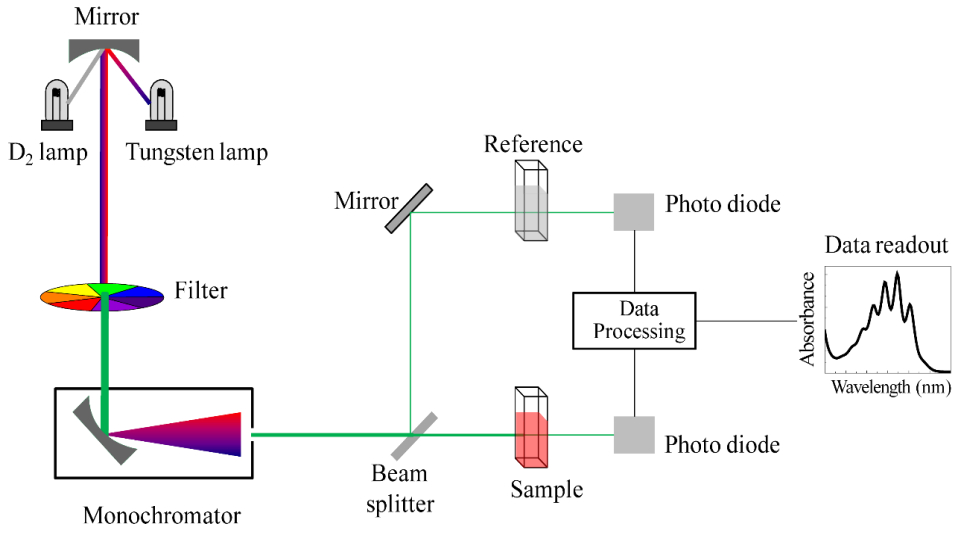

Figure 2.11. *Schematic representation of UV Vis spectroscopy* [19]

This corresponds to the concept of the Beer lambert law, that states that light absorbed by a sample is exactly proportionate to its path length and concentration.

A= log (I_0/I), where I is light intensity and is measured with respect to a reference, I_0.

***Figure 2.12**. Photograph of UV–Visible spectrometer*

UV–Visible spectrums were recorded by using UV–Vis spectrophotometer Model-1800 from Shimadzu, Japan in the absorbance range of 200–700 nm (Figure 2.12). The diluted suspension of nanomaterial was prepared in demineralized water and subjected to sonication for 5 min before recording the UV–Vis spectrum.

2.3. Soap and liquid product Analysis

2.3.1. Fatty acid composition estimation: Gas chromatography

The term gas chromatography (GC) refers to chromatographic procedures in which a gas is used as the mobile phase and either solid or liquid stationary phases are used (Figure 2.13). Gas chromatography (GC) is an investigative technique for separating and detecting the chemical compositions of a test sample in order to identify their either presence or absence, as well as their amounts. Organic molecules or gases are commonly used as chemical components. The prepared sample introduced into the apparatus is carried by a gas flow "carrier gas" helium or nitrogen into a separation tube the "column." Within the column, the different components are segregated. The sensor counts the number of components that escape the column. To evaluate a sample with an unknown concentration, a known amount reference sample is introduced into the device. To compute the concentration, the standard sample peak retention time and area are compared to the test sample [20-21].

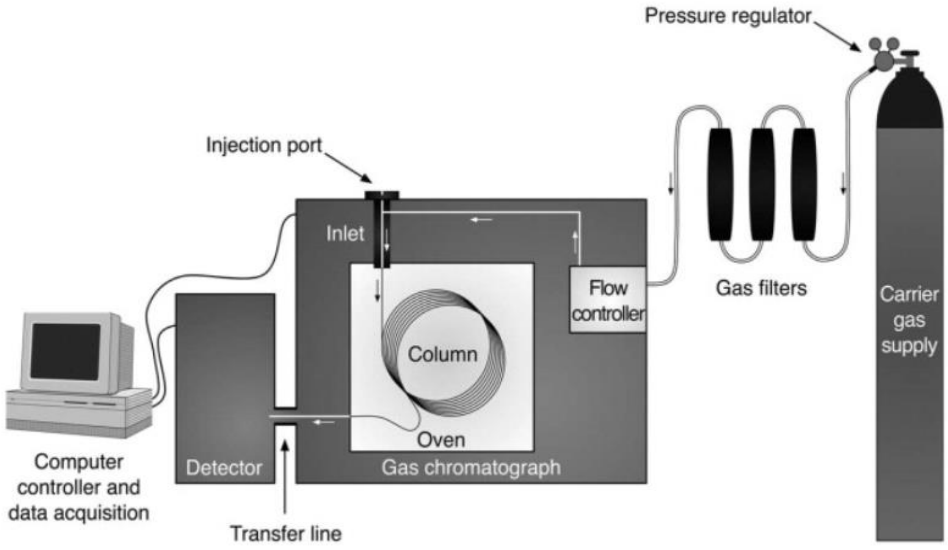

Figure 2.13. *Diagrammatic illustration of GC chromatography* [21]

The estimation of long chain fatty acids composition in soap matrix was performed using GC Agilent Technologies 7820A having capillary column HP 5MS (30 m 0.25 mm ID 0.25 mm) in conjunction with 5% diphenyl 95% dimethylpolysiloxane. Electron ionization energy 70 eV, helium gas (99.99%) used as carrier gas with a constant flow rate 1 mL/min (Figure 2.14). The injection volume is 1 mL with a split ratio of 50:1, temperature 60 C and ion source temperature 250 C.

Figure 2.14. *Photograph of GC chromatograph instrument*

2.3.2. Chloride content estimation

Chloride content was estimated using the following method, dissolve 5 g of test sample in distilled water and added calcium nitrate solution. The resultant solution was filtered through Whatman filter paper, followed by addition of methyl orange as an indicator and dilute nitric acid to neutralize the solution. This solution was further subjected to titration with silver nitrate solution, using potassium chromate solution as endpoint indicator.

$$Ag^{+} + \mathrm{Cl}^{-} \rightarrow \mathrm{AgCl}$$

During the titration, an increased amount of a silver nitrate is introduced to the test sample containing chloride ions, resulting in a silver chloride precipitation. Once most of the chloride ions have precipitated, the titration is complete.

$$2\,\mathrm{Ag}^{+} + \mathrm{CrO}_4^{2-} \rightarrow \mathrm{Ag}_2\mathrm{CrO}_4$$

Then, more silver ions react with the chromate ions present in the indicator, potassium chromate, to generate a silver chromate precipitate. Carry out a blank determination using the same quantity of all reagents but except the sample.

2.3.3. Foamability test

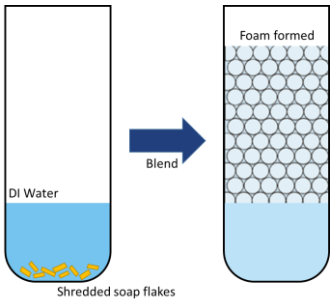

Figure 2.15. *Foam height analysis for bar and liquid soap*

Foams are generally described in terms of their foamability defined as the capacity of the surfactants to form foam irrespective of the special foam properties and foam stability describing the variations of foam height or volume, immediately after foam generation. Foamability was analysed using the following method. The aqueous solution of known quantity of soap bar was prepared and poured into a blender jar and blended at low speed for exactly 30 sec. Poured the generated foam quickly into the cylinder and measured the foam volume immediately after levelling off the top surface of the foam and noted the top height only (Figure 2.15).

2.3.4. Rheological properties of liquid cleansing product

Rheology is a broad term that refers to the discipline of analysing flow of material and deformation. The viscosity of a fluid is described as its resistance to flow. The resistance of the substance to a subjected to shear force is determined by a rheometer. Rotational viscometry is the torque needed to move an item in a liquid, such as a spindle, and it reflects the fluid's viscosity. Viscous drag is related to the force needed to move the spindle, and hence to the viscosity of a Newtonian fluid [22].

Figure 2.16. *Photograph of Rheometer*

The rheological properties of liquid cleansing product having different concentration of nanomaterials were studied on Brookfield Rheometer DV3T model (Figure 2.16), using spindle RV-5, RV-2 for rest of solutions at RPM-12, temperature-25 C, torque more than 10, test duration 1 min. Initial calibration of Rheometer was done using standard having known viscosity in centipoise (cps).

2.4. Antibacterial properties

2.4.1. Zone of inhibition: ZOI

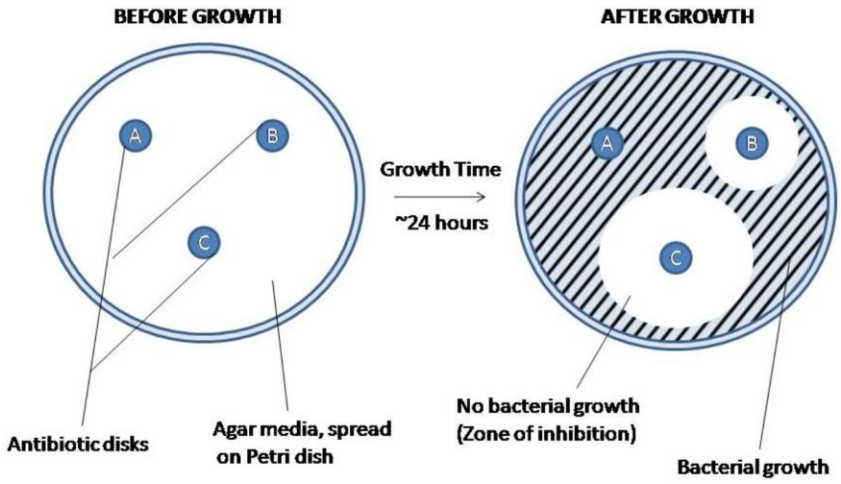

Figure 2.17. *Zone of inhibition (ZOI) illustration* [23]

Disk diffusion technique was used for evaluating the antibacterial efficacy against both Gram-positive and Gram-negative bacteria i.e., S. aureus and E. coli respectively as well as *C. acne*. These bacteria were selected as these are well known to cause various diseases among human being and animals. The bacterial strain was grown overnight and through UV spectrophotometer the optical density was adjusted to 0.1 at 600 nm to achieve 10^8 cfu/mL. The bacterial strains were spread homogeneously onto Muller & Hilton agar plates and allowed to dry. Sterile 6 mm disk were soaked in different concentration of test samples for 30 min and placed over the surface of Muller & Hilton agar plates. These plates were incubated at 37 C for 24 h, and the inhibitory actions in diameter (mm) were revealed by a clear zone (Figure 2.17) [23], [24].

2.4.2. Contact kill test: EN 1276

Quantitative suspension test was used for the assessment of bactericidal activity of sodium salt of long chain fatty acid using EN 1276 standard log reduction method. 1:1 diluted test sample was utilized and exposed with test organism suspension for contact time of 1 min followed by neutralization for specific time Figure 2.18. Placed 1 mL of above mix on agar plate and incubated for 48 h at 37 C.

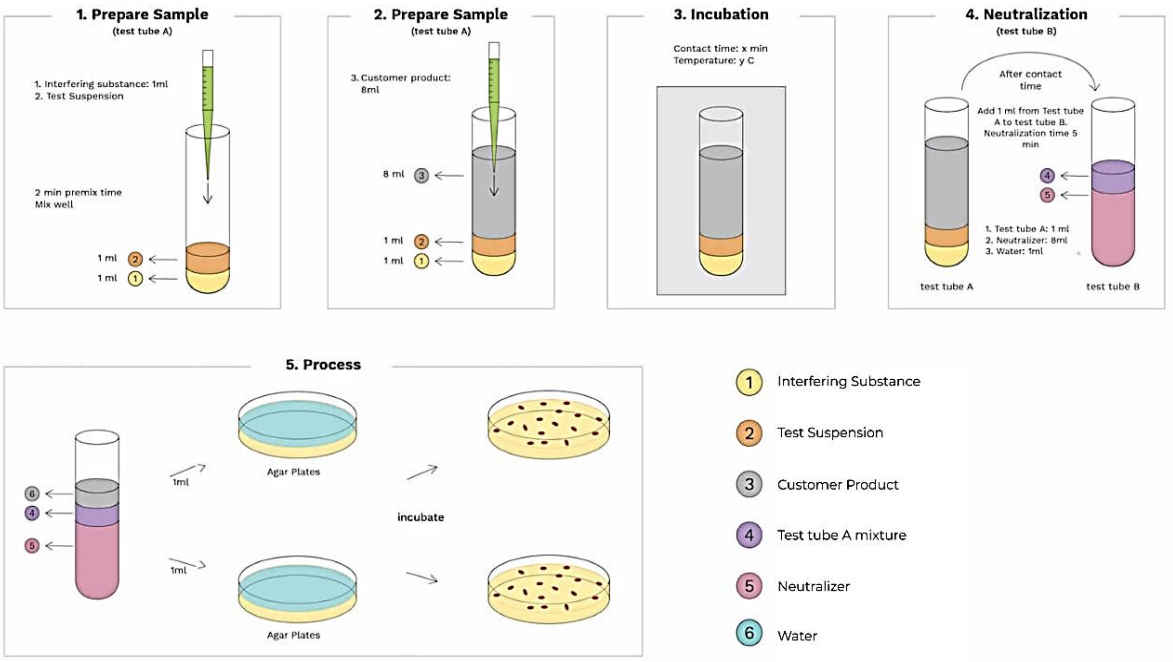

Figure 2.18. *EN 1276 illustration* [25]

2.4.3. Minimum Inhibitory Concentration (MIC)

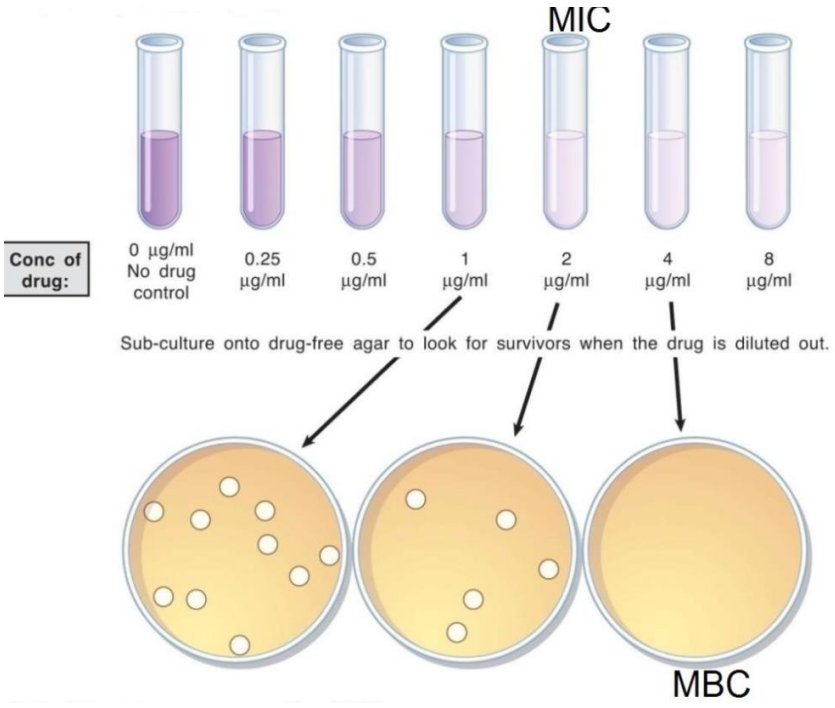

Figure 2.19. *MIC/MBC illustration* [26]

Stock solution of nanomaterial was diluted using Muller and Hinton agar to achieve some different concentrations. Mixture was vortex well and pour onto sterile petri plate and allowed to solidify. After solidification, 10^8 cfu/mL of saline suspension of test organisms *E. coli* and *S. aureus* were streaked on every plate and incubated at 37°C for 48 hours. Inhibition of growth was judged by comparison with growth in control plates. The MIC was defined as the lowest concentration of particles that showed no visible growth after incubation (Figure 2.19) [26], [27].

2.5. Antioxidant properties: Free radical scavenging potency

The anti-oxidant efficacy has been determined by using the DPPH assay. The DPPH assay is amongst the most prominent and widely used procedures for testing substances' potential to function as free radical scavengers, as well as to assess the antioxidant potential of products. Once a DPPH radical solution is combined with an antioxidant/reducing agent, the appearance of the matching hydrazine changes from purple to yellow (Figure 2.20). The capacity of antioxidants to reduce DPPH may be assessed by measuring the reduction in absorbance at 515-528 nm as the produced matching hydrazine DPPH gives a yellow solution, or by electron spin resonance.

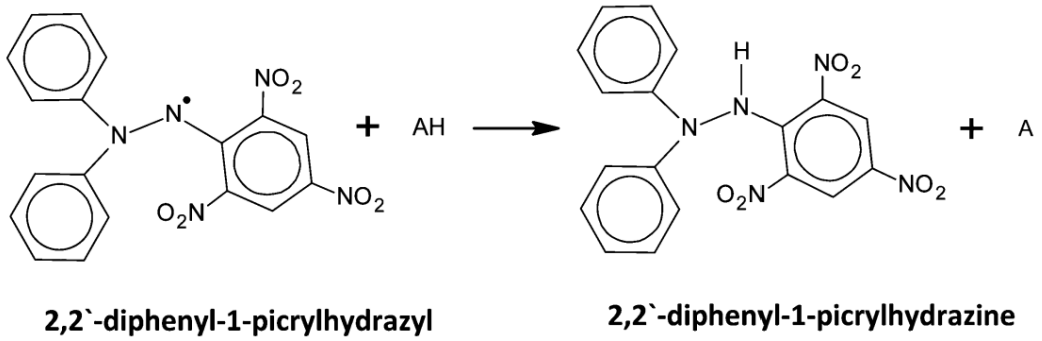

Figure 2.20. *Structure of DPPH and its reduction by an antioxidant* [28]

Methanolic solution of 1.52*10-4 M of DPPH was used in 1:1 ratio with sample at varying concentrations. Anti-oxidant efficacy percentage was examined after incubating the mixture of nanomaterial with DPPH for 30 min and recording the absorption at 517 nm. The half-maximal inhibitory concentration (IC50) is measured to study the antioxidant potency of nanoparticles to reduce the DPPH. The control samples were prepared using DPPH solution and mixed only with respective solvents (aqua/methanol) at a 1:1 ratio and measured at 517 nm.

Antioxidant efficacy % = (Control "(abs)" -Sample" (abs)")/Control" (abs)" ×100

2.6. Photostability studies

The sodium salt of long chain fatty acid infused with and without nano ZnO-SPA were placed under direct sunlight for 10 days. The product's processing, packaging, and lifespan can all be impacted by photostability. Forced degradation assessment and confirmatory analysis should be the two aspects of a product's photostability test. The goal of accelerated degradation investigations is to identify the degradation process and assess the product's overall photosensitivity. A photodegradable molecule degrades when it is exposed to photons, especially those with wavelengths similar to those of sunshine, such as infrared radiation, visible light, and ultraviolet light. However, photodegradation can also be brought on by other types of electromagnetic radiation.

Figure 2.21. *Photograph of Xrite Ci 4200*

Their photostability studies were performed by measuring their change in L, a, b values (color) using Xrite Ci 4200 (reflectance spectrophotometer) to evaluate and establish protecting effect of nano ZnO-SPA in the soap bar matrix under direct sunlight comprising high energy UV-rays (Figure 2.21). The spectrophotometer was calibrated by using white standard and black light trap standard and color ordinate measurement (L, a, b value) of test sample was measured every 2 days.

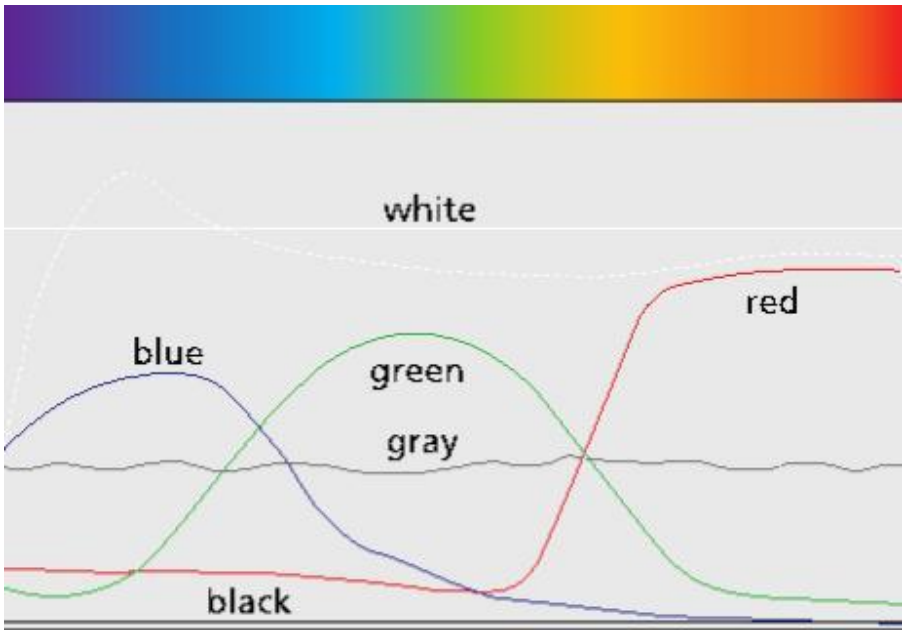

Figure 2.22. *Spectral reflectance curve*

A multi-angle spectrophotometer called X-rite was used to assess colors of various finishes like metallic, iridescent and pearlescent. This device counts the percentage of light that reflects back or passes through after illuminating a beam of light to determine color using its reflectance curve.

Since a white surface reflects all visible light energy, its reflectance curve is linear between 90 and 100% of the time (Figure 2.22). Since black absorbs practically all of the light's energy, its reflectance curve is flat and nearly zero. Near the region of the spectrum which are most reflected, different colors peak [29], [30].

References

[1] J. K. Patra and K.-H. Baek, "Green Nanobiotechnology: Factors Affecting Synthesis and Characterization Techniques," *J. Nanomater.*, vol. 2014, pp. 1–12, 2014, doi: 10.1155/2014/417305.

[2] R. Thiruvengadathan, V. Korampally, A. Ghosh, N. Chanda, K. Gangopadhyay, and S. Gangopadhyay, "Nanomaterial processing using self-assembly-bottom-up chemical and biological approaches," *Reports Prog. Phys.*, vol. 76, no. 6, p. 066501, Jun. 2013, doi: 10.1088/0034-4885/76/6/066501.

[3] V. Harish *et al.*, "Nanoparticle and Nanostructure Synthesis and Controlled Growth Methods," *Nanomaterials*, vol. 12, no. 18, p. 3226, Sep. 2022, doi: 10.3390/nano12183226.

[4] S. M. Shaban, J. Kang, and D.-H. Kim, "Surfactants: Recent advances and their applications," *Compos. Commun.*, vol. 22, p. 100537, Dec. 2020, doi: 10.1016/j.coco.2020.100537.

[5] M. S. Bakshi, "How Surfactants Control Crystal Growth of Nanomaterials," *Cryst. Growth Des.*, vol. 16, no. 2, pp. 1104–1133, Feb. 2016, doi: 10.1021/acs.cgd.5b01465.

[6] M. Lodén and W. Wessman, "The influence of a cream containing 20% glycerin and its vehicle on skin barrier properties," *Int. J. Cosmet. Sci.*, vol. 23, no. 2, pp. 115–119, Apr. 2001, doi: 10.1046/j.1467-2494.2001.00060.x.

[7] A. Venkatachalam, J. P. Jesuraj, and K. Sivaperuman, "Moringa oleifera Leaf Extract-Mediated Green Synthesis of Nanostructured Alkaline Earth Oxide (MgO) and Its Physicochemical Properties," *J. Chem.*, vol. 2021, pp. 1–22, Jun. 2021, doi: 10.1155/2021/4301504.

[8] A. Rónavári *et al.*, "Green Silver and Gold Nanoparticles: Biological Synthesis Approaches and Potentials for Biomedical Applications," *Molecules*, vol. 26, no. 4, p. 844, Feb. 2021, doi: 10.3390/molecules26040844.

[9] K. Akhtar, S. A. Khan, S. B. Khan, and A. M. Asiri, "Scanning Electron Microscopy: Principle and Applications in Nanomaterials Characterization," in *Handbook of Materials Characterization*, Cham: Springer International Publishing, 2018, pp. 113–145.

[10] K. D. Vernon-Parry, "Scanning electron microscopy: an introduction," *III-Vs Rev.*, vol. 13, no. 4, pp. 40–44, Jul. 2000, doi: 10.1016/S0961-1290(00)80006-X.

[11] B. Hecht *et al.*, "Scanning near-field optical microscopy with aperture probes: Fundamentals and applications," *J. Chem. Phys.*, vol. 112, no. 18, pp. 7761–7774, May 2000, doi: 10.1063/1.481382.

[12] "Bragg condition/law/Bragg scattering/Bragg angle." https://www.globalsino.com/EM/page3882.html.

[13] D. D. Le Pevelen, "Small Molecule X-Ray Crystallography, Theory and Workflow," in *Encyclopedia of Spectroscopy and Spectrometry*, Elsevier, 2010, pp. 2559–2576.

[14] T. M. G. Selva, J. S. G. Selva, and R. B. Prata, "Sensing Materials: Diamond-Based Materials," in *Encyclopedia of Sensors and Biosensors*, Elsevier, 2023, pp. 45–72.

[15] C. O. Colpan, Y. Nalbant, and M. Ercelik, "4.28 Fundamentals of Fuel Cell Technologies," in *Comprehensive Energy Systems*, Elsevier, 2018, pp. 1107–1130.

[16] K. Torres-Rivero, J. Bastos-Arrieta, N. Fiol, and A. Florido, "Metal and metal oxide nanoparticles: An integrated perspective of the green synthesis methods by natural products and waste valorization: applications and challenges," 2021, pp. 433–469.

[17] D. Titus, E. James Jebaseelan Samuel, and S. M. Roopan, "Nanoparticle characterization techniques," in *Green Synthesis, Characterization and Applications of Nanoparticles*, Elsevier, 2019, pp. 303–319.

[18] "UV-Vis Spectroscopy," Ucalgary.ca, 2022.

[19] "Schematic of UV- visible spectrophotometer," 2013. https://commons.wikimedia.org/wiki/File:Schematic_of_UV-_visible_spectrophotometer.png.

[20] E. Forgács and T. Cserháti, "Gas chromatography," in *Food Authenticity and Traceability*, Elsevier, 2003, pp. 197–217.

[21] E. Stauffer, J. A. Dolan, and R. Newman, "Gas Chromatography and Gas Chromatography—Mass Spectrometry," in *Fire Debris Analysis*, Elsevier, 2008, pp. 235–293.

[22] "Viscometer (BROOKFIELD) - Laboratoire MAPIEM (EA 4323)." https://mapiem.univ-tln.fr/Rheometer-BROOKFIELD-rvt.html.

[23] "Disk diffusion test," 2019.

[24] M. Azizi-Lalabadi, A. Ehsani, B. Divband, and M. Alizadeh-Sani, "Antimicrobial activity of Titanium dioxide and Zinc oxide nanoparticles supported in 4A zeolite and evaluation the morphological characteristic," *Sci. Rep.*, vol. 9, no. 1, p. 17439, Nov. 2019, doi: 10.1038/s41598-019-54025-0.

[25] I. C. MIS," Swiss Anti-Bacterial & Anti-Viral Testing Laboratory, "EN 1276 Test - Chemical Disinfectants & Antiseptics." https://microbe-investigations.com/en-1276/.

[26] A. Tankeshwar, "Minimum Inhibitory Concentration (MIC) and Minimum Bactericidal Concentration (MBC)," 2020. https://microbeonline.com/minimum-inhibitory-concentration-and-minimum-bactericidal-concentration-mbc/.

[27] K. S. Siddiqi, A. ur Rahman, Tajuddin, and A. Husen, "Properties of Zinc Oxide Nanoparticles and Their Activity Against Microbes," *Nanoscale Res. Lett.*, vol. 13, no. 1, p. 141, Dec. 2018, doi: 10.1186/s11671-018-2532-3.

[28] K. Pyrzynska and A. Pękal, "Application of free radical diphenylpicrylhydrazyl (DPPH) to estimate the antioxidant capacity of food samples," *Anal. Methods*, vol. 5, no. 17, p. 4288, 2013, doi: 10.1039/c3ay40367j.

[29] "X-Rite Color Management, Measurement, Solutions, and Software." www.xrite.com/.

[30] "What Is a Spectrophotometer?" www.xrite.com/blog/what-is-a-spectrophotometer#:~:text=types available today. (accessed Nov. 14, 2022).

Chapter 3

Surfactant Mediated Nano ZnO into Soap Matrix and Liquid Cleansing Products for Enhanced Health and Hygiene Applications

Highlights of the Chapter:

- *This research demonstrates, a facile approach to fabricate the nano ZnO system in a unique combination of surfactant-polyol-assembly (SPA) acting as a caging agent restricting the ZnO crystallite size in nano-regime.*
- *The fabricated nano ZnO in SPA were systematically characterized using various advanced and appropriate techniques. This SPA is suitable for health and hygiene products.*
- *The antibacterial efficacy of nano ZnO-SPA were investigated against Staphylococcus aureus (S. aureus) and Escherichia coli (E. coli) by Zone of Inhibition (ZOI) and European standard EN:1276.*
- *Established the impact of embedding low concentrations of nano ZnO system into the matrix of sodium salt of long chain fatty acids (soap bar) and liquid cleansing personal care products.*
- *The infused products were systematically characterized using various advanced and appropriate techniques. Soap bar without ZnO experienced photodegradation and reduction in whiteness which clearly reflects the increased photostability of soap bar.*
- *The antibacterial efficacy of infused products is investigated against Staphylococcus aureus (S. aureus) and Escherichia coli (E. coli) by Zone of Inhibition (ZOI) and European standard EN:1276. Infused products exhibited high antibacterial efficacy up to >99.99% germ kill.*

This work has been published in:

Bhalla, N., Ingle, N., Patel, H., Jayaprakash, A., Patri, S.V., Kaushik, A. and Haranath, D. (2022b), **Arabian Journal of Chemistry**, 15(6), p.103862. doi:10.1016/j.arabjc.2022.103862. **IF. 6**

3.1. Introduction

Nanoscale materials science have gained enormous attention in the last couple of decades, thereby transforming industries due to their advancements and influencing lives of people in various perspectives [1]–[6]. Transition metal oxides have played an important role since ancient times and still plays an equally pivotal role in the era of nanotechnology with applications in diverse fields like medicine, polymer composites [7], electronic technology [8], solar energy [9], personal care, cosmetic [10], food, photocatalytic activity [11][12], bio sensing, light-emitting diodes, etc. ZnO nano systems have potential applications at room-temperature UV lasers [13], and transistor sensor [14], due to its exclusive optical & electrical properties like high chemical stability, low dielectric constant, having piezoelectric and photoelectric behaviors [15], [16]. ZnO is an important member of the wurtzite family having a hexagonal crystal lattice and wide bandgap II-VI group semiconductor. Various routes to synthesize ZnO and their doped system have been reported in the literature comprising attrition method which involves the breaking of coarse particles into nano dimension using high energy ball mills [17], solvothermal [18], vaporization [19], combustion route [20], sol-gel [21], assembly assisted [22] etc.

ZnO at nanoscale due to significant benefits such as tunable morphological characteristics, dimensional stability, and chemical stability, and have been adopted as a crucial material for several photonics and electronics based advanced applications [23]. As a result, investigation of structural factors becoming increasingly important for improving the efficiency of ZnO nanomaterial related applications.

Key demerits associated with aforementioned synthesis methodologies are: (i) used solvents are expensive, possibly toxic and flammable [23] (ii) energy intensive techniques [24] (iii) solvents or generated by-products are either not permitted or affects stability of health and hygiene products and (iv) introduce harmful marine ecosystems. Therefore, there is still a lot to unleash in ZnO fabrication methodologies as well as selection of appropriate precursors.

This research is aims to address the major concerns mentioned above in the health and hygiene products by fabricating multifunctional nano ZnO-SPA system. This work may be the first or among the very few reports where authors have explored this unique surfactant and polyol combination, perfectly suitable precursors for personal care industry that aid in keeping the crystallite size of ZnO in nano-regime. SLES is an anionic surfactant that is cost effective material that is commonly used in health and hygiene industry especially cleansing products.

Glycerin is also a well-known co-surfactant for engineering nanoscale materials when additionally acts as humectant preventing the trans epidermal water loss to keep the skin moisturized [25]. Therefore, presented SPA based nano ZnO synthesis strategy has several advantages such as high compatibility with health and hygiene, personal care products especially liquid cleansing products, non-toxic, low cost solvents, low energy consuming, non-intensive process and is a one-step fast synthesis without any additional process like calcinations and milling.

The current method takes advantage of unique properties of surfactant and polyol combination such as micellar formation and their cage-like matrix to synthesize ZnO in nanoscale and restricting the particle growth. This method thus uses assemblies and caging agents specifically to make synthesized ZnO suitable for industrial applications like health and hygiene, personal care and cosmetic products. The synthesized nano ZnO-SPA has high ZOI of 13 mm in comparison to recent development reports for titanium dioxide (TiO2), zinc oxide (ZnO), and TiO_2/ZnO nanoparticles supported into 4A (alumina silicates) zeolite studied by Azizi et.al. and hybrid films containing 1%, 2%, and 4% ZnO NPs studied by Santosh Kumar et.al showing the ZOI of only 6-10 mm [26], [27]. The synthesized nano ZnO-SPA possess high specific surface area 52.99 m^2/g compared to previously explored ZnO nanoparticles having only 25–27 m^2/g reported for ZnO nanoparticles synthesized by continuous precipitation approaches [28-29].

3.2. Synthesis of nano ZnO in SPA system

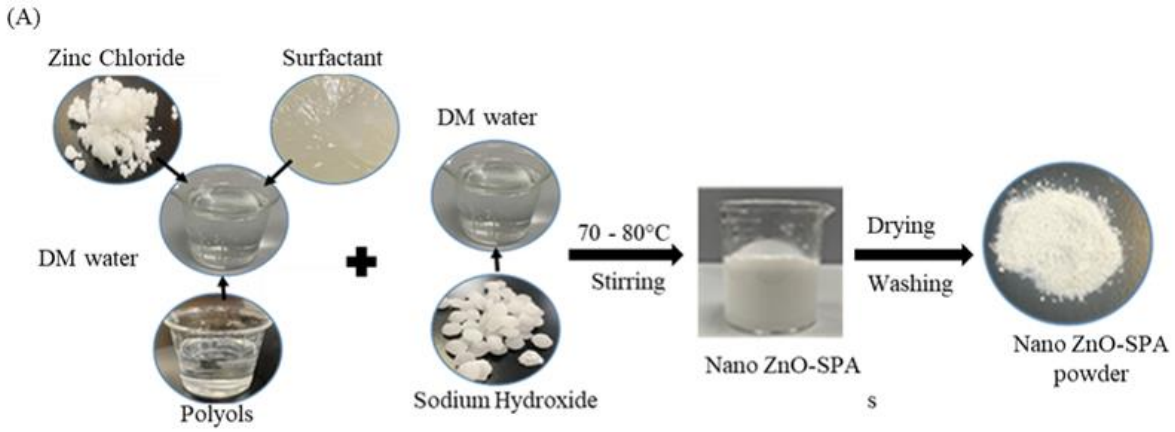

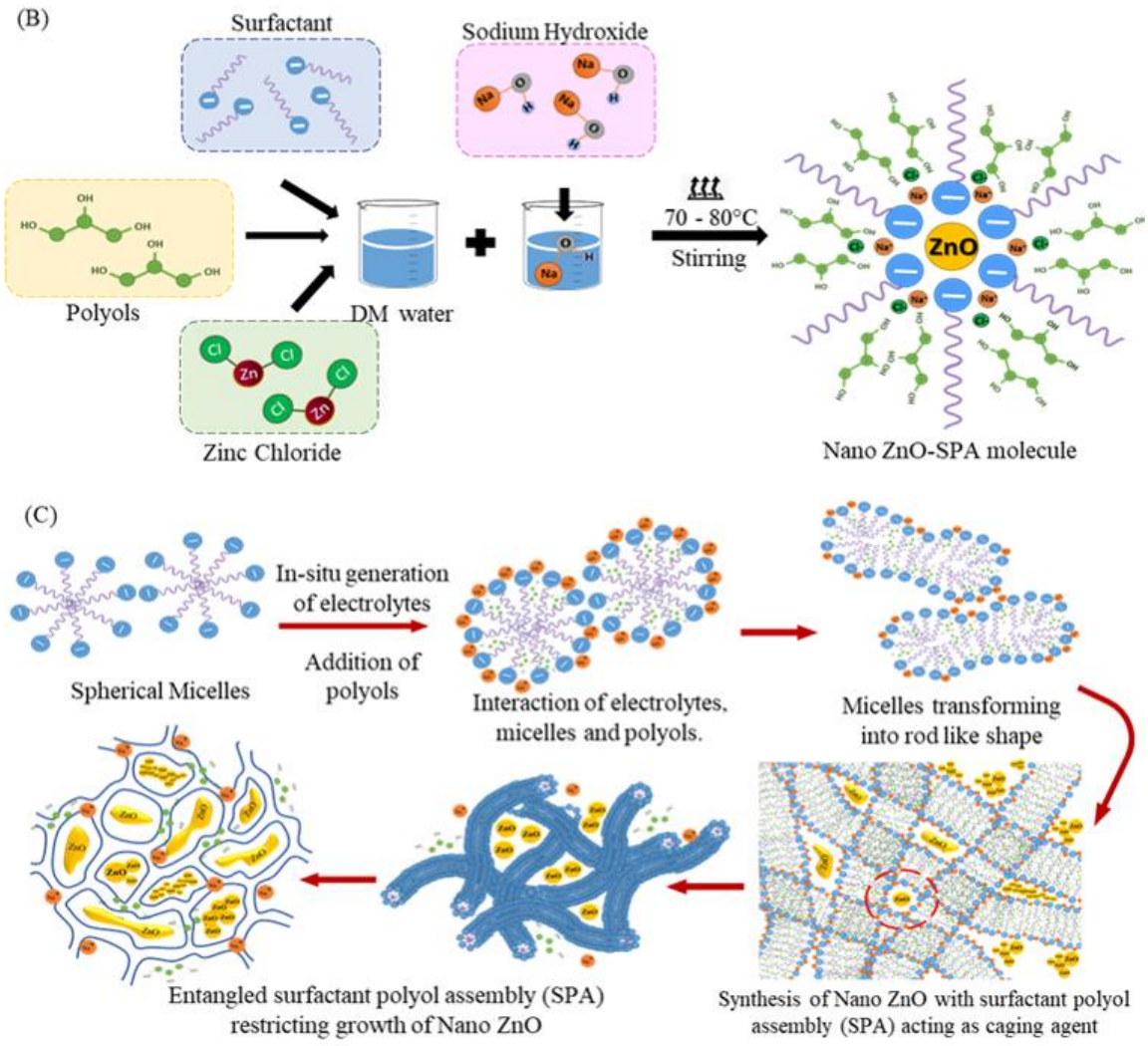

Figure 3.1: *(A and B) Systematic and mechanistic presentation to fabricate nano ZnO in SPA (C) Illustrative mechanism of caging of nano ZnO in SPA.*

3.2.1. Materials required

Zinc chloride-97% [SD Fine-chem Ltd.], distilled water pH of 5.5-7.0 with conductivity 1 µS/cm. Sodium Lauryl Ether Sulfate (SLES-2EO 70%), Cocamidopropyl Betaine (CAPB 30%) [Galaxy Surfactant India], Glycerin (Polyol) [International Foodstuffs Company (IFFCO) Malaysia, SDN BHD (IMSB)], Sodium hydroxide- 99% [VWR International], Soap noodles (65% Total Fatty Matter) [IFFCO, Egypt], Calcium nitrate, Methyl orange, Nitric acid, Phenol red indicator, Silver nitrate, Potassium chromate, Sulfuric acid, Ethylene glycol [SD Fine-chem Ltd.]. Bacterial strains *Escherichia coli (E.coli)* ATCC 10536 and *Staphylococcus. aureus (S.aureus)* ATCC 6538 were obtained from ATCC (American Type Culture Collection) in Dubai, UAE.

3.2.2. Synthesis of nano ZnO in surfactant system

The SPA in aqueous medium prepared by taking 0.57 M SLES-2EO and 1.63 M of Glycerin. To the above mixture added 0.60 M of $ZnCl_2$ followed by stoichiometric steady addition of 1.23 M NaOH solution and with continuous stirring. The temperature maintained at 70 - 80°C during reaction and mixed until uniform white homogeneous mix obtained indicating successful synthesis of nano ZnO-SPA. The reaction equation for synthesis of nano ZnO is as follows:

$$ZnCl_2 + 2NaOH \rightarrow Zn(OH)_2 + 2NaCl$$
$$Zn(OH)_2 \rightarrow ZnO + H_2O$$

Obtained morphologies in SEM correlates with proposed mechanism and hypothesis. Systematic and mechanistic presentation of synthesis of nano ZnO in SPA acting as caging agent is shown (Figure 3.1 A, B and C**).** The synthesized samples were centrifuged, washed, and dried for further evaluation.

The samples have been characterized for UV–Visible, FTIR, spectrums, SEM, EDX, XRD analysis as well as rheological properties using the techniques mentioned earlier in Chapter 3.

3.3. Results and discussion

3.3.1. UV–Visible spectroscopic studies

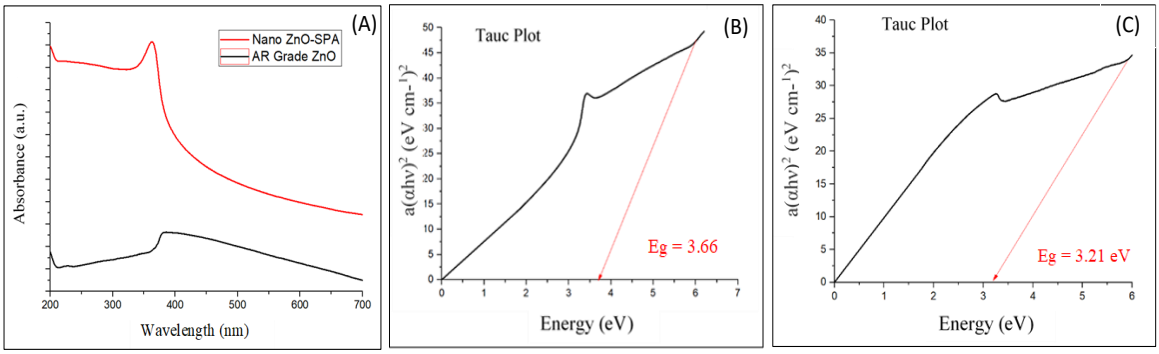

Figure 3.2: *(A) UV–Vis spectra of nano ZnO synthesized in SPA and spectrum of AR Grade ZnO. Tauc plots of $a(\alpha hv)^2$ ($eV\ cm^{-1})^2$ as function of photon energy hv (eV) for (B) nano ZnO and (C) AR Grade ZnO.*

Optical absorption spectra of synthesized nano ZnO-SPA and AR grade ZnO was recorded in the range of 200-700 nm. The absorption spectroscopy shows the typical peak absorption of ZnO in UV region and the band gap energy was determined by plotting Tauc plot. The analytical grade ZnO exhibits the absorption peak at 386 nm with energy band gap (E_g = 3.21 eV)

correspondingly nano ZnO-SPA exhibit the blue shift with absorption peak at 338 nm reflecting higher energy band gap (E_g = 3.66 eV) (Figure 3. 2 A, B and C). Blue shift of UV spectra is observed with particle size reduction of nano ZnO-SPA with respect to bulk AR grade ZnO. This could be due to multiple reasons however, can attributed to quantum confinement effect which describes that band gap energy is inversely related to particle size, and shows a blue shift as the particle size decreases [30]. When the size of the particle decreases and approaches the size of the electron-hole distance, the energy levels of that particle becomes quantum confined and discrete thus confining the motion of electron [31], [32]. It is also apparent that significant sharp absorption of nano ZnO synthesized in SPA reflects the narrow size distribution of the nano ZnO.

3.3.2. Fourier-Transform Infrared (FTIR) spectroscopy for functionality assessment

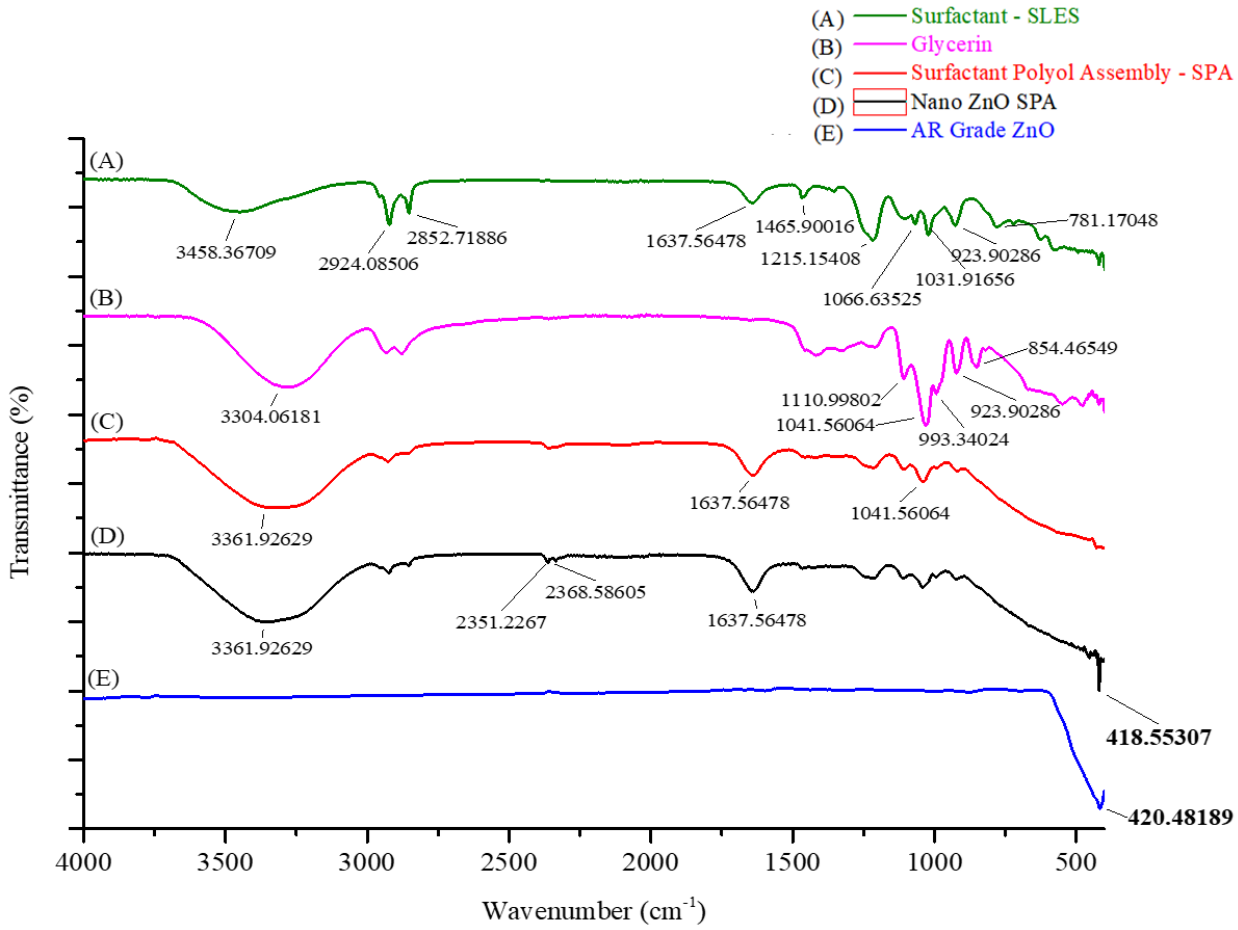

Figure 3.3: *FTIR spectrum of (A) Surfactant- SLES (B) Glycerin (C) Surfactant polyol assembly-SPA (D) Nano ZnO-SPA and (E) AR Grade ZnO in the spectral range of 400–4000 cm^{-1}.*

FTIR spectrum of Surfactant (SLES), Polyol (Glycerin), Surfactant polyol assembly- SPA, nano ZnO-SPA and AR grade ZnO exhibits the functional group in the following different regions (Figure 3.3 (A, B, C, D and E)), fingerprint region (<1500 cm^{-1}), double bond region (1500-2000 cm^{-1}), triple bond region (2000-2500 cm^{-1}), single bond region- 2500-4000 cm^{-1}). Spectrum (A, B, C and D) exhibits the sharp broad peaks in the range of 3361 cm^{-1} – 3458 cm^{-1} in single bond region it evidently specifies the existence of hydroxyl (OH) group which can be attributed to the presence of polyol (glycerol) used during synthesis and H_2O molecules. Two weak peaks at 2924 cm^{-1} & 2852 cm^{-1} observed in spectrum (A, B, C and D) are due to C-H stretching: one for symmetrical and other for asymmetrical vibrational frequency. This evidently stipulate the existence of a long-chain linear aliphatic compound of SLES-2EO surfactant. While peaks at 2351 cm^{-1} and 2368 cm^{-1} in spectrum (C and D) can be attributed to O=C=O stretching possibly due existence of impurity during synthesis or measuring environmental conditions. The peak at 1637 cm^{-1} in spectrum (A, C and D) could be related moisture or to the impurity coming through the SLES used during the synthesis. The two peaks at 1465 cm^{-1} and 781 cm^{-1} in spectrum (A) could be because of long chain linear aliphatic compounds. The peak at 1215.15 cm^{-1} exhibit the existence of S=O vibrations of sulfur-oxy compounds in SLES-2EO [33], [34]. The peak at 1110.9 cm^{-1} in spectrum (B, C and D) is due to the C-O stretching vibration of secondary alcohol group while peak around at 1041 cm^{-1} and 1031 cm^{-1} in spectrum (A, B, C and D) suggest deformation vibration of (CH) + (C-C) [35]. The peak at 993 cm^{-1} in spectrum (B, C and D) indicate the existence (C-C) vibration. The peak at 923 cm^{-1} and 854 cm^{-1} in spectrum (A, B, C and D) could be attributed for asymmetric C-O-C stretching of surfactant and polyol molecules. The peak in spectrum (D) at 418.55 cm^{-1} shows the presence of nano ZnO similar to AR grade ZnO peak at 420 cm^{-1} shown in spectrum (E). Several literatures stated the ZnO peak at 410 cm^{-1} to 440 cm^{-1}. These results are in line with reported research work [36].

3.3.3. X-Ray Diffractometer (XRD) analysis for purity assessment

The crystalline structure of nano ZnO-SPA and AR grade is shown in (Figure 3.4 A and B). XRD peaks of powder nano ZnO synthesized in SPA confirms the hexagonal wurtzite structure and the results agree with the results reported by other literatures [37]. The diffraction peaks of nano ZnO-SPA is distinguished at 2θ of 32.05°, 34.69°, 36.52°, 37.09°, 47.78°, 56.82°, 63.06°, 63.48°, 66.58°, 68.14° and 69.26° (Table 3.1). The observed planes for both the samples are well

aligned with JCPDS 36–1451, Figure 3.4 (C). Sharp and intense peaks reflect the high crystallinity of the synthesized ZnO.

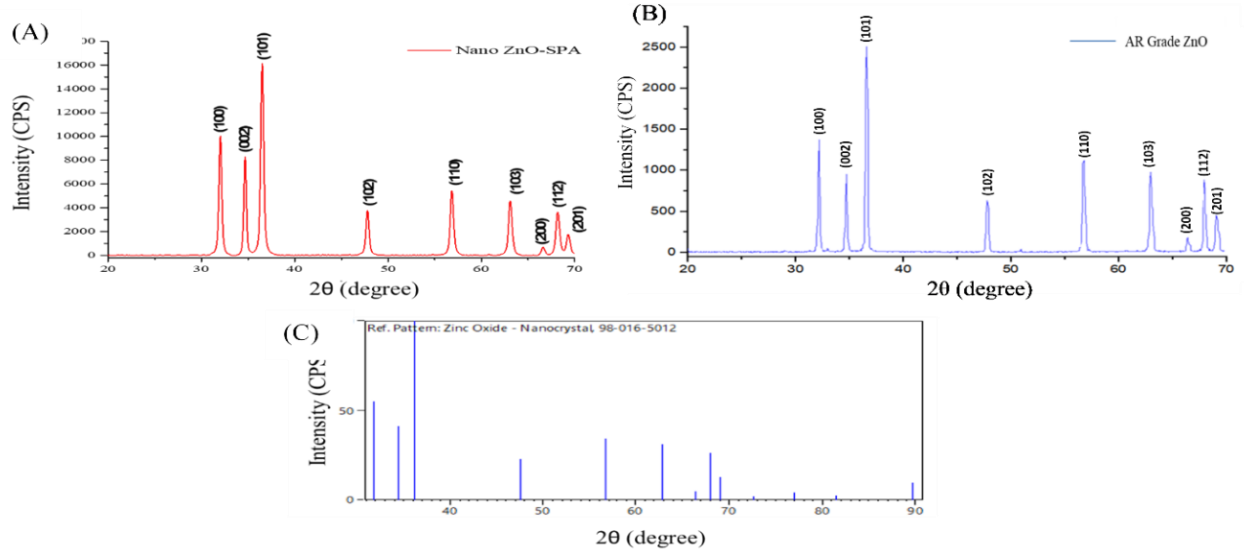

Figure 3.4: *(A) XRD pattern of nano ZnO-SPA, (B) XRD pattern of AR Grade ZnO (C) JCPDS ZnO standard card for reference.*

The average crystallites size of nano ZnO-SPA is 20.18 nm (Table 3.1) and AR grade ZnO is 30.87 nm (Table 3.2) enumerated using the Debye-Scherrer equation,

$$D = K\lambda/\beta \cos\theta$$

D-crystallites size, λ-The wavelength of X-ray, K-Scherrer constant (0.9), θ-Braggs angle in radians, β-Full width at half maxima of the peak in radians.

Table 3.1. Crystallites size and miller index of nano ZnO-SPA by XRD.

Sr. No.	Peak Position 2θ (Degree)	d-spacing (Å)	FWHM (deg)	Crystallite size D (nm)	Average crystallite size D (nm)	Miller Indices
1	32.0506	2.7903	0.3381	22.583		(100)
2	34.687	2.5832	0.2944	25.757		(002)
3	36.52	2.458	0.3594	20.991		(101)
4	47.78	1.9019	0.3471	20.926		(102)
5	56.82	1.619	0.3481	20.073	20.18	(110)
6	63.06	1.4729	0.3559	19.026		(103)
7	66.58	1.4034	0.3567	18.616		(200)
8	68.14	1.375	0.3757	17.515		(112)
9	69.26	1.3553	0.4032	16.212		(201)

Specific surface area evaluation: Specific surface area is property of solid materials which measure total surface area per unit mass of bulk volume, solid or cross-sectional area.

The specific surface area can be evaluated by using following equation,

$$S = 6 \times 10^3 / D_P \times \rho$$

where S- Specific surface area, D_P − size of particle, ρ- density of ZnO 5.61 g/cm^3.

The specific surface area of nano ZnO-SPA crystallites was found to be 52.99 m^2/g which is relatively higher specific surface area than AR grade ZnO which is 41.34 m^2.g^{-1} as seen in Table 3.2. High specific surface area could be due to obvious reason of miniaturization of particle size which is inversely proportional to specific surface area. This high specific area can play a vital role to contribute towards the high antibacterial efficacy of nano ZnO-SPA due to high surface availability and disrupting the cell wall of disease-causing germs.

Lattice Parameter evaluation: The lattice parameters a, b and c of nano ZnO-SPA and AR grade ZnO structures were calculated by using the following equations:

$$\frac{1}{d_{hkl}^2} = \frac{4}{3}\left(\frac{h^2 + hk + k^2}{a^2}\right) + \frac{l^2}{c^2}$$

where for hexagonal unit cell lattice $a=b \neq c$, λ -wavelength of the XRD, *n*- order of diffraction, d_{hkl}- interplanar spacing, *hkl* is the Miller indices. The XRD analysis reveal peaks consistent to hexagonal wurtzite ZnO crystals with (*hkl*) values corresponding to that of standard JCPDS card Table 3.2. The lattice parameter of nano ZnO-SPA is found to be a = 3.22 and c = 5.16 while the *c/a* ratio is 1.6034. The lattice parameter of AR grade ZnO is found to be a = 3.27 and c = 5.24 while the *c/a* ratio is 1.6008 which is tabulated in Table 3.2.

Table 3.2. Average crystallite size, lattice parameter and bond length of nano ZnO-SPA and AR grade ZnO using XRD.

Nano material	**Average crystallite size (nm)**	**Lattice parameters (Å)**		**Average dislocation density (δ) (lines/m^2)**	***u***	***c/a* ratio**	**Bond Length (Å)**	**Specific surface area (m^2/g)**
		a	***C***				***L***	
Nano ZnO-SPA	20.18	3.22	5.16	0.002	0.44	1.6034	1.882	52.99
AR Grade ZnO	30.87	3.27	5.24	0.0017	0.44	1.6008	1.911	41.34

The length of dislocation lines per unit volume (dislocation density) of nano ZnO-SPA and AR grade ZnO is 0.002 and 0.0017 lines/m^2 respectively calculated using the equation: $\delta = \frac{1}{D^2}$

Dislocation density is the measure of defects in a system, when there is a rise in density of delocalized electrons due to high defects the attraction of delocalized electrons and nuclei increases thus increasing stability. Rise in density of delocalized electrons have also been known to provide energetic surface to nanoparticles due to increase in percentage of surface atoms [38]–[40]. This factor contributes highly in the antibacterial efficacy of nano ZnO-SPA.

The Zn–O bond length of nano ZnO-SPA and AR grade ZnO is 1.882 and 1.911 Å respectively calculated by the following equation.

$$L = \sqrt{\frac{a^2}{3} + \left(\frac{1}{2} - u\right)^2 \, c^2}$$

Where, *u* parameter in the wurtzite structure of nano ZnO-SPA and AR grade ZnO is 0.44 calculated by following equation.

$$u = \frac{a^2}{2c^2} + 0.25$$

3.3.4. Scanning Electron Microscopy Analysis

The surface morphology analysis of powdered nano ZnO-SPA was done by scanning electron microscopy (SEM, JSM-6010 PLUS ILA) Figure 3.5 (A, B and C). Nano ZnO-SPA appeared as ultrafine rods and white spherical dots in the images with a size around 500 nm as associated with the scale. The ZnO nanoparticles asymmetrically distributed on the surface shows the agglomeration. These morphologies of nano ZnO could be due to their growth in restricted entangled cage of rod like micelles of surfactant formed in the presence of polyol and electrolyte (NaCl) generated as by product during the reaction. This electrolyte contributes towards the reduction of the gap between negative head group of surfactants resulting in the change of surfactant packing parameters and shifting the shape of micelles more towards rod like from spherical shapes. These rod-like micelles entangled with each other and enhance the viscosity of medium to a certain extent and act as caging matrix to restrict the particle growth. The EDS exhibits the quantitative elemental composition of nano ZnO powder at different sites Figure 3.5 (A, B and C)) which reflect the high purity with the elemental composition of mass % Zn – 79.64 and O - 20.36, Zn - 88.97 and O - 11.03, Zn - 77.50 and O - 22.50 shown in Figure 3.5 (D, E and F).

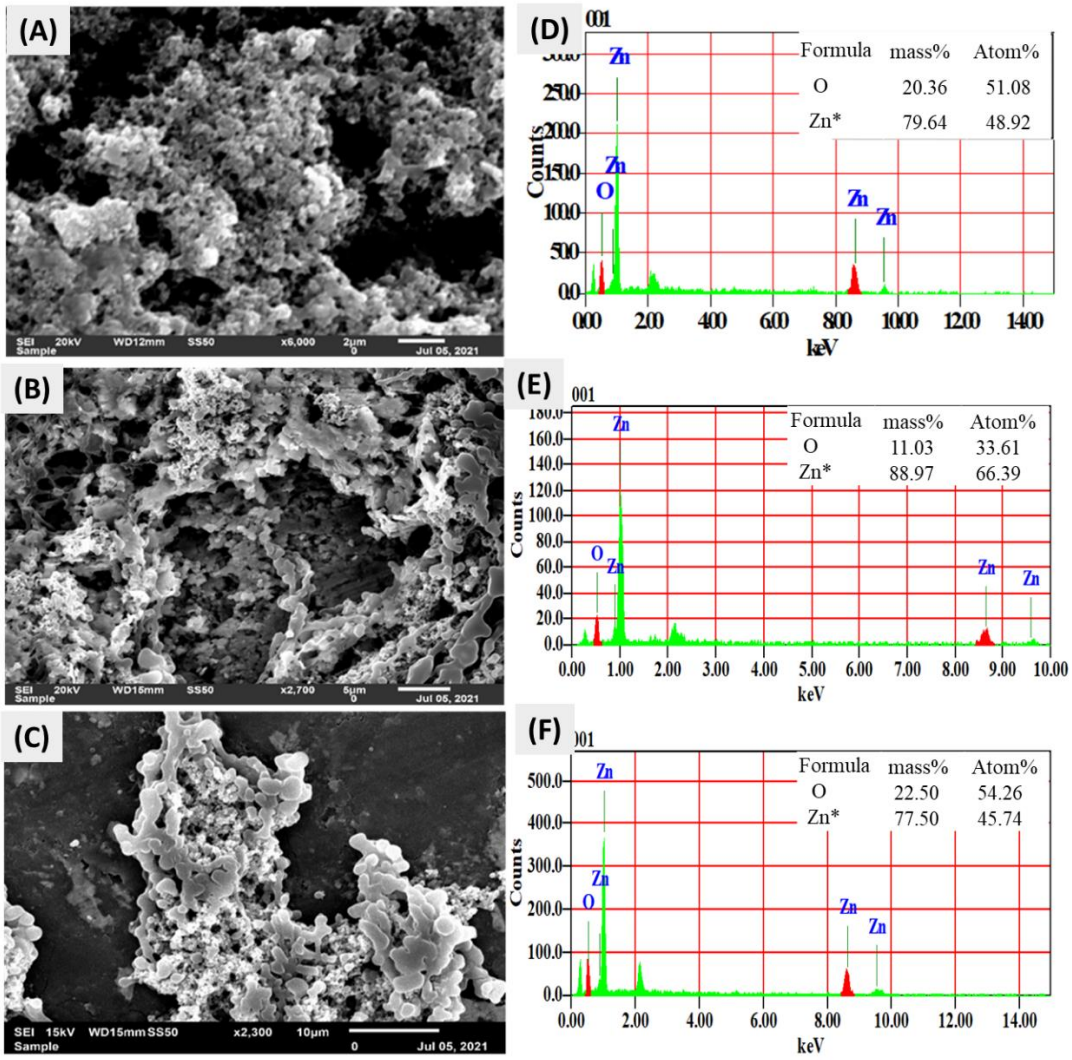

Figure 3.5: *(A, B and C) Representative SEM images of powdered nano ZnO-SPA, (D, E and F) EDS of powdered nano ZnO-SPA revealing the elemental composition in graphical and tabulated form respectively*

3.3.5. EDX-assisted elemental evaluation of nano ZnO-SPA systems

Table 3.3. Quantitative elemental analysis of nano ZnO-SPA by EDX.

Analytes	Result %	[3-sigma]	Line	Int.(cps/uA)
ZnO	53.33	0.11	ZnKα	3362.33
Cl	28.33	0.47	ClKα	50.85
SO_3	18.08	0.25	SKα	5.54

The EDX is the utmost imperative technique for quantitative elemental analysis. Nano ZnO-SPA shows the expected stoichiometric mass of 53.33% ZnO, 28.30% Cl ions, generated as a byproduct in the reaction and 18.07% sulfur trioxide (SO_3) which could be from presence of surfactant (sodium lauryl ether sulfate-2EO) in the sample (Table 3.3) while SO_3 is not present once powdered as seen in above section (Fig. 5 D, E and F). Strong peaks exhibit of ZnKα evidently confirms the presence of ZnO which is synthesized in SPA [41].

The strong peaks of ZnO measured from the line ZnKα and the 3-sigma value is 0.113 with an intensity of 3362 (cps/uA). Chloride (Cl) peak exhibits from line ClKα and the 3-sigma value 0.47, intensity 50.8533 (cps/uA), sulfur trioxide (SO_3) measured from line SKα, 3-sigma value-0.25, intensity 5.547 (cps/uA).

3.3.6. Rheological properties and pH of nano ZnO-SPA

Table 3.4. pH and viscosity of nano ZnO-SPA and constituents.

Sr. No.	Name of material	pH value	Viscosity (cps)
1.0	Surfactant Polyol Assembly (SPA)	7.30	6.07
2.0	Nano ZnO-SPA	7.60	2300
3.0	Zinc Chloride (0.61 M solution)	5.02	2.05
4.0	NaOH (1.23 M solution)	14.0	3.09
5.0	Surfactant (SLES 2EO) (0.57 M solution)	7.40	5.80
6.0	Polyol (Glycerin) (1.63 M solution)	5.50	4.01

The rheological property (viscosity) of the synthesized nano ZnO-SPA, SPA and other materials were evaluated using Brookfield Rheometer and found to be 2300 cps and 6.07 cps for nano ZnO-SPA and SPA respectively (Table 3.4). The in-situ generation of sodium chloride electrolytes during fabrication of nano ZnO-SPA in surfactant (SLES-2EO) and polyol medium cause the conversion of hexagonal surfactant micelles to rod shape micelles, this leads to increased viscosity compared to SPA. The pH of nano ZnO-SPA was found to be 7.60 which is in neutral range thus causing minimal to no effect in the pH of final products. The pH of SPA and all materials used for synthesis of nano ZnO-SPA have been tabulated in Table 3.4.

3.3.7. Antibacterial properties: Zone of inhibition using Kirby Bauer method

Antibacterial properties of nano ZnO-SPA, surfactant polyol assembly (SPA) and AR Grade ZnO were investigated by ZOI through disk diffusion method also called as Kirby Bauer method (Figure 3.6 A and B).

(A)

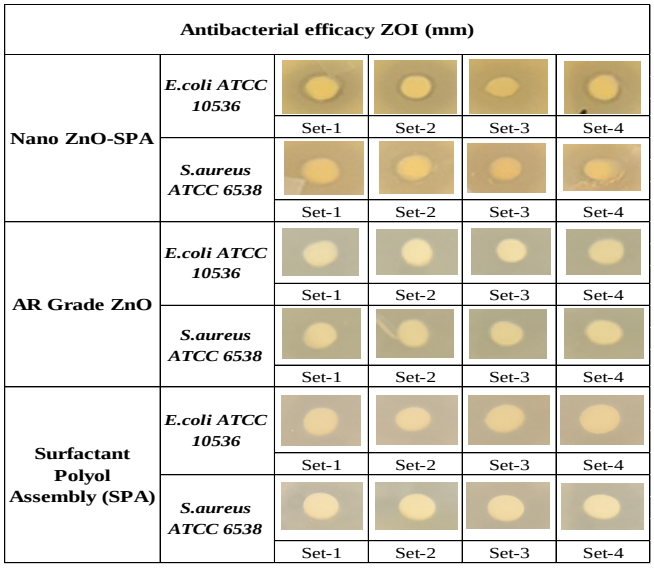

(B)

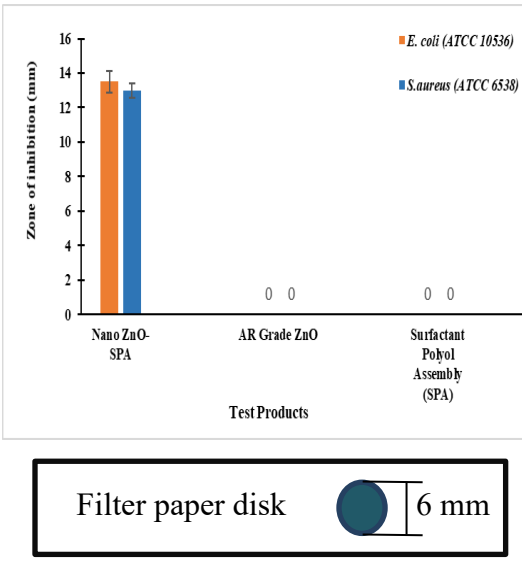

Figure 3.6: *(A) Pictorial and (B) Graphical representation of antibacterial activity (ZOI) of nano ZnO-SPA and AR Grade ZnO against S. aureus & E. coli*

Sample weight of 50 mg each was used for the ZOI study against both Gram-positive *(S. aureus)* and Gram-negative *(E. coli)* bacteria. The ZOI of SPA and AR Grade ZnO was found to be nil. However, nano ZnO-SPA have shown the average ZOI 13.5 mm, standard error 0.6, having *p-value* <0.01 there is significant difference found in the ZOI study of nano ZnO-SPA versus AR Grade ZnO (Table 3.5) [30], [31]. The higher antibacterial efficacy of nano ZnO is due to multiple reasons like higher active surface area available for the contact with microbes per unit mass. Slight lower activity against Gram-positive microbes could be due to their thicker layer of peptidoglycan in cell wall causing higher resistance to ZnO nanoparticles actions.

Table 3.5. Antibacterial activity (ZOI in mm) of nano ZnO-SPA & AR Grade ZnO against E. coli and S. aureus.

Zone of inhibition (mm)							
Sr. No.	**Name of product**	***E. coli***			***S. aureus***		
		Average	**Std. Deviation**	**Std. error**	**Average**	**Std. Deviation**	**Std. error**
1	Nano ZnO-SPA	13.5	1.291	0.645	13	0.8165	0.4082
2	AR Grade ZnO	0	0	0	0	0	0
3	Surfactant Polyol Assembly (SPA)	0	0	0	0	0	0

3.4. Product Applications in Soap Matrix and Liquid Cleansing Products

It has been suggested that not every metal oxide is allowed for cosmetic and personal care applications except a few like ZnO and TiO_2 [42]. Among the five zinc compounds that are allowed as per the list of "General Recognized as Safe (GRAS)", ZnO is a one of the listed compounds which is approved by the Food and drug administration (FDA). Additionally, nanoscale ZnO has the following advantages (i) effective blocker against both UVA and UVB radiation unlike TiO_2 (ii) non-irritating (iii) well-suited with all types of skin (iv) shields against skin irritation and therefore highly used in personal care industry [43]. Although ZnO have been previously studied for antibacterial activities, this study aims to establish increased antibacterial efficacy of health and hygiene products using nano ZnO-SPA which remains barely studied.

Major challenge nowadays is that conventional antibacterial agents used in sodium salt of long chain fatty acid (soap bars) and liquid cleansing products that have been in market for many decades are becoming extremely inefficient as antibacterial resistance grows throughout the world, making illnesses and death more problematic to manage. Most frequently used antibacterial agents such as Triclosan, Triclocarban, phenolic compounds and their carcinogenic by-products cause adverse effects, reproductive toxicity, highly destructive to the environment and are banned by the FDA since 2016 [44]. Additionally, zinc pyrithione (ZPT) an antifungal agent with extensive use in anti-dandruff shampoos that has been banned in many countries as of 2022 despite years of commercial use [45]. Therefore, once common antibacterial agents are getting phased out from the personal care products in many countries. New antibacterial agents are hence desperately required for personal care products, keeping researchers on their toes as they explore new and effective actives to fight disease-causing microbes like *Staphylococcus aureus (S. aureus), Escherichia coli (E. coli)* as well as recent world-wide pandemic Covid-19 causing respiratory syndrome. Furthermore, another major challenge is oxidation of unsaturated long chain fatty acids of soap bars causing photo-degradation under sunlight resulting into rancid and unpleasant yellow-brown colored product.

Applications of fabricated nano ZnO-SPA for health and hygiene products by infusing it into sodium salt of long chain fatty acid (soap bars) and liquid cleansing products thereby significantly enhances the antibacterial efficacy established by conducting zone of inhibition and European standard EN 1276 against Gram-positive (*S. aureus*) and Gram-negative (*E. coli*) organisms. Embedding nano ZnO-SPA, a wide band gap inorganic UV blocker, in the soap bar

reduces free radical generation thereby enhancing their photo-stability and minimize reduction of whiteness. This facile approach to fabricate multi-functional nano ZnO make it a potent and suitable material to use for various industrial applications.

3.5. Incorporation of nano ZnO-SPA in liquid cleansing product

Nano ZnO-SPA were incorporated into the liquid cleansing product having mixture of surfactant SLES-2EO, cocoamidopropyl betaine and other fundamental ingredients to establish the practical industrial applications. The liquid cleansing product was infused with different concentrations of nano ZnO-SPA i.e., 5 mg/mL, 10 mg/mL and 15 mg/mL and evaluated for antibacterial efficacy and other attributes.

3.6. Incorporation of nano ZnO-SPA in the matrix of sodium salt of long chain fatty acid

The synthesized nano ZnO-SPA were infused into the matrix of sodium salt of long chain fatty acid to establish the practical industrial applications. Sodium salt of long chain fatty acid matrix is incorporated with 0.5 mg/g, 1.5 mg/g, and 2.5 mg/g of nano ZnO-SPA. Mechanical process for soap manufacturing was followed such as mixing in sigma mixer, triple roll mill, and extrusion under vacuum to uniformly infuse nano ZnO-SPA into the sodium salt of long chain fatty acid.

3.7. Results and Discussion

3.7.1. Evaluation of sodium salt of long chain fatty acid

3.7.1.1. XRD analysis of soap matrix

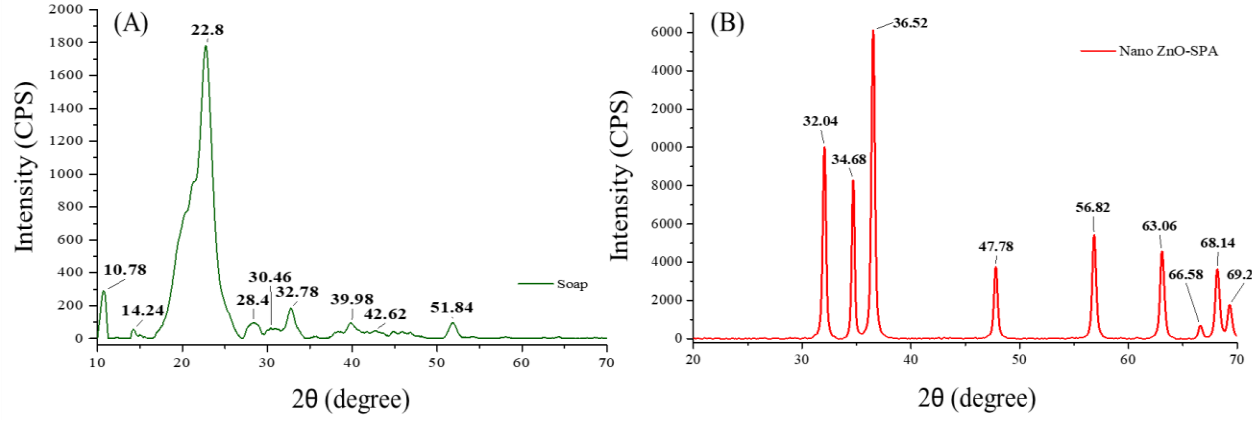

Figure 3.7 *(A) XRD pattern of sodium salt of long chain fatty acid infused with nano ZnO-SPA (B) XRD pattern of nano ZnO-SPA*

This could be the first or among the very few published scientific reports on XRD studies of sodium soap infused with nano ZnO synthesized in surfactant polyol assembly. Cation-specific interactions with carboxylate of long chain fatty acid have strong ionic forces that govern the crystalline phases of fabricated soaps. Additionally, weak van der Waals interactions between the C-H bonds in the fatty acids chain also plays a major role in soap's crystalline phases [46]. XRD patterns can be used to identify the crystalline phases of fabricated soap. It has been previously stated that sodium soap occurs in four crystalline phases namely, alpha, beta, delta, and omega. Intensity vs diffraction angles are plotted on Figure 3.7 to better observe the degree of crystallinity and pattern sharpness. However, it must be noted that relative intensity depends on crystal type as well as the scattering power of X ray atoms and thus may show discrepancy from soap to soap [47].

Table 3.6. Crystallite size of sodium salt of long chain fatty acid infused with nano ZnO-SPA by XRD.

Sr. No.	Peak Position 2 Theta (deg)	d-spacing (Å)	Intensity (I/I1)	FWHM (deg)	Crystallite size D (nm)	Average crystallite size D (nm)
1	10.7768	8.20282	197	0.75100	10.5313	7.52
2	14.3236	6.17863	40	0.53330	14.7799	
3	18.1479	4.88431	99	1.17340	6.68542	
4	20.4216	4.34534	520	2.86000	2.73366	
5	22.7956	3.89789	1199	1.80540	4.3134	
6	25.9693	3.42828	59	0.71000	10.9028	
7	28.4005	3.14009	69	1.71000	4.50371	
8	30.4627	2.93205	46	1.34660	5.69214	
9	32.7967	2.72852	126	1.08670	7.01291	
10	39.9739	2.25362	65	1.44000	5.18445	
11	42.6121	2.12000	36	2.50000	2.96045	
12	51.8540	1.76179	68	1.06670	6.69778	

XRD results reveal peak position, d spacing and intensity results in Table 3.6. The peaks observed at 10.77, 39.97 and 42.61 can be attributed to delta, omega, and beta phases of sodium palmitate respectively while the peaks at 51.85 is characteristic of alpha phase sodium stearate. Furthermore, peak at 30.46 having d spacing of 2.93 Å can be representative of sodium oleate. The peak at 32.79 having d spacing of 2.72 Å can be attributed to nano ZnO. The average crystallite size of soap was 7.51 nm.

3.7.1.2. SEM analysis of soap matrix

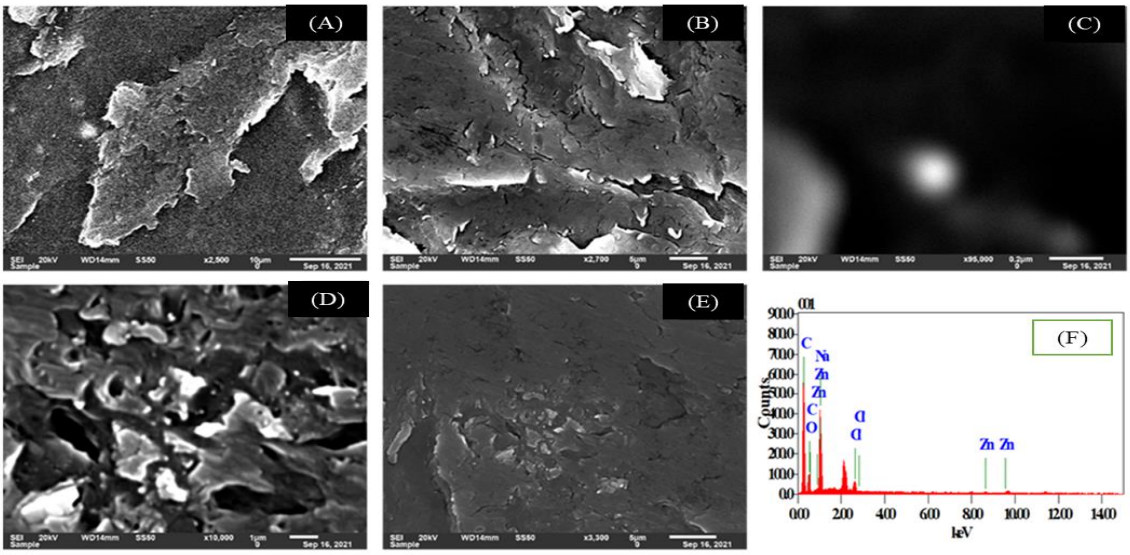

Figure 3.8. *(A-E) SEM imaging and (F) EDAX-based elemental assessment of soap matrix infused with ZnO-SPA nano system*

The SEM is an imperial tool to examine the surface morphology. The morphological evaluation of sodium salt of long chain fatty acid infused with nano ZnO-SPA done by using SEM. Different surface morphology images of soap matrix was examined revealing their layered and interconnected structure. Additionally, distribution of spherical ZnO nanoparticles and certain voids observed which also seem to be occupied by nano ZnO confirmed with further focusing on these particles and conducting the EDX, Figure 3.8. A-F). These layered structure and disruptions could be due to high shear experienced by soap during the processing like sigma mixer, roll mills and extrusion which may alter the inherent structure and rearrange the matrix.

Table 3.7. Quantitative elemental analysis of sodium salt of long chain fatty acid infused with nano-ZnO-SPA by EDX.

Formula	Mass%	Atom%	Sigma	Net	K ratio Line
C	68.48	77.95	0.13	12162	0.0059 K
O	15.70	13.42	0.26	2181	0.0036 K
Na	13.17	7.83	0.16	12148	0.0108 K
Cl	1.37	0.53	0.05	2029	0.0016 K
Zn*	1.27	0.27	0.20	309	0.0012 K
Total	100				

Table 3.7 shows the elemental analysis of soap matrix infused with nano ZnO exhibits the presence of 68.48% carbon (C) due to soap have long carbon chain fatty acids, 15.7% oxygen (O) molecule can be due to nano ZnO-SPA and $–COO^- Na^+$ group of soap, 13.17% sodium (Na) exhibits sodium salt of soap, 1.37% chloride (Cl) and 1.27% of zinc (Zn) molecule which is infused in soap.

3.7.1.3. Estimation of fatty acid composition by Gas Chromatography Flame ionization detection (GC-FID)

Table 3.8. Fatty acid composition of sodium salt of long chain fatty acid by GC-FID.

Sr. No	Name of Fatty acid	Molecular formula	Chain length	% by GC
1	Dodecanoic acid (Lauric acid)	$CH_3(CH_2)_{10}COOH$	C_{12}	5.45
2	Tetradecanoic acid (Myristic acid)	$CH_3(CH_2)_{12}COOH$	C_{14}	1.51
3	Hexadecanoic acid (Palmitic acid)	$CH_3(CH_2)_{14}COOH$	C_{16}	50.12
4	Octadecanoic acid (Stearic acid)	$CH_3(CH_2)_{16}COOH$	C_{18}	5.20
5	12-Octadecenoic acid (Oleic acid)	$C_{18}H_{32}O_2$	$C_{18:1}$	29.50
6	Linoleic acid	$C_{18}H_{32}O_2$	$C_{18:2}$	6.90

The fatty acid composition estimation of soap bar was performed using flame ionization detector (FID). Lauric, myristic, palmitic, stearic, oleic and linoleic acids are at 5.45%, 1.51%, 50.12%, 5.2%, 29.5%, and 6.9% which described in the Table 3.8. These estimated fatty acid percentages indicate a 90:10 oil blend soap having 90% palm oil (PO) and 10% palm kernel oil (PKO). Where PKO contains approximately 50% lauric acid while palmitic acid and oleic acids are abundantly present in PO.

3.7.1.4. Estimation of chloride content

Different concentrations of nano ZnO-SPA were added into the soap matrix, the chloride content into the soap matrix significantly changes from 0.5% to 0.85% which is within acceptable limits (Table 3.9.). The electrolyte plays an important role in molecular arrangement and formation of the soap phases. The electrolyte will salt-out the soaps due to ionic strength and common ion effect in the liquid phase. The result will be reducing the volume of the liquid phase and increasing the solid phase and hardness of soap [48].

3.7.1.5. Foamability test

Table 3.9. Estimation of chloride content and foamability in soap bar with different concentration of nano ZnO-SPA.

Parameters	Soap without nano ZnO-SPA	0.5 mg/g	1.5 mg/g	2.5 mg/g
Foam Improvement %	0	7.55	16.98	28.3
Chloride content	0.5	0.57	0.71	0.85

The impact on foamability due to addition of different concentrations of nano ZnO-SPA into soap matrix was studied and recorded the significant difference in the foam of soap infused with nano ZnO-SPA as compared to the base formulation. Soap infused with ZnO-SPA nano system exhibited up to 28% increase in the foam in comparison to base formulation Table 3.9. This could be due to extra surfactant coming into soap matrix along with nano ZnO-SPA. This additional surfactant plays role in influencing the critical micelle concentration (CMC) of soap and enhancing the foamability.

3.7.1.6. Photostability study of soap matrix having nano ZnO SPA

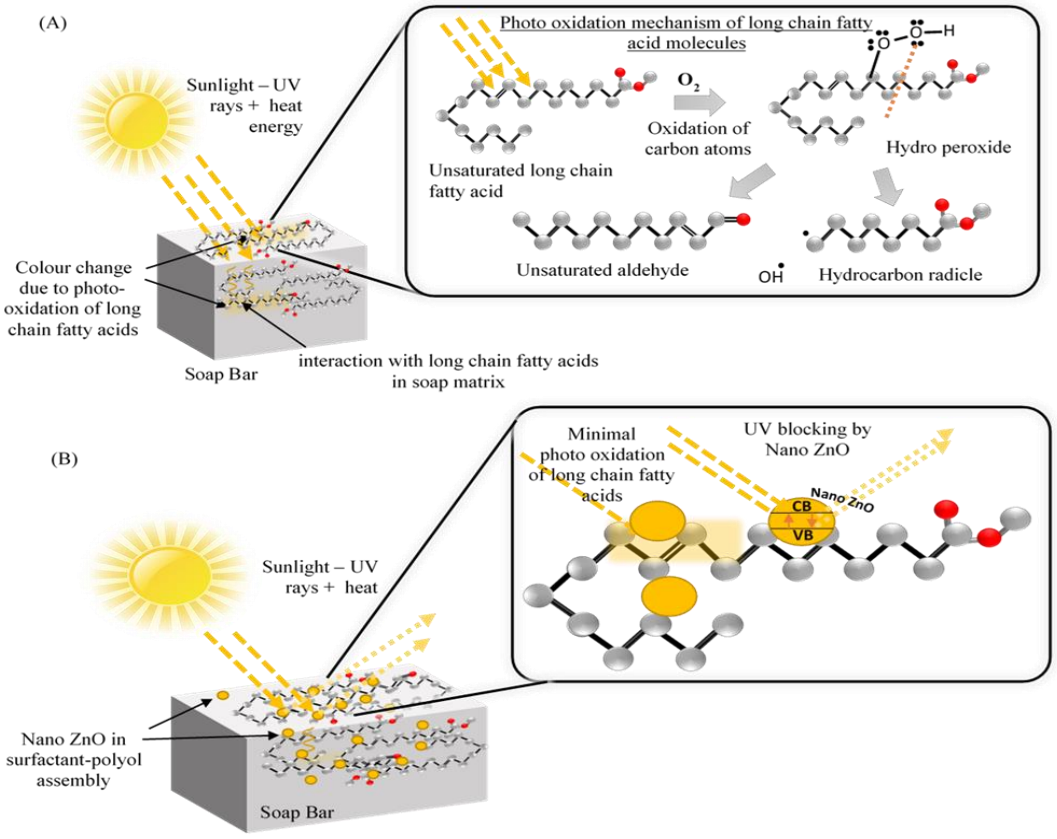

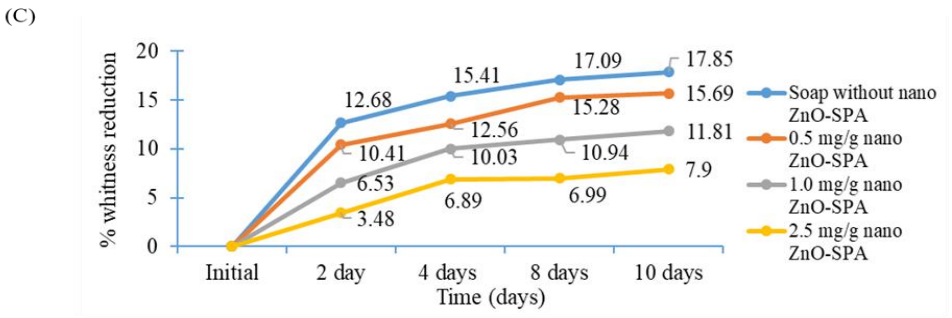

Figure 3.9. *(A) Mechanism of UV light exposure on the soap and shows the color change and free radical generation in fatty acid. (B) Systematic presentation of nano ZnO blocking phenomenon of UV rays to reduce the rate of color degradation. (C) Photostability study of soap matrix in direct sunlight for 10 days with different concentration of nano ZnO synthesized in SPA.*

Different concentrations of nano ZnO-SPA were used in soap bar (0.5 mg/g, 1.5 mg/g, 2.5 mg/g). Photostability study and color ordinate (L, a, b) measurement was carried out using Xrite Ci4200 reflectance spectrophotometer. Soap without nano ZnO shows reduction in the whiteness up to 17.85% leading towards yellow, red appearance of soap bar in comparison to initial whiteness when exposed to sunlight. However, soap bar infused with 0.5 mg nano ZnO-SPA per g of soap matrix shows a reduction in whiteness up to 15.69%, 1.5 mg nano ZnO-SPA per g of soap matrix shows a reduction in whiteness 11.81% and 2.5mg nano ZnO-SPA per g of soap exhibits reduction whiteness only up to 7.9% which is significantly better than the soap without nano ZnO-SPA infusion (Figure 3.9 C). This study evidently shows that the nano ZnO-SPA even at lower concentrations significantly protects the products from direct sunlight and heat energy by acting in multiple manner like by scattering the light, absorbing the high energy UV-radiations of the sunlight which contributes towards free radicals, blocking the unsaturated site and possibly by scavenging the free radicals and eventually enhancing the photostability of soap bar. The mechanistic representation shown in Figure 3.9 (A and B).

3.7.1.7. Antibacterial effect of nano ZnO SPA infused sodium salt of long chain fatty acid

The antibacterial efficacies of soap matrix infused without and with nano ZnO-SPA have been investigated as per EN-1276:2019 protocol. Results revealed the high potency of soap matrix with nano ZnO-SPA against both Gram-positive and Gram-negative bacteria. Soap infused with nano ZnO displayed 4.0 log reductions against Gram-positive and Gram-negative bacteria within 1 min contact time which is equivalent to killing of 99.99% of microbes. Whereas base soap without infusion of ZnO have shown nil reduction, in-fact displayed too numerous to count

(TNTC) microbes. The values of bacterial log reduction obtained from test are presented, Table 3.10. High antibacterial efficacy of soap infused with nano ZnO-SPA mainly due to active surface of ZnO disrupting the microbial cell wall, also presence of soap as a surfactant contributes in reducing the interfacial tension between ZnO and lipid bilayers of microbial cell wall.

Table 3.10. Antibacterial efficacy (EN 1276:2019) of sodium salt of long chain fatty acid infused with nano ZnO-SPA and without.

Quantity of nano ZnO SPA/Soap	Test Parameter	Initial suspension	Test Suspension	Test suspension	Final count log	Bacterial effect on log reduction
		cfu/mL	log10	cfu/mL		
Soap Base	*E. coli*	3.3×10^7	7.52	1.225×10^3	TNTC	TNTC
	S. aureus	1.25×10^7	7.10	1.225×10^3	TNTC	TNTC
2.5 mg/g	*E. coli*	3.3×10^7	7.52	1.225×10^3	3.09	4.43
	S. aureus	1.25×10^7	7.10	1.225×10^3	3.09	4.01

3.8. Evaluation of liquid cleansing product infused with nano ZnO-SPA

3.8.1. Determination of chloride content

The chloride content as NaCl was evaluated by using wet analysis method there is significant change observed in the chloride content 0.7%, 1.4% and 2.1% after addition of nano ZnO-SPA 5 mg/mL, 10 mg/mL and 15 mg/mL of liquid cleansing product Figure 3.10. (A). The possible reason to increase of chloride content because of sodium chloride liberated as by product during the synthesis of nano ZnO-SPA. This additional electrolyte content in product plays an important role in influencing the rheological properties of final product.

3.8.2. Determination of effect on rheological properties of liquid cleansing product

The rheological properties of liquid cleansing products were evaluated by Brookfield Rheometer DVT-3. The different concentrations of nano ZnO-SPA were added into the liquid cleansing product resulting into the change in rheology of liquid cleansing product. 2.17%, 4.16%, 7.69% increase in rheology (viscosity) observed after addition of 5 mg/mL, 10 mg/mL and 15 mg/mL of nano ZnO-SPA of liquid cleansing product shows in Figure 3.10. (B). Nano ZnO-SPA contain anionic surfactant (SLES-2EO) and the sodium chloride liberated as by product, most commonly

electrolyte used in the liquid cleansing product to modify the rheology. The nano ZnO-SPA composition influence shape of anionic surfactant micelles and convert them into rod shape micellar arrangement in the presence of defined level of electrolyte and entanglement of these structure results in the increase of viscosity of liquid cleansing product.

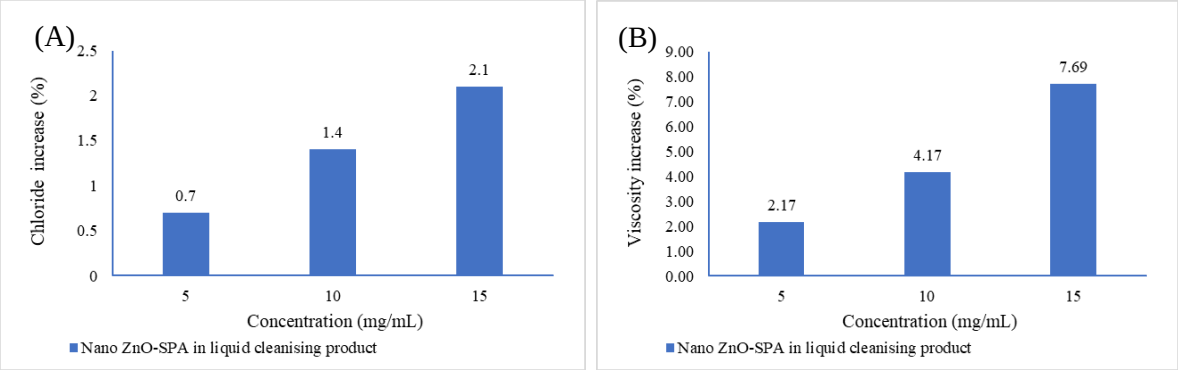

Figure 3.10. *(A) Effect of nano ZnO-SPA on chloride content of liquid cleansing product. (B) Effect of nano ZnO-SPA on rheological properties of liquid cleansing product.*

3.8.3. Antibacterial properties and application of liquid cleansing product

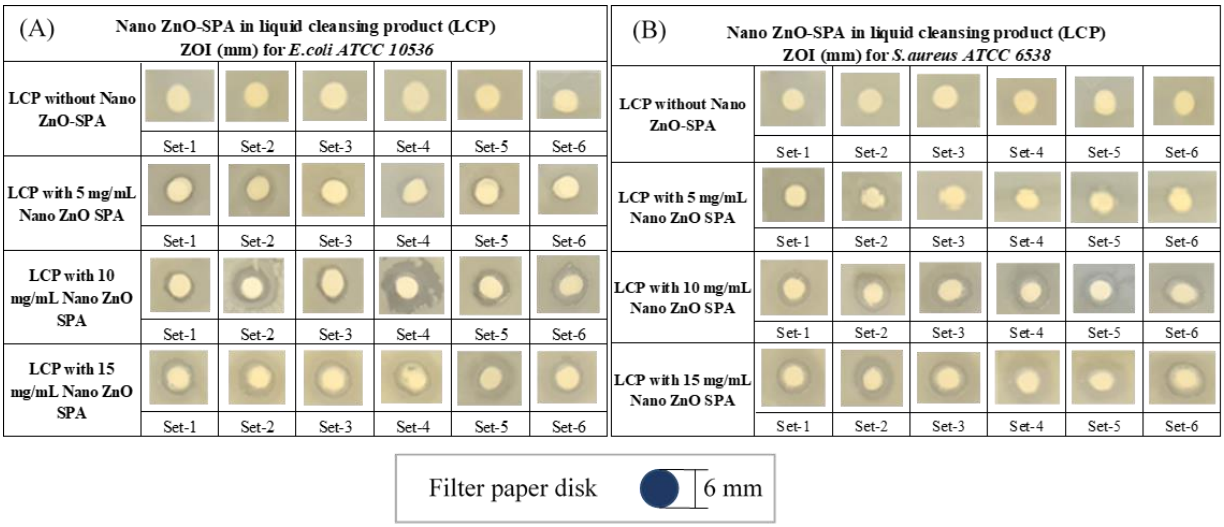

Figure 3.11. *Antibacterial efficacy (ZOI) (A) liquid cleansing product with and without nano ZnO-SPA against E. coli (B) liquid cleansing product with and without nano ZnO-SPA against S. aureus.*

Antibacterial properties of liquid cleansing products investigated by disk diffusion method (ZOI) using different concentration of nano ZnO-SPA (Figure 3.11 A and B). The antibacterial efficacy evaluation of liquid cleansing product infused with different concentration of nano ZnO-SPA was carried out using diffusion method to study ZOI.

Table 3.11. Antibacterial efficacy (ZOI in mm) of liquid cleansing product infused with nano ZnO-SPA against E. coli and S. aureus.

Test product	Zone of inhibition (mm)					
	E. coli			*S.aureus*		
	Average	**Std. Deviation**	**Std. error**	**Average**	**Std. Deviation**	**Std. error**
LCP without nano ZnO-SPA	0.000	0.000	0.000	0.000	0.000	0.000
LCP with 5 mg/mL nano ZnO-SPA	6.875	0.354	0.125	5.875	0.354	0.125
LCP with 10 mg/mL nano ZnO-SPA	9.750	0.463	0.164	9.625	0.518	0.183
LCP with 15 mg/mL nano ZnO-SPA	11.750	0.886	0.313	11.875	0.991	0.350

Four concentrations were studied for antibacterial efficacy, base liquid cleansing product does not show zone of inhibition action, nano ZnO-SPA 5 mg/mL of liquid cleansing product show the ZOI average diameter 6.87 mm, standard error 0.125, nano ZnO-SPA 10 mg/mL of liquid cleansing product shows the 9.75 mm ZOI and standard error 0.164, nano ZnO-SPA 15 mg/mL of liquid cleansing product exhibits the 11.75 mm ZOI with standard error 0.313 (Table 3.11.). There are number of factors that can affect the size of a zone of inhibition in the study, such as drug diffusion rate through agar, drug solubility, agar medium thickness, and concentration of impregnated drug into the disk.

As per the above results it can be clearly stated that liquid cleansing product infused with nano ZnO-SPA shows the high antibacterial efficacy against both Gram-positive and Gram-negative pathogens. High antibacterial potency of nano ZnO-SPA could be due to multiple reasons like high active surface, defects, and surface charges.

References

[1] S. Saleem *et al.*, "Modification in structural, optical, morphological, and electrical properties of zinc oxide (ZnO) nanoparticles (NPs) by metal (Ni, Co) dopants for electronic device applications," *Arab. J. Chem.*, vol. 15, no. 1, p. 103518, Jan. 2022, doi: 10.1016/j.arabjc.2021.103518.

[2] A. Nazir *et al.*, "Zinc oxide nanoparticles fabrication using Eriobotrya japonica leaves extract: Photocatalytic performance and antibacterial activity evaluation," *Arab. J. Chem.*, vol. 14, no. 8, p. 103251, Aug. 2021, doi: 10.1016/j.arabjc.2021.103251.

[3] H. Zhang, Z. Liang, J. Zhang, W. Wang, H. Zhang, and Q. Lu, "Zinc oxide nanoparticle synthesized from Euphorbia fischeriana root inhibits the cancer cell growth through modulation of apoptotic signaling pathways in lung cancer cells," *Arab. J. Chem.*, vol. 13, no. 7, pp. 6174–6183, Jul. 2020, doi: 10.1016/j.arabjc.2020.05.020.

[4] D. Rajamanickam and M. Shanthi, "Photocatalytic degradation of an organic pollutant by zinc oxide – solar process," *Arab. J. Chem.*, vol. 9, pp. S1858–S1868, Nov. 2016, doi: 10.1016/j.arabjc.2012.05.006.

[5] M. Imran, S. Haider, K. Ahmad, A. Mahmood, and W. A. Al-masry, "Fabrication and characterization of zinc oxide nanofibers for renewable energy applications," *Arab. J. Chem.*, vol. 10, pp. S1067–S1072, Feb. 2017, doi: 10.1016/j.arabjc.2013.01.013.

[6] Z. Samavati *et al.*, "Enhancement of organic solar cell efficiency by altering the zinc oxide photoanode nanostructure morphology," *J. Nanostructure Chem.*, vol. 12, no. 6, pp. 1119–1130, Dec. 2022, doi: 10.1007/s40097-021-00453-2.

[7] S. Kumar, R. Seth, S. Panwar, K. K. Goyal, V. Kumar, and R. K. Choubey, "Morphological and Optical Studies of ZnO-Silica Nanocomposite Thin Films Synthesized by Time Dependent CBD," *J. Electron. Mater.*, vol. 50, no. 6, pp. 3462–3470, Jun. 2021, doi: 10.1007/s11664-021-08863-2.

[8] S. Mishra *et al.*, "Enhanced output of ZnO nanosheet-based piezoelectric nanogenerator with a novel device structure," *Eng. Res. Express*, vol. 3, no. 4, p. 045022, Dec. 2021, doi: 10.1088/2631-8695/ac34c3.

[9] V. Khullar, S. Soni, and H. Tyagi, "Nanoparticle-Laden Flow for Solar Absorption," in *Handbook of Multiphase Flow Science and Technology*, Singapore: Springer Singapore, 2016, pp. 1–30.

[10] C. Cole, "Sunscreen Formulation: Optimizing Efficacy of UVB and UVA Protection," in *Principles and Practice of Photoprotection*, Cham: Springer International Publishing, 2016, pp. 275–287.

[11] E. D. M. Isa, K. Shameli, N. W. C. Jusoh, and R. Hazan, "Rapid photodecolorization of methyl orange and rhodamine B using zinc oxide nanoparticles mediated by pullulan at different calcination conditions," *J. Nanostructure Chem.*, vol. 11, no. 1, pp. 187–202, Mar. 2021, doi: 10.1007/s40097-020-00358-6.

[12] M. Rajapriya *et al.*, "Correction to: Synthesis and Characterization of Zinc Oxide Nanoparticles Using Cynara scolymus Leaves: Enhanced Hemolytic, Antimicrobial, Antiproliferative, and Photocatalytic Activity," *J. Clust. Sci.*, vol. 31, no. 4, pp. 803–803, Jul. 2020, doi: 10.1007/s10876-019-01734-1.

[13] M. H. Huang *et al.*, "Room-Temperature Ultraviolet Nanowire Nanolasers," *Science (80-.).*, vol. 292, no. 5523, pp. 1897–1899, Jun. 2001, doi: 10.1126/science.1060367.

[14] B. Cai *et al.*, "Conductive SnO 2 :Sb nanobelts as electrodes for detection of NO 2 in ppb level with ultrahigh sensitivity," *Appl. Phys. Lett.*, vol. 104, no. 7, p. 073112, Feb. 2014, doi: 10.1063/1.4866275.

[15] X. Y. Kong and Z. L. Wang, "Spontaneous Polarization-Induced Nanohelixes, Nanosprings, and Nanorings of Piezoelectric Nanobelts," *Nano Lett.*, vol. 3, no. 12, pp. 1625–1631, Dec. 2003, doi: 10.1021/nl034463p.

[16] D. G. Beasley and T. A. Meyer, "Characterization of the UVA Protection Provided by Avobenzone, Zinc Oxide, and Titanium Dioxide in Broad-Spectrum Sunscreen Products," *Am. J. Clin. Dermatol.*, vol. 11, no. 6, pp. 413–421, Dec. 2010, doi: 10.2165/11537050-000000000-00000.

[17] S. Wirunchit, P. Gansa, and W. Koetniyom, "Synthesis of ZnO nanoparticles by Ball-milling process for biological applications," *Mater. Today Proc.*, vol. 47, pp. 3554–3559, 2021, doi: 10.1016/j.matpr.2021.03.559.

[18] G. V. Ovidiu Oprea, Ecaterina Andronescu, Bogdan Stefan Vasile and C. C. O. OPREA , E. ANDRONESCU, B. S. VASILE, G. VOICU, "SYNTHESIS AND CHARACTERIZATION OF ZnO NANOPOWDER BY NON-BASIC ROUTE," *Dig. J. Nanomater. Biostructures*, vol. 6, no. 3, pp. 1393–1401, 2011, [Online]. Available: https://www.researchgate.net/publication/236024051_Synthesis_and_characterization_of_ZnO_nanopowder_by_non-basic_route.

[19] S. Sánchez-Martín, S. M. Olaizola, E. Castaño, E. Urionabarrenetxea, G. G. Mandayo, and I. Ayerdi, "Study of deposition parameters and growth kinetics of ZnO deposited by aerosol assisted chemical vapor deposition," *RSC Adv.*, vol. 11, no. 30, pp. 18493–18499, 2021, doi: 10.1039/D1RA03251H.

[20] O.-R. Vasile *et al.*, "Synthesis and characterization of nanostructured zinc oxide particles synthesized by the pyrosol method," *J. Nanoparticle Res.*, vol. 14, no. 12, p. 1269, Dec. 2012, doi: 10.1007/s11051-012-1269-7.

[21] J. N. Hasnidawani, H. N. Azlina, H. Norita, N. N. Bonnia, S. Ratim, and E. S. Ali, "Synthesis of ZnO Nanostructures Using Sol-Gel Method," *Procedia Chem.*, vol. 19, pp. 211–216, 2016, doi: 10.1016/j.proche.2016.03.095.

[22] S. Goktas and A. Goktas, "A comparative study on recent progress in efficient ZnO based nanocomposite and heterojunction photocatalysts: A review," *J. Alloys Compd.*, vol. 863, p. 158734, May 2021, doi: 10.1016/j.jallcom.2021.158734.

[23] D. Haranath, N. Bhalla, H. Chander, Rashmi, M. Kar, and R. Kishore, "Controlled growth of ZnS:Mn nanophosphor in porous silica matrix," *J. Appl. Phys.*, vol. 96, no. 11, pp. 6700–6705, Dec. 2004, doi: 10.1063/1.1806552.

[24] S. Kumar *et al.*, "Variation in chemical bath pH and the corresponding precursor concentration for optimizing the optical, structural and morphological properties of ZnO thin films," *J. Mater. Sci. Mater. Electron.*, vol. 30, no. 19, pp. 17747–17758, Oct. 2019, doi: 10.1007/s10854-019-02125-y.

[25] M. Lodén and W. Wessman, "The influence of a cream containing 20% glycerin and its vehicle on skin barrier properties," *Int. J. Cosmet. Sci.*, vol. 23, no. 2, pp. 115–119, Apr. 2001, doi: 10.1046/j.1467-2494.2001.00060.x.

[26] M. Azizi-Lalabadi, A. Ehsani, B. Divband, and M. Alizadeh-Sani, "Antimicrobial activity of Titanium dioxide and Zinc oxide nanoparticles supported in 4A zeolite and evaluation the morphological characteristic," *Sci. Rep.*, vol. 9, no. 1, p. 17439, Nov. 2019, doi: 10.1038/s41598-019-54025-0.

[27] S. Kumar, A. Mudai, B. Roy, I. B. Basumatary, A. Mukherjee, and J. Dutta, "Biodegradable Hybrid Nanocomposite of Chitosan/Gelatin and Green Synthesized Zinc Oxide Nanoparticles for Food Packaging," *Foods*, vol. 9, no. 9, p. 1143, Aug. 2020, doi: 10.3390/foods9091143.

[28] K. L. Isamai M. A. Taha K.K. Modwi A., "ZnO nanoparticles: Surface and X-ray profile analysis," *J. Ovonic Res.*, vol. 14, no. 5, pp. 381–393, 2018, [Online]. Available: https://www.researchgate.net/publication/328026905_ZnO_nanoparticles_Surface_and_X-ray_profile_analysis.

[29] İ. Boz, S. Kaluza, M. Ş. Boroğlu, and M. Muhler, "Synthesis of high surface area ZnO powder by continuous precipitation," *Mater. Res. Bull.*, vol. 47, no. 5, pp. 1185–1190, May 2012, doi: 10.1016/j.materresbull.2012.02.005.

[30] M. K. Debanath and S. Karmakar, "Study of blueshift of optical band gap in zinc oxide (ZnO) nanoparticles prepared by low-temperature wet chemical method," *Mater. Lett.*, vol. 111, pp. 116–119, Nov. 2013, doi: 10.1016/j.matlet.2013.08.069.

[31] A. Goktas, F. Aslan, B. Yeşilata, and İ. Boz, "Physical properties of solution processable n-type Fe and Al co-doped ZnO nanostructured thin films: Role of Al doping levels and annealing," *Mater. Sci. Semicond. Process.*, vol. 75, pp. 221–233, Mar. 2018, doi: 10.1016/j.mssp.2017.11.033.

[32] M. Nabil, I. V. Perez-Quintana, M. Acosta, J. A. Mendez-Gamboa, and R. Castro-Rodriguez, "Morphological, Structural, and Optical Bandgap Characterization of Extracted ZnO Nanoparticles from Commercial Paste," *Adv. Mater. Sci. Eng.*, vol. 2021, pp. 1–7, Oct. 2021, doi: 10.1155/2021/9926544.

[33] C. Stoian. and G. Z. Sandu PERETZ, Manuela FLOREA-SPIROIU, Dan F. ANGHEL, "CHITOSAN MICROPARTICULATE SYSTEMS PREPARED BY POLYMER-SURFACTANT INTERACTION," *Rev. Roum. Chim.*, vol. 58, no. 2–3, pp. 275–281, 2013, [Online]. Available: https://www.researchgate.net/publication/287412842_Chitosan_microparticulate_systems_prepared_by_polymer-surfactant_interaction.

[34] S. Cunliffe, P. Martin, M. Baker, O. Mihailova, and P. Martin, "Near infrared absorption spectroscopy for the quantification of unsulfated alcohol in sodium lauryl ether sulfate," *J. Near Infrared Spectrosc.*, vol. 29, no. 1, pp. 11–23, Feb. 2021, doi: 10.1177/0967033520963825.

[35] A. Y. Hammoudeh, S. M. Obeidat, E. K. Abboushi, and A. M. Mahmoud, "FT-IR Spectroscopy for the Detection of Diethylene Glycol (DEG) Contaminant in Glycerin-Based Pharmaceutical Products and Food Supplements," *Acta Chim. Slov.*, vol. 67, no. 2, pp. 530–536, Jun. 2020, doi: 10.17344/acsi.2019.5553.

[36] M. Hasan *et al.*, "Bioinspired synthesis of zinc oxide nano-flowers: A surface enhanced antibacterial and harvesting efficiency," *Mater. Sci. Eng. C*, vol. 119, p. 111280, Feb. 2021, doi: 10.1016/j.msec.2020.111280.

[37] Y. Lei, F. Qu, and X. Wu, "Assembling ZnO Nanorods into Microflowers through a Facile Solution Strategy: Morphology Control and Cathodoluminescence Properties," *Nano-Micro Lett.*, vol. 4, no. 1, pp. 45–51, Mar. 2012, doi: 10.1007/BF03353691.

[38] P. Gnanamozhi *et al.*, "Enhanced antibacterial and photocatalytic degradation of reactive red 120 using lead substituted ZnO nanoparticles prepared by ultrasonic-assisted co-precipitation method," *Ceram. Int.*, vol. 46, no. 11, pp. 19593–19599, Aug. 2020, doi: 10.1016/j.ceramint.2020.05.020.

[39] M. Shaban, F. Mohamed, and S. Abdallah, "Production and Characterization of Superhydrophobic and Antibacterial Coated Fabrics Utilizing ZnO Nanocatalyst," *Sci. Rep.*, vol. 8, no. 1, p. 3925, Mar. 2018, doi: 10.1038/s41598-018-22324-7.

[40] M. Gomathi, P. V. Rajkumar, and A. Prakasam, "Study of dislocation density (defects such as Ag vacancies and interstitials) of silver nanoparticles, green-synthesized using Barleria cristata leaf extract and the impact of defects on the antibacterial activity," *Results Phys.*, vol. 10, pp. 858–864, Sep. 2018, doi: 10.1016/j.rinp.2018.08.011.

[41] H. Bahadur, A. Srivastava, R. Sharma, and S. Chandra, "Morphologies of Sol–Gel Derived Thin Films of ZnO Using Different Precursor Materials and their Nanostructures," *Nanoscale Res. Lett.*, vol. 2, no. 10, p. 469, Oct. 2007, doi: 10.1007/s11671-007-9089-x.

[42] T. Smijs and Pavel, "Titanium dioxide and zinc oxide nanoparticles in sunscreens: focus on their safety and effectiveness," *Nanotechnol. Sci. Appl.*, p. 95, Oct. 2011, doi: 10.2147/NSA.S19419.

[43] M. Abendrot and U. Kalinowska-Lis, "Zinc-containing compounds for personal care applications," *Int. J. Cosmet. Sci.*, vol. 40, no. 4, pp. 319–327, Aug. 2018, doi: 10.1111/ics.12463.

[44] R. U. Halden, "On the Need and Speed of Regulating Triclosan and Triclocarban in the United States," *Environ. Sci. Technol.*, vol. 48, no. 7, pp. 3603–3611, Apr. 2014, doi: 10.1021/es500495p.

[45] "BREAKING NEWS: The Ban on the Cosmetic Anti-dandruff Agent Zinc Pyrithione (ZPT) in the EU will come into force on March 1, 2022 - Regulatory News - Personal and Home Care Products," 2022. https://www.cirs-group.com/en/cosmetics/breaking-news-the-ban-on-the-cosmetic-anti-dandruff-agent-zinc-pyrithione-zpt-in-the-eu-has-come-into-force-on-march-1-2022.

[46] R. J. Jandacek and W. B. Broering, "X-Ray diffraction study of sodium soaps of monounsaturated and polyunsaturated fatty acids," *Lipids*, vol. 24, no. 12, pp. 1008–1013, Dec. 1989, doi: 10.1007/BF02544070.

[47] G. S. HATTIANCDI, "Characterization of some commercial soaps by X-ray diffraction.," *J. Res. Natl. Bur. Stand. (1934).*, vol. 42, no. 4, pp. 331–341, 1949, doi: 10.6028/jres.042.027.

[48] N. Hall, "Implications of Soap Structure for Formulation and User Properties," in *Soap Manufacturing Technology*, Elsevier, 2016, pp. 1–33.

Chapter 4

Surfactant Mediated Silver doped Nano ZnO for Advanced Germicidal Efficacy of Health and Hygiene Products

Highlights of the Chapter:

- *This chapter explores a strategic approach to fabricate nano scale silver (100-2000 ppm) doped zinc oxide (ZnOS) in a unique Surfactant-Polyol-Assembly (SPA) that acts as a caging agent, restricting the growth of particles.*

- *This highly suitable approach for health and hygiene products is among the few works of literature exploring the fabrication and infusion of nano ZnOS to elevate the germicidal efficacy of liquid cleansing products significantly.*

- *Infused products with 0.2% of ZnOS exhibit ZOI up to 13.25 mm with a log reduction of 2.13 while nano ZnOS 2000 ppm shows ZOI up to 11.75 mm with a log reduction of 5.41 which corresponds to >99.999% germ kill.*

This work has been published in:

Bhalla, N., Jayaprakash, A., Ingle, N., Patel, H., Patri, S.V. and Haranath, D. (2022), **Journal of Science: Advanced Materials and Devices**, 7(4), p.100487. doi:10.1016/j.jsamd.2022.100487. **IF. 8**

4.1. Introduction

The emergence of nanoscience was regarded as a major scientific breakthrough that opened the way for the creation of high-quality goods in several sectors [1]–[6]. Nanotechnology is the use of materials with morphologies in nano scale dimensions for the development of materials or mechanisms with unique or considerably enhanced characteristics owing to their nano-size. Nanostructures are gaining popularity across the world as it is commonly regarded as having enormous promise in a broad array of applications. Nanoscale silver integrated into textile, nano gold used for photocatalysis, nanoscale TiO_2 and ZnO for sun protection are examples of nanoparticles that have been used in the personal care and garments industry [7]–[9]. In the current research work authors aim to improve the germicidal efficacy of health and hygiene products by fabricating nanoscale silver doped ZnO in Surfactant-Polyol-Assembly (SPA) having high germicidal potency.

Zinc oxide (ZnO) is a hexagonal wurtzite-structured broad bandgap based II-VI semiconductor having high luminosity and electronic conductivity [10], [11]. Nanoscale ZnO has several significant benefits such as (i) tunable morphological characteristics, (ii) chemical stability, (iii) efficient blockers of sun rays and ultraviolet radiations (iv) non-irritant (v) compatible with various skin types (vi) protects the skin from inflammation and have thus used as a crucial material for applications in diverse fields in personal care and electronic among others [12]–[14]. As a result, investigation of structural factors is becoming increasingly important for improving the efficiency of ZnO nano material related applications. Silver nanoparticles have inspired a wave of academic curiosity among noble metallic nanoparticles because of their distinctive characteristics, such as catalyst, excellent conductivity and their wide variety of prospective high germicidal activities [15], [16]. The morphology, structure, and percentage of Ag nanoparticles influence the photonic as well as the bactericidal characteristics of zinc oxide nanomaterials [17], [18]. Moreover, metal-doping methods have recently been utilized to enhance the physical and chemical characteristics of ZnO nanoparticles. Since Surface Plasmon Resonance (SPR) occurs across the visible region of the spectrum, noble metal inclusion into the zinc oxide matrix enhances the optical absorption. This increases the electron-hole pair formation, thus, advancing ROS generation and germicidal efficacy. Silver, platinum, and gold metals, in particular, are the most popular materials because of their significant SPR properties. Platinum and gold, on the one hand, remain less used due to the expense for

commercial applications. However, silver is very inexpensive and is acceptable for practical implementations. Metal doping could impact the molecular structure of ZnO resulting in significant improvements in application sectors [19], [20].

Several disadvantages are present in the existing synthesis methods and solvents. Among them, the three disadvantages are (i) cost, time and labour intensive (ii) solvents used and by-products released are not allowed in health and hygiene applications and (iii) solvents could be harmful to flora and fauna [21]–[23]. Hence it is of utmost importance to develop advanced methodologies involving appropriate solvents and products suitable for industrial applications.

Liquid cleansing products make our lives easier with merchandise for skin care, hair care and domestic care for disinfection of various household items and textile cleaning. As a result, it's no surprise that liquid cleansing products have grown in demand since their emergence in the mid-1950s. However, due to the increase in various diseases including COVID-19, there is a growing public awareness about the importance of disease control and personal hygiene products. To address growing customer awareness and interest, novel formulations with enhanced germicidal potency are in high demand.

Challenges in developing advanced germicidal agents have also been increasing in recent times. Within the past five years the Food and Drug Administration (FDA) has banned the incorporation of triclosan, triclocarban and 18 other antimicrobial chemicals from household personal care products like soaps and hand wash [24]. This is due to the concerns about the toxic, highly damaging and carcinogenic effects of these chemicals on human, wildlife and environment. In 2021, the European Commission officially issued Zinc Pyrithione (ZPT), an anti-fungal agent with decades of usage in anti-dandruff shampoos, as a prohibited ingredient due to its cell toxicity [25]. Moreover, over time mutations in disease-causing germs form resistant organisms that no longer respond to the germicidal agents used in products widely the past decades. As a result, in several countries, popular agents are being transitioned out of personal care products. Thus, novel germicidal agents are highly required in personal care industry. The work contributes immensely for advanced germicidal health and hygiene products.

In the current work, authors have fabricated nano scale ZnOS in unique SPA with high germicidal efficacy to address these concerns for health and hygiene application in liquid cleansing product. This is perhaps one of the few papers to develop synthesis method in which precursors and all byproducts are safe to use in personal care industry. SLES is a low-cost

anionic surfactant widely utilized in the health and hygiene industries, particularly in personal care products. Glycerin is a very well-used co-surfactant for designing nanoscale structures, and it also functions as a moisturizing agent, limiting trans epidermal water loss and keeping the skin hydrated. As a result, the discussed SPA based nano ZnOS fabrication strategy has many benefits, including high suitability with health and hygiene, personal care products, particularly liquid cleansing products, non-irritating, minimal solvents, lower power consumption, non-intensive process, and one-step quicker fabrication without any additional process, such as thermal treatment and milling.

In order to fabricate nano-sized ZnOS and confine nanoparticle growth, the current approach utilizes the unique capabilities of surfactant and polyol combinations such as micellar assembly and their caging structure. Arrangements and caging agents are used in this approach to create fabricated ZnOS suited for industrial purposes such as health and hygiene, personal care, and cosmetics. The synthesized nano ZnOS 2000 ppm has a high ZOI (11.75 mm) in contrast to recent reported literature. For instance, zinc oxide (ZnO) nanoparticles reinforced into alumina silicates explored by Azizi et.al. and metal (namely iron, silver) doped zinc oxide nanoparticles studied by Samreen et.al showing the ZOI less than 10 mm. [26], [27]. The fabricated nano ZnOS 2000 ppm has a low crystallite size (15.14 nm) when compared to previously explored silver doped ZnO nanoparticles having as high as 54.1 nm and 59.07 nm reported for silver doped ZnO nanoparticles synthesized using green extract route and simple solution method [28], [29]. The application of synthesized ZnOS into the liquid cleansing product for the health and hygiene industry enhances their germicidal efficacy established by conducting zone of inhibition and European standard EN 1276 against both Gram-positive bacteria i.e. *Staphylococcus aureus* (*S. aureus*) and Gram-negative bacteria i.e. *Escherichia coli* (*E. coli*).

Their toxicity to microbes at low concentrations has the potential to be revolutionary addition in many industries. Nano ZnOS in SPA can be infused into products in the health and hygiene industry for detergent based cleaning and antibacterial effects. Nano ZnOS can be used in animal/ floor disinfectants due to their minimal surfactant concentrations and high microbicidal efficacy. Moreover, fabricating silver doped ZnO nanosystem is not limited to personal care, it shows potential in the home care and textile industries due to its germicidal, UV protection and/or photocatalytic efficacies. This system also has the potential use of surfactant based nanomaterials to enhance existing wastewater treatments.

4.2. Fabrication of nano ZnO in SPA system

4.2.1. Materials required

Zinc nitrate hexahydrate ($Zn(NO_3)_2.6H_2O$) [S D Fine-chem limited, India], Sodium hydroxide (NaOH) [S D Fine-chem limited, India] and silver nitrate ($AgNO_3$) [CARLO ERBA Reagents S.A.S] were used as raw materials for synthesis of ZnOS nanomaterials. Sodium Lauryl Ether Sulfate containing 2 mol of ethylene oxide (SLES 2EO 70% Surfactant) [Galaxy Surfactants, India] and Glycerin (Polyol) [International Foodstuffs (IFFCO) Malaysia] were used as capping and caging agents and Zinc oxide AR [S D Fine-chem limited, India] was used in the study. De-ionized water having a pH of 5.5-7.0 with conductivity 1 µS/cm was used as solvent during the experimentation. All the reagents were used as received without further purification. Bacterial strains *Escherichia coli* (*E. coli*) ATCC 10536, *Staphylococcus aureus* (*S. aureus*) ATCC 6538, *Pseudomonas aeruginosa* (*P. aeruginosa*) ATCC 15442 and *Enterococcus hirae* (*E. hirae*) ATCC 10541 were obtained from ATCC (American Type Culture Collection) in Dubai.

4.2.2. Synthesis of nano ZnOS in Surfactant-Polyol-Assembly (SPA)

0.615 M zinc nitrate (hexahydrate) ($Zn(NO_3)_2.6H_2O$) was added into de ionized water (H_2O) and stirred well for 10 min then SPA containing 1.62 M glycerin and 0.54 M SLES-2EO 70% was added as a capping and stabilizing agent. The whole mixture was subjected to continuous stirring (300 rpm) at 50-60 ^oC until uniformity was achieved. To study the impact of silver doping on ZnO network, silver nitrate ($AgNO_3$) was added to the above homogeneous mixture with following concentrations of silver: 0 ppm, 100 ppm, 500 ppm, 1000 ppm and 2000 ppm. After the mixture was further stirred, 1.23 M NaOH solution was added drop wise until even color was observed. The resultant samples were centrifuged, washed and dried.

The possible mechanism of silver doping on ZnO system is the following [30]:

$$Zn^{2+} + 4OH^- \rightarrow Zn(OH)_4^{2-}$$

$$Ag^+ + 2OH^- \rightarrow Ag(OH)^{2-}$$

$$Zn(OH)_4^{2-} + 2Ag(OH)^{2-} \rightarrow Ag_2O/ZnO + 2H_2O + 4OH^-$$

$$Ag_2O/ZnO \rightarrow Ag/ZnO + O_2$$

Surfactants are interfacial active complexes. They consist of a polar head group and a non-polar hydrocarbon chain.

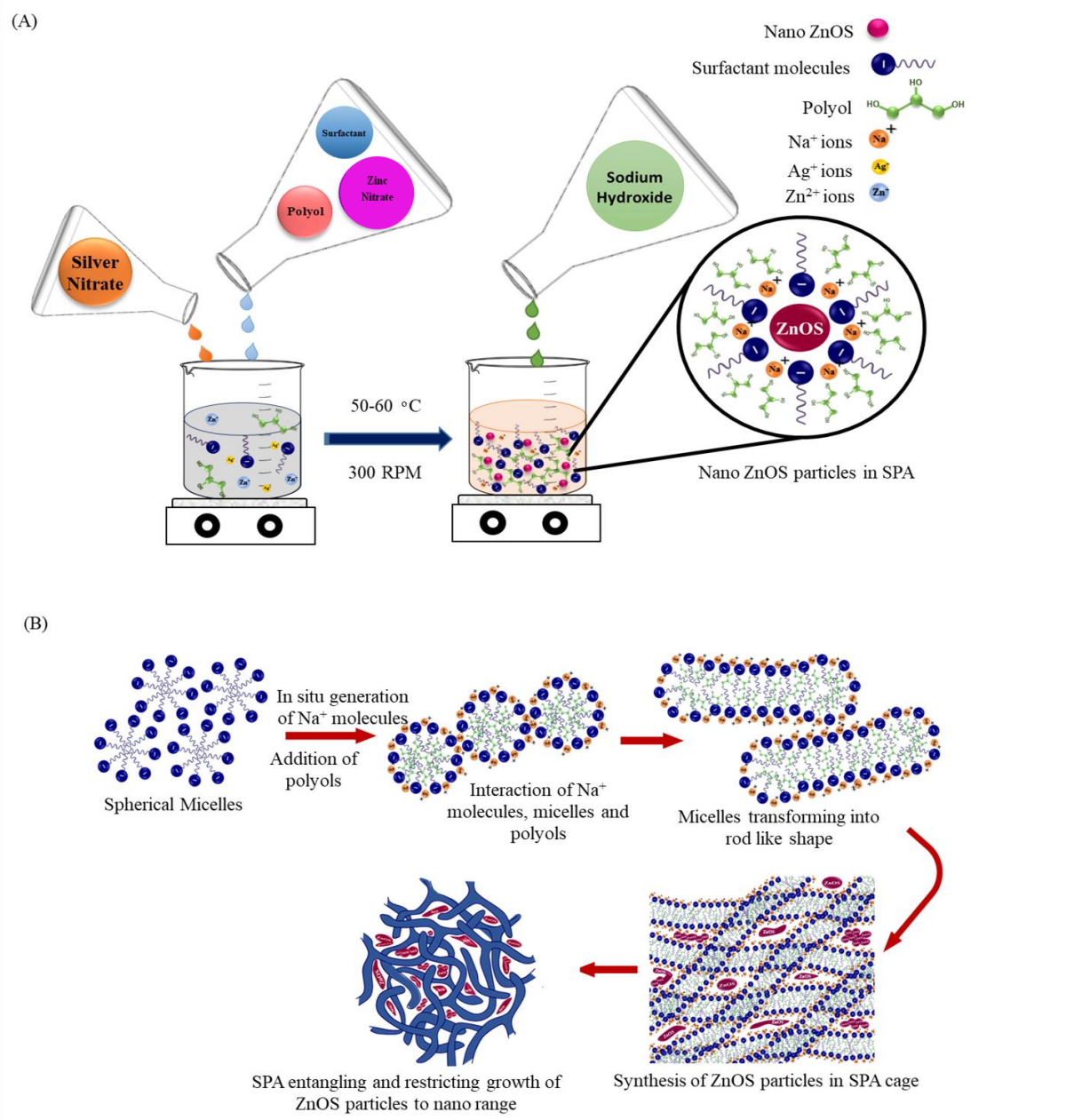

Figure 4.1. *(a) Illustrative synthesis mechanism of ZnOS (b) Illustration of SPA acting as caging agent*

Owing to their two-part structure, surfactants adsorb at interfaces where they can find their most energetically advantageous conditions. Surfactant molecules in SPA thus tend to form spherical micelles. Upon addition of polyol and in-situ generation of electrolyte during the reaction these spherical micelles having negative head groups get attracted toward the positively charged electrolytes. This causes a transformation of spherical micelles to rod-like shapes with polyols altering the packing parameters of the surfactants from <1/3 to >1/3 up to 1.

These rod shape surfactant micelles interact and entangle with each other resulting in higher viscosity leading to a cage-like effect and causing SPA to act as caging agents. This caging effect of SPA restrict the growth of particle size and at the same time deters any further collision or agglomeration of fabricated nano ZnOS particle that might cause an increase in size [7]. Entrapment of nano ZnOS particles provides control over the particle growth, and self-assembly of the macromolecules allows the defined arrangement of nanoparticles that is suitable and compatible with personal care products. These functionalized nanoparticles encaged in surfactant and polyol assembly act as antibacterial agents and reduce the requirement for preservatives. Functionalizing ZnO and silver, materials that are already approved safe to use in the health and hygiene industry is critical since several existing antibacterial agents are progressively getting banned or facing microbial resistance. An illustrative presentation of the synthesis of nano ZnOS in SPA acting as caging agent is shown (Figure 4.1 (a & b)).

4.3. Infusion of nano ZnOS in liquid cleansing product

In this study, a liquid cleaning product developed with the required concentrations of anionic and amphoteric surfactants and other fundamental ingredients were precisely quantified and dispersed in distilled water at a medium stirring. The liquid cleansing products were infused using different concentration levels of synthesized nano ZnOS i.e. 0.1%, 0.125%, and 0.2%. Further, to study the germicidal efficacy, disc diffusion method and EN 1276 studies have been conducted against Gram-positive and Gram-negative pathogens.

4.4. Results and Discussion

4.4.1. UV vis spectroscopy

UV-Vis spectra of AR grade ZnO, nano ZnO and nano ZnOS was recorded in the 300-500 nm wavelength range. UV-Vis spectroscopy was performed to determine the effect of doping silver concentration on the optical properties of the ZnO nanoparticles. Figure 4.2 (a) shows the UV-Vis spectra of the ZnOS nanoparticles. Spectrum for the AR grade ZnO is also provided for comparison. AR grade ZnO nanoparticles show UV absorption edge at 386 nm while all the spectra of synthesized nano ZnOS showed the typical broad absorption, with a blue shift in absorption peak in the range of 340-351 nm indicating successful synthesis of nano ZnO.

However, a blue shift of UV absorbance edge is observed with increasing silver doping, indicating an increase in the band gap indicating the Burstein-Moss effect.

Based on UV absorption edge, the band gap (Eg) was calculated with formula:

$$E = \frac{hc}{\lambda}$$

where: h = 6.626 x 10^{-34} Joules sec is the Plancks constant, c = 3.0 x 10^{8} m/s is the speed of light and λ is the wavelength

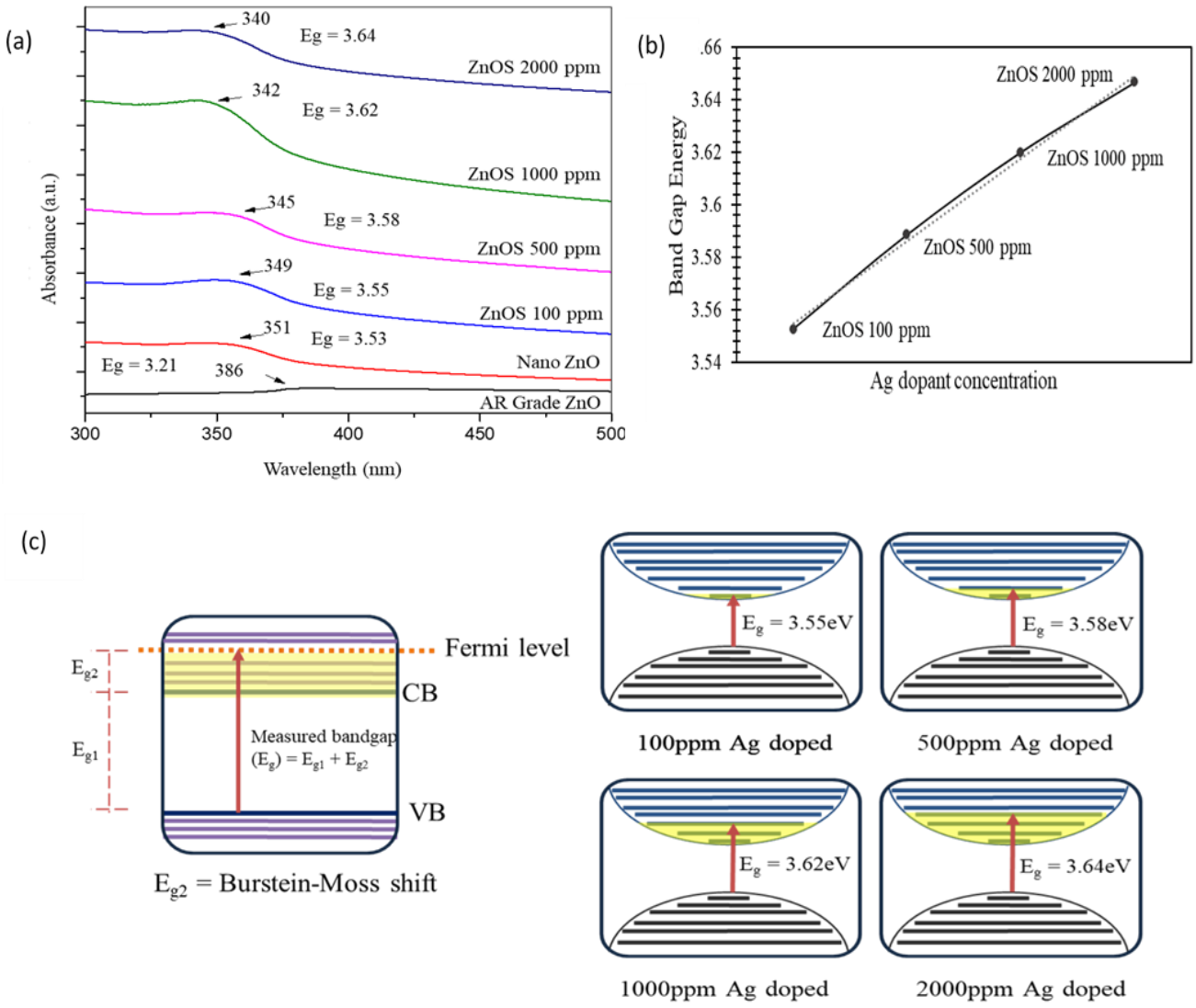

Figure 4.2. *(a) UV-vis spectra and band gap energy of the synthesized ZnO and nano ZnOS (b) Band gap energy (Eg) of samples as a function of silver contents (c) Schematic view of the Burstein-Moss effect in nano ZnOS*

The values of the optical band gap of nano ZnOS show a widening up to 3.64 eV for nano ZnOS 2000 ppm as compared to that of 3.21 eV obtained for AR grade ZnO. The optical band gap for nano ZnO is 3.53 eV and further, an increase in Eg is observed from nano ZnOS 100-2000 ppm from 3.55 eV to 3.64 eV i.e. with increased silver doping there is an increase in band gap energy (Figure 4.2 (b)). This widening of the band gap can be due to the Burstein-Moss effect in the metal doped system. With an increase in silver doping, there is a possibility of more impurity in mid-gap states, occupying initial levels of the conduction band thus leading to a noteworthy shift in the energy band gap. It can be suggested that the Fermi level shifts upward within the conduction band from the lower edge of the conduction band (Figure 4.2 (c)) [31], [32].

4.4.2. Fourier-Transform Infrared (FT-IR) Spectroscopy

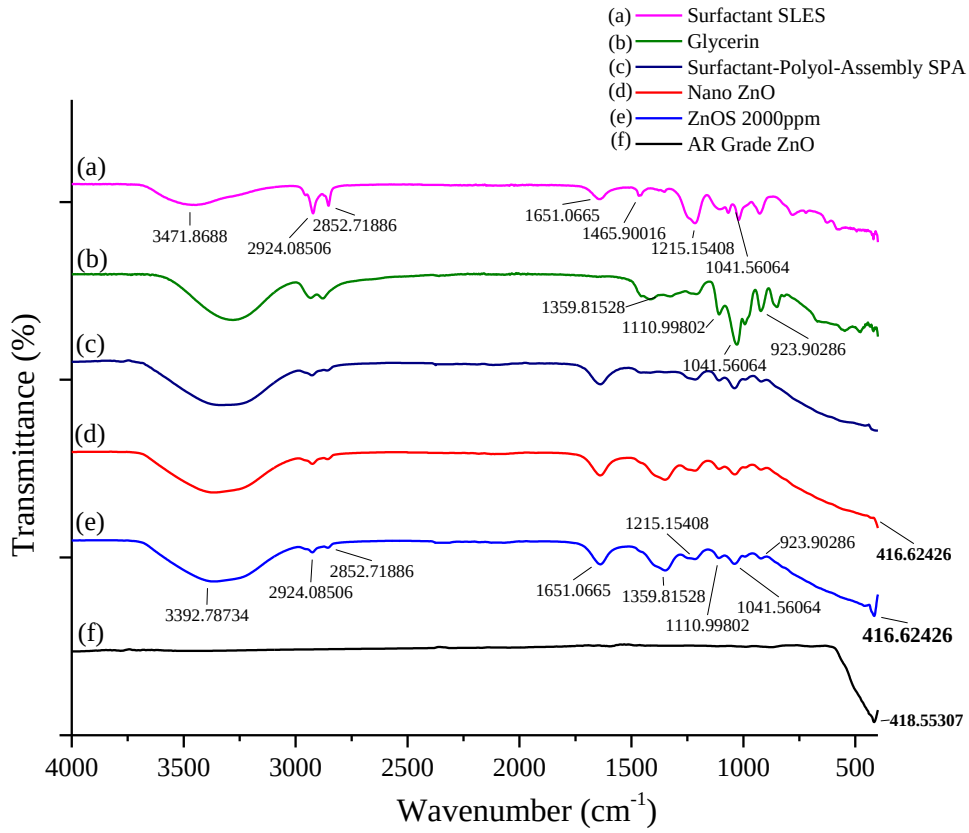

Figure 4.3. *FT-IR spectra of (a) surfactant SLES (b) glycerin (c) SPA (d) nano ZnO (e) nano ZnOS 2000 ppm and (f) AR grade ZnO, in the range of 400–4000 cm^{-1}*

The FT-IR spectrum of fabricated nano ZnOS, nano ZnO and its components shows absorption bands in different regions indicating the presence of specific functional groups

(Figure 4.3). The absorbance peak at 3471 - 3392 cm^{-1} in all spectra corresponds to the O-H stretching vibrations due to H_2O present during synthesis. The absorbance bands at 2924 cm^{-1} and 2852.71 cm^{-1} seen in all spectra can be attributed to the symmetrical and asymmetrical stretching due to C-H. Additionally, absorbance peaks at 1651 cm^{-1} and 1359 cm^{-1} present in spectra (a, c, d and e) are attributed to carbon bond vibrations present in SLES and glycerin respectively. The peak at 1215 cm^{-1} in spectra (a, c, d and e) could be because of the S=O vibration of sulfur-oxy compounds in SLES 2EO [33]. The peak at 1110 cm^{-1} could be due to the C-O stretching vibration of the secondary alcohol group while the peaks at 1042 cm^{-1} and 923 cm^{-1} suggest deformation vibration of (CH), (C-C) and C-O-C stretching due to the presence of surfactant (SLES 2EO) and glycerin [34]. The absorption peak at about 416 - 418 cm^{-1} is related to a typical FT-IR absorption peak of ZnO which originates from the stretching mode of the Zn-O bond [35], [36]. No vibrations concerning silver were detected in doped ZnO samples due to the low content of silver doping. Except for the absorption bands mentioned above, no other distinguished peak related to any other functional group is detected in the FTIR spectrum which reflects that the synthesized product is without any significant impurity.

4.4.3. Scanning Electron Microscope Analysis (SEM) and Energy Dispersive X-ray Spectrophotometer (EDX)

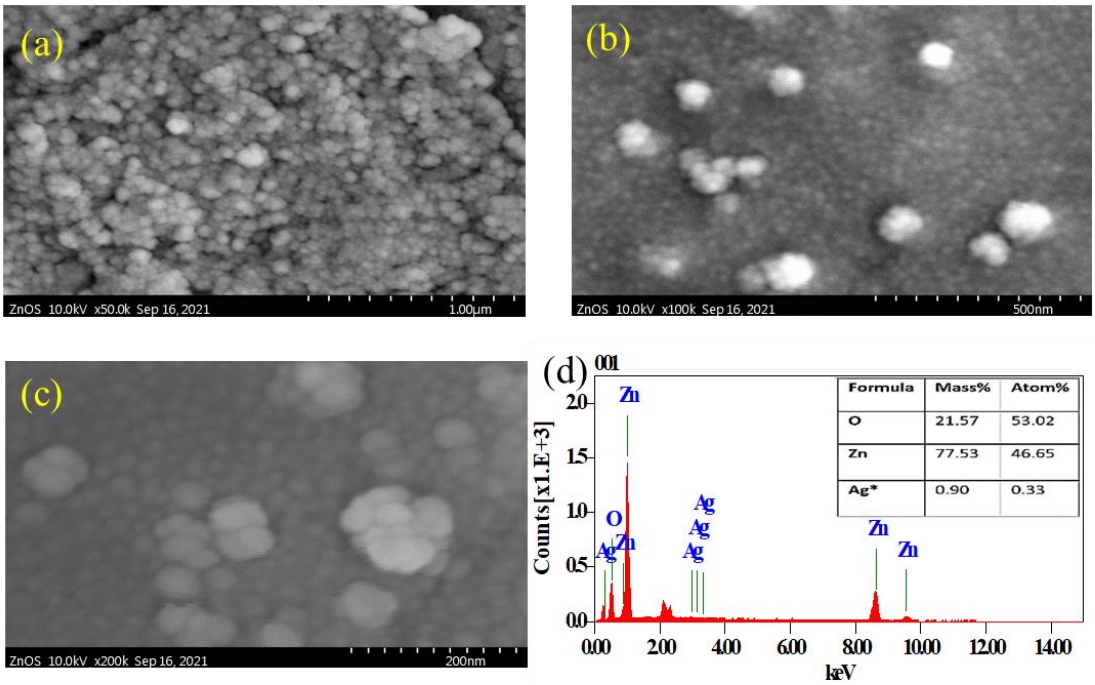

Figure 4.4. *(a-c) Representative electron micrographs of nano ZnOS 2000 ppm (d) EDX analysis of nano ZnOS 2000 ppm in graphical tabulated form*

The surface morphology of the nano ZnOS 2000 ppm were analyzed by SEM. Electron micrographs taken from SEM are shown in Figure 4.4 (a-c). These figures suggest spherical nanoparticles of highly similar size less than 100 nm as seen by the scale evenly distributed on the surface. Observed morphologies can be possibly attributed to the fabrication approach in SPA and in-situ generation of electrolytes influencing packing parameters. The energy dispersive X-ray spectroscopic analysis of the nano ZnOS also confirms the presence of silver in the doped ZnO. Figure 4.4 (d) is the EDX spectrum of nano ZnOS 2000 ppm. The compositional distribution ratio of nanomaterials was determined using an EDX spectroscopy (Figure 4.4 (d)), with the observations indicating the presence of Zn, Ag, and O in the nanomaterial. Atom % of Zn, O and Ag was shown to be 46.65, 53.02 and 0.33 respectively. The silver maximum at 2.5 keV shows relevant signal, indicating that silver is present in the ZnO nanostructures.

4.4.4. X-Ray Diffractometer Analysis

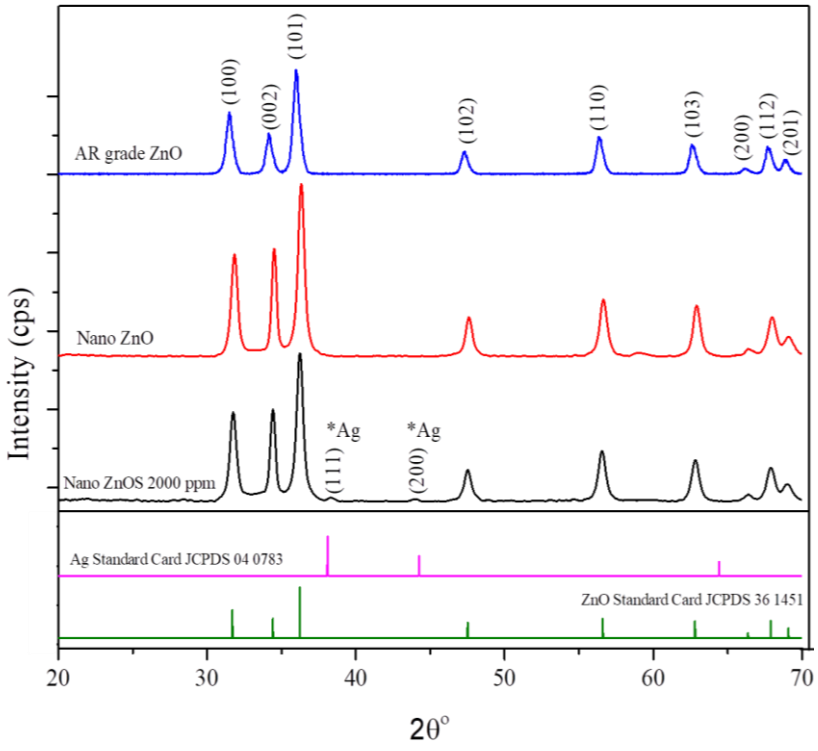

Figure 4.5. *XRD spectra of AR grade ZnO, synthesized nano ZnOS 2000 ppm and nano ZnO with JCPDS standard card of ZnO and Ag for reference*

Figure 4.5 Shows the XRD patterns of the nano ZnOS 2000 ppm nanoparticles synthesized in the SPA. XRD pattern of the AR grade ZnO and nano ZnO without any doping is also shown for

comparison. The diffractograms are illustrative for the samples centrifuged and dried at 50ºC after being synthesized in SPA. The XRD pattern can be indexed using the hexagonal wurtzite crystal structure of nano ZnO and no other crystalline phases were detected. The diffraction peaks of ZnO were distinguished on 2θ of 31.77°, 34.43°, 36.24°, 47.52°, 62.79°, 66.35°, and 68.95° according to the JCPDS 36-1451 (Figure 4.5) suggests hkl values of (100), (002), (101), (102), (110), (103), (200), (112) and (201) respectively. However, the ZnOS 2000 ppm revealed some additional diffraction peaks at 38.38° and 44° which corresponds to (111) and (200) sets of lattice planes associated with the face centered cubic phase of metallic Ag (JCPDS file No. 04-0783) as shown in Figure 4.5 [37]. The doping of silver nanoclusters on the grain boundaries of nano ZnO was confirmed since there is no shift in ZnO peaks. The XRD patterns and angles, as well as the Miller indices data for the produced nanomaterial, align with existing works of literatures [38], [39].

4.4.5. Physical characteristics evaluation from XRD

The lattice parameters a, b and c of nano ZnOS 2000 ppm and nano ZnO structures were calculated by using the following equations:

$$\frac{1}{d_{hkl}^2} = \frac{4}{3}\left(\frac{h^2 + hk + k^2}{a^2}\right) + \frac{l^2}{c^2}$$

where for hexagonal unit cell lattice a=b ≠ c, d_{hkl} is the interplanar spacing and hkl is the Miller indices

The average crystallite size (D) of the synthesized nano ZnOS was determined from the XRD data using the Debye-Scherer's equation (Table 4.1):

$$D_{hkl} = \frac{0.94\lambda}{\beta_{hkl}\, cos\theta}$$

where $\lambda_{CuK\alpha}$=1.5406 Å, β_{hkl} is the full-width at half maximum intensity (FWHM) of the XRD peaks in radians and θ is the Bragg's angle of the diffraction peak

For nano ZnO and nano ZnOS 2000 ppm, the crystalline size associated to the maximum peak in the XRD spectra was determined to be 15.14 nm and 15.16 nm, respectively this suggests that doping low levels of silver into the ZnO system does not affect the crystallite size significantly. The crystalline size of AR grade ZnO is however 30.87 nm. The appearance of strong peaks in XRD data and crystalline sizes smaller than 100 nm indicated that the synthesized was nanocrystalline.

The characteristic of solid materials that measures total surface area per unit mass of bulk volume area is known as specific surface area. The following equation can be used to calculate the specific surface area:

$$S = \frac{6 \times 10^3}{\mathrm{D} \times \rho}$$

where S- specific surface area, D – size of particle, ρ- density of ZnO i.e. 5.606 g/cm^3.

The specific surface area of nano ZnO and nano ZnOS crystallites was found to be 70.56 m^2. g^{-1} and 70.68 m^2. g^{-1} respectively and of AR grade ZnO was only 41.34 m^2. g^{-1}. Due to increased surface availability, there is higher ROS and/or ion generation resulting in a consequently increased disruption of bacterial cell walls. Thus high specific area will play a critical role in contributing to the high germicidal activity of nano ZnOS [40].

Additionally, toughness, density, opacity, and dispersion are all influenced by the level of crystallinity hence the effect of crystallinity is calculated using following formula:

$$Crystallinity = \frac{\text{Area of crystalline peaks}}{\text{Area of total peaks (crystalline + amorphous)}} \times 100$$

The crystallinity of nano ZnO and nano ZnOS crystallites was found to be 97.04% and 97.62% respectively while for AR grade ZnO it was only 95.57%.

The length of dislocation lines per unit volume i.e. dislocation density (δ) is calculated using the equation: $\delta = \frac{1}{D^2}$

Dislocation density is the number of defects present in the material. When there is a rise in these defects, the density of delocalized electrons increases causing a higher affinity between the delocalized electrons and the nucleus, which increases the stability of the material. An increase in dislocation density has also been recognized to be responsible for nanoparticles with high surface energy due to an increase in the ratio of surface atoms, which consequently leads to higher germicidal efficacy [41]–[43].

The results calculated from the above equations are tabulated in Table 4.1.

Table 4.1. Structural and optical parameters of AR grade ZnO, nano ZnO and nano ZnOS 2000 ppm.

Nano material	**Average Crystallite Size (D) (nm)**	**Lattice Parameters (Å)**		**Dislocation Density (δ) (lines/m^2)**	**Specific surface area (S) (m^2. g^{-1})**	**Crystallinity (%)**
		a	**c**			
AR Grade ZnO	30.87	3.27	5.24	0.0017	41.34	95.57
Nano ZnO	15.16	3.24	5.19	0.0055	70.56	97.04
Nano ZnOS 2000 ppm	15.14	3.24	5.20	0.0064	70.68	97.62

The supercell was chosen as a 3×3×2 growth of the nanoscale ZnO cell, thus comprising 36 Zn atoms and 36 O atoms [44]. It is further observed from Table 4.1 that crystallinity, crystalline size and lattice parameters are comparable in both nano ZnO and nano ZnOS nanomaterials, unlike bulk AR grade ZnO. At ambient conditions, the thermodynamically stable phase of nano ZnO is the Wurtzite structure, in which every zinc atom is tetrahedrally coordinated with four oxygen atoms. The optimal sites for silver molecules are determined by calculating the formation energies of different doped ratios. Dopant silver at the Zn site, dopant Ag at the O site, and Ag at the interstitial site are the three doping situations studied. Their respective positions are depicted in Figure 4.6 (b-d). It has been observed previously by Yanlu Li et.al [45] that the silver atom favors the zinc atom substitution site under both zinc and oxygen-rich environments, and silver substitution of the zinc atom is the energetically favorable configuration. The formation energy of silver substitution of zinc atom is considerably decreased under an oxygen-rich environment that silver possibly opts not to replace oxygen site nor occupy interstitial sites. While silver may substitute oxygen atom site when in a zinc-rich environment i.e. silver and zinc precursors are in excess. It has also been noted that the formation energy of the stable silver substitution in interstitial configuration is very high, making it undesirable to occupy any interstitial site of the ZnO network under either zinc or oxygen-rich environments [45].

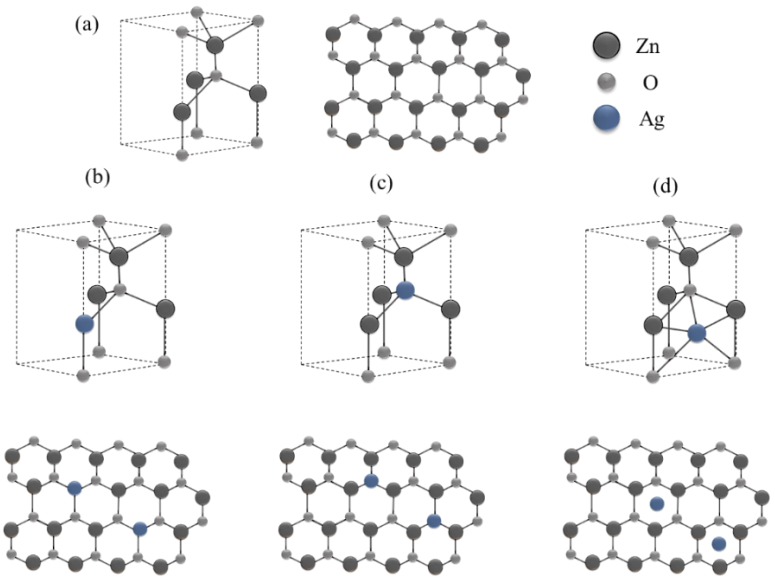

Figure 4.6. *An illustration of Stick-and-ball stacking model of (a) ZnO crystals and atomic substitution locations of Ag (b) Zn substitution (c) O substitution (d) interstational*

4.4.6. Rheological properties and pH of nano ZnO-SPA

The viscosity of the fabricated nano ZnO, nano ZnOS, SPA, and reagents was measured using the Brookfield Rheometer and determined as 2381 cps for nano ZnOS and 5.87 cps for SPA, respectively (Table 4.2). During the synthesis of nano ZnOS in surfactant (SLES-2EO) and polyol solution, in-situ formation of NaCl ions causes the conversion of spherical surfactant micellar to rod-shaped micelles, resulting in enhanced viscosity relative to SPA. Nano ZnOS has a pH of 7.64, which is in the neutral region, meaning it has little to no influence on the pH of finished products. Table 4.2 lists the pH of SPA, nano ZnO, and nano ZnOS 2000 ppm as well as the components utilized in the fabrication of nano ZnOS.

Table 4. 2. pH and viscosity of SPA, nano ZnO, nano ZnOS and reagents.

Sr. No.	Name of material	pH value	Viscosity (cps)
1.	SPA	7.50	5.87
2.	Nano ZnO	7.80	2254
3.	Nano ZnOS	7.64	2381
4.	Zinc Nitrate (0.615 M solution)	5.52	1.98
5.	NaOH (1.23 M solution)	13.67	4.11
6.	Surfactant (SLES 2EO) (0.54 M solution)	7.60	5.41
7.	Polyol (Glycerin) (1.62 M solution)	6.01	4.23

4.5. Germicidal Efficacy

4.5.1. ZOI of SPA, AR grade ZnO, nano ZnO and nano ZnOS

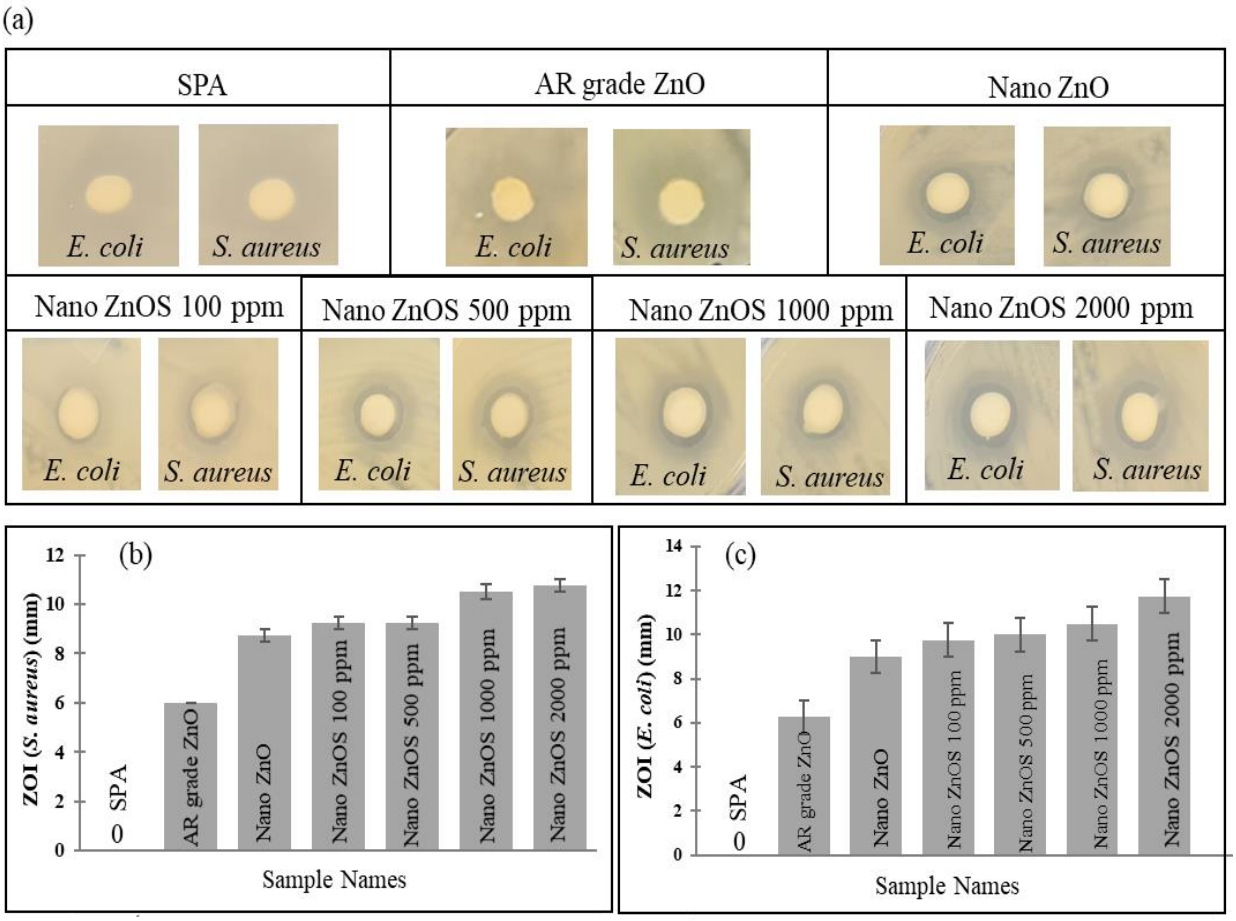

Figure 4.7. *(a) Pictorial and Graphical representation of germicidal disc diffusion method with (b) S. aureus and (c) E. coli on agar plates with SPA, AR grade ZnO, synthesized nano ZnO and nano ZnOS (100-2000 ppm)*

The ZOI was used to evaluate the germicidal activity of nano ZnOS nanomaterials as a function of silver concentration**.** Germicidal potency shown to improve significantly compared to AR grade ZnO when the silver concentration was increased. It is reasonable to infer that when particle size decreases, the number of particles in a solution increases, leading to greater surface area and reactive oxygen species production. Germicidal experiments with AR grade ZnO, nano ZnO and ZnOS at different percentages are shown in Figure 4.7.

Table 4.3: Zone of inhibition, standard deviation and error for SPA, AR grade ZnO, nano ZnO and nano ZnOS (100 ppm-2000 ppm) against E. coli and S. aureus

Sample details	*E.coli*			*S.aureus*		
	ZOI (mm)	Std. Deviation	Std. Error	ZOI (mm)	Std. Deviation	Std. Error
SPA	0.00	0.00	0.00	0.00	0.00	0.00
AR grade ZnO	6.25	0.50	0.25	6.00	0.00	0.00
Nano ZnO	9.00	0.82	0.41	8.75	0.50	0.25
Nano ZnOS 100 ppm	9.75	0.50	0.25	9.25	0.50	0.25
Nano ZnOS 500 ppm	10.00	0.82	0.41	9.25	0.50	0.25
Nano ZnOS 1000 ppm	10.50	1.00	0.50	10.50	0.58	0.29
Nano ZnOS 2000 ppm	11.75	0.96	0.48	10.75	0.50	0.25

The results displayed in Figure 4.7 and Table 4.3 suggests that there is an increase in germicidal efficacy with silver doping. The efficacy increases significantly with increasing doping concentration in both Gram-negative and Gram-positive bacteria. Nano ZnOS 2000 ppm shows significantly higher germicidal efficacy when compared to undoped nano ZnO and base SPA. This was confirmed by running statistics showing probability values (p-values) less than 0.05 (i.e. significantly more than 95%). Nano ZnOS 2000 ppm showed significantly higher germicidal activity against nano ZnO and SPA having p-value of 0.0027 and 0.00045 respectively.

4.5.2. Germicidal Efficacy: EN 1276 of SPA, nano ZnO and nano ZnOS

The germicidal efficacy of nano ZnO and the synthesized nano ZnOS 2000 ppm in the SPA was further tested using the EN 1276 protocol. They were tested against the following microbes, *E. coli* and *S. aureus*. It can be observed that nano ZnO has a log reduction of 2.97 and 2.86 while nano ZnOS 2000 ppm has an impressive log reduction of up to 5.41 indicating germ kill >99.999% (Table 4.4). The phrase "$\log_{10}$ reduction" refers to a 10 times or 90% decline in the amount of live microbes. The term "3 log" reduction means a decrease of 99.9% in the number of live microbes. The term "5 log" reduction refers to the 99.999% microbes are inactive.

Table 4.4: EN 1276 results for SPA, nano ZnO and nano ZnOS against E. coli and S. aureus

Sample details	**SPA**		**Nano ZnO**		**Nano ZnOS 2000 ppm**	
Test parameter	*E.coli*	*S.aureus*	*E.coli*	*S.aureus*	*E.coli*	*S.aureus*
Bactericidal effect log_{10} reduction	Too numerous to count	Too numerous to count	2.97	2.86	5.41	4.57

The morphological variations in the bacterium cell wall are among the major motivations for evaluating both Gram-positive and Gram-negative bacteria. Gram-positive bacteria have a cellular structure consisting largely of a thick peptidoglycan substrate but lack an outer lipid membrane. Gram-negative bacteria have a relatively complicated cellular structure due to the existence of an external membrane made primarily of lipopolysaccharide (LPS) and a small peptidoglycan layer [46]. As a result, examining the germicidal activity of nanomaterials against both kinds will provide extensive information on their broad-spectrum efficacy. Additionally, numerous factors can influence ZnO nanoparticles' germicidal effectiveness, including their size and hence surface area, along with their ability to work in tandem with other germicidal compounds. However, overall significantly high germicidal efficacy makes these synthesized nanomaterials a very suitable and potent candidate for various product applications.

4.6. Industrial Application in Liquid Cleansing Product

Novel liquid cleansing products are fabricated with the addition of doped and undoped ZnO in different ratios and characterized to evaluate the germicidal properties against both *E. coli* and *S. aureus.*

4.7. Germicidal efficacy

4.7.1. Zone of Inhibition (ZOI) of Liquid Cleansing Product

The base formulation of the liquid cleansing product shows Nil germicidal activity i.e. no antimicrobial action. This base formulation was then enhanced by adding 0.1%, 0.125%, and 0.2% of AR grade ZnO, prepared nano ZnO and the synthesized nano ZnOS 1000 ppm and 2000 ppm in the SPA.

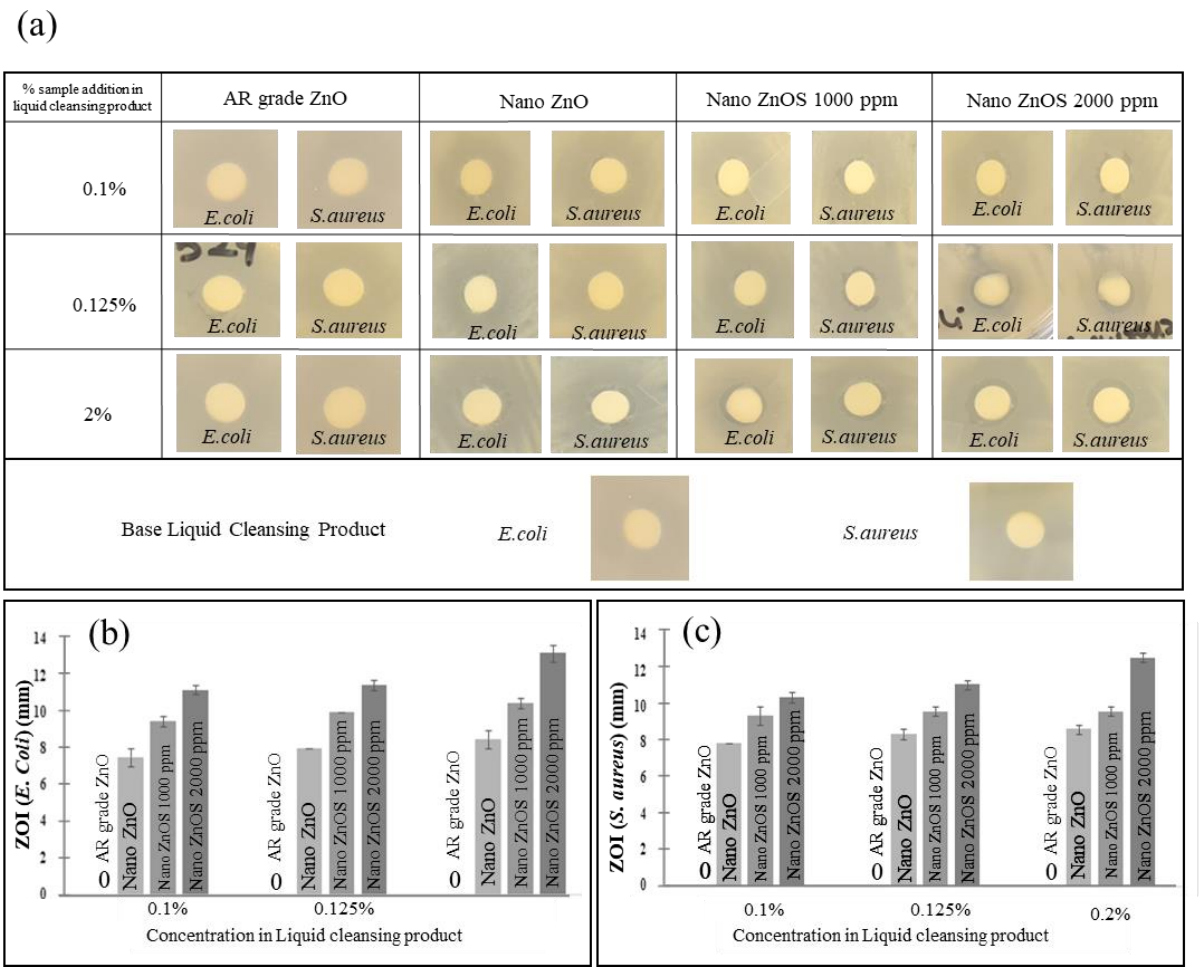

Figure 4.8. *(a) Pictorial results of E. coli and S. aureus on agar plates with base liquid cleansing product enhanced with AR grade ZnO, nano ZnO and nano ZnOS (1000 ppm and 2000 ppm) using concentrations 0.1%, 0.125%, and 0.2% with base liquid cleansing product for reference (b) Graphical representation of results against E. coli (c) Graphical representation of results against S. aureus*

Figure 4.8 and Table 4.5 show the ZOI in mm conducted by the disc diffusion method. It can be seen that there is a significant increase with a 0.2% addition of nano ZnOS but no activity with AR grade ZnO. Within 0.2% addition, both nano ZnOS 1000 and 2000 ppm show significantly higher germicidal efficacy compared to undoped nano ZnO having a p-value less than 0.05 (i.e. significantly more than 95%). ZnOS 1000 ppm showed significantly higher germicidal activity against undoped nano ZnO having a p-value of 0.0066. ZnOS 2000 ppm also exhibits significantly higher germicidal activity against undoped ZnO having a p-value 0.0005. The highest ZOI for both Gram-positive and Gram-negative bacteria has been displayed by nano ZnOS 2000 ppm.

Table 4.5. Zone of inhibition, standard deviation and error for liquid cleansing product enhanced with AR grade ZnO, nano ZnO and nano ZnOS (1000 ppm and 2000 ppm) using concentrations 0.1%, 0.125%, and 0.2% with E. coli and S. aureus

		E.coli			*S.aureus*		
Concentration in industrial cleansing product		0.1%	0.125%	0.2%	0.1%	0.125%	0.2%
Base Liquid cleansing product	ZOI(mm)	0	0	0	0	0	0
AR grade ZnO	ZOI(mm)	0	0	0	0	0	0
Nano ZnO	ZOI(mm)	7.50	8	8.50	8.00	8.50	8.75
	Standard Deviation	1.00	0	1.00	0	0.58	0.50
	Standard error	0.50	0	0.50	0	0.29	0.25
Nano ZnOS 1000 ppm	ZOI(mm)	9.50	10.00	10.50	9.50	9.75	9.75
	Standard Deviation	0.58	0.05	0.58	1.00	0.50	0.50
	Standard error	0.29	0.025	0.29	0.50	0.25	0.25
Nano ZnOS 2000 ppm	ZOI(mm)	11.25	11.5	13.25	10.5	11.25	12.75
	Standard Deviation	0.50	0.58	0.96	0.58	0.50	0.50
	Standard error	0.25	0.29	0.48	0.29	0.25	0.25

4.7.2. EN 1276 of Liquid Cleansing Product

The germicidal efficacy of prepared liquid cleansing products was enhanced by adding 0.2% as prepared nano ZnO and the synthesized nano ZnOS 2000 ppm in the SPA which was further tested using EN 1276 protocol. It can be observed that ZnO and 2000pm ZnOS liquid cleansers have a significant log reduction between 1.96 and 3.85 (Table 4.6).

Table 4.6: Liquid cleansing product enhanced with nano ZnO and nano ZnOS 2000 ppm using concentrations 0.1%, 0.125%, and 0.2%

Sample details	**0.2% nano ZnO in Liquid Cleansing Product**				**0.2% nano ZnOS 2000 ppm in Liquid Cleansing Product**			
Test parameter	***E.coli***	***S.aureus***	***P.aeruginosa***	***E.hirae***	***E.coli***	***S.aureus***	***P.aeruginosa***	***E.hirae***
Bactericidal effect log reduction	1.98	1.96	1.84	2.15	2.13	2.26	3.85	2.25

References

[1] T. T. Doanh, N. Van Hieu, T. N. Quynh Trang, and V. T. Hanh Thu, "In situ synthesis of hybrid zinc oxide-silver nanoparticle arrays as a powerful active platform for surface-enhanced Raman scattering detection," *J. Sci. Adv. Mater. Devices*, vol. 6, no. 3, pp. 379–389, Sep. 2021, doi: 10.1016/j.jsamd.2021.03.007.

[2] L. S. R. Yadav *et al.*, "Green synthesis of Ag ZnO nanoparticles: Structural analysis, hydrogen generation, formylation and biodiesel applications," *J. Sci. Adv. Mater. Devices*, vol. 4, no. 3, pp. 425–431, Sep. 2019, doi: 10.1016/j.jsamd.2019.03.001.

[3] A. Elhalil *et al.*, "Novel Ag-ZnO-La2O2CO3 photocatalysts derived from the Layered Double Hydroxide structure with excellent photocatalytic performance for the degradation of pharmaceutical compounds," *J. Sci. Adv. Mater. Devices*, vol. 4, no. 1, pp. 34–46, Mar. 2019, doi: 10.1016/j.jsamd.2019.01.002.

[4] P. Karthikeyan, S. Sathishkumar, K. Pandian, L. Mitu, and R. Rajavel, "Novel copper doped Halloysite Nano Tube/silver-poly(pyrrole-co-3,4-ethylenedioxythiophene) dual layer coatings on low nickel stainless steel for anti-corrosion applications," *J. Sci. Adv. Mater. Devices*, vol. 3, no. 1, pp. 59–67, Mar. 2018, doi: 10.1016/j.jsamd.2017.12.003.

[5] S. Suresh, S. Karthikeyan, and K. Jayamoorthy, "FTIR and multivariate analysis to study the effect of bulk and nano copper oxide on peanut plant leaves," *J. Sci. Adv. Mater. Devices*, vol. 1, no. 3, pp. 343–350, Sep. 2016, doi: 10.1016/j.jsamd.2016.08.004.

[6] H. Ehtesabi, "Application of carbon nanomaterials in human virus detection," *J. Sci. Adv. Mater. Devices*, vol. 5, no. 4, pp. 436–450, Dec. 2020, doi: 10.1016/j.jsamd.2020.09.005.

[7] N. Bhalla *et al.*, "A facile approach to fabricate and embed multifunctional nano ZnO into soap matrix and liquid cleansing products for enhanced antibacterial and photostability for health and hygiene applications," *Arab. J. Chem.*, vol. 15, no. 6, p. 103862, Jun. 2022, doi: 10.1016/j.arabjc.2022.103862.

[8] M. A. Mitchnick, D. Fairhurst, and S. R. Pinnell, "Microfine zinc oxide (Z-Cote) as a photostable UVA/UVB sunblock agent," *J. Am. Acad. Dermatol.*, vol. 40, no. 1, pp. 85–90, Jan. 1999, doi: 10.1016/S0190-9622(99)70532-3.

[9] T. Singh, A. Jayaprakash, M. Alsuwaidi, and A. A. Madhavan, "Green synthesized gold nanoparticles with enhanced photocatalytic activity," *Mater. Today Proc.*, vol. 42, pp. 1166–1169, 2021, doi: 10.1016/j.matpr.2020.12.531.

[10] M. Shaban, F. Mohamed, and S. Abdallah, "Production and Characterization of Superhydrophobic and Antibacterial Coated Fabrics Utilizing ZnO Nanocatalyst," *Sci. Rep.*, vol. 8, no. 1, p. 3925, Mar. 2018, doi: 10.1038/s41598-018-22324-7.

[11] A. Bachvarova-Nedelcheva, R. Iordanova, A. Stoyanova, R. Gegova, Y. Dimitriev, and A. Loukanov, "Photocatalytic properties of ZnO/TiO2 powders obtained via combustion gel method," *Open Chem.*, vol. 11, no. 3, pp. 364–370, Mar. 2013, doi: 10.2478/s11532-012-0167-2.

[12] B. Abebe, E. A. Zereffa, A. Tadesse, and H. C. A. Murthy, "A Review on Enhancing the Antibacterial Activity of ZnO: Mechanisms and Microscopic Investigation," *Nanoscale Res. Lett.*, vol. 15, no. 1, p. 190, Dec. 2020, doi: 10.1186/s11671-020-03418-6.

[13] C.-T. Lee, "Fabrication Methods and Luminescent Properties of ZnO Materials for Light-Emitting Diodes," *Materials (Basel).*, vol. 3, no. 4, pp. 2218–2259, Mar. 2010, doi: 10.3390/ma3042218.

[14] S. Kumar, R. Seth, S. Panwar, K. K. Goyal, V. Kumar, and R. K. Choubey, "Morphological and Optical Studies of ZnO-Silica Nanocomposite Thin Films Synthesized by Time Dependent CBD," *J. Electron. Mater.*, vol. 50, no. 6, pp. 3462–3470, Jun. 2021, doi: 10.1007/s11664-021-08863-2.

[15] C. Baker, A. Pradhan, L. Pakstis, D. Pochan, and S. I. Shah, "Synthesis and Antibacterial Properties of Silver Nanoparticles," *J. Nanosci. Nanotechnol.*, vol. 5, no. 2, pp. 244–249, Feb. 2005, doi: 10.1166/jnn.2005.034.

[16] M. Guzman, J. Dille, and S. Godet, "Synthesis and antibacterial activity of silver nanoparticles against gram-positive and gram-negative bacteria," *Nanomedicine Nanotechnology, Biol. Med.*, vol. 8, no. 1, pp. 37–45, Jan. 2012, doi: 10.1016/j.nano.2011.05.007.

[17] L. Motelica *et al.*, "Innovative Antimicrobial Chitosan/ZnO/Ag NPs/Citronella Essential Oil Nanocomposite—Potential Coating for Grapes," *Foods*, vol. 9, no. 12, p. 1801, Dec. 2020, doi: 10.3390/foods9121801.

[18] B. Ranjithkumar *et al.*, "Evaluation of structural, surface morphological and thermal properties of Ag-doped ZnO nanoparticles for antimicrobial activities," *Phys. E Low-dimensional Syst. Nanostructures*, vol. 133, p. 114801, Sep. 2021, doi: 10.1016/j.physe.2021.114801.

[19] K. Kalwar and D. Shan, "Antimicrobial effect of silver nanoparticles (AgNPs) and their mechanism – a mini review," *Micro Nano Lett.*, vol. 13, no. 3, pp. 277–280, Mar. 2018, doi: 10.1049/mnl.2017.0648.

[20] R. Rajendran and A. Mani, "Photocatalytic, antibacterial and anticancer activity of silver-doped zinc oxide nanoparticles," *J. Saudi Chem. Soc.*, vol. 24, no. 12, pp. 1010–1024, Dec. 2020, doi: 10.1016/j.jscs.2020.10.008.

[21] S. Goktas and A. Goktas, "A comparative study on recent progress in efficient ZnO based nanocomposite and heterojunction photocatalysts: A review," *J. Alloys Compd.*, vol. 863, p. 158734, May 2021, doi: 10.1016/j.jallcom.2021.158734.

[22] S. Kumar *et al.*, "Variation in chemical bath pH and the corresponding precursor concentration for optimizing the optical, structural and morphological properties of ZnO thin films," *J. Mater. Sci. Mater. Electron.*, vol. 30, no. 19, pp. 17747–17758, Oct. 2019, doi: 10.1007/s10854-019-02125-y.

[23] V. Rajendar, T. Dayakar, C. H. S. Chakra, and K. V. Rao, "Systematic Approach on the Fabrication of Ag Doped ZnO Nanoparticles by Novel Auto Combustion Method for Antibacterial Applications," *Nanomedicine and Nanobiology*, vol. 2, no. 1, pp. 21–27, Dec. 2015, doi: 10.1166/nmb.2015.1013.

[24] R. U. Halden, "On the Need and Speed of Regulating Triclosan and Triclocarban in the United States," *Environ. Sci. Technol.*, vol. 48, no. 7, pp. 3603–3611, Apr. 2014, doi: 10.1021/es500495p.

[25] S. D. Lamore, C. M. Cabello, and G. T. Wondrak, "The topical antimicrobial zinc pyrithione is a heat shock response inducer that causes DNA damage and PARP-dependent energy crisis in human skin cells," *Cell Stress Chaperones*, vol. 15, no. 3, pp. 309–322, May 2010, doi: 10.1007/s12192-009-0145-6.

[26] M. Azizi-Lalabadi, A. Ehsani, B. Divband, and M. Alizadeh-Sani, "Antimicrobial activity of Titanium dioxide and Zinc oxide nanoparticles supported in 4A zeolite and evaluation the morphological characteristic," *Sci. Rep.*, vol. 9, no. 1, p. 17439, Nov. 2019, doi: 10.1038/s41598-019-54025-0.

[27] S. Kumar, A. Mudai, B. Roy, I. B. Basumatary, A. Mukherjee, and J. Dutta, "Biodegradable Hybrid Nanocomposite of Chitosan/Gelatin and Green Synthesized Zinc Oxide Nanoparticles for Food Packaging," *Foods*, vol. 9, no. 9, p. 1143, Aug. 2020, doi: 10.3390/foods9091143.

[28] Swati *et al.*, "Antimicrobial potential of ag-doped ZnO nanostructure synthesized by the green method using moringa oleifera extract," *J. Environ. Chem. Eng.*, vol. 8, no. 3, p. 103730, Jun. 2020, doi: 10.1016/j.jece.2020.103730.

[29] N. Sharma, J. Kumar, S. Thakur, S. Sharma, and V. Shrivastava, "Antibacterial study of silver doped zinc oxide nanoparticles against Staphylococcus aureus and Bacillus subtilis," *Drug Invent. Today*, vol. 5, no. 1, pp. 50–54, Mar. 2013, doi: 10.1016/j.dit.2013.03.007.

[30] P. Bhattacharya and S. Neogi, "Antibacterial properties of doped nanoparticles," *Rev. Chem. Eng.*, vol. 35, no. 7, pp. 861–876, Oct. 2019, doi: 10.1515/revce-2017-0116.

[31] E. Burstein, "Anomalous Optical Absorption Limit in InSb," *Phys. Rev.*, vol. 93, no. 3, pp. 632–633, Feb. 1954, doi: 10.1103/PhysRev.93.632.

[32] Q. Zhu, J. Lu, Y. Wang, F. Qin, Z. Shi, and C. Xu, "Burstein-Moss Effect Behind Au Surface Plasmon Enhanced Intrinsic Emission of ZnO Microdisks," *Sci. Rep.*, vol. 6, no. 1, p. 36194, Nov. 2016, doi: 10.1038/srep36194.

[33] S. Cunliffe, P. Martin, M. Baker, O. Mihailova, and P. Martin, "Near infrared absorption spectroscopy for the quantification of unsulfated alcohol in sodium lauryl ether sulfate," *J. Near Infrared Spectrosc.*, vol. 29, no. 1, pp. 11–23, Feb. 2021, doi: 10.1177/0967033520963825.

[34] A. Y. Hammoudeh, S. M. Obeidat, E. K. Abboushi, and A. M. Mahmoud, "FT-IR Spectroscopy for the Detection of Diethylene Glycol (DEG) Contaminant in Glycerin-Based Pharmaceutical Products and Food Supplements," *Acta Chim. Slov.*, vol. 67, no. 2, pp. 530–536, Jun. 2020, doi: 10.17344/acsi.2019.5553.

[35] L. A. Berglund and I. Burgert, "Bioinspired Wood Nanotechnology for Functional Materials," *Adv. Mater.*, vol. 30, no. 19, p. 1704285, May 2018, doi: 10.1002/adma.201704285.

[36] O. Bechambi, M. Chalbi, W. Najjar, and S. Sayadi, "Photocatalytic activity of ZnO doped with Ag on the degradation of endocrine disrupting under UV irradiation and the investigation of its antibacterial activity," *Appl. Surf. Sci.*, vol. 347, pp. 414–420, Aug. 2015, doi: 10.1016/j.apsusc.2015.03.049.

[37] G. Y. Nigussie *et al.*, "Antibacterial Activity of Ag-Doped TiO 2 and Ag-Doped ZnO Nanoparticles," *Int. J. Photoenergy*, vol. 2018, pp. 1–7, 2018, doi: 10.1155/2018/5927485.

[38] R. S. Zeferino, M. B. Flores, and U. Pal, "Photoluminescence and Raman Scattering in Ag-doped ZnO Nanoparticles," *J. Appl. Phys.*, vol. 109, no. 1, p. 014308, Jan. 2011, doi: 10.1063/1.3530631.

[39] H. A. Habeeb Alshamsi and B. S. Hussein, "Hydrothermal Preparation of Silver Doping Zinc Oxide Nanoparticles: Studys, Characterization and Photocatalytic Activity," *Orient. J. Chem.*, vol. 34, no. 4, pp. 1898–1907, Aug. 2018, doi: 10.13005/ojc/3404025.

[40] A. Abdal Dayem *et al.*, "The Role of Reactive Oxygen Species (ROS) in the Biological Activities of Metallic Nanoparticles," *Int. J. Mol. Sci.*, vol. 18, no. 1, p. 120, Jan. 2017, doi: 10.3390/ijms18010120.

[41] P. Gnanamozhi *et al.*, "Enhanced antibacterial and photocatalytic degradation of reactive red 120 using lead substituted ZnO nanoparticles prepared by ultrasonic-assisted co-precipitation method," *Ceram. Int.*, vol. 46, no. 11, pp. 19593–19599, Aug. 2020, doi: 10.1016/j.ceramint.2020.05.020.

[42] P. Bindu and S. Thomas, "Estimation of lattice strain in ZnO nanoparticles: X-ray peak profile analysis," *J. Theor. Appl. Phys.*, vol. 8, no. 4, pp. 123–134, Dec. 2014, doi: 10.1007/s40094-014-0141-9.

[43] M. Gomathi, P. V. Rajkumar, and A. Prakasam, "Study of dislocation density (defects such as Ag vacancies and interstitials) of silver nanoparticles, green-synthesized using Barleria cristata leaf extract and the impact of defects on the antibacterial activity," *Results Phys.*, vol. 10, pp. 858–864, Sep. 2018, doi: 10.1016/j.rinp.2018.08.011.

[44] Y. S. Avadhut, J. Weber, E. Hammarberg, C. Feldmann, and J. Schmedt auf der Günne, "Structural investigation of aluminium doped ZnO nanoparticles by solid-state NMR spectroscopy," *Phys. Chem. Chem. Phys.*, vol. 14, no. 33, p. 11610, 2012, doi: 10.1039/c2cp41139c.

[45] Y. Li, X. Zhao, and W. Fan, "Structural, Electronic, and Optical Properties of Ag-Doped ZnO Nanowires: First Principles Study," *J. Phys. Chem. C*, vol. 115, no. 9, pp. 3552–3557, Mar. 2011, doi: 10.1021/jp1098816.

[46] T. J. Silhavy, D. Kahne, and S. Walker, "The Bacterial Cell Envelope," *Cold Spring Harb. Perspect. Biol.*, vol. 2, no. 5, pp. a000414–a000414, May 2010, doi: 10.1101/cshperspect.a000414.

Chapter 5

Green Approach to Synthesize Nano Zinc Oxide via Moringa Oleifera Leaves for Enhanced Health & Wellness Applications

Highlights of the Chapter:

- *In this present study phytochemical analysis have been done on the aqueous and methanolic Moringa leaves extracts using GCMS and their free radical scavenging potency (FRSP) studied for further applications.*
- *These extracts can act as very powerful antioxidants, anti-inflammatory ingredient for various applications in diverse field of food, cosmetics, medicine etc.*
- *Moringa oleifera comprises various phytochemicals that act as non-toxic stabilizing and reducing agents. Green synthesized ZnO nanoparticles (GsZnO-Nps) were investigated for their morphological and physicochemical properties using various advanced characterizing techniques.*
- *Anti-oxidant activity is recommended to improve general health by helping to neutralize free radicals in our systems. Strong anti-acne efficacy established against C. acne bacteria which is mostly responsible for causing acne on skin, the average inhibition zone was 33.00 mm.*
- *Antibacterial efficacy of GsZnO-Nps was established at different concentrations (10, 50, 100, and 200 µg/mL) against Gram-positive and Gram-negative pathogens by zone-of-inhibition (ZOI) method with respect to standard drugs.*

This work has been published in:

N. Bhalla, N. Ingle, A. Jayaprakash, H. Patel, S.V. , Patri, and D. Haranath, (2022), **Arabian Journal of Chemistry,** 13(16), p.104506. doi:10.1016/j.arabjc.2022.104506. **IF. 6**

N. Bhalla, N. Ingle, S. V. Patri, and D. Haranath, **Saudi Journal of Biological Sciences**, vol. 28, no. 12, pp. 6915–6928, Dec. 2021, doi: 10.1016/j.sjbs.2021.07.075. **IF. 4.4**

Part-1: Phytochemical Analysis of Moringa oleifera Leaves Extracts by GC-MS and Free Radical Scavenging Potency for Industrial Applications

5.1. Introduction

Plants and extracts of their various sections have been used for their medical characteristics and to cure specific ailments as well as general tonics, meals, and other methods to increase the body's immunity and vigor since ancient times [1]–[4]. However, since last few decades the interest of researchers has gone up dramatically to understand their detailed compositions and also to explore and establish their potential applications in diverse areas. In fact, it is the need of the hour to leverage the vital power of the nature to combat proliferating diseases like cancer, heart attacks, diabetes, rapid skin aging etc. and upcoming varieties of new alarming health concerns like recent concerns of Coronavirus disease in 2019 (COVID-19), which affects the respiratory system acutely [5], [6].

Different parts like seeds, roots, stem, bark, leaves, flower and fruits of the plant have their own phytochemical compositions and potential medicinal properties. Moringa have various species across the globe which are known for their variety of usages few examples of Moringa species are *Moringa longituba, Moringa drouhardii, Moringa ovalifolia* etc. [7]. *Moringa oleifera* is one of the magical plants considered in India due to its high medicinal properties. However, there is still a lot to unleash the potential of *Moringa oleifera* by understanding their phytocomponents and variation in extraction due to solvents, understanding their potential properties and to establish their applications in various fields. The present study is focused to investigate the phytochemical composition of the *Moringa oleifera* leave's aqueous and alcoholic extracts by GC-MS and their free radical scavenging potencies, which make them useful for their further applications in cosmetic products to prevent skin damage due to free radicals generated because of pollution, UV from sunlight, smoke, also for animal feed etc.

5.2. Materials and Methods

5.2.1. Materials

Methanol of 99.8% purity, HPLC grade from SD fine chemical limited, distilled water having pH 5.3-7 and conductivity 2 µS/cm. Raw leaves powder of *Moringa oleifera* of India origin grown in the climate of tropics and sub tropics were used for the investigation. Extra pure 2,2-Diphenyl-1-Picrylhydrazyl (DPPH) from SRL Pvt. Ltd was used for the free radical scavenging studies.

5.2.2. Preparation of Aqueous and Methanolic extracts

The suspension of 5% Moringa Oleifera leaves were prepared in distilled water and in Methanol separately and were subjected to continuous stirring at 45-50 °C for 8 hours respectively. The resultant samples were filtered through Whatman filter paper 1 to extract the phytochemicals. The filtrates were concentrated by evaporating the solvents and were used to prepare the samples for further analysis.

5.3. Results and Discussion

5.3.1. Phytocomponent identification by GC MS of Aqueous extract of M. Oleifera leave powder

The GC-MS profile of the aqueous extract of M. Oleifera leaves is shown in Figure 5.1, which reflects 25 peaks of biomolecules. Table 5.1 presents the phytocomponents, their retention time, peak area percentage and Molecular weight. Chemical structure of active components and their known key applications like medicinal, cosmetics etc. are tabulated in Table 5.2. Few major compounds found with high percent peak area are Carbonic acid, butyl 2-pentyl ester (20.64%), 2-Isopropoxyethyl propionate (16.87%), 4H-Pyran-4-one, 2,3-dihydro-3,5-dihydroxy-6-methyl- (8.98%), and 1,3-Dioxolan-2-one, 4,5-dimethyl- (6.16%) additional compounds with reasonable percentage of peak area are Tetra acetyl-d-xylonic nitrile (5.03%), Azetidin-2-one 3,3-dimethyl-4-(1-aminoethyl)- (4.67%), 1,3-Dihydroxyacetone dimer (3.85%), Alpha-D-Glucose (3.44%), and Butanedioic acid, 2-hydroxy-2-methyl-, (3.14%) which is rarely been detected in plant extracts and have various applications.

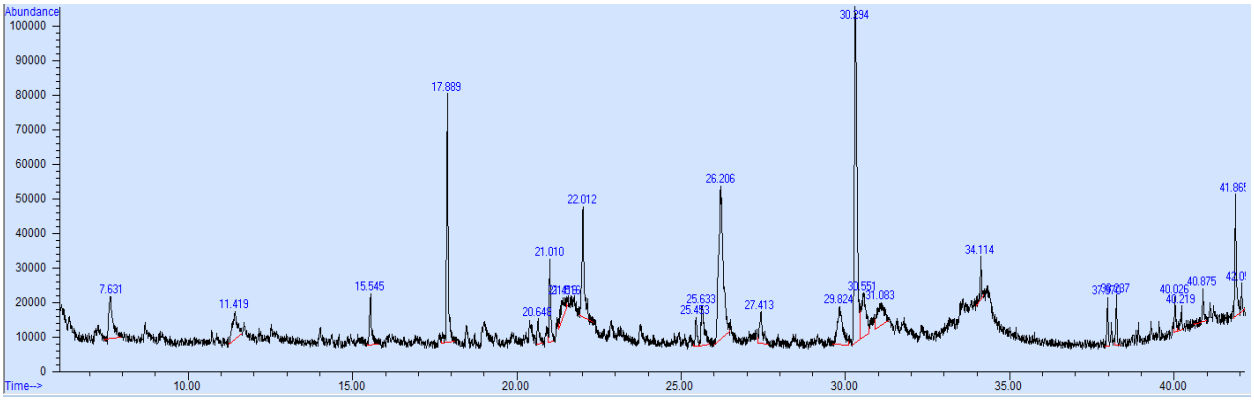

Figure 5.1. *GC MS of M. Oleifera leaves aqueous extract*

Table 5.1. List of phytochemicals identified in aqueous extract of M. Oleifera leaves, their retention time and peak area% with molecular weight (grams/mole).

Sr. No.	RT	Peak Area %	Library/ID	Molecular Weight (g/mol)
1	7.63	3.8551	1,3-Dihydroxyacetone dimer	180
2	11.42	3.2396	Acetic acid, [(aminocarbonyl)amino]oxo-	132
3	15.54	2.2433	4(1H)-Pyrimidinone, 2,6-diamino-	126
4	17.89	8.9858	4H-Pyran-4-one, 2,3-dihydro-3,5-dihydroxy-6-methyl-	144
5	20.65	1.1214	2-Hexynoic acid	112
6	21.01	3.1422	Butanedioic acid, 2-hydroxy-2-methyl-, (S)-	148
7	21.42	1.9275	3,3'-Iminobispropylamine	131
8	21.52	0.0774	1-Hexanamine	101
9	22.01	6.1627	1,3-Dioxolan-2-one, 4,5-dimethyl-	116
10	25.45	1.3083	2-Butenethioic acid, 3-(ethylthio)-, S-(1-methylethyl) ester	204
11	25.63	3.0349	Propanamide, N,N-dimethyl-	101
12	26.21	16.8738	2-Isopropoxyethyl propionate	160
13	27.41	2.5622	D-Mannoheptulose	210
14	29.82	4.6738	Azetidin-2-one 3,3-dimethyl-4-(1-aminoethyl)-	142
15	30.29	20.6431	Carbonic acid, butyl 2-pentyl ester	188
16	30.55	5.0379	Tetra acetyl-d-xylonic nitrile	343
17	31.08	3.445	.alpha.-D-Glucose	180
18	34.11	1.2587	1H-Cyclopenta[c]furan-3(3aH)-one, 6,6a-dihydro-1-(1,3-dioxolan-2-yl)-, (3aR,1-trans,6a-cis)-	196
19	37.97	1.5253	3-[1-(4-Cyano-1,2,3,4-tetrahydronaphthyl)]propanenitrile	210
20	38.24	1.4067	Quinolinium, 1-ethyl-, iodide	285
21	40.03	0.9462	N-Isopropyl-3-phenylpropanamide	191
22	40.22	0.7335	Propanamide	73
23	40.88	0.8805	1,2-Ethanediamine, N-(2-aminoethyl)-	103
24	41.87	4.3169	1,4-Benzenediol, 2-methyl-	124
25	42.05	0.5981	Ethene, ethoxy-	72

Table 5.2. Phytochemicals in aqueous extract of M. Oleifera leaves, their structure from NIST library and known potential applications wherever applicable

Ingredients	Structure	Key Applications (if any readily available)
1,3-Dihydroxyacetone dimer	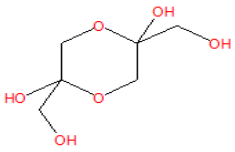	Synthesis of polymeric biomaterials [8]
Acetic acid, [(aminocarbonyl)amino]oxo-	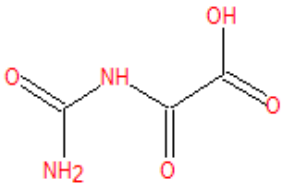	
4(1H)-Pyrimidinone, 2,6-diamino-	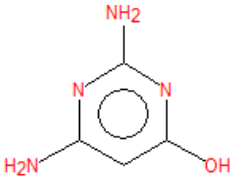	Hydroxy and amino Pyrimidines are of great interest in natural products and in the development of new drugs for various diverse areas like anti-cancer [9]
4H-Pyran-4-one, 2,3-dihydro-3,5-dihydroxy-6-methyl-	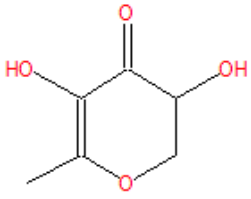	Strong Anti-oxidant[10], [11]
2-Hexynoic acid	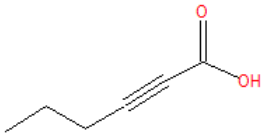	As precursor for synthesizing various biological metabolites like leucotrienes, oxylipins [12]
Butanedioic acid, 2-hydroxy-2-methyl-, (S)-	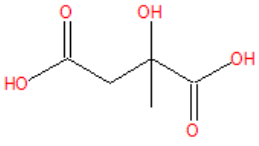	One of the rarely identified component in plant extracts. Mobilize the Phosphates in soil for agricultural applications to enhance the P availability [13]

3,3'-Iminobispropylamine	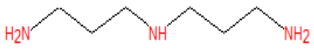	This is also among the rare component identified in plant have various role in plant as well as medicinal antitumor active[14]–[16]
1-Hexanamine		
1,3-Dioxolan-2-one, 4,5-dimethyl-	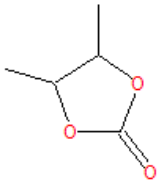	Precursor for various drugs and cyclic Carbonates have applications in Electrochemical energies [17], [18]
2-Butenethioic acid, 3-(ethylthio)-, S-(1-methylethyl) ester	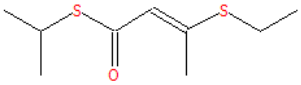	
Propanamide, N,N-dimethyl-	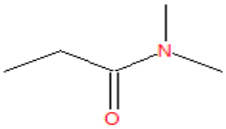	
2-Isopropoxyethyl propionate	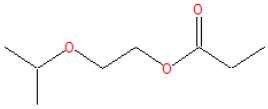	
D-Mannoheptulose	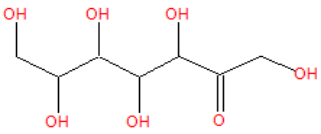	D-Mannoheptulose widely studied for its activity against breast cancer and to suppress the D-glucose induced insulin release. [19], [20]
Azetidin-2-one 3,3-dimethyl-4-(1-aminoethyl)-	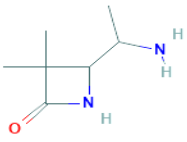	Anti-inflammatory, ulcerogenic, and analgesic activities [21]

Carbonic acid, butyl 2-pentyl ester	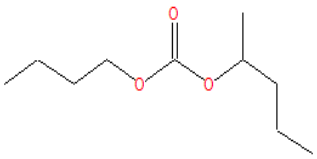	
Tetra acetyl-d-xylonic nitrile	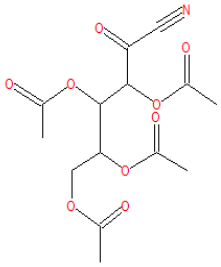	Anti-tumor and Anti-oxidant [22], [23]
Alpha-D-Glucose	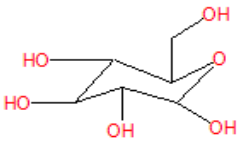	Source of energy, highly effective and used in food, medicine and its derivatives also have many medicinal use. [24], [25]
1H-Cyclopenta[c]furan-3(3aH)-one, 6,6a-dihydro-1-(1,3-dioxolan-2-yl)-, (3aR,1-trans,6a-cis)-	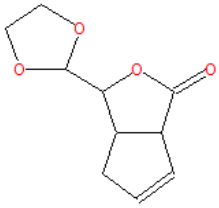	
3-[1-(4-Cyano-1,2,3,4-tetrahydronaphthyl)]propanenitrile	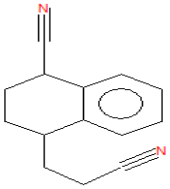	
Quinolinium, 1-ethyl-, iodide	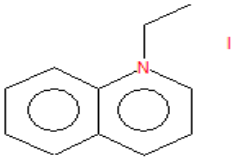	
N-Isopropyl-3-phenylpropanamide	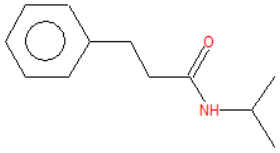	

Propanamide	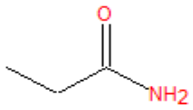	Propanamide derivatives studied for antimicrobial and antiviral efficacy [26]
1,2-Ethanediamine, N-(2-aminoethyl)-	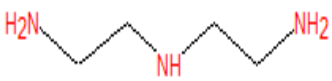	
1,4-Benzenediol, 2-methyl-	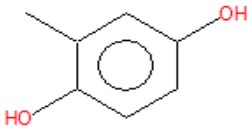	
Ethene, ethoxy-		

5.3.2. Phytocomponent identification by GC MS of Methanolic extract of M. Oleifera leaves

The GC-MS profile of the methanolic extract of M. Oleifera leaves is shown in Figure 5.2, which reflects 54 peaks of biomolecules. Table 5.3 presents the phytocomponents, their retention time, peak area percentage and Molecular weight. Chemical structure of active components and their known key applications like medicinal, cosmetics etc. are tabulated in Table 5.4. Few major compounds found with high percent peak area are 1,3-Propanediol, 2-ethyl-2- (hydroxymethyl)- (21.19%), Propionic acid, 2-methyl-, octyl ester (15.02%), Ethanamine, N-ethyl-N-nitroso- (5.21%), and 9,12,15-Octadecatrienoic acid, (Z,Z,Z)- (5.00%) additional compounds with reasonable percentage of peak area are 4H-Pyran-4-one, 2,3-dihydro-3,5-dihydroxy-6-methyl- (4.18%), Benzeneacetonitrile, 4-hydroxy- (3.47%), 3-Deoxy-d-mannoic lactone (3.29%), n-Hexadecanoic acid (2.57%) and Monomethyl malonate (2.56%).

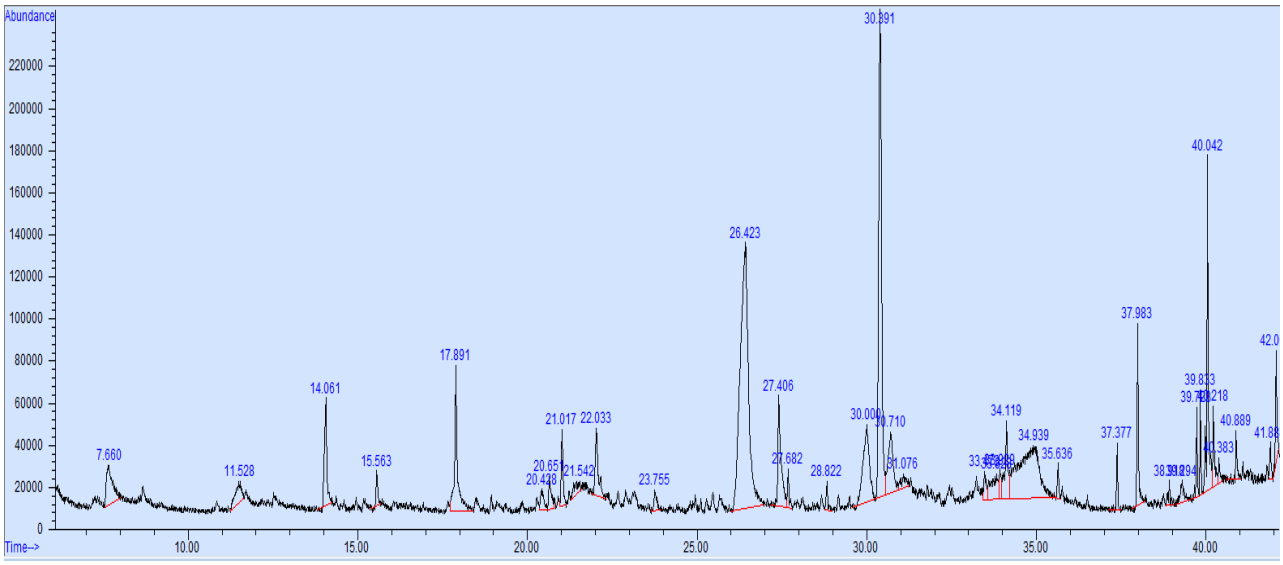

Figure 5.2. *GC MS of M. Oleifera leaves methanolic extract*

Table 5.3. List of phytochemicals identified in methanolic extract of M. Oleifera leaves, their retention time and peak area% with molecular weight (grams/mole).

Sr.No	RT	Peak Area %	Library/ID	Molecular Weight (g/mol)
1	7.66	2.4651	Dihydroxyacetone	90
2	11.5285	1.8656	Glycerin	92
3	11.7064	0.5327	Erythritol	122
4	14.0612	2.5684	Monomethyl malonate	118
5	15.5626	0.6434	4,5-Diamino-6-hydroxypyrimidine	126
6	17.8911	4.1801	4H-Pyran-4-one, 2,3-dihydro-3,5-dihydroxy-6-methyl-	144
7	18.9343	0.2105	Furan, 2,3-dihydro-4-methyl-	84
8	20.4278	0.6806	Catecholborane	120
9	20.6515	0.8121	2-Fluoropyridine	97
10	21.017	1.4375	1,2,3-Propanetriol, 1-acetate	134

11	21.2273	0.1746	3,4-Furandiol, tetrahydro-, trans-	104
12	21.4101	0.5114	1-Nitro-.beta.-d-arabinofuranose, tetraacetate	363
13	21.5424	0.1172	1,8-Diamino-3,6-dioxaoctane	148
14	22.033	1.7997	1,7-Diaminoheptane	130
15	22.6606	0.454	N,N-Dimethylacetamide	131
16	22.8934	0.5466	2-Oxoglutaric acid	146
17	23.1495	0.9008	Oxazolidine, 2-ethyl-2-methyl-	115
18	23.7541	0.7112	Heptanal	114
19	25.4554	0.4293	6-Methoxy-3-pyridazinethiol	142
20	25.6675	0.5971	3-Piperidinol	101
21	26.4192	21.1909	1,3-Propanediol, 2-ethyl-2-(hydroxymethyl)-	134
22	27.4032	3.4763	Benzeneacetonitrile, 4-hydroxy-	133
23	27.6817	0.395	Benzenebutanal, .gamma.,4-dimethyl-	176
24	28.8207	0.4491	2(4H)-Benzofuranone, 5,6,7,7a-tetrahydro-4,4,7a-trimethyl-	180
25	30.0026	5.2161	Ethanamine, N-ethyl-N-nitroso-	102
26	30.3938	15.0279	Propanoic acid, 2-methyl-, octyl ester	200
27	30.7101	3.2947	3-Deoxy-d-mannoic lactone	162
28	31.0768	0.3814	d-Glycero-d-ido-heptose	210
29	31.1206	0.3314	D-erythro-Pentose, 2-deoxy-	134
30	32.4351	0.5345	N-Methoxy-1-ribofuranosyl-4-imidazolecarboxylic amide	273
31	33.2282	0.5847	Formamide, N,N-dimethyl-	73
32	33.4717	0.5651	d-Talonic acid lactone	178
33	33.7365	0.482	Sorbitol	182
34	33.9282	0.5189	Allo-Inositol	180

35	34.1181	1.595	D-chiro-Inositol, 3-O-(2-amino-4-((carboxyiminomethyl)amino)-2,3,4,6-tetradeoxy-.alpha.-D-arabino-hexopyranosyl)-	379
36	34.3555	1.1254	Allo-Inositol	180
37	34.5368	1.1121	Scyllo-Inositol	180
38	34.7792	2.0264	Muco-Inositol	180
39	34.8409	0.8749	Allo-Inositol	180
40	34.8998	2.0545	Inositol	180
41	35.6364	0.4822	Cyclohexane, 1-methyl-4-(2-hydroxyethyl)-	142
42	37.3767	0.8519	Hexadecanoic acid, methyl ester	270
43	37.9829	2.5703	n-Hexadecanoic acid	256
44	38.9185	0.3737	Phenol, 2-methyl-	108
45	39.2935	0.967	(1S)-Propanol, (2S)-[(tert.butyloxycarbonyl)amino]-1-phenyl-	251
46	39.7227	1.0307	9-Octadecenoic acid (Z)-, methyl ester	296
47	39.8325	0.9664	Phytol	296
48	40.0418	5.0063	9,12,15-Octadecatrienoic acid, (Z,Z,Z)-	278
49	40.2184	1.2051	Octadecanoic acid	284
50	40.3832	0.4257	4-Allyl-3-(dimethylhydrazono)-2-methylhexane-2,5-diol	228
51	40.8886	0.6056	Benzyl .beta.-d-glucoside	270
52	41.0816	0.1698	4,6-dimethyl-2-propyl-1,3,5-dithiazinane	191
53	41.8877	0.545	1,3-Benzenediol, 2-methyl-	124
54	42.0626	1.4694	9-Octadecenamide, (Z)-	281

Table 5.4. Phytochemicals in methanolic extract of M. Oleifera leaves, their structure from NIST library and known potential applications wherever applicable.

Ingredients	Structure	Key applications (if any readily known)
Dihydroxyacetone	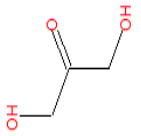	Dihydroxyacetone (DHA) are being used in Sunless tanning type of products [27]
Glycerin	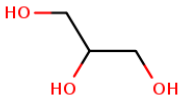	Used as humectant, Moisturizer having application in cosmetics and Medicines [28]
Erythritol	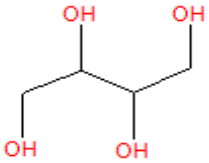	Antioxidant Improve blood vessel function in people with type 2 diabetes [29]
Monomethyl malonate	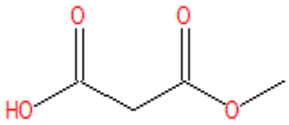	
4,5-Diamino-6-hydroxypyrimidine	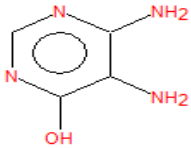	Analogues are used for various Medicinal properties like antimicrobial [30]
4H-Pyran-4-one, 2,3-dihydro-3,5-dihydroxy-6-methyl-	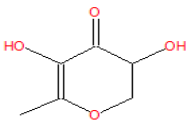	Strong Anti-oxidant [10], [11]
Furan, 2,3-dihydro-4-methyl-	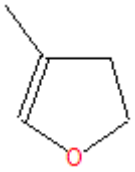	

Catecholborane	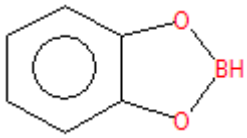	Versatile compound for various organic synthesis [31], [32]
2-Fluoropyridine	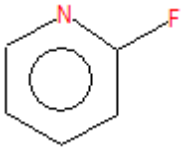	
1,2,3-Propanetriol, 1-acetate	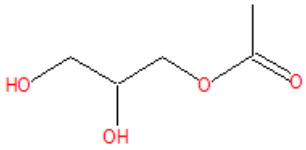	
3,4-Furandiol, tetrahydro-, trans-	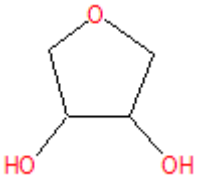	
1-Nitro-.beta.-d-arabinofuranose, tetraacetate	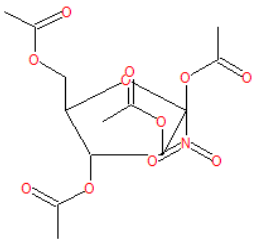	
1,8-Diamino-3,6-dioxaoctane		
1,7-Diaminoheptane	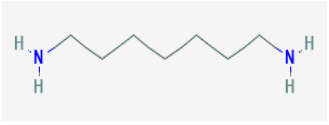	Malaria treatment [33]
N,N-Dimethylacetamide	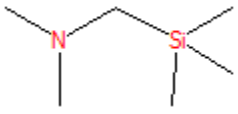	Novel antiviral agent [34]

2-Oxoglutaric acid	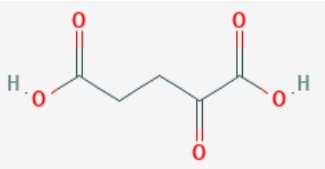	Biosynthesis of Carotenoids in Chloroplasts [35]
Oxazolidine, 2-ethyl-2-methyl-	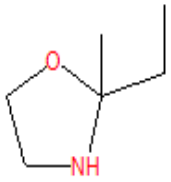	
Heptanal		
6-Methoxy-3-pyridazinethiol	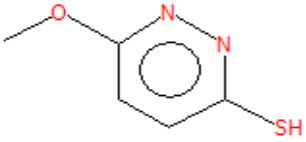	
3-Piperidinol	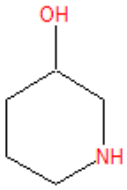	Anti-tuberculosis agent [36]
1,3-Propanediol, 2-ethyl-2-(hydroxymethyl)-	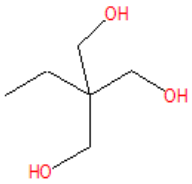	
Benzeneacetonitrile, 4-hydroxy-	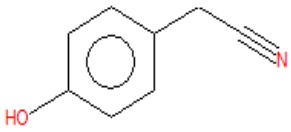	
Benzenebutanal, .gamma.,4-dimethyl-	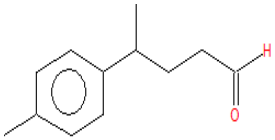	

2(4H)-Benzofuranone, 5,6,7,7a-tetrahydro-4,4,7a-trimethyl-	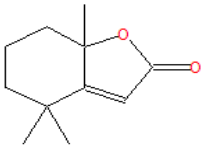	Anti-arthritic activity [37]
Ethanamine, N-ethyl-N-nitroso-	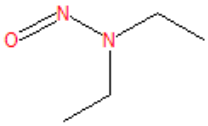	Boost immune system [38]
Propanoic acid, 2-methyl-, octyl ester	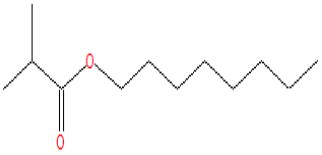	Anti-Microbial properties [39]
3-Deoxy-d-mannoic lactone	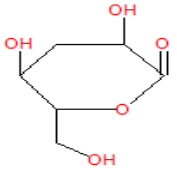	
d-Glycero-d-ido-heptose	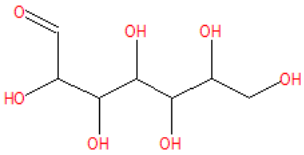	Inhibition of insulin secretion & Hexokinase [40]
D-erythro-Pentose, 2-deoxy-	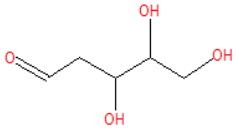	
N-Methoxy-1-ribofuranosyl-4-imidazolecarboxylic amide	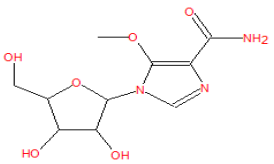	
Formamide, N,N-dimethyl-	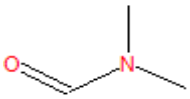	
d-Talonic acid lactone	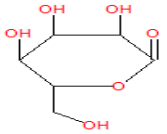	

Sorbitol	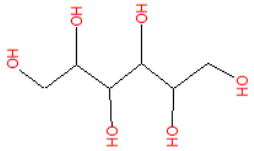	Help to prevent hyperglycemia [41] Protect and rejuvenation of skin from oxidative stress [42]
Allo-Inositol	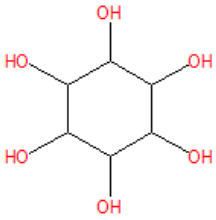	Control the il6 level to reduce the inflammation [43]
D-chiro-Inositol, 3-O-(2-amino-4-((carboxyiminomethyl)amino)-2,3,4,6-tetradeoxy-.alpha.-D-arabino-hexopyranosyl)-	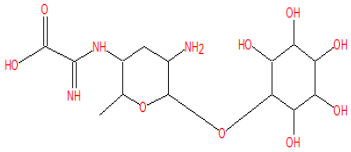	Type 2 Diabetes Treatment [44]
Allo-Inositol	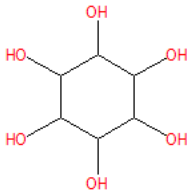	Control the il6 level to reduce the inflammation [43]
Scyllo-Inositol	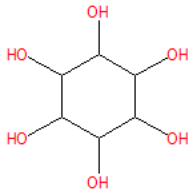	Treat mild to moderate Alzheimer's disease [45]
Muco-Inositol	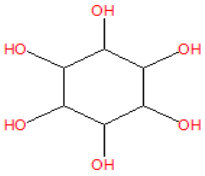	Oligomer of muco-inositol act as glycosidase inhibitors [46]
Allo-Inositol	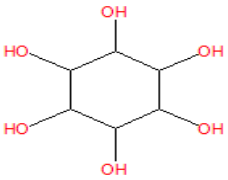	Control the il6 level to reduce the inflammation [43]

Inositol	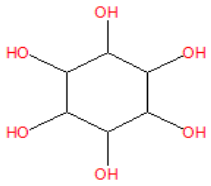	Inositol and its derivative are known for treatment of PCOS [47], [48]
Cyclohexane, 1-methyl-4-(2-hydroxyethyl)-	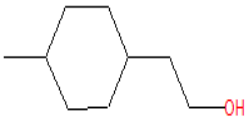	
Hexadecanoic acid, methyl ester		Anti-inflammatory [49]
n-Hexadecanoic acid (palmitic acid)		Anti-inflammatory [50]
Phenol, 2-methyl-	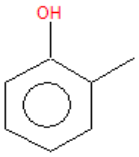	
(1S)-Propanol, (2S)-[(tert.butyloxycarbonyl)amino]-1-phenyl-	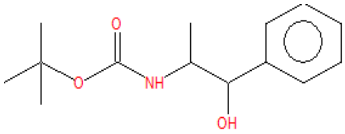	HIV-1 Protease Inhibitors [51]
9-Octadecenoic acid (Z)-, methyl ester	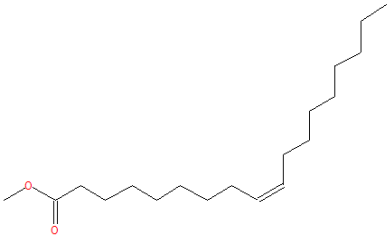	Lubricant [52]
Phytol	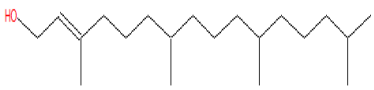	Control Ganoderma boninense (Plant disease) [53] Antioxidant, Anti-inflammatory [54]

9,12,15-Octadecatrienoic acid, (Z,Z,Z)-	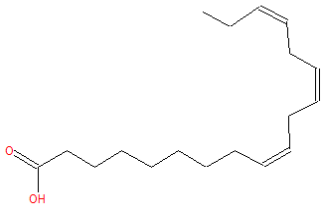	Reduce complications in Covid-19 patients. [55] Neuroprotective Properties [56]
Octadecanoic acid	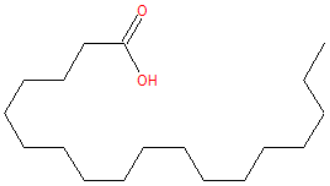	Play role in food reward [57] Lowers HDL cholesterol [58]
4-Allyl-3-(dimethylhydrazono)-2-methylhexane-2,5-diol	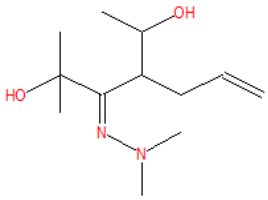	
Benzyl .beta.-d-glucoside	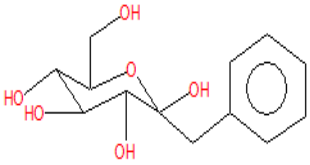	
4,6-dimethyl-2-propyl-1,3,5-dithiazinane	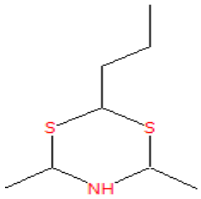	
1,3-Benzenediol, 2-methyl-	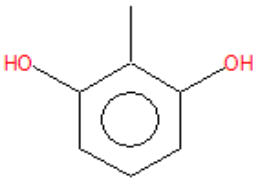	
9-Octadecenamide, (Z)-	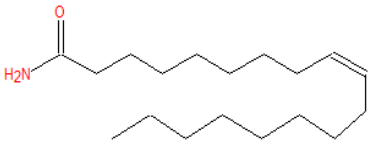	Anti-depressive effects [59]

5.4. Free Radical Scavenging efficacy of aqueous and methanolic extracts of Moringa leaves at varying concentrations

The aqueous extract of Moringa leaves have the IC_{50} at concentration of 4.65 µL/mL after incubating for 30 minutes Figure 5.3 whereas the IC_{50} of methanolic extract was found 1.83 µL/mL Figure 5.4 which is significantly lower than the IC_{50} of Moringa aqueous extract. Various concentrations (1 µL/mL to 5 µL/mL) of Moringa aqueous and methanolic extracts were also evaluated and compared at the defined interval of incubation time up to 160 minutes to identify the maximum FRSP for each concentration and the results are showcased in Figure 5.5.

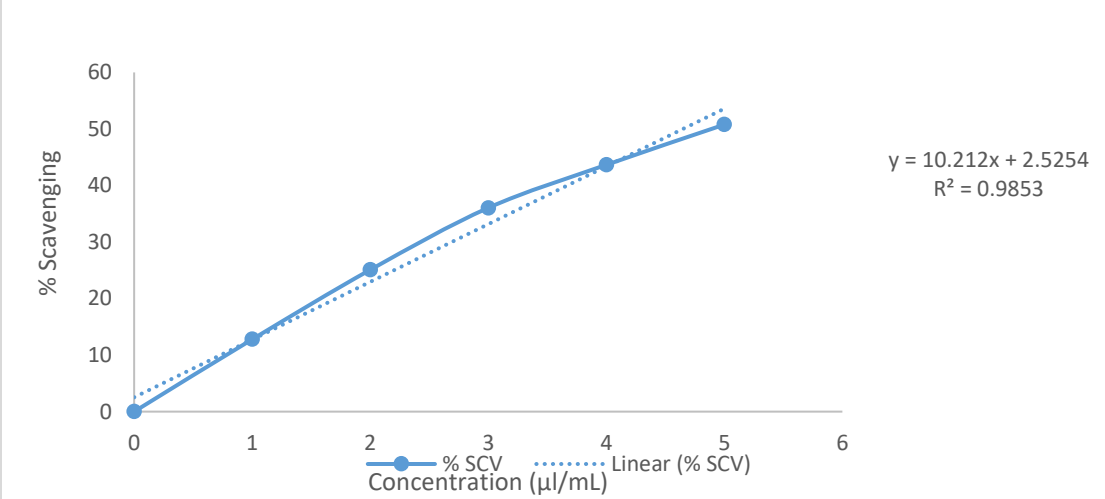

Figure 5.3. *IC_{50} of M. Oleifera leaves aqueous extract*

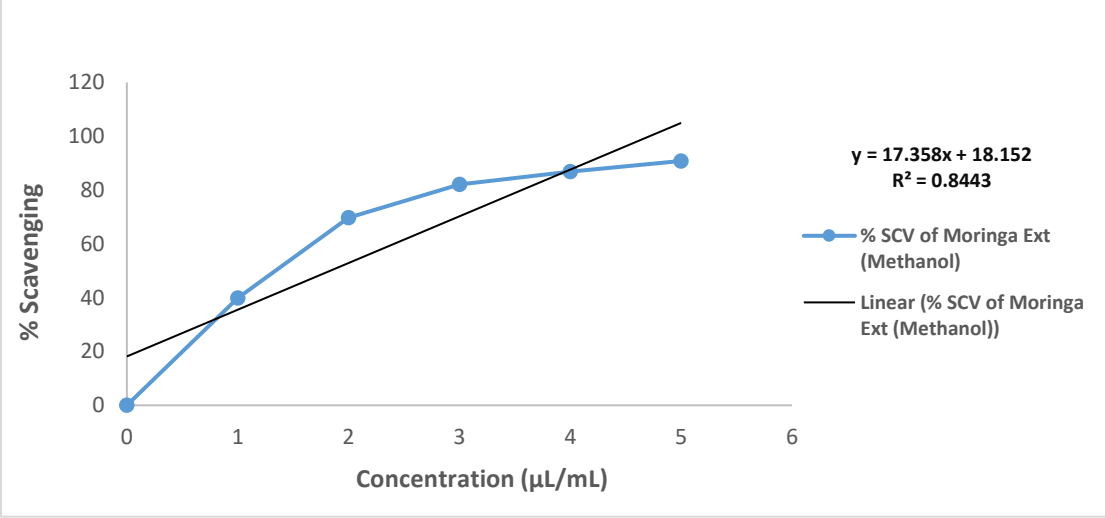

Figure 5.4. *IC_{50} of M. Oleifera leaves methanolic extract*

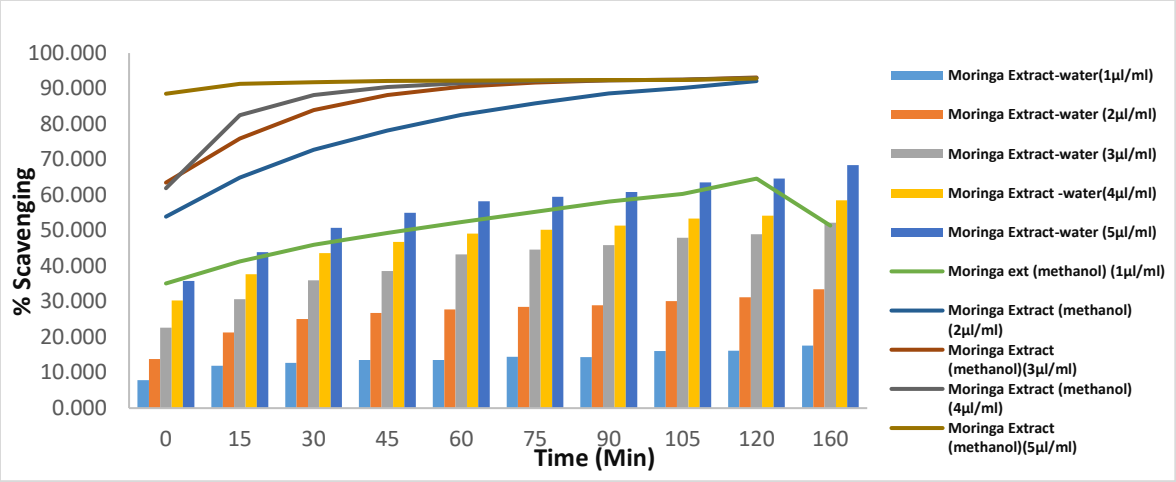

Figure 5.5. *Free radical scavenging potency (FRSP) comparison of aqueous and methanolic extract of varying concentration at various incubation time points*

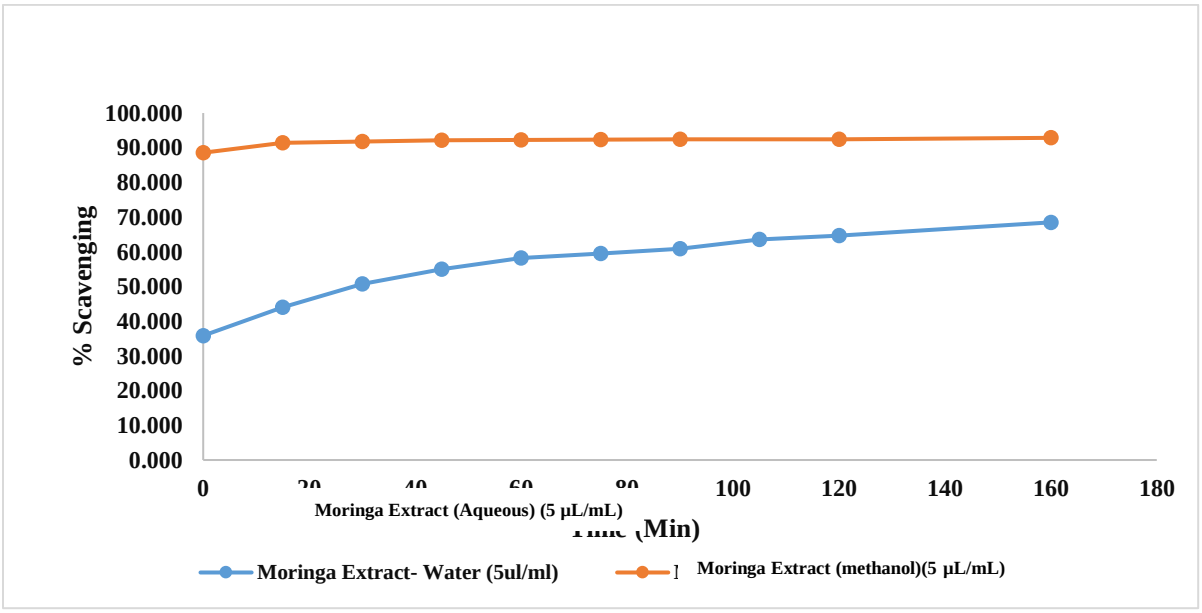

Figure 5.6. *Free radical scavenging potency (FRSP) comparison of aqueous and methanoic extract of 5 µL/mL concentration at various incubation time points*

This study is among the very few reports where the phytochemical profile of Moringa extracts with their free radical scavenging potency studies have been reported. In this study, higher number of phytochemicals in methanolic extract (Table 5.3) of Moringa extract in comparison to aqueous (Table 5.1) could be due to difference in their polarity, which could have led to difference in the extraction of phytochemicals. These, phytochemicals have various

industrial applications and medicinal properties like anti-tumor, anti-cancer, Insulin regulation, anti-oxidant etc. which makes it really a magical plant for food, medicine and suitable natural ingredient to explore its further applications in diverse areas like in cosmetics, personal care products etc.

Natural antioxidants are always of very high importance for health as a part of food and as a part of cosmetics for topical applications to combat the detrimental effects of free radicals on internal and external organs like skin aging etc. Both aqueous and methanolic Moringa extracts have excellent anti-oxidant/FRSP. However, in relative terms methanolic extract found to have lower IC_{50} (1.83 µL/mL) Figure 5.4 reflecting higher free radical scavenging ability in comparison to of aqueous extract having higher IC_{50} (4.65 µL/mL) Figure 5.3. This could be mainly due to higher number of polyphenolic component extracted in methanolic extracts and relatively at higher percentages, which is contributing towards higher scavenging potency at lower concentration. It has been found that methanolic extract at 5 µL/mL gives the 88.5% FRSP and does not change significantly over the period of time and reaches maximum level of 92.8% FRSP. Whereas aqueous extract at 5 µL/mL show 35.8% FRSP at the initial time point and which further scavenge the DPPH free radical significantly up to 68.4% in 160 minutes Figure 5.6, however still less FRSP of Moringa aqueous extract than the methanolic extract could be due to the same reason as explained above of having more polyphenolic components in methanolic extract of Moringa as reflected in GC-MS results.

Part-2: Green Approach to Synthesize Nano Zinc Oxide for Enhanced Anti-oxidant, Anti-acne, Anti-bacterial Properties

5.5. Background

Nanotechnology and nanoscience have seen a tremendous increase in industrial applications in the past decade. Plant-based synthesis of nanoparticles is a unique approach that has various applications in cosmetics, medicine, food, and agriculture industries [60]–[64]. *Moringa oleifera* leaves, notably, are well-known for their prophylactic and therapeutic powers and are often devoured in meals. Extracts obtained from the leaves have powerful antioxidant capabilities. Additionally, phytochemicals in *Moringa oleifera* leaves show incredible properties such as anti-cancer, anti-inflammatory, anti-diabetics and are suitable for applications in different industries such as foodstuff, cosmetics, and drug delivery [65].

Drug delivery, nanomedicine, gene delivery and biosensing are the new horizon of the nanoscience field [66], [67]. Plant-derived methods using such biological agents help in stabilizing and reducing particles into nano scale having a high shelf life. The plant-based synthesis methods have inherent variability due to the presence of several phytochemicals like phenolic compounds, flavonoids, vitamins, and carbohydrates. These phytochemicals contain amine, carbonyl, and hydroxyl functional groups which help in the reduction of metals ions and convert them into nano-scale particles [68], [69]. However, it has been seen that most favorably phenolic and flavonoid-containing functional groups play a vital role in the green synthesis of nanoparticles [70], [71]. Green synthesized nanomaterials are found to be non-toxic, cost-effective and biodegradable in nature [72]–[75]. Being an eco-friendly approach, the green synthesis method helps to reduce the consumption of hazardous chemicals and use natural materials such as roots, leaves, flower, bark extract and even microbes like algae, fungus, bacteria, etc. [76]–[78]. Recent literatures show the importance of nanoparticles of metal and their oxides synthesized by green route like zinc, silver, copper, nickel, gold, etc. [79]–[81].

ZnO is commonly generally recognized as safe and shows a high potential to kill the disease-causing germs in humans and animals [82]–[84]. The high specific surface area of the nanoparticles and phytochemicals of plants shows the remarkable and exclusive properties which can play a very important role in their antibacterial, anti-oxidant and photocatalytic application [85]–[87].

Numerous routes to synthesize ZnO nanoparticles have been reported in the literature, the non-basic route [88], high energy ball mills technique [89], combustion route [90], vaporization [91], assembly assisted [92] and sol-gel technique [93], etc. However, certain drawbacks of these synthesis methods of nano ZnO are: high energy consumption, time, cost, labor-intensive, solvents used, and byproducts released are not permissible in most industrial applications. Moreover, nanoparticles synthesized using chemical methods have limited opportunity for medicinal sector applications due to their possible toxicity and harmful byproducts. Hence, the present study explores eco-friendly and sustainable method which is suitable for different industrial applications.

In recent times there are huge challenges in evolving and innovating strong antibacterial agents. As per the last 5 years, the Food and Drug Administration (FDA) have banned the most common antimicrobial agent like triclosan, triclocarban, and 18 others from the personal care industry [94]. This action was taken due to major apprehensions about the carcinogenic effects, cell toxicity of these materials on the environment, humans and wildlife. Recently, in 2021 the European Commission declared Zinc Pyrithione (ZPT) well known antifungal agent as a prohibited ingredient due to its cell toxicity [95]. Moreover, microbes no longer respond to existing germicidal agents because of mutations and resistant built against them. As a result, novel, natural, strong antimicrobial agents are extremely required for the home and personal care industry.

In our previous research article, we have reported 25 phytochemicals in aqueous *Moringa oleifera* leave extract evaluated by GC-MS along with their free radicle scavenging potency [65]. *Moringa oleifera* leaves extract acts as a biodegradable, natural and non-toxic reducing agent for fabrication of nano-scale ZnO. The evaluation and characterizations of GsZnO-Nps are done by using advanced technical tools like UV Vis, FTIR, XRD, SEM-EDX. Moreover, the antioxidant of GsZnO-Nps and AR Grade ZnO has been evaluated using 2,2-diphenyl-1-picrylhydrazyl (DPPH) standard free radical. The IC_{50} concentration GsZnO-Nps was significantly lower than AR-Grade ZnO.

This may be the first or among the very few researches that have established the potency of green synthesized zinc oxide using Moringa leaves extract against *C. acne* and additionally demonstrated efficacy equivalent to standard drugs with respect to *S. aureus* and *E. coli* bacterium. The present research work mainly aims on reporting eco-friendly and sustainable

methods of green synthesized ZnO nanoparticles (GsZnO-Nps) using *Moringa oleifera* leaves for addressing the rapidly growing needs of advanced antibacterial and anti-oxidant agent for health & wellness applications. This research will further help to increase the application of green synthesized versatile nanomaterials in the medicine, health & wellness, cosmetic, personal care sector.

5.6. Materials and Methods

5.6.1. Materials

Zinc Acetate 99.5% ($C_4H_6Zn.2H_2O$) from S D Fine-chem limited, Mumbai, India. *Moringa oleifera leaves* powder from Holy Natural, India. Extra pure 2,2-Diphenyl-1-Picrylhydrazyl (DPPH) from SRL Pvt. Ltd. Distilled water having pH 5.5-7.0 & 1µS/cm conductivity. Bacterial cultures *E. coli* ATCC 10536, *C. acne* ATCC 11827 and *S. aureus* ATCC 6538 were purchase through ATCC bank (American Type of Culture Collection) and standard drugs (Doxycycline, Azithromycin, Cefpodoxime) from local pharmacies.

5.6.2. Green synthesis ZnO nanoparticles (GsZnO-Nps)

Prepare decoction of *Moringa oleifera leaves* powder with distilled water at 1:20 ratio under continuous stirring at 80-90 °C for 6 hours. Filter the above mixture using Whatman filter paper-1 to get separated solid leaf pieces from the *Moringa oleifera* leaves extract. Add 0.272 moles of zinc acetate dihydrate (final concentration in mixture to be 0.0597 g/mL) to the filtered plant extract with continuously stirring for 2-3 hours at 80-90 ºC until precipitation is observed. Set the solution aside for 18 hours in room temperature in order to facilitate the reaction completion and formation of ZnO nanoparticles. A dark green mixture having a pH of 7.45 and settled precipitates is observed. Centrifuge the solution at 3000 rpm to collect GsZnO-Nps and dry at 50 °C to make it powder for further evaluation Figure 5.7. The possible mechanism of green synthesis of nano ZnO formation, using herbal extract is described as,

$$nZn^{2+} + 2Ar - (OH)_n \rightarrow nZn^{\circ} + 2nAr = O + 2nH^{+}$$

$$2(x+1)Zn^{\circ} + 2Ar = y + yO_2 \rightarrow 2(Zn^{\circ} - Zn_x O_y - Ar = O)$$

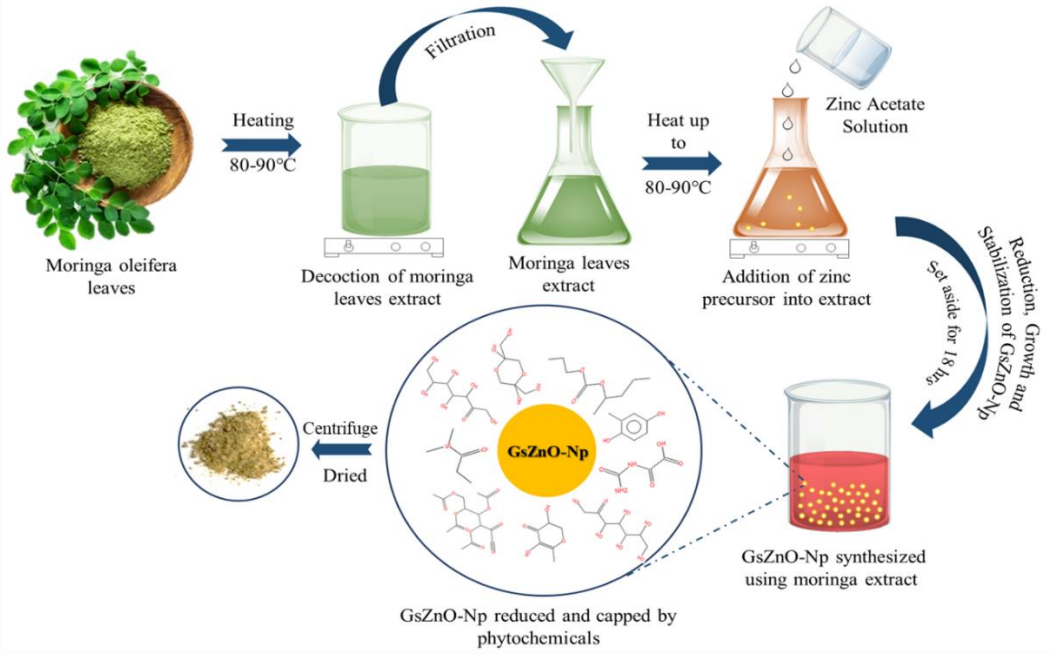

Figure 5.7. *Systematic presentation of synthesis of GsZnO-Nps via Moringa oleifera leaves*

The phytochemicals such as phenolic compounds and flavonoids (Ar-(OH) n) present in *Moringa oleifera* leaves extract are responsible for synthesis of GsZnO-Nps. (Ar-(OH) n) losses an electron for the reduction of Zn^{2+} to Zn^{o} and possible formation of Zn°-phenolate complex by chelation effect which helps in the synthesis of ZnO nanoparticle at 80-90 °C [96].

5.7. Results and Discussion

5.7.1. UV-Vis spectrum

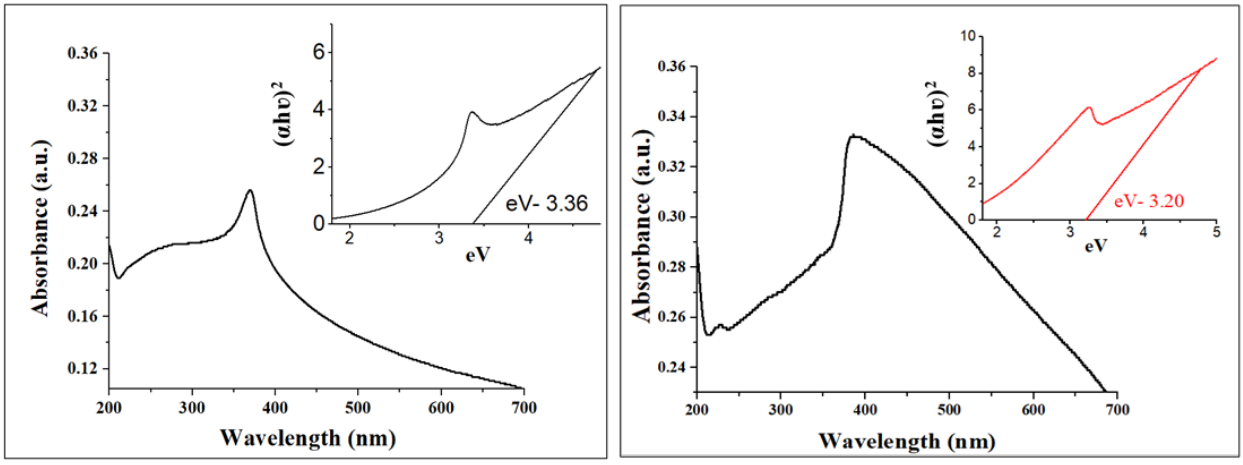

Figure 5.8. *The UV-Vis absorption spectrum and band gap energy of (A) GsZnO-Nps (B) UV-Vis spectrum AR grade ZnO given for comparative study.*

The UV-Visible absorption spectrum of GsZnO-Nps and AR grade ZnO was examined by a UV-Vis spectrophotometer in the range of 200-700 nm. The AR Grade ZnO exhibits the absorption peak at 386 nm with an energy bandgap of 3.20 eV correspondingly GsZnO-Nps exhibits a typical absorption peak in the UV range at 368.5 nm having bandgap energy of 3.36 eV shown in Figure 5.8 (A and B).

Based on UV wavelength, the band gap (Eg) was calculated with formula [4]:

$$E = h\frac{c}{\lambda}$$

where: h = 6.626 x 10^{-34} Joules sec is the Planks constant, c = 3.0 x 10^{8} m/s^{2} is the speed of light and λ is the wavelength.

The high band gap energy of GsZnO-Nps clearly indicate the successful synthesis of nanoparticles. A blue shift of absorption bands was observed in the GsZnO-Nps spectra unlike bulk AR grade ZnO. The blue shift could be because of several reasons, like the quantum confinement effect explaining the bandgap energy inversely proportional to particle size, and shows a blue shift as the particle size decreases. The particle size decreases and approaches the size of the electron-hole distance, particle energy levels become quantum confined and separate thus confining the motion of the electron [97].

5.7.2. Fourier-Transform Infrared (FT-IR) spectroscopy:

IR spectrum of Moringa extract and GsZnO-Nps exhibits the functional group in different regions as shown in Figure 5.9. Spectrum (A, B, and C) shows the sharp broad peak in the single bond region with a shift from 3076.63 to 3302.13 cm^{-1} suggests the existence of the hydroxyl (OH) group which can be attributed to the presence of H_2O molecules. Spectrum (A) shows the two peaks at 2918.29 cm^{-1} and 2848.86 cm^{-1} could be due to symmetrical and asymmetrical C-H stretching of phytochemicals [98]. Small peak at 2362.79 cm^{-1} observed Spectrum (C) could be due to O=C=O stretching probably due to the impurity during synthesis or measuring condition. The peak at 1635.63 cm^{-1} and 1639.49 cm^{-1} in spectrum (A & C) could be attributes to the stretching of (C=C) group of phenolic compounds [98]. The peaks at 1550.76, 1552.69 and 1350.17 cm^{-1} in spectrum (B & C) could be due to asymmetrical and symmetrical stretching bonds of COO^{-} [96]. Peak at 1408.03 to 1433.11 cm^{-1} in spectrum (A, B & C) could be attributed to the –C–H bending vibration. The peaks 1244.08 cm^{-1} could be C–O stretching vibration. While 1045.41 cm^{-1} peak is the due to the C-OH bending of carbohydrates present in Moringa

extract. The peak 1018.41 cm^{-1} in spectrum B could be due to C-CH_3 framework originated from zinc acetate [99]. While the peak at 956.69 cm^{-1} exhibit the existence of vinyl C-H out-of-plane bend. The peak at 686.65 and 611.43 cm^{-1} could be due to out-of-plane bend of OH vibration. Spectrum (C and D) shows the peaks at 420.48 cm^{-1} and 410.83 cm^{-1} indicating the presence of ZnO similar to previously reported literatures. [96], [100].

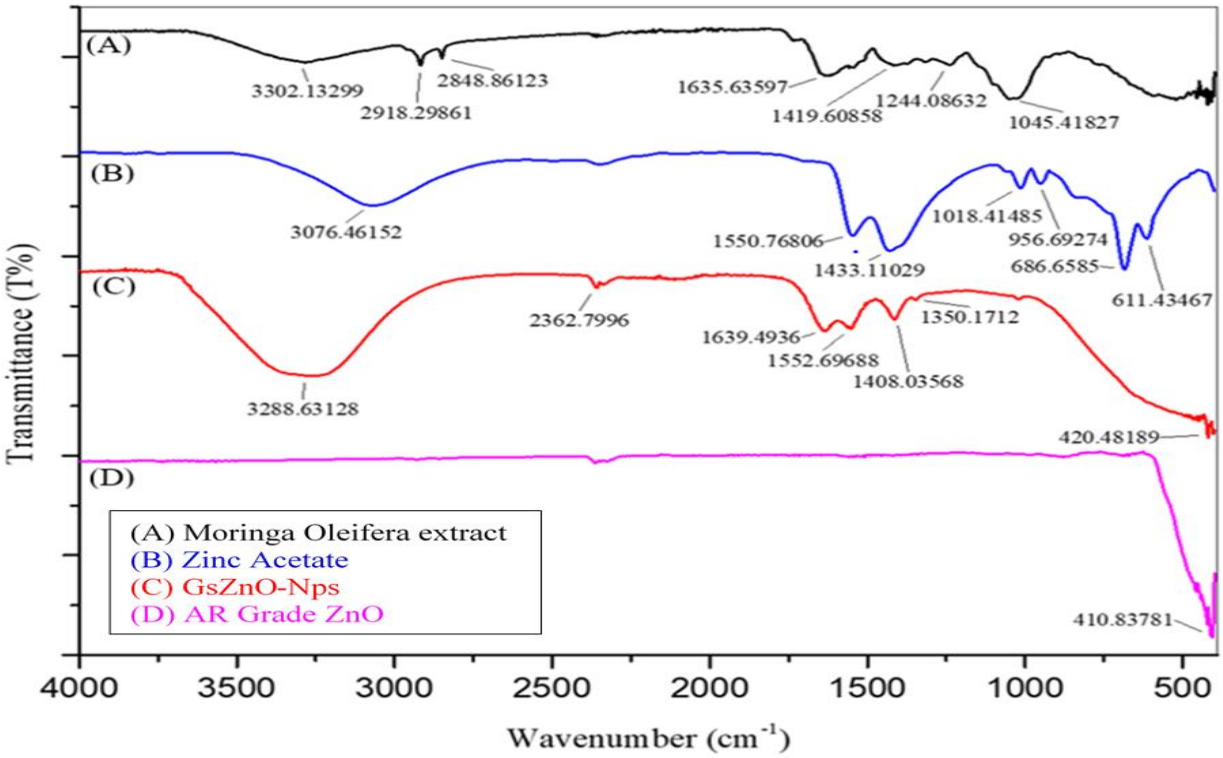

Figure 5.9. *FT-IR spectrum of (A) Moringa oleifera leaves powder (B) Zinc acetate (C) GsZnO-Nps (D) AR Grade Zinc oxide in the spectral range of 400–4000 cm^{-1}*

5.7.3. X-Ray Diffraction Analysis

The crystalline structure of GsZnO-Nps was analyzed by an X-ray diffractometer. The diffractogram confirms the hexagonal wurtzite structure of GsZnO-Nps [101]. The diffraction peaks were found at 2θ values of 31.53°, 34.19°, 36.02°, 47.31°, 56.37°, 62.63°, 66.16°, 67.72°, and 68.86°. These peaks are in line with JCPDS standard card 36-1451 of ZnO shown in Figure 5.10 (A, B and C) which is in line with previously published literatures [63], [64], [76]. The average crystallites size of GsZnO-Nps is 13.82 nm (Table 5.5) which is significantly lower than AR Grade ZnO is 30.87 nm and other previous reported literature[102]. Debye-Scherrer equation was used for evaluation of crystallite size,

$$D = K\lambda/\beta \cos\theta$$

D- Crystallites size, λ- The wavelength of X-ray, K-Scherrer constant (0.9), θ-Braggs angle in radians and β-Full width at half maxima of the peak in radians.

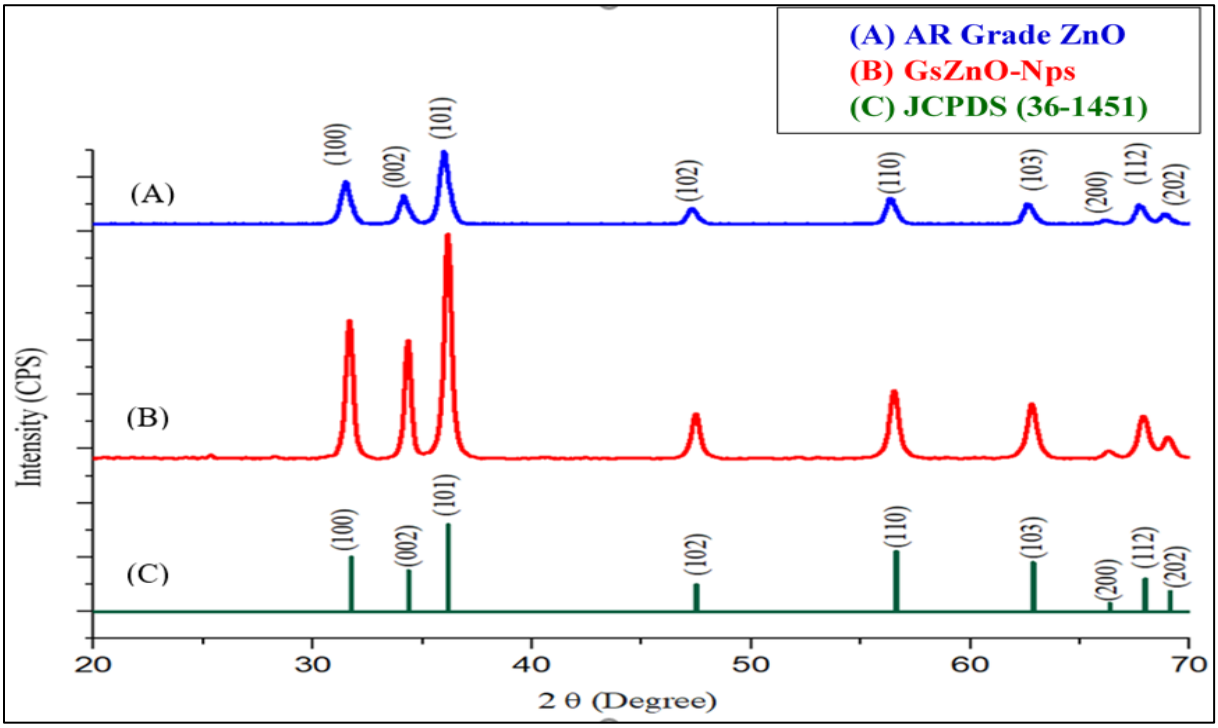

Figure 5.10. *XRD spectrum of (A) AR Grade ZnO (B) GsZnO-Nps and (C) JCPDS Standard card no. 36-1451 given for reference.*

Table 5.5. Average crystalline size, Total crystallinity and specific surface area of GsZnO-Nps and AR grade ZnO

Name of materials	Average crystallite size (nm)	Total crystallinity (%)	Specific surface area (m^2/g)
GsZnO-Nps	13.82	95.91	77.38
AR Grade ZnO	30.87	95.50	42.64

Specific surface area:

Specific surface area is the property of solid materials which measure total surface area per unit mass of bulk volume, solid or cross-sectional area. The specific surface area can be evaluated by using the following equation,

$$S = 6 \times 10^3 / D_P \times \rho$$

Where S- specific surface area, D_P – particle size (average crystallite), ρ- density of ZnO 5.61 g/cm^3.

The Specific surface area of GsZnO-Nps and AR Grade ZnO was found to be 77.38 m^2/g and 42.64 m^2/g. GsZnO-Nps has significantly higher specific surface area than AR Grade ZnO as well as nano ZnO in other reported literature [102]. The specific area can play important role in the antibacterial efficacy due to high surface availability and destruction of the cell wall of microorganisms.

***Total crystallinity**:* The total crystallinity of GsZnO-Nps and AR Grade ZnO was found to be 95.91% and 95.50 % respectively calculated by following equation,

$$\text{Total crysatallinity } \% = \frac{\text{Area of crystalline peaks}}{\text{Area of total peaks (crystalline + amorphous)}} \times 100$$

The high crystallinity of nanomaterials significantly increases the release of Zn^{2+}, which interacts with the negatively charged cell membrane of bacteria through electrostatic interaction subsequently destruction of cell membrane and protein structure results in high antibacterial efficacy [103].

5.7.4. Scanning Electron Microscope Analysis (SEM):

The surface morphology of the GsZnO-Nps was examined by using a scanning electron microscope having x50k and x100 k magnification. Figure 5.11 (A, B, and C) shows monodispersed spherical particles of GsZnO-Nps having approximately 50 nm particle size as deduced from the cited scale. Figure 5.11 (D) shows the energy-dispersive X-ray spectroscopy (EDS) analysis which reveals the quantitative elemental composition of GsZnO-Nps. The elemental analysis of green synthesis nanoparticles shows a mass % of Zn-77.07 and O- 22.93.

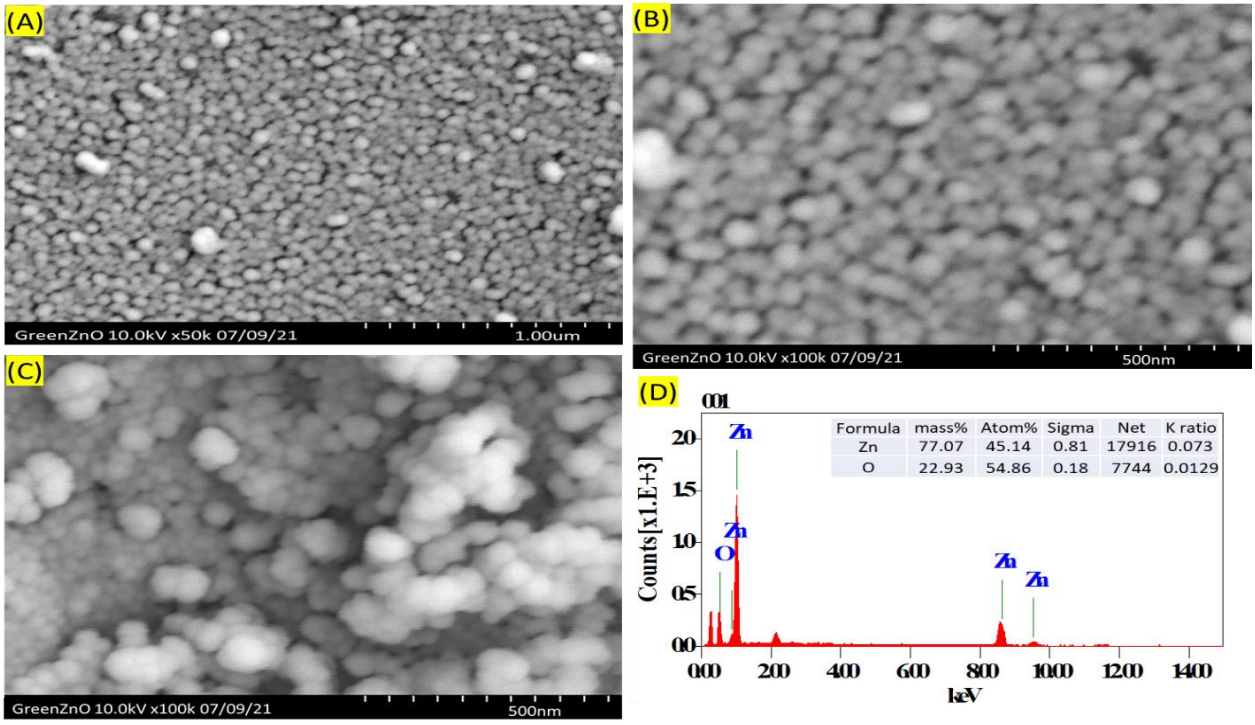

Figure 5.11. *(A, B and C) Scanning Electron Microscopic images reveal the morphology of GsZnO-Nps shows spherical nanoparticles, (D) EDS of GsZnO-Nps revealing the elemental composition in graphical and tabulated form.*

5.8. Anti-Oxidant efficacy of GsZnO-Nps

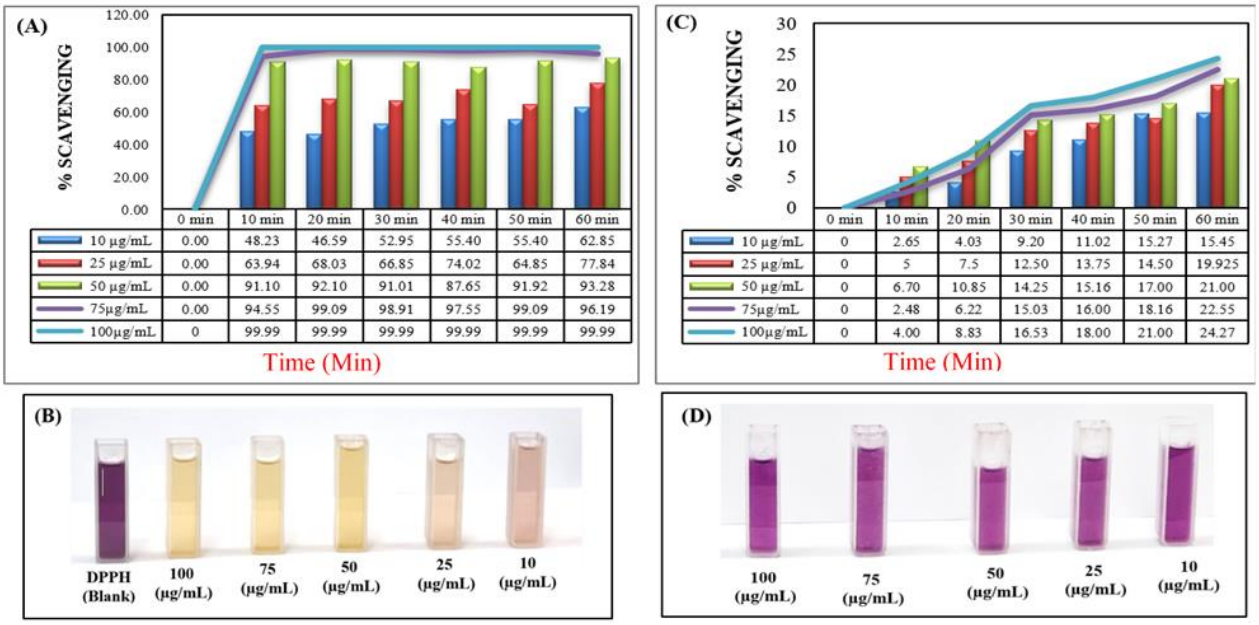

(A)	0 min	10 min	20 min	30 min	40 min	50 min	60 min
10 µg/mL	0.00	48.23	46.59	52.95	55.40	55.40	62.85
25 µg/mL	0.00	63.94	68.03	66.85	74.02	64.85	77.84
50 µg/mL	0.00	91.10	92.10	91.01	87.65	91.92	93.28
75µg/mL	0.00	94.55	99.09	98.91	97.55	99.09	96.19
100µg/mL	0	99.99	99.99	99.99	99.99	99.99	99.99

(C)	0 min	10 min	20 min	30 min	40 min	50 min	60 min
10 µg/mL	0	2.65	4.03	9.20	11.02	15.27	15.45
25 µg/mL	0	5	7.5	12.50	13.75	14.50	19.925
50 µg/mL	0	6.70	10.85	14.25	15.16	17.00	21.00
75µg/mL	0	2.48	6.22	15.03	16.00	18.16	22.55
100µg/mL	0	4.00	8.83	16.53	18.00	21.00	24.27

Figure 5.12. *(A) Anti-oxidant efficacy of GsZnO-Nps different concentration (10 to 100 µg/mL vs Time), (B) Pictorial representation Anti-oxidant efficacy of GsZnO-Nps, (C) Anti-oxidant efficacy of AR Grade ZnO, (D) Pictorial representation Anti-oxidant efficacy of AR Grade ZnO given of comparison.*

Anti-oxidant efficacy of GsZnO-Nps and AR Grade ZnO were evaluated at different concentrations (10 to 100 µg/mL) by using nitrogen-centered free radical i.e. DPPH. The anti-oxidant efficacy of GsZnO-Nps and AR Grade ZnO was shown in Figure 5.12 (A and C) up to 60 min. The systematic pictorial representation of scavenging of free radical color change due to GsZnO-Nps and AR Grade ZnO shown Figure 5.12 (B and D). The free radical scavenging potency "FRSP" of GsZnO-Nps at concentration 50, 75 and 100 µg/mL shows 91% to 99.99% after 30 min. However, FRSP of AR Grade ZnO was 14% to 16%. The IC_{50} concentration of GsZnO-Nps was 21.72 µg/mL and AR Grade ZnO was 345.57 µg/mL which is shown in Figure 5.13 (A and B). The free radicle scavenging potency of GsZnO-Nps is significantly higher than in reported literature [104]. The high FRSP could be because of several reasons, influence of phytochemicals of *Moringa oleifera* leaves extract and their bioactive attraction towards charged nanoparticles ($ZnO = Zn^{2+} + O^{2-}$) which synergistically increase the bioactivity, formation of nanoscale particles, high specific surface area. The activity effects commonly depend on the attachment sites of the metals and their subsequent impact on the potency of the free radical scavenging [105].

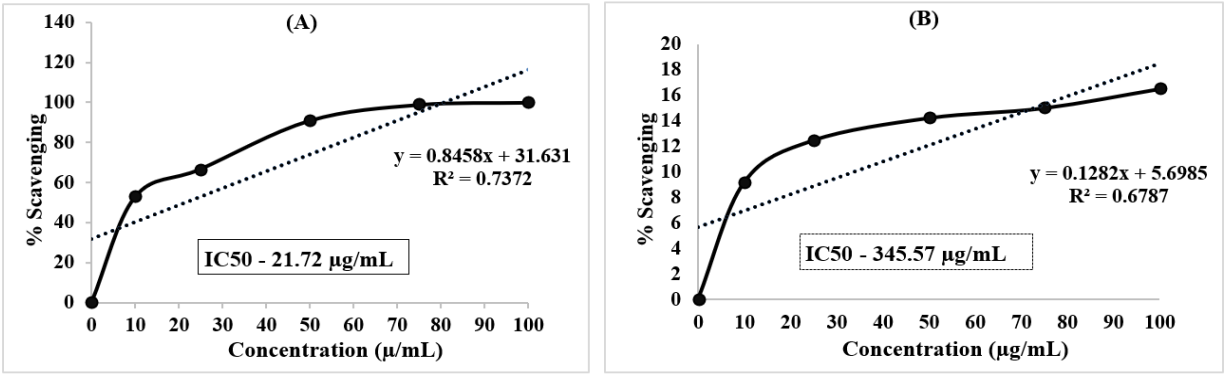

Figure 5.13. *IC_{50} concentration (A) GsZnO-Nps and (B) AR Grade ZnO which is given for comparison.*

5.9. Antimicrobial efficacy GsZnO-Nps

5.9.1. Anti-Acne efficacy

The anti-acne efficacy of 0.0183 g/mL GsZnO-Nps and zinc acetate dihydrate was evaluated by disk diffusion technique against *C. acne* bacteria which is mainly responsible for causing acne on skin. The study was carried out in four different sets to minimize the experimental error. The average inhibition zone of GsZnO-Nps against *C. acne* was 33 mm having a standard deviation

of 1.155 mm and a standard error of 0.557 mm. ZOI of zinc acetate dihydrate was 10.7 mm having a standard deviation of 0.559 mm and the standard error was 0.279 mm which is shown in Figure 5.14 (A and B) and Table 5.6. The robust anti-acne efficacy could be due to several reasons like the influence of active chemical constituents of *Moringa oleifera*, the particle size of metal oxide in nano regime, generation of reactive oxygen species, the release of Zn^{2+} ions which can rupture the micro-organism cell walls and potentially damage the internal organelle of the bacterial cell. The anti-acne efficacy is significantly higher than other reported literature [106].

Figure	Sample details	Zone of inhibition in mm for *C. acne* ATCC 11827	
A	GsZnO-Nps (0.0183 g/mL)	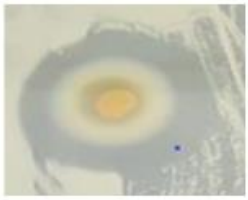	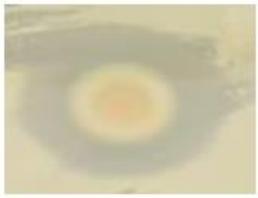
B	Zinc acetate dihydrate (0.0183 g/mL)		

Figure 5.14. *Representative images of anti-acne study against C. acne bacteria (A) ZOI of GsZnO-Nps (B) ZOI of Zinc acetate dihydrate salt.*

Table 5.6. GsZnO-Nps anti-acne efficacy measured in inhibition zone against C. acne.

Sr. No.	Sample details	Zone of inhibition in mm for *C. acne* ATCC 11827				Average (mm)	Std. deviation	Std. error
		Set 1	Set 2	Set 3	Set 4			
1	GsZnO-Nps (0.0183 g/mL)	34.00	34.00	32.00	32.00	33.00	1.155	0.577
2	Zinc acetate dihydrate (0.0183 g/mL)	11.1	10.5	10.00	11.2	10.70	0.559	0.279

5.9.2. ZOI: Disk diffusion method

(A) **Anti-bacterial efficacy against *S. aureus***

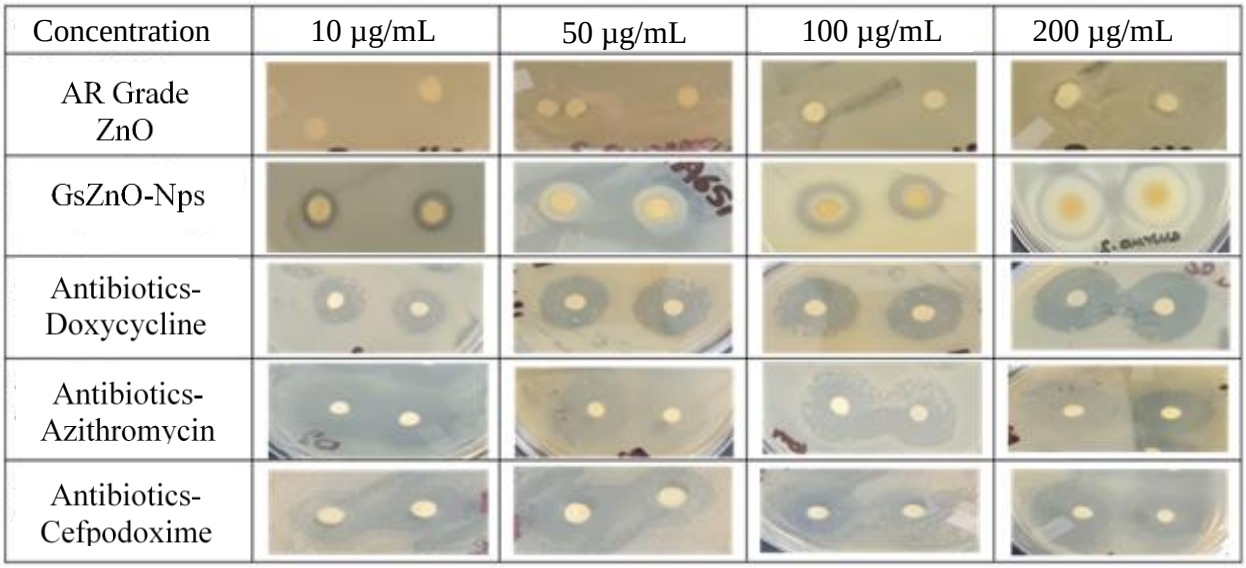

(B) **Anti-bacterial efficacy against *E. coli***

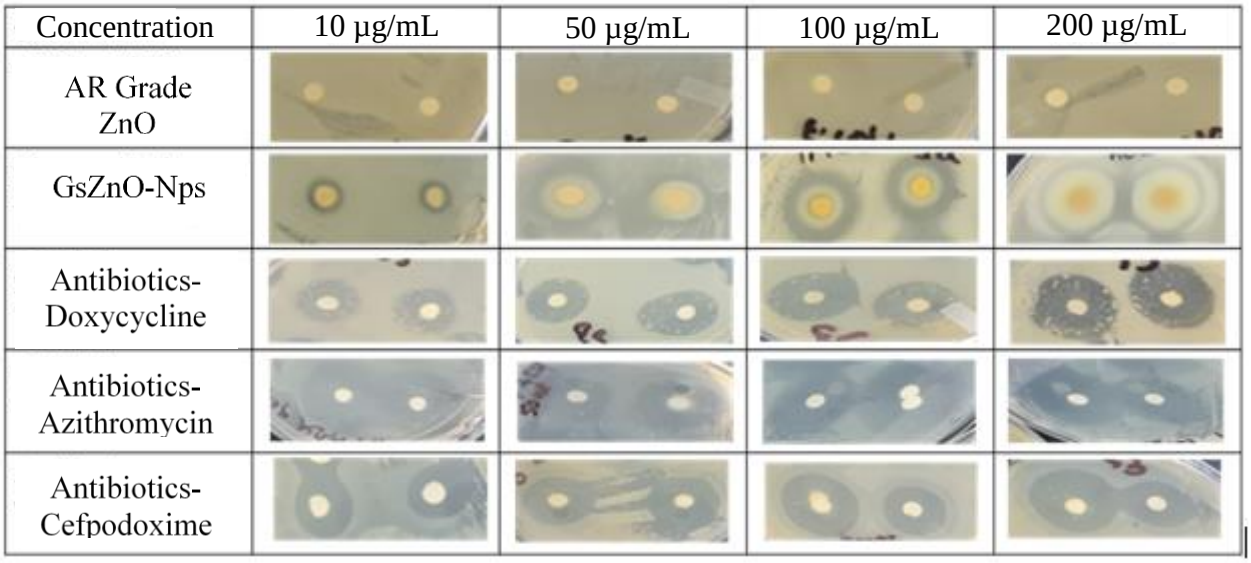

Figure 5.15. *Antibacterial efficacy of AR Grade ZnO, GsZnO-Nps, Vs standard drugs antibiotics (Doxycycline, Azithromycin and Cefpodoxime) against both gram-positive and gram-negative organism (A) S. aureus and (B) E. coli*

Anti-bacterial properties of GsZnO-Nps, AR Grade ZnO and standard drug were investigated by disk diffusion method. Different concentration like 10 µg/mL, 50 µg/mL, 100 µg/mL, 200 µg/mL of GsZnO-Nps, AR Grade ZnO and same for standard drugs used for the ZOI study against both Gram-positive *(S. aureus)* and Gram-negative *(E. coli)* pathogens which

is shown in Figure 5.15 (A and B). There is no inhibition zone observed in AR Grade ZnO. However, the higher concentration of GsZnO-Nps (200 µg/mL) have shown the average ZOI 26.75 mm against (*E. coli)* and 30.00 mm against *(S. aureus).* Standard drug (antibiotics) Doxycycline show the inhibition zone 24.0 mm and 22.5 mm against (*E. coli)* and 30.00 mm against *(S. aureus),* Azithromycin shows the strong inhibition zone against both (*E. coli)* and *(S. aureus)* respectively 31.00 mm and 30.00 mm as well as Cefpodoxime shows the inhibition zone approximately 20.25 mm and 19.75 mm against both (*E. coli)* and *(S. aureus).* The inhibition zone of GsZnO-Nps is directionally higher than standard drugs Doxycycline, Cefpodoxime and at par to Azithromycin inhibition zone at 200 µg/mL which is tabulated in Table 5.7.

Table 5.7. Anti-bacterial efficacy measured in ZOI (mm) of AR Grade ZnO, GsZnO-Nps vs Standard drug.

Name of Test product	Conc. (µg/mL)	*E. coli* Inhibition Zone (mm)		*S. aureus* Inhibition Zone (mm)	
		Average	Std. dev.	Average	Std. dev.
AR Grade ZnO	10	0.00	0.00	0.00	0.00
	50	0.00	0.00	0.00	0.00
	100	0.00	0.00	0.00	0.00
	200	0.00	0.00	0.00	0.00
GsZnO-Nps	10	6.50	0.58	6.75	0.50
	50	14.50	1.73	14.25	0.96
	100	19.25	0.50	18.25	0.96
	200	26.75	1.50	30.00	1.83
Doxycycline	10	14.00	1.41	15.25	0.50
	50	18.25	0.96	17.75	1.89
	100	22.00	0.82	20.50	1.29
	200	24.00	1.83	22.50	1.73
Azithromycin	10	15.75	0.96	16.00	0.82
	50	21.75	0.50	22.25	0.96
	100	23.00	2.16	24.25	0.96
	200	31.00	1.41	30.00	1.41
Cefpodoxime	10	11.75	0.96	11.00	0.50
	50	15.00	1.83	16.25	0.96
	100	18.75	1.26	17.00	0.40
	200	20.25	0.96	19.75	0.96

The anti-bacterial efficacy of GsZnO-Nps is significantly higher that reported literatures possibly due to influence of phytochemicals, high active specific surface area available for the interaction with microorganisms per unit mass, release of zinc ions, interaction of particles to cell membrane and generation of reactive oxygen species [107].

5.9.3. Minimum Inhibitory concentration:

The MIC of GsZnO-Nps and AR Grade ZnO was determined against *E. coli* and *S. aureus* bacteria. MIC of GsZnO-Nps was found to be 500 µg/mL which is significantly lesser as to AR Grade ZnO (>900 µg/mL) shown in Table 5.8 which is in line with previous published literature [108].

Table 5.8. MIC of GsZnO-Nps and AR Grade ZnO against both E. coli and S. aureus organism

Material	Pathogen	Concentration (µg/mL)	Observation	MIC (µg/mL)
AR Grade ZnO	*E. coli*	*900*	Growth	>900
		700	Growth	
		500	Growth	
		300	Growth	
		100	Growth	
	S. aureus	900	Growth	>900
		700	Growth	
		500	Growth	
		300	Growth	
		100	Growth	
GsZnO-Nps	*E. coli*	900	No Growth	500
		700	No Growth	
		500	No Growth	
		300	Growth	
		100	Growth	
	S. aureus	900	No Growth	500
		700	No Growth	
		500	No Growth	
		300	Growth	
		100	Growth	

Both, the inhibition zone and the MIC allow a prediction of therapeutic success. Concentration of GsZnO-Nps can be vary in both ZOI & MIC because while the MIC is a direct measurement of a concentration needed at the site of growth for bactericidal effect and the inhibition zone is that a given sample inhibits in whatsoever way the growth of the target bacterium and express bacteriostatic property [108]. Numbers of factors are responsible for anti-bacterial activity like reactive oxygen species (ROS), release of Zn^{2+} and direct contact of ZnO nanoparticles.

References

[1] R. Ullah, A. S. Alqahtani, O. M. A. Noman, A. M. Alqahtani, S. Ibenmoussa, and M. Bourhia, "A review on ethno-medicinal plants used in traditional medicine in the Kingdom of Saudi Arabia," *Saudi J. Biol. Sci.*, vol. 27, no. 10, pp. 2706–2718, Oct. 2020, doi: 10.1016/j.sjbs.2020.06.020.

[2] A. M. Ageel, N. S. Parmar, J. S. Mossa, M. A. Al-Yahya, M. S. Al-Said, and M. Tariq, "Anti-inflammatory activity of some Saudi Arabian medicinal plants," *Agents Actions*, vol. 17, no. 3–4, pp. 383–384, Jan. 1986, doi: 10.1007/BF01982656.

[3] E. E. G. Gamal, S. A. K. Khalifa, A. S. Gameel, and M. A. Emad, "Traditional medicinal plants indigenous to Al-Rass province, Saudi Arabia," *J. Med. Plants Res.*, vol. 4, no. 24, pp. 2680–2683, Dec. 2010, doi: 10.5897/JMPR09.556.

[4] R. Purena, R. Seth, and R. Bhatt, "Protective role of Emblica officinalis hydro-ethanolic leaf extract in cisplatin induced nephrotoxicity in Rats," *Toxicol. Reports*, vol. 5, pp. 270–277, 2018, doi: 10.1016/j.toxrep.2018.01.008.

[5] S. P. Varahachalam *et al.*, "Nanomedicine for the SARS-CoV-2: State-of-the-Art and Future Prospects," *Int. J. Nanomedicine*, vol. Volume 16, pp. 539–560, Jan. 2021, doi: 10.2147/IJN.S283686.

[6] P. Paliwal, S. Sargolzaei, S. K. Bhardwaj, V. Bhardwaj, C. Dixit, and A. Kaushik, "Grand Challenges in Bio-Nanotechnology to Manage the COVID-19 Pandemic," *Front. Nanotechnol.*, vol. 2, Nov. 2020, doi: 10.3389/fnano.2020.571284.

[7] A. Leone, A. Spada, A. Battezzati, A. Schiraldi, J. Aristil, and S. Bertoli, "Cultivation, Genetic, Ethnopharmacology, Phytochemistry and Pharmacology of Moringa oleifera Leaves: An Overview," *Int. J. Mol. Sci.*, vol. 16, no. 12, pp. 12791–12835, Jun. 2015, doi: 10.3390/ijms160612791.

[8] A. N. Zelikin and D. Putnam, "Poly(carbonate−acetal)s from the Dimer Form of Dihydroxyacetone," *Macromolecules*, vol. 38, no. 13, pp. 5532–5537, Jun. 2005, doi: 10.1021/ma050049v.

[9] J. Skoweranda, M. Bukowska-Strzyzewska, R. Bartnik, and W. Strzyżewski, "Molecular structure and some reactivity aspects of 2,6-diamino-4(3H)-pyrimidinone monohydrate," *J. Crystallogr. Spectrosc. Res.*, vol. 20, no. 2, pp. 117–121, Apr. 1990, doi: 10.1007/BF01160962.

[10] X. Yu, M. Zhao, F. Liu, S. Zeng, and J. Hu, "Identification of 2,3-dihydro-3,5-dihydroxy-6-methyl-4H-pyran-4-one as a strong antioxidant in glucose–histidine Maillard reaction products," *Food Res. Int.*, vol. 51, no. 1, pp. 397–403, Apr. 2013, doi: 10.1016/j.foodres.2012.12.044.

[11] L. Čechovská, K. Cejpek, M. Konečný, and J. Velíšek, "On the role of 2,3-dihydro-3,5-dihydroxy-6-methyl-(4H)-pyran-4-one in antioxidant capacity of prunes," *Eur. Food Res. Technol.*, vol. 233, no. 3, pp. 367–376, Sep. 2011, doi: 10.1007/s00217-011-1527-4.

[12] E. K. Starostin, M. A. Lapitskaya, A. V. Ignatenko, K. K. Pivnitsky, and G. I. Nikishin, "Practical synthesis of hex-5-ynoic acid from cyclohexanone," *Russ. Chem. Bull.*, vol. 49, no. 1, pp. 81–84, Jan. 1990, doi: 10.1007/BF02499070.

[13] R. Khorassani, U. Hettwer, A. Ratzinger, B. Steingrobe, P. Karlovsky, and N. Claassen, "Citramalic acid and salicylic acid in sugar beet root exudates solubilize soil phosphorus," *BMC Plant Biol.*, vol. 11, no. 1, p. 121, Dec. 2011, doi: 10.1186/1471-2229-11-121.

[14] B. Rodriguez-Garay, G. C. Phillips, and G. D. Kuehn, "Detection of Norspermidine and Norspermine in Medicago sativa L. (Alfalfa)," *Plant Physiol.*, vol. 89, no. 2, pp. 525–529, Feb. 1989, doi: 10.1104/pp.89.2.525.

[15] P. S. Sunkara, J. H. Zwolshen, N. J. Prakash, and T. L. Bowlin, "Mechanism of Antitumor Activity of Norspermidine, a Structural Homologue of Spermidine," 1988, pp. 707–716.

[16] T. Nishio, Y. Yoshikawa, C.-Y. Shew, N. Umezawa, T. Higuchi, and K. Yoshikawa, "Specific effects of antitumor active norspermidine on the structure and function of DNA," *Sci. Rep.*, vol. 9, no. 1, p. 14971, Oct. 2019, doi: 10.1038/s41598-019-50943-1.

[17] Y. TAKEBE, K. Osaka IUCHI, G. Nara-ken TSUKAMOTO, and Osaka-fu, "4-CHLORO-4-METHYL-5-METHYLENE-1,3-DIOXOLAN-2-ONE," EP 0 147 472 B1, 1984.

[18] K. Hagiyama *et al.*, "Physical Properties of Substituted 1,3-Dioxolan-2-ones," *Chem. Lett.*, vol. 37, no. 2, pp. 210–211, Feb. 2008, doi: 10.1246/cl.2008.210.

[19] A. G. Al-Ziaydi, M. I. Hamzah, A. M. Al-Shammari, H. S. Kadhim, and M. S. Jabir, "The anti-proliferative activity of D-mannoheptulose against breast cancer cell line through glycolysis inhibition," 2020, p. 020023, doi: 10.1063/5.0032958.

[20] P. Courtois, A. Sener, and W. Malaisse, "D-mannoheptulose phosphorylation by hexokinase isoenzymes," *Int. J. Mol. Med.*, Apr. 2001, doi: 10.3892/ijmm.7.4.359.

[21] H. K. . K. A. M. B. S.BISWAL, U.SAHOO, S.SETHY, "INDOLE: THE MOLECULE OF DIVERSE BIOLOGICAL ACTIVITIES," *Asian J. Pharm. Clin. Res.*, vol. 5, no. 1, 2012.

[22] H. H. Imad, J. H. Hussein, A. K. Muhanned, and S. H. Nidaa, "Identification of five newly described bioactive chemical compounds in methanolic extract of Mentha viridis by using gas chromatography - mass spectrometry (GC-MS)," *J. Pharmacogn. Phyther.*, vol. 7, no. 7, pp. 107–125, Jul. 2015, doi: 10.5897/JPP2015.0349.

[23] S. Kanhar and A. K. Sahoo, "Ameliorative effect of Homalium zeylanicum against carbon tetrachloride-induced oxidative stress and liver injury in rats," *Biomed. Pharmacother.*, vol. 111, pp. 305–314, Mar. 2019, doi: 10.1016/j.biopha.2018.12.045.

[24] A. M. Shendurse and C. D. Khedkar, "Glucose: Properties and Analysis," in *Encyclopedia of Food and Health*, Elsevier, 2016, pp. 239–247.

[25] J. Cancelas, A. Acitores, M. L. Villanueva-Penacarrillo, W. J. Malaisse, and I. Valverde, "Activation of glycogen synthase a in hepatocytes exposed to alpha-D-glucose pentaacetate.," *Int. J. Mol. Med.*, Aug. 2000, doi: 10.3892/ijmm.6.2.197.

[26] S. Ölgen, N. Altanlar, E. Karataylı, and M. Bozdayı, "Antimicrobial and Antiviral Screening of Novel Indole Carboxamide and Propanamide Derivatives," *Zeitschrift für Naturforsch. C*, vol. 63, no. 3–4, pp. 189–195, Apr. 2008, doi: 10.1515/znc-2008-3-405.

[27] A. Huang, N. Brody, and T. N. Liebman, "Dihydroxyacetone and sunless tanning: Knowledge, myths, and current understanding," *J. Am. Acad. Dermatol.*, vol. 77, no. 5, pp. 991–992, Nov. 2017, doi: 10.1016/j.jaad.2017.04.1117.

[28] A. E. Sagiv, S. Dikstein, and A. Ingber, "The efficiency of humectants as skin moisturizers in the presence of oil," *Ski. Res. Technol.*, vol. 7, no. 1, pp. 32–35, Feb. 2001, doi: 10.1034/j.1600-0846.2001.007001032.x.

[29] G. J. M. den Hartog *et al.*, "Erythritol is a sweet antioxidant," *Nutrition*, vol. 26, no. 4, pp. 449–458, Apr. 2010, doi: 10.1016/j.nut.2009.05.004.

[30] Z. A. A. Abbas, N. M. J. Abu-Mejdad, Z. W. Atwan, and N. A. Al-Masoudi, "Synthesis and Biological Evaluation of New Dipyridylpteridines, Lumazines, and Related Analogues," *J. Heterocycl. Chem.*, vol. 54, no. 2, pp. 895–903, Mar. 2017, doi: 10.1002/jhet.2651.

[31] H. C. Brown, "Economical and convenient procedures for the synthesis of catecholborane," US6204405B1, 1999.

[32] *Encyclopedia of Reagents for Organic Synthesis*. Wiley, 2001.

[33] A. Kaiser, A. Gottwald, C. Wiersch, B. Lindenthal, W. Maier, and H. Seitz, "Effect of drugs inhibiting spermidine biosynthesis and metabolism on the in vitro development of Plasmodium falciparum," *Parasitol. Res.*, vol. 87, no. 11, pp. 963–972, Nov. 2001, doi: 10.1007/s004360100460.

[34] Y. He, J. L. H. Johnson, and S. H. Yalkowsky, "Oral formulation of a novel antiviral agent, PG301029, in a mixture of Gelucire 44/14 and DMA (2∶1, wt/wt)," *AAPS PharmSciTech*, vol. 6, no. 1, pp. E1–E5, Mar. 2005, doi: 10.1208/pt060101.

[35] S. Liu, L. He, and K. Yao, "The Antioxidative Function of Alpha-Ketoglutarate and Its Applications," *Biomed Res. Int.*, vol. 2018, pp. 1–6, 2018, doi: 10.1155/2018/3408467.

[36] S. D. Markad *et al.*, "Novel lead generation of an anti-tuberculosis agent active against non-replicating mycobacteria: exploring hybridization of pyrazinamide with multiple fragments," *Med. Chem. Res.*, vol. 24, no. 7, pp. 2986–2992, Jul. 2015, doi: 10.1007/s00044-015-1352-6.

[37] Z.-I. Rhew, J. H. Lee, and Y. Han, "Aster yomena has anti-arthritic activity against septic arthritis induced by Candida albicans: its terpenoid constituent is the most effective and has synergy with indomethacin," *Adv. Tradit. Med.*, vol. 20, no. 2, pp. 213–221, Jun. 2020, doi: 10.1007/s13596-019-00405-w.

[38] N. V. Zaitseva, T. S. Ulanova, O. V. Dolgikh, T. V. Nurislamova, and O. A. Mal'tseva, "Diagnostics of Early Changes in the Immune System Due to Low Concentration of N-Nitrosamines in the Blood," *Bull. Exp. Biol. Med.*, vol. 164, no. 3, pp. 334–338, Jan. 2018, doi: 10.1007/s10517-018-3984-2.

[39] A. Hamedi, A. Pasdaran, and A. Pasdaran, "Antimicrobial Activity and Analysis of the Essential Oils of Selected Endemic Edible Apiaceae Plants Root from Caspian Hyrcanian Region (North of Iran)," *Pharm. Sci.*, vol. 25, no. 2, pp. 138–144, Jun. 2019, doi: 10.15171/PS.2019.21.

[40] A. S. & W. J. M. O. Scruel, C. Vanhoutte, "Interference of D-mannoheptulose with D-glucose phosphorylation, metabolism and functional effects: Comparison between liver, parotid cells and pancreatic islets," *Mol. Cell. Biochem.*, vol. 187, pp. 113–120, 1998, [Online]. Available: https://link.springer.com/article/10.1023/A:1006812300200.

[41] A. N. Wick, M. C. Almen, and L. Joseph, "The Metabolism of Sorbitol*," *J. Am. Pharm. Assoc. (Scientific ed.)*, vol. 40, no. 11, pp. 542–544, Nov. 1951, doi: 10.1002/jps.3030401104.

[42] M. L. Manca *et al.*, "Sorbitol-penetration enhancer containing vesicles loaded with baicalin for the protection and regeneration of skin injured by oxidative stress and UV radiation," *Int. J. Pharm.*, vol. 555, pp. 175–183, Jan. 2019, doi: 10.1016/j.ijpharm.2018.11.053.

[43] D. A. Mariano Bizzarri, Antonio Simone Laganà and Vittorio Unfer, "Inositol and pulmonary function. Could myo-inositol treatment downregulate inflammation and cytokine release syndrome in SARS-CoV-2?," *Eur. Rev. Med. Pharmacol. Sci.*, vol. 24, pp. 3426–3432, 2020, doi: 10.26355/eurrev_202003_20715.

[44] B. Pintaudi, G. Di Vieste, and M. Bonomo, "The Effectiveness of Myo-Inositol and D-Chiro Inositol Treatment in Type 2 Diabetes," *Int. J. Endocrinol.*, vol. 2016, pp. 1–5, 2016, doi: 10.1155/2016/9132052.

[45] J.-K. Choi, I. Carreras, A. Dedeoglu, and B. G. Jenkins, "Detection of increased scyllo-inositol in brain with magnetic resonance spectroscopy after dietary supplementation in Alzheimer's disease mouse models," *Neuropharmacology*, vol. 59, no. 4–5, pp. 353–357, Sep. 2010, doi: 10.1016/j.neuropharm.2010.03.011.

[46] S. Freeman and T. Hudlicky, "New oligomers of conduritol-F and muco -inositol. Synthesis and biological evaluation as glycosidase inhibitors," *Bioorg. Med. Chem. Lett.*, vol. 14, no. 5, pp. 1209–1212, Mar. 2004, doi: 10.1016/j.bmcl.2003.12.050.

[47] Z. Kamenov and A. Gateva, "Inositols in PCOS," *Molecules*, vol. 25, no. 23, p. 5566, Nov. 2020, doi: 10.3390/molecules25235566.

[48] G. C. M. Bizzarri, "Inositol: history of an effective therapy for Polycystic Ovary Syndrome," *Eur. Rev. Med. Pharmacol. Sci.*, vol. 18, no. 13, pp. 1896–1903, 2014, [Online]. Available: https://www.europeanreview.org/article/7565.

[49] N. M. Saeed, E. El-Demerdash, H. M. Abdel-Rahman, M. M. Algandaby, F. A. Al-Abbasi, and A. B. Abdel-Naim, "Anti-inflammatory activity of methyl palmitate and ethyl palmitate in different experimental rat models," *Toxicol. Appl. Pharmacol.*, vol. 264, no. 1, pp. 84–93, Oct. 2012, doi: 10.1016/j.taap.2012.07.020.

[50] V. Aparna, K. V. Dileep, P. K. Mandal, P. Karthe, C. Sadasivan, and M. Haridas, "Anti-Inflammatory Property of n-Hexadecanoic Acid: Structural Evidence and Kinetic Assessment," *Chem. Biol. Drug Des.*, vol. 80, no. 3, pp. 434–439, Sep. 2012, doi: 10.1111/j.1747-0285.2012.01418.x.

[51] A. K. Ghosh *et al.*, "Structure-Based Design of Potent HIV-1 Protease Inhibitors with Modified P1-Biphenyl Ligands: Synthesis, Biological Evaluation, and Enzyme–Inhibitor X-ray Structural Studies," *J. Med. Chem.*, vol. 58, no. 13, pp. 5334–5343, Jul. 2015, doi: 10.1021/acs.jmedchem.5b00676.

[52] E. Faujdar and R. K. Singh, "Methyl oleate derived multifunctional additive for polyol based lubricants," *Wear*, vol. 466–467, p. 203550, Feb. 2021, doi: 10.1016/j.wear.2020.203550.

[53] S. D. ABDUL AZIZ, "PHYTOL-CONTAINING SEAWEED EXTRACTS AS CONTROL FOR Ganoderma boninense," *J. Oil Palm Res.*, May 2019, doi: 10.21894/jopr.2019.0018.

[54] M. T. Islam *et al.*, "Phytol: A review of biomedical activities," *Food Chem. Toxicol.*, vol. 121, pp. 82–94, Nov. 2018, doi: 10.1016/j.fct.2018.08.032.

[55] P. Weill, C. Plissonneau, P. Legrand, V. Rioux, and R. Thibault, "May omega-3 fatty acid dietary supplementation help reduce severe complications in Covid-19 patients?," *Biochimie*, vol. 179, pp. 275–280, Dec. 2020, doi: 10.1016/j.biochi.2020.09.003.

[56] N. Blondeau, R. H. Lipsky, M. Bourourou, M. W. Duncan, P. B. Gorelick, and A. M. Marini, "Alpha-Linolenic Acid: An Omega-3 Fatty Acid with Neuroprotective Properties—Ready for Use in the Stroke Clinic?," *Biomed Res. Int.*, vol. 2015, pp. 1–8, 2015, doi: 10.1155/2015/519830.

[57] Y. Li *et al.*, "Diet containing stearic acid increases food reward-related behaviors in mice compared with oleic acid," *Brain Res. Bull.*, vol. 164, pp. 45–54, Nov. 2020, doi: 10.1016/j.brainresbull.2020.08.012.

[58] M. A. van Rooijen, J. Plat, W. A. M. Blom, P. L. Zock, and R. P. Mensink, "Dietary stearic acid and palmitic acid do not differently affect ABCA1-mediated cholesterol efflux capacity in healthy men and postmenopausal women: A randomized controlled trial," *Clin. Nutr.*, vol. 40, no. 3, pp. 804–811, Mar. 2021, doi: 10.1016/j.clnu.2020.08.016.

[59] L. Ge *et al.*, "Differential proteomic analysis of the anti-depressive effects of oleamide in a rat chronic mild stress model of depression," *Pharmacol. Biochem. Behav.*, vol. 131, pp. 77–86, Apr. 2015, doi: 10.1016/j.pbb.2015.01.017.

[60] P. Malik, R. Shankar, V. Malik, N. Sharma, and T. K. Mukherjee, "Green Chemistry Based Benign Routes for Nanoparticle Synthesis," *J. Nanoparticles*, vol. 2014, pp. 1–14, Mar. 2014, doi: 10.1155/2014/302429.

[61] V. N. Kalpana and V. Devi Rajeswari, "A Review on Green Synthesis, Biomedical Applications, and Toxicity Studies of ZnO NPs," *Bioinorg. Chem. Appl.*, vol. 2018, pp. 1–12, Aug. 2018, doi: 10.1155/2018/3569758.

[62] I. S. G. MRITUNJAI SINGH, SHINJINI SINGH, S. PRASAD, "NANOTECHNOLOGY IN MEDICINE AND ANTIBACTERIAL EFFECT OF SILVER NANOPARTICLES," *Dig. J. Nanomater. Biostructures*, vol. 3, no. 3, pp. 115–122, 2008, [Online]. Available: https://www.researchgate.net/publication/256463087_Nanotechnology_in_medicine_and_antibacterial_effect_of_silver_nanoparticles.

[63] N. Bhalla *et al.*, "A facile approach to fabricate and embed multifunctional nano ZnO into soap matrix and liquid cleansing products for enhanced antibacterial and photostability for health and hygiene applications," *Arab. J. Chem.*, vol. 15, no. 6, p. 103862, Jun. 2022, doi: 10.1016/j.arabjc.2022.103862.

[64] N. Bhalla, A. Jayaprakash, N. Ingle, H. Patel, S. V. Patri, and D. Haranath, "Fabrication and infusion of potent silver doped nano ZnO aimed to advance germicidal efficacy of health and hygiene products," *J. Sci. Adv. Mater. Devices*, vol. 7, no. 4, p. 100487, Dec. 2022, doi: 10.1016/j.jsamd.2022.100487.

[65] N. Bhalla, N. Ingle, S. V. Patri, and D. Haranath, "Phytochemical analysis of Moringa Oleifera leaves extracts by GC-MS and free radical scavenging potency for industrial applications," *Saudi J. Biol. Sci.*, vol. 28, no. 12, pp. 6915–6928, Dec. 2021, doi: 10.1016/j.sjbs.2021.07.075.

[66] C. Jianrong, M. Yuqing, H. Nongyue, W. Xiaohua, and L. Sijiao, "Nanotechnology and biosensors," *Biotechnol. Adv.*, vol. 22, no. 7, pp. 505–518, Sep. 2004, doi:

10.1016/j.biotechadv.2004.03.004.

[67] X. Zhang, Q. Guo, and D. Cui, "Recent Advances in Nanotechnology Applied to Biosensors," *Sensors*, vol. 9, no. 2, pp. 1033–1053, Feb. 2009, doi: 10.3390/s90201033.

[68] N. O. K. V V Makarov , A J Love , O V Sinitsyna , S S Makarova , I V Yaminsky , M E Taliansky, "'Green' nanotechnologies: synthesis of metal nanoparticles using plants," *Acta Naturae*, vol. 6, no. 1, pp. 35–44, 2014, [Online]. Available: https://pubmed.ncbi.nlm.nih.gov/24772325/.

[69] V. ARYA, "LIVING SYSTEMS: ECO-FRIENDLY NANOFACTORIES," *Dig. J. Nanomater. Biostructures*, vol. 5, no. 1, pp. 9–21, 2010, [Online]. Available: https://www.researchgate.net/publication/266093859_Living_systems_Eco-friendly_nanofactories.

[70] B. Biswas, K. Rogers, F. McLaughlin, D. Daniels, and A. Yadav, "Antimicrobial Activities of Leaf Extracts of Guava (Psidium guajava L.) on Two Gram-Negative and Gram-Positive Bacteria," *Int. J. Microbiol.*, vol. 2013, pp. 1–7, 2013, doi: 10.1155/2013/746165.

[71] J. Virkutyte and R. S. Varma, "Green synthesis of metal nanoparticles: Biodegradable polymers and enzymes in stabilization and surface functionalization," *Chem. Sci.*, vol. 2, no. 5, pp. 837–846, 2011, doi: 10.1039/C0SC00338G.

[72] M. N. Nadagouda and R. S. Varma, "Green synthesis of silver and palladium nanoparticles at room temperature using coffee and tea extract," *Green Chem.*, vol. 10, no. 8, p. 859, 2008, doi: 10.1039/b804703k.

[73] M. Darroudi, Z. Sabouri, R. Kazemi Oskuee, A. Khorsand Zak, H. Kargar, and M. H. N. Abd Hamid, "Green chemistry approach for the synthesis of ZnO nanopowders and their cytotoxic effects," *Ceram. Int.*, vol. 40, no. 3, pp. 4827–4831, Apr. 2014, doi: 10.1016/j.ceramint.2013.09.032.

[74] S. Iravani, "Green synthesis of metal nanoparticles using plants," *Green Chem.*, vol. 13, no. 10, p. 2638, 2011, doi: 10.1039/c1gc15386b.

[75] M. Behravan, A. Hossein Panahi, A. Naghizadeh, M. Ziaee, R. Mahdavi, and A. Mirzapour, "Facile green synthesis of silver nanoparticles using Berberis vulgaris leaf and root aqueous extract and its antibacterial activity," *Int. J. Biol. Macromol.*, vol. 124, pp. 148–154, Mar. 2019, doi: 10.1016/j.ijbiomac.2018.11.101.

[76] P. Rajiv, S. Rajeshwari, and R. Venckatesh, "Bio-Fabrication of zinc oxide nanoparticles using leaf extract of Parthenium hysterophorus L. and its size-dependent antifungal activity against plant fungal pathogens," *Spectrochim. Acta Part A Mol. Biomol. Spectrosc.*, vol. 112, pp. 384–387, Aug. 2013, doi: 10.1016/j.saa.2013.04.072.

[77] A. A. Menazea, A. M. Ismail, and A. Samy, "Novel Green Synthesis of Zinc Oxide Nanoparticles Using Orange Waste and Its Thermal and Antibacterial Activity," *J. Inorg. Organomet. Polym. Mater.*, vol. 31, no. 11, pp. 4250–4259, Nov. 2021, doi: 10.1007/s10904-021-02074-2.

[78] J. S. Moodley, S. B. N. Krishna, K. Pillay, Sershen, and P. Govender, "Green synthesis of silver nanoparticles from Moringa oleifera leaf extracts and its antimicrobial potential," *Adv. Nat. Sci. Nanosci. Nanotechnol.*, vol. 9, no. 1, p. 015011, Mar. 2018, doi: 10.1088/2043-

6254/aaabb2.

[79] T. Singh, A. Jayaprakash, M. Alsuwaidi, and A. A. Madhavan, "Green synthesized gold nanoparticles with enhanced photocatalytic activity," *Mater. Today Proc.*, vol. 42, pp. 1166–1169, 2021, doi: 10.1016/j.matpr.2020.12.531.

[80] J. Suresh, G. Pradheesh, V. Alexramani, M. Sundrarajan, and S. I. Hong, "Green synthesis and characterization of zinc oxide nanoparticle using insulin plant (Costus pictus D. Don) and investigation of its antimicrobial as well as anticancer activities," *Adv. Nat. Sci. Nanosci. Nanotechnol.*, vol. 9, no. 1, p. 015008, Feb. 2018, doi: 10.1088/2043-6254/aaa6f1.

[81] N. J. Sushma, B. Mahitha, K. Mallikarjuna, and B. D. P. Raju, "Bio-inspired ZnO nanoparticles from Ocimum tenuiflorum and their in vitro antioxidant activity," *Appl. Phys. A*, vol. 122, no. 5, p. 544, May 2016, doi: 10.1007/s00339-016-0069-9.

[82] A. Kołodziejczak-Radzimska and T. Jesionowski, "Zinc Oxide—From Synthesis to Application: A Review," *Materials (Basel).*, vol. 7, no. 4, pp. 2833–2881, Apr. 2014, doi: 10.3390/ma7042833.

[83] A. A. Menazea and N. S. Awwad, "Antibacterial activity of TiO2 doped ZnO composite synthesized via laser ablation route for antimicrobial application," *J. Mater. Res. Technol.*, vol. 9, no. 4, pp. 9434–9441, Jul. 2020, doi: 10.1016/j.jmrt.2020.05.103.

[84] J. Iqbal *et al.*, "Green synthesis of zinc oxide nanoparticles using Elaeagnus angustifolia L. leaf extracts and their multiple in vitro biological applications," *Sci. Rep.*, vol. 11, no. 1, p. 20988, Oct. 2021, doi: 10.1038/s41598-021-99839-z.

[85] Z. Q. Zheng, J. D. Yao, B. Wang, and G. W. Yang, "Light-controlling, flexible and transparent ethanol gas sensor based on ZnO nanoparticles for wearable devices," *Sci. Rep.*, vol. 5, no. 1, p. 11070, Jun. 2015, doi: 10.1038/srep11070.

[86] S. Yedurkar, C. Maurya, and P. Mahanwar, "Biosynthesis of Zinc Oxide Nanoparticles Using Ixora Coccinea Leaf Extract—A Green Approach," *Open J. Synth. Theory Appl.*, vol. 05, no. 01, pp. 1–14, 2016, doi: 10.4236/ojsta.2016.51001.

[87] M. F. H. Abd El-Kader, M. T. Elabbasy, A. A. Adeboye, M. G. M. Zeariya, and A. A. Menazea, "Morphological, structural and antibacterial behavior of eco-friendly of ZnO/TiO2 nanocomposite synthesized via Hibiscus rosa-sinensis extract," *J. Mater. Res. Technol.*, vol. 15, pp. 2213–2220, Nov. 2021, doi: 10.1016/j.jmrt.2021.09.048.

[88] C. C. O. OPREA , E. ANDRONESCU, B. S. VASILE, G. VOICU, "SYNTHESIS AND CHARACTERIZATION OF ZnO NANOPOWDER BY NON-BASIC ROUTE," *Dig. J. Nanomater. Biostructures*, vol. 6, no. 3, pp. 1393–1401, 2011, [Online]. Available: https://www.researchgate.net/publication/236024051_Synthesis_and_characterization_of_ZnO_nanopowder_by_non-basic_route.

[89] S. Wirunchit, P. Gansa, and W. Koetniyom, "Synthesis of ZnO nanoparticles by Ball-milling process for biological applications," *Mater. Today Proc.*, vol. 47, pp. 3554–3559, 2021, doi: 10.1016/j.matpr.2021.03.559.

[90] O.-R. Vasile *et al.*, "Synthesis and characterization of nanostructured zinc oxide particles synthesized by the pyrosol method," *J. Nanoparticle Res.*, vol. 14, no. 12, p. 1269, Dec. 2012, doi: 10.1007/s11051-012-1269-7.

[91] S. Sánchez-Martín, S. M. Olaizola, E. Castaño, E. Urionabarrenetxea, G. G. Mandayo, and I. Ayerdi, "Study of deposition parameters and growth kinetics of ZnO deposited by aerosol assisted chemical vapor deposition," *RSC Adv.*, vol. 11, no. 30, pp. 18493–18499, 2021, doi: 10.1039/D1RA03251H.

[92] S. Goktas and A. Goktas, "A comparative study on recent progress in efficient ZnO based nanocomposite and heterojunction photocatalysts: A review," *J. Alloys Compd.*, vol. 863, p. 158734, May 2021, doi: 10.1016/j.jallcom.2021.158734.

[93] J. N. Hasnidawani, H. N. Azlina, H. Norita, N. N. Bonnia, S. Ratim, and E. S. Ali, "Synthesis of ZnO Nanostructures Using Sol-Gel Method," *Procedia Chem.*, vol. 19, pp. 211–216, 2016, doi: 10.1016/j.proche.2016.03.095.

[94] K. Z. Sanidad, G. Wang, A. Panigrahy, and G. Zhang, "Triclosan and triclocarban as potential risk factors of colitis and colon cancer: Roles of gut microbiota involved," *Sci. Total Environ.*, vol. 842, p. 156776, Oct. 2022, doi: 10.1016/j.scitotenv.2022.156776.

[95] S. D. Lamore, C. M. Cabello, and G. T. Wondrak, "The topical antimicrobial zinc pyrithione is a heat shock response inducer that causes DNA damage and PARP-dependent energy crisis in human skin cells," *Cell Stress Chaperones*, vol. 15, no. 3, pp. 309–322, May 2010, doi: 10.1007/s12192-009-0145-6.

[96] M. Hasan *et al.*, "Bioinspired synthesis of zinc oxide nano-flowers: A surface enhanced antibacterial and harvesting efficiency," *Mater. Sci. Eng. C*, vol. 119, p. 111280, Feb. 2021, doi: 10.1016/j.msec.2020.111280.

[97] M. K. Debanath and S. Karmakar, "Study of blueshift of optical band gap in zinc oxide (ZnO) nanoparticles prepared by low-temperature wet chemical method," *Mater. Lett.*, vol. 111, pp. 116–119, Nov. 2013, doi: 10.1016/j.matlet.2013.08.069.

[98] R. Joshi *et al.*, "Application of Fourier Transform Infrared Spectroscopy and Multivariate Analysis Methods for the Non-Destructive Evaluation of Phenolics Compounds in Moringa Powder," *Agriculture*, vol. 12, no. 1, p. 10, Dec. 2021, doi: 10.3390/agriculture12010010.

[99] W. Phoohinkong, T. Foophow, and W. Pecharapa, "Synthesis and characterization of copper zinc oxide nanoparticles obtained via metathesis process," *Adv. Nat. Sci. Nanosci. Nanotechnol.*, vol. 8, no. 3, p. 035003, Jul. 2017, doi: 10.1088/2043-6254/aa7223.

[100] O. Bechambi, M. Chalbi, W. Najjar, and S. Sayadi, "Photocatalytic activity of ZnO doped with Ag on the degradation of endocrine disrupting under UV irradiation and the investigation of its antibacterial activity," *Appl. Surf. Sci.*, vol. 347, pp. 414–420, Aug. 2015, doi: 10.1016/j.apsusc.2015.03.049.

[101] Y. Lei, F. Qu, and X. Wu, "Assembling ZnO Nanorods into Microflowers through a Facile Solution Strategy: Morphology Control and Cathodoluminescence Properties," *Nano-Micro Lett.*, vol. 4, no. 1, pp. 45–51, Mar. 2012, doi: 10.1007/BF03353691.

[102] A. Jayachandran, A. T.R., and A. S. Nair, "Green synthesis and characterization of zinc oxide nanoparticles using Cayratia pedata leaf extract," *Biochem. Biophys. Reports*, vol. 26, p. 100995, Jul. 2021, doi: 10.1016/j.bbrep.2021.100995.

[103] C. Shuai *et al.*, "Enhanced Crystallinity and Antibacterial of PHBV Scaffolds Incorporated with Zinc Oxide," *J. Nanomater.*, vol. 2020, pp. 1–12, Jul. 2020, doi: 10.1155/2020/6014816.

[104] C. O. Tettey and H. M. Shin, "Evaluation of the antioxidant and cytotoxic activities of zinc oxide nanoparticles synthesized using scutellaria baicalensis root," *Sci. African*, vol. 6, p. e00157, Nov. 2019, doi: 10.1016/j.sciaf.2019.e00157.

[105] B. Kumar, K. Smita, L. Cumbal, and A. Debut, "Green Approach for Fabrication and Applications of Zinc Oxide Nanoparticles," *Bioinorg. Chem. Appl.*, vol. 2014, pp. 1–7, 2014, doi: 10.1155/2014/523869.

[106] J. Y. Bae and S. N. Park, "Evaluation of anti-microbial activities of ZnO, citric acid and a mixture of both against Propionibacterium acnes," *Int. J. Cosmet. Sci.*, vol. 38, no. 6, pp. 550–557, Dec. 2016, doi: 10.1111/ics.12318.

[107] M. Gupta, R. S. Tomar, S. Kaushik, R. K. Mishra, and D. Sharma, "Effective Antimicrobial Activity of Green ZnO Nano Particles of Catharanthus roseus," *Front. Microbiol.*, vol. 9, Sep. 2018, doi: 10.3389/fmicb.2018.02030.

[108] M. A. Ansari, H. M. Khan, A. A. Khan, A. Sultan, and A. Azam, "Synthesis and characterization of the antibacterial potential of ZnO nanoparticles against extended-spectrum β-lactamases-producing Escherichia coli and Klebsiella pneumoniae isolated from a tertiary care hospital of North India," *Appl. Microbiol. Biotechnol.*, vol. 94, no. 2, pp. 467–477, Apr. 2012, doi: 10.1007/s00253-011-3733-1.

Chapter 6

Conclusions and Scope for Future Work

Highlights of the Chapter:

- *The current chapter summarizes the thesis's significance and noteworthy successes.*
- *Details of novelty along with key findings and remarks developed in the present study.*
- *The scope for future work has also been discussed.*

6.1. Conclusions

Nanotechnology and nano scale metal oxide particles was known to humankind for over several years. However, even after years of major development with the discovery of zinc oxide nanoparticles, there exists a very few number of information based on its synthesis in a suitable media permitted for application in personal care products. Majority of existing fabrication methods for zinc oxide nanoparticles involve the use of harsh chemicals or by products that pose danger if exposed to human skin hence not permitted to be applied in personal care products. These methods also are often energy, expensive and labor extensive to be carried out in large scale industrial production. Moreover, there is a significant rise in antimicrobial resistant (AMR) microorganisms that defeat drugs designed to kill them. The existing antibacterial agents are proving inefficient and few agents like Triclosan, Triclocarbon, and ZPT etc. have been recently banned due to recent discoveries that they cause harmful diseases to humans on repeated exposure. Although green plant based products are being introduced in the market there is a dearth of personal care products involving moringa synthesized zinc oxide antibacterial agents.

Inspired by the information provided above, the research effort in this thesis has primarily concentrated on fabrication nanomaterials using appropriate techniques, evaluating and establishing their potential properties suited for health and hygiene products. Zinc oxide and silver doped zinc oxide nanomaterials were fabricated using surfactant polyol matrix suitable for health and hygiene applications and moringa oleifera based green synthesis. The synthesis causes in-situ generation of electrolyte influencing packing parameters of assembly and controlling the crystallite size in nano regime. The methodology adopted involved an analysis and comparison of the structural, morphological, antioxidant and antibacterial characteristics of both bulk commercial zinc oxide and synthesized nanomaterial. The thesis explored the characteristics of the as prepared samples for their structural and morphological analysis using techniques like Scanning Electron Microscopy (SEM), X-Ray Diffraction (XRD), UV-Visible spectroscopy and Fourier transform infrared Spectroscopy (FTIR).

Preparation of nanoparticles for industrial use in soap bars and liquid cleansing products to improve anti-oxidant and anti-microbial characteristics. Since this integration of nanoparticles improved the varied characteristics of soap bars and liquid cleansing products, efforts were undertaken to investigate the effect of nanomaterials in these systems. Antibacterial effectiveness

of prepared samples as measured by zone of inhibition (ZOI), minimal inhibitory concentration (MIC), and contact kill test (EN 1276). While antibacterial activity is affected by particle size, attempts were undertaken to investigate the influence of particle size by comparing synthesized nano zinc oxide samples to commercial bulk zinc oxide samples.

In addition to above mentioned details, properties and characteristics of moringa oleifera leaves are explored. Phytochemical study and identification was conducted and their antioxidant and antibacterial efficacy's were studied. The moringa oleifera was utilized to synthesize zinc oxide nanoparticles and the effects of moringa phytochemicals on the properties of zinc oxide nanoparticles were explored including anti-acne, antibacterial and antioxidant efficacies.

6.2. Novelty and Key findings of Research Work

Surfactant mediated Fabrication and application of nano ZnO and doped system:

- **Facile and unique combination approach**: This is among the very few researches to establish a facile approach to fabricate nano ZnO in a unique combination of surfactant polyol assembly (SPA) while generating in-situ electrolyte and transforming the micellar structures to rod shaped, acting as caging agent to restrict the particle growth in nano regime, named nano ZnO-SPA. This SPA matrix is suitable for health and hygiene products and such optimized technique rarely being explored to study the impact of embedding low concentrations of nano ZnO-SPA system into the matrix of sodium salt of long chain fatty acids (soap bar) and liquid cleansing personal care products.

- **Application** of the nano ZnO-SPA into sodium salt of long chain fatty acids matrix and liquid cleansing products confirmed significant antibacterial efficacies against disease causing germs. Multifunctional nano ZnO-SPA in soap matrix act as an inorganic physical UV ray blocker reducing the rate of degradation of unsaturated fatty acids resulting into significant enhancement of photostability of soap and protect the whiteness of soap bar >50% in comparison to soap without infusion.

- **Significant antibacterial efficacy through products** demonstrated by ZOI and EN 1276 methodologies up to 4.43 log reduction equivalent to 99.99% germ kill exhibited. High antibacterial activity of nano ZnO-SPA materials were established using agar disk diffusion method and capturing the ZOI against Gram-positive (S. aureus) and Gram-negative organisms (E. coli).

- **Strategic approach established to fabricate nano scale silver (100 -2000 ppm) doped zinc oxide (ZnOS)**. This highly suitable approach for health and hygiene products is among the few works of literature exploring the fabrication and infusion of nano ZnOS to elevate the germicidal efficacy of liquid cleansing products significantly.

- **Silver doped zinc oxide (ZnOS)** having an average crystalline size 15.14 nm with a blue shift in absorbance peaks 349 nm–340 nm observed possibly due to Burstein-Moss effect in metal doped system. Crystallite size, dislocation density, specific surface area and crystallinity parameters have been explored using XRD diffractogram analysis. The SEM result shows the surface morphology of nano ZnOS as closely packed spherical particles.

- **Advanced germicidal efficacy of liquid cleansing product**: Germicidal behavior of AR grade ZnO, nano ZnO and ZnOS investigated confirmed that nano ZnOS possessed higher germicidal activity than the AR grade or nano ZnO. Disk diffusion method and EN 1276:2019 confirmed that base formula of liquid cleansing product showed no microbial activity while ZnOS nanomaterial addition increased the germicidal activity of liquid cleansing product significantly i.e >99.999% germ kill.

Green approach -GsZnO-Nps and applications:

- **Moringa extracts**: aqueous extract and identified twenty-five phytochemicals and similarly in Methanolic extract fifty-four phytochemical components were identified. Few of phytochemicals reported here are rarely detected in plant extracts like 3,30-Iminobispropylamine, Butanedioic acid, 2-hydroxy-2-methyl- etc. and have potential applications.

- **Substantial free radical scavenging potency**: IC50 of Moringa aqueous extract observed is 4.65 ml/ml and for methanolic extract 1.83 ml/ml. Methanolic extract at 5 µl gives maximum level of 92.8% FRSP. Aqueous extract at 5 µl scavenge the DPPH free radical significantly up to 68.4%. These high FRSP make them very suitable ingredients for various applications like food, animal feed medicines, cosmetic etc.

- **Green synthesis**: Moringa Oleifera leaves extract is effectively used for the green synthesis as a strategic and sustainable route to fabricate potent zinc oxide nanoparticles. This may be the first or among the very few researches that have established the potency of green synthesized zinc oxide using moringa leaves extract against *C. acne* and additionally demonstrated efficacy equivalent to standard drugs with respect to S. aureus and E. coli bacterium.

- **Green synthesized ZnO nanoparticle's (GsZnO-Nps)**: Particle size 50 nm, high specific surface area (77.38 m^2/g), and total crystallinity 95.91%. UV-Vis spectra displayed the absorption band at 368.5 nm having band gap energy 3.36 eV has a blue shift in relation to AR grade ZnO.

- **Significantly high antioxidant activity of GsZnO-Nps**: having a half-maximal inhibitory concentration (IC50) of 21.72 µg/mL. Antioxidant activity is recommended to improve general health by helping to neutralize free radicals in our systems.

- **Advanced antimicrobial activity of GsZnO-Nps comparable to antibiotics**: having inhibition zone 26.75 mm and 30.00 mm against E. coli and S. aureus bacteria which is higher or equal to the standard drug (antibiotics) while MIC of GsZnO-Nps was found to be 500 µg/mL which is much less when compared to AR Grade zinc oxide.

6.3. Dermatologically Tested Products: Products comprising Moringa extract and Moringa with Zinc (GsZnO-Nps) has been dermatologically tested by ISO certified center for safety as per ethics committee approval and direct supervision of dermatologist and Principal investigator as per IS 4011:2018.

MASCOT SPINCONTROL

clinical research centre

ISO 9001:2015 Certified

This is to certify that

Savannah Body Lotion Moringa

was evaluated upon Ethics Committee approval for safety on human volunteer and is -

- Dermatologically tested for Safety
- Non-Irritant to skin

Mrs. Mumtaz Lalvani
Chief Executive Officer

Date: 25/04/2023

NOTE: The clinical ***study coded D01-6Q01-LC-AL23,*** *was conducted under the direct supervision of Dermatologist & Principal Investigator as per IS 4011:2018 3rd Revision Methods of test for safety evaluation of cosmetics at Mascot Spincontrol.*

MASCOT SPINCONTROL

clinical research centre

ISO 9001:2015 Certified

This is to certify that

Savannah Anti–Acne Cream With Moringa & Zinc

was evaluated upon Ethics Committee approval for safety on human volunteer and is -

- Dermatologically tested for Safety
- Non-Irritant to skin

Mrs. Mumtaz Lalvani
Chief Executive Officer

Date: 25/04/2023

NOTE: The clinical ***study coded D01-6Q01-LC-AL23,*** *was conducted under the direct supervision of Dermatologist & Principal Investigator as per IS 4011:2018 3rd Revision Methods of test for safety evaluation of cosmetics at Mascot Spincontrol.*

6.4. Scope for Future Work

New novel nanomaterial fabrication methods are essential requirement in elevating industrial application opportunities. However, the conventional methods of synthesis are just not adequate to meet the high demands and safety regulations in the health and hygiene sector. Metal and metal oxide nanomaterials possessing high antibacterial and antioxidant, has found ever-increasing commercial interest in this decade, especially, because of their usage in large number of fields including medicine, packaging, cosmetics, personal care, additives, etc. Fabrication of zinc oxide nanoparticles using surfactant and green based methods that are suitable for application in personal care industry is a very remarkable aspect in product development. Recommendations for future work are as follows:

- There is a massive demand for non-toxic antibacterial and antimicrobial agents for health and hygiene products. It is thus worthy to develop non-toxic antibacterial and antimicrobial nanocomposites using materials such as zinc oxide, titanium dioxide etc. to establish different synergistic combinations for advanced efficacies and more precise application.
- In addition, careful incorporation of various dopant and co-dopants can be done to boost the properties of the nanomaterial and efficacy in the final product after application.
- Impact of bivalent ions and dielectric permittivity of the solvents on morphologies and efficacies
- The most serious hazard to animal husbandry health is infectious illness due to bacteria, fungus and viruses. Fabricated products can be used as the antimicrobial active for such animal disinfectants and also be explored for potency against larger collection of gram positive, gram negative bacteria, virus, fungi etc.
- There have been evaluations on self-sterilizing antimicrobial packaging coatings, but none have offered a full picture of the uses of active packaging to reduce fungal deterioration. ZnO-SPA, silver doped ZnO, and GsZnO np have yet to be investigated as self-sterilizing coatings.
- Observed high free radicle scavenging and antimicrobial potency of the fabricated materials make them very suitable ingredients for various applications like food, animal feed medicines, cosmetic etc. Application of the same in products for topical application having skin benefits like prevention of skin damage, aging, anti-acne etc. are yet to be studied as well as in vivo analysis such as trans epidermal water loss, high-quality image analysis, clinical data of erythema and dryness etc. need to be explored.
- It will be highly recommended and to take up the challenge of commercial large scale production of personal care products explored currently in just lab scale for the practical industrial application.

Product Application of Surfactant Mediated and Green Approach Based Nano ZnO

Research Publications to Scholar's Credit

(A) Publications related to Ph.D. Thesis:

SCI Journal Publications

1. Green approach to synthesize nano zinc oxide via Moringa oleifera leaves for enhanced anti-oxidant, anti-acne and anti-bacterial properties for health & wellness applications, **Nitesh Bhalla**, N. Ingle, A. Jayaprakash, H. Patel, S. V. Patri, D. Haranath, *Arabian Journal of Chemistry*. 16 (2023) 104506. *https://doi.org/10.1016/j.arabjc.2022.104506* **[IF. = 6]**

2. Fabrication and infusion of potent silver doped nano ZnO aimed to advance germicidal efficacy of health and hygiene products, **Nitesh Bhalla**, A. Jayaprakash, N. Ingle, H. Patel, S. V. Patri and D. Haranath, *Journal of Science: Advanced Materials and Devices*, 07 (2022) 100487. *https://doi.org/10.1016/j.jsamd.2022.100487* **[IF. = 8]**

3. A Facile approach to fabricate and embed multifunctional nano ZnO into soap matrix and liquid cleansing products for enhanced antibacterial and photostability for health and hygiene applications, **Nitesh Bhalla**, N. Ingle, H. Patel, A. Jayaprakash, S. V. Patri, A. Kaushik and D. Haranath, *Arabian Journal of Chemistry*, 15 (2022) 103862. *https://doi.org/10.1016/j.arabjc.2022.103862* **[IF. = 6]**

4. Phytochemical analysis of Moringa Oleifera leaves extracts by GC-MS and free radical scavenging potency for industrial applications, **Nitesh Bhalla**, N. Ingle, S. V. Patri and D. Haranath, *Saudi Journal of Biological Sciences* 28 (2021) 6915-6928. **[IF. = 4.4]** https://doi.org/10.1016/j.sjbs.2021.07.075

International/National Conferences and Seminars attended

1. **As Keynote address** International E-Conference on Advances in Nano Technology ANT-2021 "*Smart Nano engineered ZnO and its industrial applications*, held at Vaagdevi Degree and PG College, Telangana, India.

2. **As an Invited speaker** National Conference on Luminescence and Applications (NCLA-2020) on the title "*Anti-microbial Fluorescent ZnO and industrial applications*", held at National Institute of Technology (NIT) Warangal, Telangana, India.

(B) Patents other than Ph.D. Thesis:

1. **Nitesh Bhalla,** Mhaskar, S., Gode, V., & Kalghatgi, B. "Composition for Relieving Stress" India, 2632/MUM/2009; (Granted)
2. **Nitesh Bhalla** & Pramanik "A Zinc Complex, Process for Preparation Thereof and A Method for Treating Fabric Therewith" 1047/Mum/2007 · Issued Sep 12, 2012 (Granted)
3. **Nitesh Bhalla** & Pramanik, A. "A Zinc Complex, Process for Preparing Thereof and a Method for Treating Fabric Therewith" Europe, PCT/EP2008/055143 (28 Apr 2008)

(C) SCI Journal Publications and conferences other than Ph.D. Thesis:

1. **Nitesh Bhalla**, Dharmadhikari R., Bell F., Chandani P., Mamniya C. & Rastogi, P. (29 Aug 2014), "The Hair Damage Dilemma" (awarded as the Best Poster) at 3rd International Conference of Trichology

2. Kamath Y., Gode V., **Nitesh Bhalla**, Kalghatgi B. & Mhaskar S. (2012) - "Quantitative Measurement of the Penetration of Coconut Oil into Human Hair using Radiolabelled Coconut Oil" *Journal of Cosmetic Science*, 63, 27–31

3. Kamath Y., Gode V., **Nitesh Bhalla**, Kalghatgi B. & Mhaskar S (2010) - "Effect of Grooming Practices on Physical Characteristics of Hair" *International Journal of Applied Science*, 136 (11)

4. Haranath D., Sharma P., Chander H., Ali A., **Nitesh Bhalla** & Halder S.K. (2007)-"Role of Boric Acid in Synthesis and Tailoring the Properties of Rare Earth Doped Calcium Aluminate Phosphor"-*Material Chemistry and Physics*, 101, 163

5. Haranath D., Chander H., **Nitesh Bhalla**, Sharma P. & Sood K.N. (2005), "Surface Distribution Studies and Improved Photoluminescence Characteristics of Silica Coated Zns: Mn Nanophosphor Layers" *Applied Physics Letter* 86, 201904

6. Haranath D., Chander H., **Nitesh Bhalla**, Sood K.N., Singh S. & Kishore R (2004), "Morphological Investigation of ZnS: Mn Nanophosphor Embedded in Transparent Silica Gel"-Electron Microscopy and Allied Fields, EMSI-2004, National Physical Laboratory, New Delhi, p. 236

7. Sharma P., Chander H., Haranath D., **Nitesh Bhalla**, Singh S. & Kishore R. (2004), "Structure & Photoluminescence of Nano-SrAl2O4:Eu2+, Dy3+, Phosphor"-Electron Microscopy & Allied Fields, EMSI-2004, National Physical Laboratory, Delhi, p. 208

8. Haranath D., Chander H., **Nitesh Bhalla**, & Sharma P. (2004), "Luminescence of ZnS: Mn Nanophosphor Embedded in Porous Silica Matrix using Sol-Gel Method"-National Conference on Materials and their Applications (NCMA-2004), Department of Physics, Kurukshetra University, Kurukshetra, p. 41

9. Haranath D., **Nitesh Bhalla,** Chander, H. Rashmi, Kar M. & Kishore R. (2004), "Controlled Growth of ZnS: Mn Nanophosphor in Porous Silica Matrix"-*Journal of Applied Physics*, 96 (11), 6700

NITESH BHALLA

R&D | Strategic Leadership | Innovation & Change | Expert Advisor | Development of Executive Talent

- Qualified R&D leader with a proven career in conceiving & implementing effective ideas / strategies in FMCG sector that can add value to organization through inspiring leadership, rich experience & innovation excellence

bhalla.nitesh@gmail.com / niteshb7@yahoo.co.in

https://www.linkedin.com/in/nitesh-bhalla-77a893b/

+971 508242787

+971 562592555

Executive Profile

- **Dynamic career of over 19 years** that reflects rich Indian, Chinese, UAE experience & year-on-year success in **Research & Development** across FMCG industry involving inventing, developing & implementing new technologies to deliver novel & superior sensorial for products by identifying, incubating & market readying disruptive innovations that have potential to be future core in traditional businesses
- **Tactful & articulate** in driving vision and championing the cause; proficient in accelerating, protecting & differentiating our innovations and working on global venture & product line demanding unique skill set & distinct experience
- Directed **cross-functional & multi-cultural teams** (India, China, UAE) using interactive & motivational leadership; acknowledged for leading & mentoring various team members to achieve resource wise productivity & optimization
- A forward-thinking person with **strong communication, analytical & organizational** skills; well organized with a track record that demonstrates self-motivation & creativity to achieve corporate & personal goals

Career Timeline

Sep'03-Nov'04: National Physical Laboratory (a CSIR Lab), Luminescent Material & Devices Group as Research Intern

Nov'04-Apr'07: Unilever Limited (Discovery Center), Synthetic Chemistry Group as Research Associate

Apr'07-Jun'09: Marico Limited, Advanced Technology Group as R&D Assistant Manager

Jun'09-Jun'18: Hindustan Unilever Limited (Unilever Limited) as R&D Sr. Manager at Shanghai, China & India

Since Jun'18: IFFCO Beauty, As R&D lead for personal care, at Dubai

Behavioral Traits

Professional Experience

Since Jun'18: IFFCO Beauty, Dubai

Jun'09-Jun'18: Hindustan Unilever Limited (Unilever Limited), Mumbai

Growth Path / Assignments Handled:

Jun'09-Sep'11: Assistant Manager - R&D, Homecare Category *(Unilever Limited, Mumbai, India)*

Oct'11-Feb'13: Formulation Design Manager - R&D, Laundry, Global Design Center *(Unilever Limited, Mumbai, India)*

Mar'13-Jan'15: R&D Sr. Manager - Product Evaluation & Advertising Claims, Hair South Asia Deploy Center *(Unilever Limited, Mumbai, India)*

Feb'15-Jul'17: R&D Sr. Manager - Product Evaluation, Consumer Insight & Advertising Claims - Hair Global Design Center *(Unilever Co. Limited, Shanghai, China)*

Since Aug'17: R&D Sr. Manager - Technical Project Leader (TPL) - Hair (S. Asia Deploy Centre) *(Hindustan Unilever Limited)*

Most Proud of

3Ds – Experienced in 3 pillars of R&D i.e. Discover, Design & Deploy

3Cs – Cross-category (Hair, Skin & Homecare), Cross-function (Product Development, Product Evaluation, Consumer Technical Insight & Claims) and Cross-countries

3Ps: Product, Patents and Publications

Unilever R&D Laureate Award for best performance in the market (2014); Awardee as a R&D contributor to achieve 1 billion Euro milestones of Laundry Business in S. Asia (2011)

Bagged a prestigious award of Marico Ltd. for innovation & launch of Parachute "Revitalizing Hot Oil" (Apr'09)

Received award for best performance at Unilever (Discovery Centre) in 2005 & 2006

Awarded for delivering projects & communicating the value of bias for action (2008) in Marico Ltd.

Key Impact Areas

- **Research & Development**
- **New Product Development**
- **Budgeting / Costing**
- **Claims & Capability Roadmaps**
- **Project Management**
- **Consumer Insights**
- **Hair, Skin, Household and Laundry**
- **Competitor Intelligence**
- **People Leadership**
- **Quality**

Role:

As R&D & QA Head- IFFCO Beauty

- Building ***R&D strategies***, in line with Org. strategies. Leading ***new product development (NPD*)** projects and setup processes.
- **Leading R&D & QA team** and keeping them motivated to deliver business objectives
- Establishing the development and ***evaluation capabilities*** for personal care products e.g. Shampoos, Body wash, Soap, Anti-bac Hand wash, Skin creams, lotions
- ***New site expansions***: Leading and defining critical process parameters and provide inputs for all technical requirements
- Leading **packaging team** member and initiatives for new products and value engineering program
- **Saponification**: Defining & designing strategies for oil blend flexibility program. Oil blends like 80:20, 90:10 for different TFM soap noodles 65, 72, 78 TFM based on SWING, SAGE, DFA, DPFAD etc. Process and their technical specifications to ensure the quality products.
- Leading ***QA/QC*** and ensure the implementation of ***GMP ISO 22716-2007***, QMS, Halal certification, EcoVadis CSR certifications.
- Regulatory: Ensuring product meet the regulatory requirements and Standards of the country like GSO, SASO, JS, BIS, EU etc.
- Ensuring documentation and product registrations in different countries, meeting with FDA, Municipality. like Jordan FDA, Egypt FDA, ESMA, Saudi FDA, SABER, Dubai Municipality (Montaji) etc.
- Defining R&D strategies for ***Pvt. Label and leading projects*** example Carrefour, Lulu hyper market, Panda, Nesto etc.

As R&D Sr. Manager - Technical Project Leader (TPL) - Hair (S. Asia Deploy Centre):

- Created strategies to land ***male grooming*** innovations successfully
- Led the ***NPD project teams***, a range of male grooming products (***Brylcreem***-Shampoo, Beard balm, Beard oil, Styling Wax, beard wash) developed and launched exclusive on e-com. channel.
- Headed Project Team and ensured efficient delivery of 8 variants ***TRESemme*** Innovations / Business led G Projects in S. Asia
- Defined ***strategies to maximize the technology impact*** for hair category across brands for S. Asia
- Formulated strategies on ***claims & delivering demos for e-com*** to have the high business impact

As R&D Sr. Manager - Product Evaluation, Consumer Insight & Advertising Claims - Hair Global Design Center:

- Defined strategies for: Active ***technology & haircare formulation*** to drive consumer benefit platform
- ***Hair Fall platform***, BPS, and claims roadmap integrated with key technologies & innovation pipelines
- Steered creative approach and established a new reporting system which saved up to 30% of time on routine procedures
- Developed ***strategic partners*** for advanced & routine measurements, product performance evaluation, partners for data endorsements to communicate strong product claims
- Assured on-time full (OTIF) deliveries of ***global claim support packages*** meeting countries regulations via innovation projects of ***iTO €20-50 Mln***. in 1-3 years
- Led ***consumer technical insight (CTI)*** function globally for Hair Fall (HF) platform, conducted qualitative & quantitative ***consumer studies*** and worked closely with R&D, external partners & marketing stakeholders
- Drove ***new insight generation***, hair fall and dandruff platform while defining the study brief / objectives, inclusion / exclusion criteria, ***protocols and clinical end points*** as per the innovation pipeline
- Realized the diversification impact and applied claims for hair fall innovations using Pack, TVC, Print, Digital Communications, ***Digital Demo Strategies*** in store, point of sale & other media
- Conducted ***business intelligence globally for hair fall platform***, reviewed & assessed competitors and generated innovative ideas for gaining competitive advantages

As R&D Sr. Manager - Product Evaluation & Advertising Claims, Hair South Asia Deploy Center:

- ***Headed a team*** of Consumer Technical Insight, Claim and Appraisal for South Asia to cater the communication need ***across hair care brands*** (like Dove & Tresemme) and formats (Shampoo, Oil & LOT) in the region
- Designed ***claims roadmap*** linked to brand agenda of innovation pipeline of 5 years to drive growth of Clinic Plus
- Formulated strategies, attained the best results for consecutive years and ***won in-out challenges in 2014***
- Drove regional claim forum with ***cross-functional team and stakeholders*** of Marketing, R&D, Legal and Regulatory
- Rolled-out various consumer relevant and differentiated demos to maximize the technology impact using media like TVCs, digital, conferences and in-store activations

As Formulation Design Manager - R&D, Laundry, Global Design Center:

- Formulated strategies for ***big bold projects of total saving potential of €20-40 Mln***. through collaboration with strategic partner to evaluate the best suitable technologies
- Drove simplification, delivered multiple projects to ***improve gross margins (GM)*** and meet the set targets by realizing annual saving of €2-5 Mln.
- ***Headed Project Team of 10-15 members of different culture*** (supply chain, procurement, processing, marketing & regulatory)
- Performed ***business intelligence for laundry*** globally while reporting on competitor launches / re-launches, pack claims, formulation changes & performance evaluation and ***forecasting on further strategies***

As Assistant Manager - R&D, Homecare Category:

- Executed Innovation Projects including ***household & laundry*** and ensured their implementation in key areas locally & globally
- Assured effective management of ***Innovation and Value Improvement Programs (VIP)***
- Re-launched dish wash (DW) Vim Bar in India and established clear ***superiority versus competition***, thereby regaining share lost to regional brands & adding incremental ***turnover (iTO) of €25+ Mln***. within 3 years
- Managed virtual team members in a project of white space entry for dish wash (DW) business in Pakistan for ***formats of bars & liquid concentrates*** with potential of more than €30 Mln. iTO within 1-5 years
- Delivered ***Technology Transfer Document*** (TTD) covering claim substantiation & all technical components in details like Chemistry, Manufacturing and Controls (CMC)

Previous Experience

Apr'07-Jun'09: Marico Limited, Advanced Technology Group, Mumbai, India as R&D Assistant Manager
Nov'04-Apr'07: Unilever Limited (Discovery Center), Synthetic Chemistry Group, Bangalore as Research Associate
Sep'03-Nov'04: National Physical Laboratory (a CSIR Lab), Luminescent Material & Devices Group, New Delhi as Research Intern

Education

- **Pursuing Ph.D. in Chemistry**, National Institute of Technology, Warangal (NITW) 2019, India
- **M.Sc. in Organic Chemistry** from Kurukshetra University, Kurukshetra in 2003
- **B.Sc. in Industrial Chemistry** from Kurukshetra University, Kurukshetra in 2001

Trainings

- "**Leading People: Leading, Not Managing People**" training course completed, 2021
- Successfully completed the program titled "**Strategy Development and Execution: The ADEPTT Model**"
- "**Leading Change: McKinsey's 7-S Change Model**", 2021
- Successfully completed the program titled "**Strategies for Achieving Goals**", 2021
- "**Leading @ IFFCO Workshop - for MM and HD only**", 2019
- Successfully completed the program titled "**Leading with Your Strengths**", 2019
- Successfully completed the program titled "**Feedback and Coaching Essentials**", 2019
- ***DuPont*** Course in ***Managing Safety*** Techniques that Works for Line Supervisors in 2006
- Laborate Pharmaceuticals India Limited, ***Quality Control Lab***, Panipat, Haryana during May'02-Jun'02
- Indian Oil Corporation Limited (IOCL), ***Panipat Refinery, Sulphur Recovery Unit***, Haryana during May'00-Jun'00
- Indian Oil Corporation Limited (IOCL), ***Panipat Refinery, Quality Lab***, Haryana, India during May'99-Jun'99

Patents

- **Bhalla, N.**, Mhaskar, S., Gode, V., & Kalghatgi, B. "Composition for Relieving Stress" India, 2632/MUM/2009; (Granted)
- **Bhalla, N.** & Pramanik "A Zinc Complex, Process for Preparation Thereof and A Method for Treating Fabric Therewith" 1047/Mum/2007 · Issued Sep 12, 2012 (Granted)
- **Bhalla, N.** & Pramanik, A. "A Zinc Complex, Process for Preparing Thereof and a Method for Treating Fabric Therewith" Europe, PCT/EP2008/055143 (issued on 28 Apr 2008)

Publications & Presentations

- **Bhalla N.,** Ingle N., Jayaprakash A., Patel H., Patri S., Haranath D., (2023), "Green approach to synthesize nano zinc oxide via Moringa oleifera leaves for enhanced anti-oxidant, anti-acne and anti-bacterial properties for health & wellness applications"" Arabian Journal of Chemistry, Elsevier
- **Bhalla N.,** Jayaprakash A., Ingle N., Patel H. Patri S., Haranath D., (2022), "Fabrication and infusion of potent silver doped nano ZnO aimed to advance germicidal efficacy of health and hygiene products" Journal of Science: Advanced Materials and Devices, 7, 100487.
- **Bhalla N.,** Ingle N., Patel H., Jayaprakash A., Patri S., Kaushik A., Haranath D., (2022), "A Facile approach to fabricate and embed multifunctional nano ZnO into soap matrix and liquid cleansing products for enhanced antibacterial and photostability for health and hygiene applications" Arabian Journal of Chemistry, Elsevier
- **Bhalla N.,** Ingle N., Patri S., Haranath D (2021), "Phytochemical analysis of Moringa Oleifera leaves extracts by GC-MS and free radical scavenging potency for industrial applications" Saudi Journal of Biological Sciences, Vol. 28 issue 12. Elsevier
- **Bhalla N.,** as an **Invited Speaker** (2020)- "Anti-microbial Fluorescent Nano ZnO and its Industrial Applications" at National Conference on Luminescence and its Applications (NCLA), National Institute of Technology, Warangal, India

- **Bhalla N.,** as an **Invited Speaker** 2016- “In-vitro Advanced Measurements in Hair Care” at International Technical Forum for Healthcare and Beauty Products. June 2016 GuangZhou, China
- **Bhalla N.,** Dharmadhikari R., Bell F., Chandani P., Mamniya C. & Rastogi, P. (29 Aug 2014), “The Hair Damage Dilemma” (awarded as the Best Poster) at 3rd International Conference of Trichology
- Kamath Y., Gode V., **Bhalla N.,** Kalghatgi B. & Mhaskar S. (2012) - “Quantitative Measurement of the Penetration of Coconut Oil into Human Hair using Radiolabelled Coconut Oil” Journal of Cosmetic Science, 63, 27–31
- Kamath Y., Gode V., **Bhalla N.,** Kalghatgi B. & Mhaskar S (2010) - "Effect of Grooming Practices on Physical Characteristics of Hair" International Journal of Applied Science, 136 (11)
- Mhaskar S., Shirhatti V., Gode V., **Bhalla N.,** Agarwal N. & Augustin P. (Sept 2009), “Coconut Oil - A Natural Do Good Hair Conditioner”-HairS’09, DWI an der RWTH Aachen E.V., Germany
- Haranath D., Sharma P., Chander H., Ali A., **Bhalla N.** & Halder S.K. (2007)-"Role of Boric Acid in Synthesis and Tailoring the Properties of Rare Earth Doped Calcium Aluminate Phosphor"-Material Chemistry and Physics, 101, 163
- Haranath D., Chander H., **Bhalla N.,** Sharma P. & Sood K.N. (2005), “Surface Distribution Studies and Improved Photoluminescence Characteristics of Silica Coated Zns: Mn Nanophosphor Layers” Applied Physics Letter 86, 201904
- Haranath D., Chander H., **Bhalla N.,** Sood K.N., Singh S. & Kishore R (2004), “Morphological Investigation of ZnS: Mn Nanophosphor Embedded In Transparent Silica Gel”-Electron Microscopy and Allied Fields, EMSI-2004, National Physical Laboratory, New Delhi, p. 236
- Sharma P., Chander H., Haranath D., **Bhalla N.,** Singh S. & Kishore R. (2004), “Structure & Photoluminescence of Nano-$SrAl_2O_4:Eu^{2+}$, Dy^{3+}, Phosphor”-Electron Microscopy & Allied Fields, EMSI-2004, National Physical Laboratory, Delhi, p. 208
- Haranath D., Chander H., **Bhalla N.,** & Sharma P. (2004), “Luminescence of ZnS: Mn Nanophosphor Embedded in Porous Silica Matrix using Sol-Gel Method”-National Conference on Materials and their Applications (NCMA-2004), Department of Physics, Kurukshetra University, Kurukshetra, p. 41
- Haranath D., **Bhalla, N**. Chander, H. Rashmi, Kar M. & Kishore R. (2004), “Controlled Growth of ZnS: Mn Nanophosphor in Porous Silica Matrix”-Journal of Applied Physics, 96 (11), 6700

Other Information

I am married to Rashmi my sweetheart and we are blessed with two sons- Gunmay (14 yr) and Yatharth (8yr). Both are studying and building their intellect to embrace the journey of life confidently.
My interests include writing Hindi poetry and listening to some spiritual music. I also love martial arts since childhood and bagged medals at National levels.

Personal Details

Date of Birth: 07/07/81
Address: 2B-602, N.G. Suncity Phase-2, Thakur Village, Kandivali, Mumbai-400101, Maharashtra, India
Languages Known: English and Hindi
Industry Preference: FMCG / Speciality Chemical / Pharma
Location Preference: Europe / Australia /North Asia/ Canada / North & South America / UAE / India / South East Asia/ME